2018

Identification and Characterization of Hells-CDCA7, a Nucleosome Remodeling Complex Required for Mitotic Chromosome Structure

Christopher Jenness

IDENTIFICATION AND CHARACTERIZATION OF HELLS-CDCA7, A NUCLEOSOME REMODELING COMPLEX REQUIRED FOR MITOTIC CHROMOSOME STRUCTURE

A Thesis Presented to the Faculty of

The Rockefeller University

in Partial Fulfillment of the Requirements for

the degree of Doctor of Philosophy

by

Christopher Jenness

June 2018

IDENTIFICATION AND CHARACTERIZATION OF HELLS-CDCA7, A NUCLEOSOME REMODELING COMPLEX REQUIRED FOR MITOTIC CHROMOSOME STRUCTURE

Christopher Jenness, Ph.D.

The Rockefeller University 2018

The major components of mitotic chromosomes including histones, topoisomerase II and condensin are known to compact and shape the chromatin into rod-like chromatids. However, a complete picture of the proteins involved in shaping mitotic chromatin is unsettled.

Here, I perform mass spectrometry on chromatin isolated from *Xenopus* egg extracts. By comparing interphase and M phase, I reveal how the chromatin proteome is affected by the cell cycle. I find that although topoisomerase II associates with chromatin throughout the cell cycle, its catalytic activity is greatly enhanced in mitosis where it can act on nucleosomal substrates. In contrast, condensin is specifically recruited to M phase chromatin and prefers a non-nucleosomal substrate. I show that nearly all proteins involved in nucleosome assembly and remodeling are evicted from mitotic chromosomes, concurrent with a reduction in mitotic nucleosome assembly and discuss a role for these phenomena in shaping mitotic chromosomes.

In analyzing my mass spectrometry data, I noticed that subunits of stoichiometric chromatin-bound complexes behaved similarly across a variety of conditions. Using this principle, I identify a novel nucleosome remodeling complex comprising HELLS and CDCA7, two proteins known to be causative for Immunodeficiency, centromeric region instability, facial anomalies (ICF) syndrome, a rare immunodeficiency disease. Consistent with previous literature, HELLS alone fails to remodel nucleosomes, but the HELLS-CDCA7 complex possesses robust nucleosome remodeling activity. CDCA7 is essential for loading HELLS onto chromatin, and CDCA7 harboring patient ICF mutations fails to recruit the complex to chromatin. Finally, I show that the HELLS-CDCA7 complex is required for proper mitotic chromosome structure. Together, my study identifies a unique bipartite nucleosome remodeling complex where the functional remodeling activity is split between two proteins.

These data lead me to a unifying model for ICF syndrome where all known ICF mutations converge on defective DNA methylation. I propose that HELLS-CDCA7 mediated remodeling of juxtacentromere heterochromatic nucleosomes facilitates DNMT3B-mediated methylation and discuss this model alongside alternative models for ICF syndrome. Finally, I consider the role of CDCA7 paralogs in differentially regulating HELLS, and present an outlook on the future of ICF syndrome research.

ACKNOWLEDGEMENTS

I would like to thank members of the Funabiki laboratory for their help during my time at The Rockefeller University. Christian Zierhut, Dave Wynne, Pavan Choppakatla, Michael Wheelock, Simona Giunta, Hironori Funabiki, David Allis, and Brian Chait provided valuable discussions, which helped the direction of the project.

Additionally, I am grateful for Tom Muir accommodating me into his lab in September of 2014 where I learned a very different perspective on science under the mentorship of Manuel Muller.

Many people provided reagents and technical advice including Geneviève Almouzni, Shawn Amed, Yoshiaki Azuma, Noah Dephoure, Joseph Fernandez, Rebecca Heald, Tatsuya Hirano, Nathan Gamarra, Hiroshi Kimura, Lance Langston, Geeta Narlikar, Atsuya Nishimaya, Miachel O'Donnell, Dirk Remus, Johannes Walter, Martin Whur, and Henry Zebroski.

TABLE OF CONTENTS

LIST OF FIGURES

LIST OF TABLES

CHAPTER 1: INTRODUCTION

The cell cycle

The cell cycle

For a cell to become two cells, it must duplicate and segregate its entire genome. These two process are temporally separated into interphase (the growth and duplication phase) and mitosis (the division phase) and repeat in turn for every cellular division. In interphase cells duplicate their cellular contents including their DNA and other organelles. Once duplicated in constitution, in mitosis the cellular components are divided in two, each daughter receiving an entire copy of genomic DNA and organelles (detailed below). This coordinated progression results in two cells, each with an entire genomic set, and the cycle can start over. Since the original discovery of genetic factors involved in the regulation of the cell cycle(Hartwell et al., 1970), many of the molecular details have been elucidated.

Mitosis

Mitosis is the phase of the cell cycle where the duplicated genome is split into two separate cells (reviewed in (Morgan, 2007)). The main driver of all aspects of mitosis is the protein kinase Cyclin Dependent Kinase (Cdk1)(Coudreuse and Nurse, 2010). Activated by mitotic expression of cyclin B(Jeffrey et al., 1995; Murray and Kirschner, 1989; Murray et al., 1989), Cdk1-cyclin B initiates and controls all downstream mitotic stages. Prophase, the first visible stage of mitosis, is where chromosomes condensation and individualization begins. Nuclear envelope breakdown

occurs and the machinery to segregate the chromosomes assembles on chromatin during prometaphase. At metaphase, chromosomes are attached to microtubules and aligned at the metaphase plate. Individual chromosomes can easily be visualized, with identically replicated sister chromatids held together with cohesin. Once chromosomes are aligned at the metaphase plate, cohesin(Ciosk et al., 1998) and cyclin B(Irniger et al., 1995; Murray et al., 1989) are degraded, leading to Cdk1 inactivation, sister chromatid segregation, chromosome decondensation, nuclear envelope formation, and the beginning of the next cell cycle.

In addition to Cdk1, a variety of other mitotic kinases facilitate proper chromosome segregation. Aurora B, the kinase component of the chromosome passenger complex (CPC), phosphorylates numerous substrates, performing many mitotic functions, which include mitotic spindle assembly and ensuring that chromosomes are properly oriented in the spindle (Carmena et al., 2012). The CPC is recruited to mitotic chromosomes by the mitotic phosphorylation of threonine 3 on histone H3, which is phosphorylated by haspin(Kelly et al., 2010; Wang et al., 2010; Yamagishi et al., 2010). Specifically, the CPC subunit survivin recognizes H3T3ph to localize and active the complex. Polo like kinase (Plk1) is required to release cohesin, the molecule responsible for linking together replicated sister chromatids, from chromosome arms during prophase(Sumara et al., 2002). These kinases are specifically activated in mitosis, downstream of Cdk1, to coordinate mitotic events.

Chromatin throughout the cell cycle

Chromatin, the nucleic acid-protein complex comprising the cellular genetic material, undergoes dramatic morphological changes throughout the cell cycle. In interphase, chromatin is loosely packaged into the nucleus (reviewed in (Dixon et al., 2016)). This “open” chromatin state is important for DNA based transactions including transcription, replication, and DNA damage repair. Although, densely packaged heterochromatin is inherently refractory to DNA based processes including transcription(Lorentz et al., 1992), DNA repair(Cowell et al., 2007), and DNA methylation(Lyons and Zilberman, 2017), the cell has specialized mechanisms to overcome these barriers.

How chromatin is organized in the genome has been a topic of intense study. Recently, the technique Hi-C has been developed to probe the local and long range interactions between genomic loci(Lieberman-Aiden et al., 2009). In Hi-C, the genome is fixed and digested with nucleases. Following digestion, the genome is re-ligated and sequenced. DNA that has re-ligated with new sequences in the genome is indicative of a spatial interaction between the two loci. This technique has yielded immense insight into the organization of interphase chromatin. Most importantly, the genome is organized into megabase-sized topological domains in which DNA preferentially interacts with other DNA in the domain and not with DNA outside of the domain(Dixon et al., 2012). Genes within topological domains tend to be transcriptionally co-regulated(Le Dily et al., 2014), and disruption of topological domains results in strong transcriptional defects. Furthermore, the topological domains are compartmentalized into “active” and

“repressed” regions, termed A/B compartments, which correlates with their gene expression(Lieberman-Aiden et al., 2009).

As opposed to interphase, mitotic chromosomes reproducibly individualize into discrete chromosomes, and can often be seen as compact rod-like sturctures. Compaction of chromosomes begins in prophase(Nagasaka et al., 2016), and continues through metaphase when condensed chromosomes are aligned on the metaphase plate. As sister chromatids are pulled apart, chromosomes arms axially compact further in anaphase to prevent segregation errors, in an Aurora B dependent manner(Mora-Bermudez et al., 2007). Interestingly, mitotic chromosome structure is consistent across a variety of tested cell types(Naumova et al., 2013), whereas the compartmentalization of interphase chromatin is highly cell type dependent. Since mutants affecting the compaction of chromosomes result in non-individualized, catenated chromosomes, the main role of mitotic chromosome condensation is to facilitate decatenation and ultimately separation of sister chromatids(Nasmyth, 2001). Additionally, chromosomal compaction is required to accommodate the spatial constraints of mitosis(Schubert and Oud, 1997). Although mitotic chromatin is highly condensed, experiments surprisingly showed that pentameric GFP molecules can diffuse freely through mitotic chromatin, suggesting that the dense chromatin is still accessible through diffusion(Nozaki et al., 2013). The molecular determinants of mitotic chromosome structure are detailed below.

Chromatin

The nucleosome

The fundamental unit of packaging DNA into the interphase nucleus and mitotic chromosomes is the nucleosome. Eight core histones, comprising a tetramer of $(H3\text{-}H4)_2$ and two H2A-H2B dimers, are wrapped in ~147 base pairs of DNA and form a nucleosomal monomer(Luger et al., 1997). The nucleosome is assembled in a step-wise fashion (Smith and Stillman, 1991) where DNA first wraps an H3-H4 tetramer, forming a stable intermediate. Consistent with the H3-H4 tetramer embedded within the nucleosome, there is very little turnover of H3-H4 on cellular chromatin measured by FRAP on GFP-H3 and GFP-H4(Kimura and Cook, 2001). This implies that even during active processes like transcription, the H3-H4 core tetramer is very stable. Following tetrasome formation, H2A-H2B dimers are incorporated externally to the H3-H4 tetramer within the core particle. In contrast to H3-H4 the surface of the nucleosome is actively exchanged; nearly 40% of chromatinized H2A-H2B is turned over within hours in cells(Kimura and Cook, 2001). Much of this turnover depends on transcription suggesting that processes that require access to DNA can result in the eviction of H2A-H2B dimers.

In addition to core histones (H3, H4, H2A, H2B), nucleosomes contain lysine-rich histones, termed linker histones, that associate with the peripheral surface of the nucleosome particle. However, not every cellular nucleosome is associated with a linker histone. The stoichiometry of linker histones to nucleosomes varies between cell types and organisms, but linker histone occupancy ranges from 60-100%(Van Holde, 1989).

H1, the most well studied linker histone, was shown to dock on the nucleosome dyad by cryo-EM, interacting with core DNA and linker DNA simultaneously(Bednar et al., 2017). Through interacting with flanking DNA entering and exiting the nucleosome, H1 constrains the dynamics of DNA linking adjacent nucleosomes, which is hypothesized to compact nucleosomal arrays. Many in vitro studies have led to the hypothesis that H1 compacts nucleosomal arrays into a precise repetitive structure termed the 30-nm fiber(Chen and Li, 2017), including in a recent cryo-EM structure(Song et al., 2014). Unfortunately, there is little evidence for the 30-nm fiber in vivo(Eltsov et al., 2008; Nishino et al., 2012), suggesting that the 30-nm fiber may be an in vitro artifact that can only form under precise conditions or in specialized contexts such as chicken erythrocytes(Langmore and Schutt, 1980) and starfish sperm(Woodcock, 1994). Regardless of the specific structure, the constraints that H1 imposes on linking DNA is predicted to have a direct consequence on arrays of nucleosomes.

Forming a mitotic chromosome: Histones

As nucleosomes are the fundamental underlying unit of mitotic chromatin, they were assumed to be a prerequisite for mitotic chromosome structure, however, accessing the role of histones in vivo is technically difficult. Each core histone is present in multiple non-allelic copies in the genome, and in some species up to hundreds of repeats (reviewed in (Van Holde, 1989)), which makes traditional genetic manipulation difficult. Nevertheless, a recently study showed that mitotic chromosomes can still form in the absence of core histones. Using *Xenopus* egg extracts, which can assemble

mitotic chromosomes from exogenous DNA substrates, it was shown that histone-free rod-like mitotic chromosomes can form in extracts depleted of HIRA(Shintomi et al., 2017), a factor required to load H3-H4 onto chromatin(Ray-Gallet et al., 2007). The mitotic chromosomes retained their three-dimensional structure but were less condensed, suggesting that the role of histones is to compact DNA locally but not dictate the global structure of the mitotic chromosome. This finding is consistent with historic data showing that the central axis metaphase chromosomes can be retained even after washing off histones (Paulson and Laemmli, 1977).

Linker histones possess similar technical challenges as core histones. Humans possess at least ten H1 variants, with most somatic cells expressing approximately six different variants(Van Holde, 1989). Although each H1 variant is typically only located once in the genome, combinatorial deletion of multiple H1 variants is lethal, and H1 variants have overlapping functions(Fan et al., 2003). Because of these challenges, the role of H1 in shaping mitotic chromosomes is conveniently studied in *Xenopus* egg extracts, as there is a single H1 variant present in the maternal egg(Dworkin-Rastl et al., 1994) which can be immunodepleted from the extract(Dimitrov et al., 1994). Assembly of mitotic chromosomes in H1 depleted *Xenopus* egg extract results in rod-like mitotic chromosomes that are mostly normal(Maresca et al., 2005). However, one pronounced defect is that H1 depleted chromosomes are axially elongated and radially thinner than wildtype mitotic chromosomes. H1 depleted chromosomes appear fragile and unable to resist forces from microtubules causing them to appear “stringy” in the mitotic spindle (Maresca et al., 2005). It is hypothesized that H1’s effect on chromosome compaction is

direct because no other major chromosomal proteins are affect after H1 depletion; however, the contribution of minor proteins cannot be excluded. This is consistent with in vitro studies showing that H1 has a direct effect on the structure of chromatin(Fyodorov et al., 2017).

Forming a mitotic chromosome: Non-histone proteins

Since depletion of core histones only prevents compaction but does not prevent the shaping of mitotic chromosomes(Shintomi et al., 2017), there must be other factors involved in this process. After core histones and H1, the most abundant protein components of mitotic chromosomes are condensins and topoisomerase II(Hirano and Mitchison, 1994; Saitoh et al., 1994), which play important roles in shaping mitotic chromosomes, discussed below and summarized in Figure 1-1.

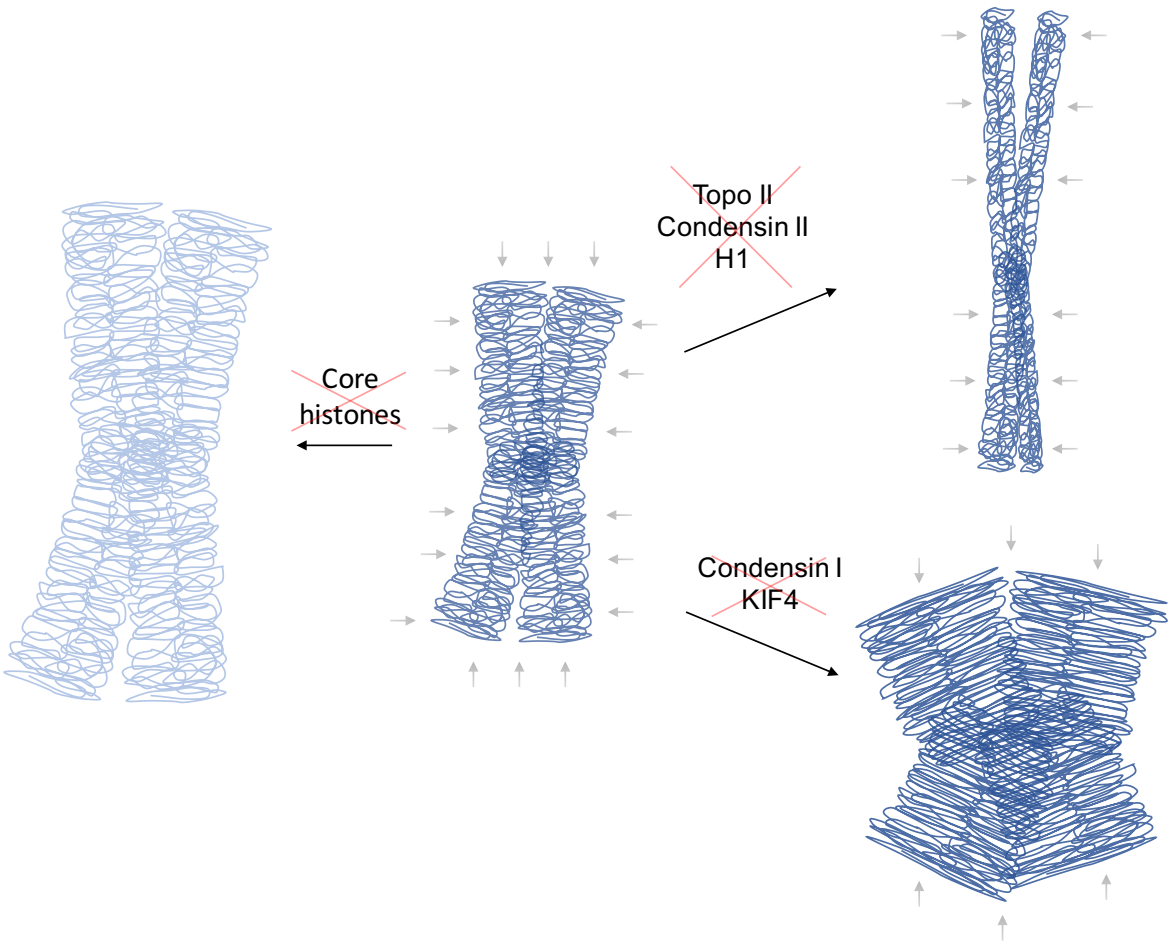

Figure 1-1. Factors influencing the compaction and shaping of mitotic chromosomes. Shown is a schematic depiction of wildtype mitotic chromosomes (center) that form stereotypical compact rod-like chromatids. Depletion of core histones (left) still maintains rod-like structure, however, the DNA is decompacted. To shape mitotic chromosomes, condensin I and KIF4 are required for lateral compaction of mitotic chromosomes (bottom right) while topoisomerase II, condensin II, and H1 are required for axial compaction of mitotic chromosomes.

Topoisomerase II is an ATP-dependent enzyme which transiently creates a double strand break in a DNA molecule to allow the passage of a second strand of DNA through the break(Berger et al., 1996). This activity is important in the untangling of DNA for proper resolution of sister chromatids during chromosome segregation(Nagasaka et al., 2016). Although the mechanism remains unclear, topoisomerase II localizes to the central axis of mitotic chromosomes and is required for mitotic chromosome formation in *Xenopus* egg extract(Cuvier and Hirano, 2003). Specifically, it appears that topoisomerase II depleted chromosomes become axially elongated(Sakaguchi and Kikuchi, 2004; Samejima et al., 2012). It was originally thought that topoisomerase II formed a requisite scaffold for mitotic chromosome structure, however it was shown that topoisomerase II could be washed off of chromosomes without majorly affecting the chromatid rod-like structure(Hirano and Mitchison, 1993).

Condensin is a five subunit complex which can supercoil DNA in an ATP dependent manner(Kimura and Hirano, 1997). Similar to topoisomerase II, condensin localizes to the chromatid central axis and is required for mitotic chromosome formation in *Xenopus* egg extract(Hirano and Mitchison, 1994). The ATPase activity of condensin is required for this process, suggesting that the supercoiling activity of condensin is important in this process(Kinoshita et al., 2015). There are two condensin complexes (condensin I and II); the exact defect of condensin depletion on chromosome structure depends on the specific condensin complex(Green et al., 2012). Depleting condensin I, comprising SMC2, SMC4, CAPG, CAPH, and CAPD2, results in laterally decompact

chromosomes. Depleting condensin II, comprising SMC2, SMC4, CAPG2, CAPH2, and CAPD3, results in axially decompact chromosomes which are reminiscent of topoisomerase II and H1 depletion. Interestingly, there may be interplay between condensin and topoisomerase II where positive supercoiling by condensin facilitates active decatenation by topoisomerase II(Baxter et al., 2011; Cuvier and Hirano, 2003). Finally, another protein located at the chromosome central axis, KIF4, has been shown to be required for the lateral compaction of mitotic chromosomes(Mazumdar et al., 2004; Samejima et al., 2012), similar to condensin I.

Drawing from these experiments, it was recently shown that mitotic chromatid formation from sperm chromatin could be reconstituted from purified components using only core histones, histone chaperones (nucleoplasmin, Nap1 and FACT), topoisomerase II and condensin, indicating that these are the minimum set of factors involved in mitotic chromosome formation(Shintomi et al., 2015).

It is likely that axial and lateral compaction of mitotic chromosomes are competing activities, where axial compaction prevents excess lateral compaction and vice versa(Samejima et al., 2012). Accordingly, KIF4 depleted lateral chromosome elongation can be rescued by double depletion of KIF4 (a lateral compacter) and topoisomerase II (an axial compacter). This raises the question of whether axially elongated H1 or topoisomerase II depleted chromosomes are inherently defects of under-compaction or over-compaction; H1 or topoisomerase II depletion could directly increase lateral compaction resulting in axial elongation or alternatively could directly

decrease axial elongation that results in lateral compaction. As their mechanism of compaction is unknown, either hypothesis is possible.

There is a major gap in understanding how the biochemical properties of topoisomerase II (DNA decatenation) and condensin (ATP dependent DNA supercoiling) lead to properly shaped mitotic chromosomes. The proteinaceous central axis of mitotic chromosomes is thought to be a key determinant of mitotic chromosome structure. In a widely accepted, but not well studied model, mitotic chromosomes are thought to be composed of DNA loops, where the anchor of loops are positioned at the chromatid axis. This arrangement was first visualized by electron microscopy on histone extracted HeLa chromosomes, which indicated that the axis-loop structure did not require histones(Paulson and Laemmli, 1977). In a landmark study, spatial contact data from Hi-C experiments was used to show that mitotic chromosomes form a homogenous structure that is not dictated by the DNA sequence(Naumova et al., 2013). Indeed, data from this study were consistent with the previously proposed DNA looping model and estimated the loop size to be 80-120kb. A key insight from this study was that loop anchors are randomly positioned between cells, reconciling the inability to identify loop anchoring DNA sequences or motifs. Strikingly, mitotic loop formation depends entirely on condensin in fission yeast and condensin depletion results in mitotic chromatin that essentially resembles interphase chromatin in Hi-C(Kakui et al., 2017), indicating that condensin is a key driver of this process.

But how does condensin form mitotic loops? At present, only untested theoretical models exist. However, in a recent single molecule study(Eeftens et al., 2017), it was

shown that condensin can bind DNA in the absence of ATP but can only topologically entrap DNA following ATP hydrolysis. After entrapment, condensin can compact DNA against force. Most importantly, condensin was shown to be a motor that can walk along DNA(Terakawa et al., 2017). In addition to its motor activity, it can bind a separate strand of DNA while walking. These activities have been shown to theoretically be sufficient for loop formation and chromosome compaction(Goloborodko et al., 2016), further supporting the notion that condensin mediated loops may facilitate mitotic chromosome shaping.

Nucleosome Remodeling Complexes

Nucleosome remodeling

DNA is packaged into nucleosomes to facilitate packing into the nucleus or mitotic chromosomes, but nucleosomes are refractory to a variety of processes that must use the DNA within. In interphase, nucleosomes prevent transcription factor binding(Adams and Workman, 1995), RNA synthesis(Teves et al., 2014), DNA replication(Gasser et al., 1996), and DNA repair(Hara et al., 2000). In mitosis, nucleosomes occlude condensin binding(Toselli-Mollereau et al., 2016) and may inhibit topoisomerase II mediated decatenation of DNA(Capranico et al., 1990). Due to these repressive effects of nucleosomes, eukaryotes utilize nucleosome remodeling complexes to facilitate access to the underlying DNA(Clapier and Cairns, 2009).

Nucleosome remodelers expose nucleosomal DNA by hydrolyzing ATP to slide, evict, or restructure nucleosomes (Figure 1-2). The mechanism of sliding is best

characterized in the ISWI remodeler. Single molecule studies show that ISWI first forces 7 bp out of the nucleosome(Deindl et al., 2013), which results in an intermediate nucleosome that is sterically strained. To accommodate this strain, nucleosome remodelers have been shown to distort the histone octamer(Sinha et al., 2017), indicating that they are not strictly moving the DNA around a stationary octamer. DNA is then entered the nucleosome, resulting in an unstrained nucleosome that has translocated. Interestingly, another well studied remodeler, CHD1, does not distort the histone octamer while remodeling(Farnung et al., 2017), suggesting that different remodelers may utilize fundamentally different principles to remodel nucleosomes.

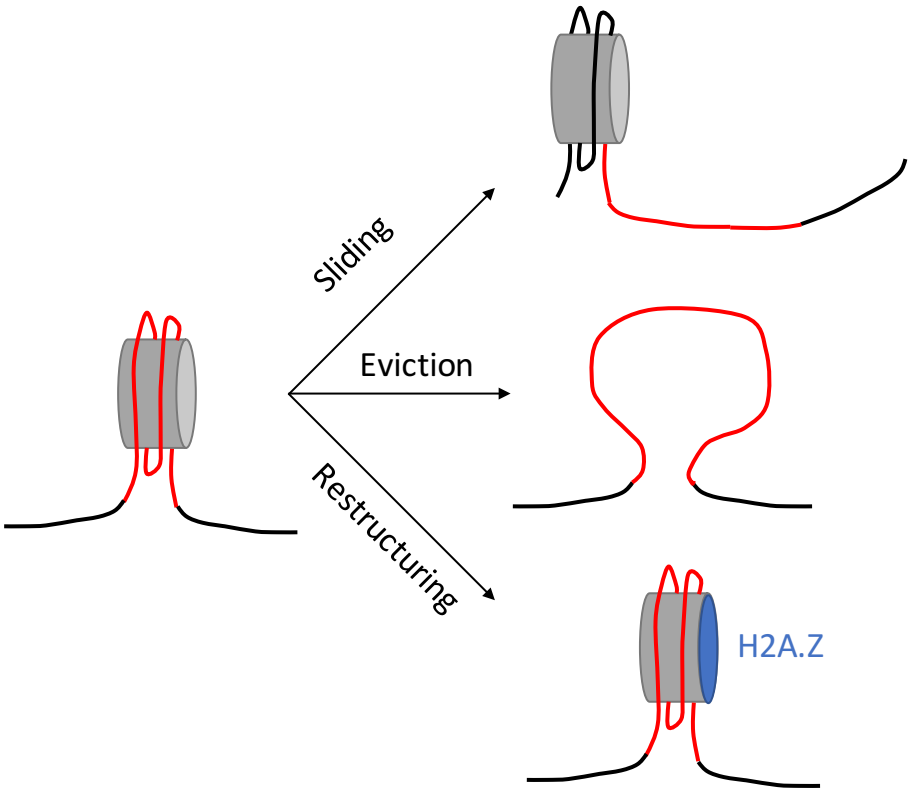

Figure 1-2. Nucleosome remodeling activities. Nucleosome remodelers provide access to nucleosomal DNA by sliding (top), evicting (middle), or restructuring (bottom) histone octamers.

In contrast to nucleosome sliding, the mechanism of nucleosome eviction by remodeling proteins is less characterized. Nucleosome remodelers can slide neighboring nucleosomes into each other(Ulyanova and Schnitzler, 2005), which is hypothesized to create a stable intermediate whereby DNA continuously wraps around a canonical histone octamer and a hexamer lacking an H2A/H2B dimer(Kato et al., 2017). Further remodeling can displace the hexamer, resulting in an evicted nucleosome(Dechassa et al., 2010). The regulation and detailed mechanism of this process in unknown.

Finally, nucleosome remodelers can restructure the histone octamer. By loosening histone-DNA contacts within the nucleosome, remodelers can facilitate exchange of H2A/H2B dimers(Bruno et al., 2003). This mechanism is commonly employed by Ino80 and Swr1 to incorporate and remove H2A.Z throughout the genome(Brahma et al., 2017; Mizuguchi et al., 2004). Incorporation of H2A.Z nucleosomes destabilizes interactions between H2A/H2B dimers and H3-H4 tetramers within the nucleosomes and facilitates transcriptional activation(Suto et al., 2000).

Nucleosome remodeling proteins

The SNF2 family of helicases (Figure A-1) are a subfamily of ATP-dependent helicases within the SF2 family. Many members of this family are ATPases with nucleosome remodeling activity. The family can be further divided into 5 clades, SNF2-like, Swr1-like, SSO1653-like, Rad54-like, and Rad5/16-like, named after archetypal

members within each clade. Here, I focus on SNF2-like remodelers including ALC1, ISWI, CHD1, HELLS, Mi-2, and SNF2.

Although remodeling factors can evict and restructure nucleosomes, the primary biochemical activity within the Snf2-like family of nucleosome remodelers is the ability to slide nucleosomes. All known remodelers within the Snf2-like have a single core ATPase subunit that can slide nucleosomes in vitro, which is summarized in Figure 1-3. The exception to this is HELLS, which possess DNA-dependent ATPase activity but lacks any detectable nucleosome sliding activity(Burrage et al., 2012).

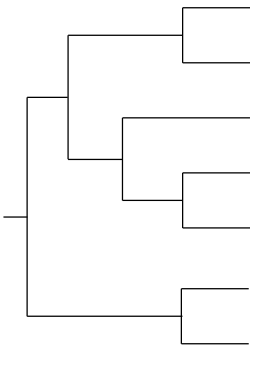

	Intrinsic Remodeling Activity	References
ALC1	Yes	(Ahel et al., 2009)
ISWI	Yes	(Corona et al., 1999)
CHD7	Yes	(Bouazoune and Kingston, 2012)
CHD1	Yes	(Lusser et al., 2005)
Mi-2	Yes	(Wang and Zhang, 2001)
HELLS	No	(Burrage et al., 2012)
Snf2	Yes	(Phelan et al., 1999)

Figure 1-3. Phylogeny of Snf2-like nucleosome remodeling proteins. Tree of Snf2-like remodelers (adapted from (Flaus et al., 2006)) indicating which proteins possess intrinsic nucleosome remodeling activity.

Regulation by accessory subunits

Within the Snf2-like family of nucleosome remodelers, the core nucleosome remodeling catalytic subunit is commonly found in complex with non-catalytic subunits. For example, hSWI/SNF forms large complexes of 9-12 auxiliary subunits, which are stable in 0.5 M NaCl washing(Wang et al., 1996). The effect of non-catalytic subunits on the biochemistry and functions of the complex varies depending on the specific remodeler and auxiliary subunits, with a few examples detailed below.

Auxiliary subunits can stimulate the rate of nucleosome sliding. For example, ISWI in complex with ACF1 can slide nucleosomes at approximately six times the rate of the core ATPase subunit alone(Yang et al., 2006). Similarly, ALC1 has detectable, yet minimal nucleosome sliding activity in vitro(Ahel et al., 2009), but this activity is greatly enhanced by forming a stable complex with PARP1(Gottschalk et al., 2012). Although the ATPase domain of ALC1 is a functional remodeler, it is largely autoinhibited by its N-terminal macrodomain. This inhibition is relieved by PARP1(Singh et al., 2017). Large multi-protein remodeling complexes can also form, such as hSWI/SNF whose core remodeler is BRG and is stimulated by three auxiliary subunits BAF155, BAF170 and INI1(Phelan et al., 1999), and associates with many other proteins including BAF60a/b/c, BAF57, BAF53a/b and beta-actin.

In addition to modulating the rate of nucleosome sliding, auxiliary subunits can alter the biochemical properties of nucleosome sliding in vitro, which is best exemplified by ISWI(Oppikofer et al., 2017). The core remodeling subunit, SNF2H, will partition a mononucleosome randomly throughout at 270 bp DNA fragment. Adding the auxiliary

subunit RSF causes the remodeling complex to specifically slide the nucleosome to the end of the DNA fragment, while the auxiliary subunit BAZ1A shifts the mononucleosome to the middle of the DNA fragment. These directionality changes are dictated by the auxiliary subunits and not the core ATPase since similar results are observed when the ATPase subunit is switched from SNF2H to SNF2L, a closely related ATPase. Although dramatic, the physiological significance of these biochemical differences is unclear.

Lastly, non-catalytic subunits in nucleosome remodeling complexes can be used to direct the core ATPase subunit to specific genomic loci. Many remodeling complexes harbor domains that can bind specific histone post-translational modifications, which can be used to target them throughout the genome. In a seminal study(Wysocka et al., 2006), it was shown that the PHD finger of BPTF, an auxiliary subunit of ISWI, binds H3K4 trimethylation to direct the complex to transcriptional start sites. Accordingly, loss of H3K4 trimethylation results in mislocalized ISWI and downstream developmental defects. In a recent high-throughput assay(Dann et al., 2017), using a library of 115 mononucleosomes containing different post-translational modifications, it was shown that ISWI in complex with seven distinct subsets of auxiliary proteins was highly susceptible to histone modifications throughout the nucleosome and especially within the acidic patch, the region on the nucleosome where many chromatin binders engage.

While Snf2-like remodelers are typically configured as a core remodeling protein in complex with numerous auxiliary subunits, an exception to this paradigm is thought to be HELLS. HELLS was shown to exist as a monomer in nuclear extracts by size exclusion chromatography and sucrose density centrifugation(Myant and Stancheva,

2008). It is still possible that HELLS forms larger complexes, however, they are likely neither stable nor highly abundant.

Regulation by H1

As H1 is intimately associated with nucleosomes, it is likely that H1 has dramatic effects on nucleosome remodeling. Indeed, H1 and the remodeler CHD1 bind to similar positions on the nucleosome(Farnung et al., 2017), which causes H1 to dramatically impede CHD1 mediated remodeling(Lusser et al., 2005). Importantly, remodelers are differentially affected by H1, since the remodeler ACF1 seems unaffected by H1(Lusser et al., 2005). Similar to non-catalytic accessory subunits, H1 can alter the directionality of nucleosome remodelers; in vitro, hSWI/SNF moves nucleosomes to ends of DNA fragments, but in the presence of H1, it moves nucleosomes to the center of the same fragments(Ramachandran et al., 2003). An interesting case is Arabidopsis DDM1, thought to be a HELLS ortholog, which is hypothesized to specifically remodel H1 containing nucleosomes in vivo based on in vivo DNA methylation patterns(Zemach et al., 2013); however, this activity has not been recapitulated in vitro. Currently, only a few H1 variants and nucleosome remodelers have individually been studied at present so a complete picture on how H1 affects nucleosome remodeling is lacking. However, H1 is reported to affect nucleosome spacing in mice(Fan et al., 2003), supporting the possibility that H1 influences nucleosome remodelers in vivo.

Mitotic regulation and function of nucleosome remodeling complexes

The role that nucleosome remodeling complexes play in mitosis, if any, has remained a mystery. Intriguingly, many nucleosome remodeling complexes are evicted from mitotic chromatin including ISWI(MacCallum et al., 2002), CHD1(Stokes and Perry, 1995) and Ino80(Hur et al., 2010). Additionally, SWI/SNF is phosphorylated in mitosis, which entirely inactivates its remodeling activity(Sif et al., 1998). However, upon mitotic exit, nucleosome remodelers are required to re-establish gene expression patterns in interphase cells(Krebs et al., 2000). Concurrent with the loss of remodelers known to precisely position nucleosomes, mitotic chromatin has been reported to lack any defined nucleosome position(Komura and Ono, 2005). Regardless, the physiological role of mitotic eviction by nucleosome remodelers is not established. It has been hypothesized that nucleosome remodeler eviction is required to facilitate the silencing of many genes that is known to occur during mitosis(Palozola et al., 2017). In contrast, it has been shown that nucleosome remodeler mediated nucleosome eviction is required to load condensin on mitotic chromatin(Toselli-Mollereau et al., 2016), indicating that nucleosome remodeling may not be completely absent on mitotic chromatin. Finally, it was shown that ISWI binds microtubules during mitosis and is required for chromosome segregation and microtubule dynamics during anaphase(Yokoyama et al., 2009), suggesting that nucleosome remodelers may also have mitotic functions other than sliding nucleosomes.

ICF syndrome

ICF patients

Since mitotic chromosome architecture is important for transmitting genetic material, there are a variety of diseases which cause defects in mitotic chromosome formation. One of these, Immunodeficiency, centromeric instability and facial dimorphism (ICF Syndrome) is an extremely rare disease with less than 70 reported cases as of 2013(Ehrlich et al., 2006; Weemaes et al., 2013). Mitotic chromosome formation is defective in ICF patients' lymphocytes following mitogen stimulation. Specifically, chromosomes 1, 9, and 16 harbor long blocks of satellite II and III repetitive elements adjacent to the centromere that are typically methylated and heterochromatinized. This juxtacentromeric heterochromatin is typically stretched and hypothemylated in ICF patients (summarized in Figure 1-4). Additionally, patients show variable immunodeficiencies and facial anomalies. Ultimately, patients with ICF syndrome usually die of severe recurrent infections prior to adulthood.

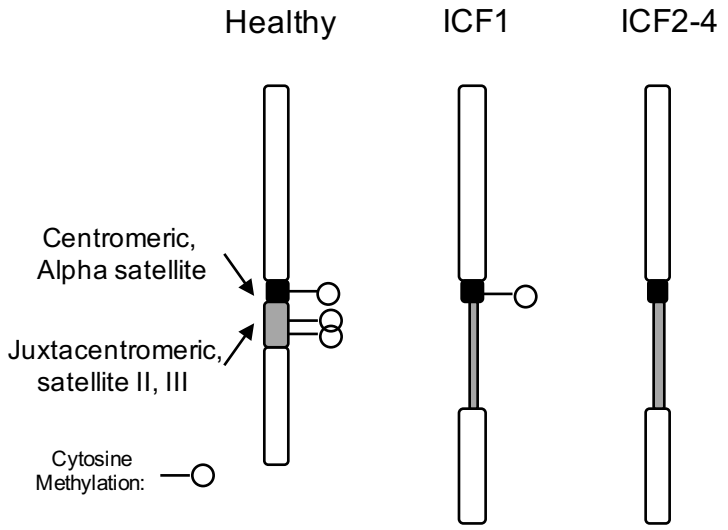

Figure 1-4. Chromosome defects in ICF syndrome. Healthy chromosomes 1, 9 and 16 contain methylated centromeric alpha satellite DNA and methylated juxtacentromeric satellite II and III DNA. ICF1, ICF2, ICF3, and ICF4 patients have stretched and hypomethylated juxtacentromeric DNA, while only ICF2-4 patients have hypomethylated alpha satellite DNA.

Genetic causes of ICF

A variety of mutations have been identified as causative for ICF syndrome (Figure 1-5). Mutations in DNMT3B, a de novo DNA methyltransferase, were the first genetic causes identified for ICF syndrome(Hansen et al., 1999; Xu et al., 1999). Most DNMT3B ICF mutations map to the C-terminal methyltransferase domain, indicating that these patients do not possess a fully functional DNMT3B. Although some patients contain DNMT3B null alleles, DNMBT3B is a required gene so these patients are always found to have heterozygous compound mutations with a less severe DNMT3B mutation.

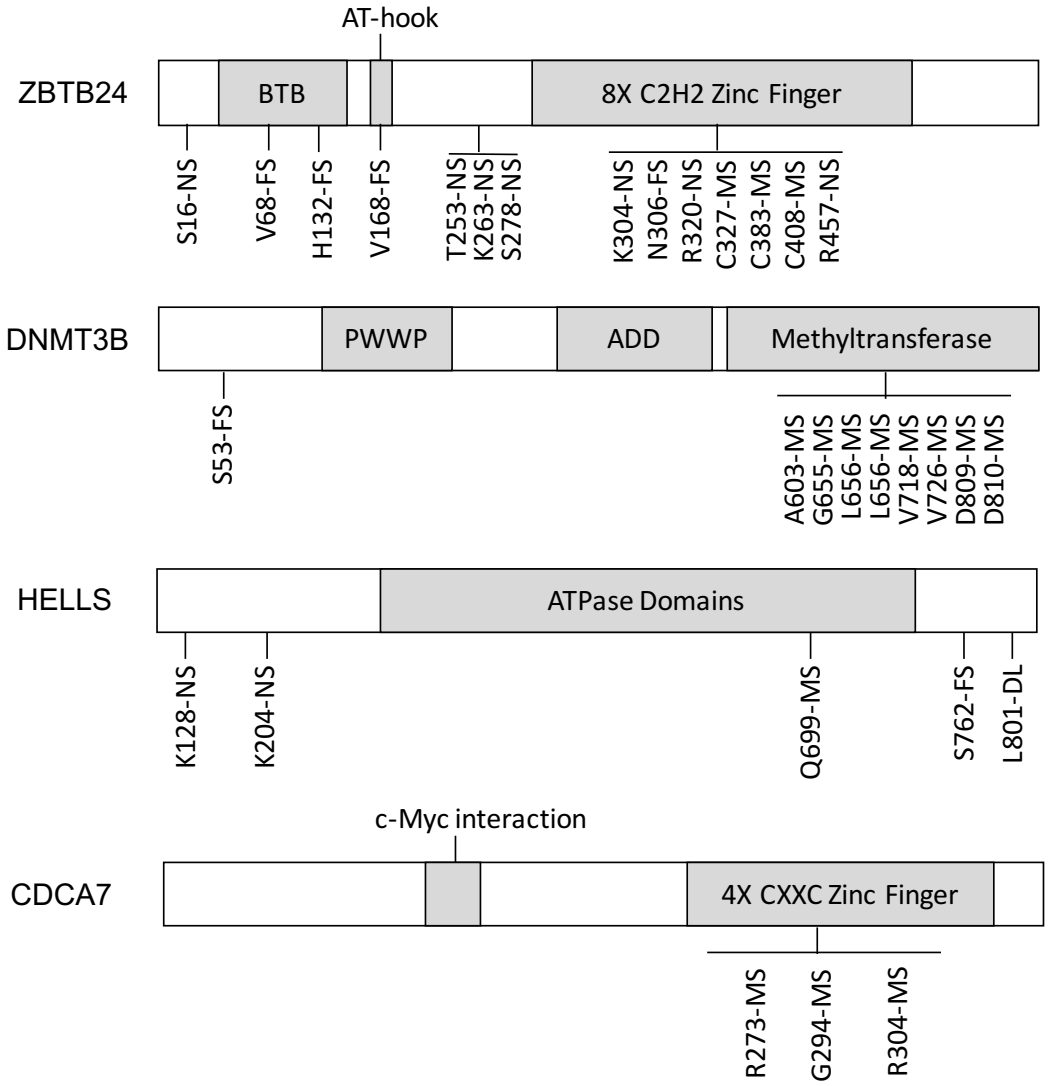

Figure 1-5. Mutational landscape of ICF syndrome. Missense (MS), nonsense (NS), frameshift (FS), and deletion (DL) mutations identified in ICF patients. Note, many DNMT3B mutations have been identified, only a subset of which are displayed. Data was aggregated from(de Greef et al., 2011; Nitta et al., 2013; Robertson and Wolffe, 2000; Thijssen et al., 2015; van den Boogaard et al., 2017).

More recently, ICF patients have been identified with mutations in ZBTB24, HELLS, and CDCA7. ZBTB24 is a transcription factor, harboring a DNA-binding AT-hook domain, eight C2H2 zinc fingers, and a BTB domain thought to facilitate homodimerization. ICF patient mutations have been found throughout these domains(de Greef et al., 2011), emphasizing the importance of ZBTB24 in ICF syndrome. While the exact nature of the ICF mutation's effect on ZBTB24 function is unclear, the BTB and AT-hook domains are required for ZBTB24 activity, indicating that the ICF mutations in these domains may partially interfere with ZBTB24 activity(Wu et al., 2016).

HELLS (discussed below), is a putative nucleosome remodeler. Most ICF patient mutations in HELLS are expected to produce null proteins either by frameshift or by missense mutations in the conserved ATPase domain(Thijssen et al., 2015). Interestingly, mutations in HELLS have been identified that are predicted to only affect the C-terminus, suggesting that this domain may be important in ICF syndrome.

CDCA7 (discussed below) is an uncharacterized CXXC zinc finger containing protein. CDCA7 is thought to be a transcription factor under control of c-MYC(Osthus et al., 2005), however the molecular function of CDCA7 is not well defined. All known CDCA7 ICF mutations map to the highly conserved zinc finger domain(Thijssen et al., 2015) but their effect on CDCA7 function is unknown.

Molecular Causes of ICF

ICF syndrome is thought to be caused by defects in de novo DNA methylation, since the majority of patients harbor DNMT3BB mutations. Indeed, patient mutations

engineered into DNMT3B show reduced, but not eliminated DNA methyltransferase activity(Gowher and Jeltsch, 2002). Complete lack of DNMT3B is lethal(Okano et al., 1999), indicating that ICF is only a partial defect in DNA methylation. DNMT3B ICF patient mutations map to the DNA methyltransferase domain, suggesting that defective methylation is causative, rather than other reported functions of DNMT3B, such as DNA methylation independent transcriptional repression, which maps to the central domain(Bachman et al., 2001). In agreement with DNA methylation defects causing ICF, stretched juxtacentromeres in ICF patient lymphocytes phenocopy healthy lymphocytes treated with 5-azacytidine, a non-methylatable cytidine analog ICF(Viegas-Pequignot and Dutrillaux, 1976).

ICF patients show heterogeneous DNA methylation defects throughout the genome including at Alu elements, centromeric alpha-satellites, and certain imprinted genes(Miniou et al., 1997a; Miniou et al., 1997b; Schuffenhauer et al., 1995). However, the defining feature in ICF patients is hypomethylation at the juxtacentromeric heterochromatin of chromosomes 1, 9, and 16, the same region at which is stretched cytologically(Mora-Bermudez et al., 2007). Since there is only a 7% decrease in total genomic cytosine methylation in ICF patient tissue compared to healthy patient tissue(Tuck-Muller et al., 2000), it has been suggested that DNA methylation defects at this specific genomic locus is the causative molecular defect (Tuck-Muller et al., 2000). How (and if) juxtacentromeric hypomethylation directly leads to ICF syndrome is unclear.

It is also unclear how genetic defects of ICF other than DNMT3B mutations cause the disease, however, it is assumed that they all converge on DNA methylation defects(Ehrlich et al., 2006). Accordingly, siRNA mediated knockdown of ZBTB24, HELLS or CDCA7 in fibroblasts results in reduced satellite DNA methylation(Thijssen et al., 2015). Additionally, HELLS has been shown in mouse to facilitate DNMT3B mediated DNA methylation(Myant and Stancheva, 2008; Zhu et al., 2006), which may explain the contribution of HELLS to ICF syndrome. Recently, it was shown that ZBTB24 is required for robust CDCA7 expression(Wu et al., 2016), but how ZBTB24 and CDCA7 contributes to the HELLS-DNMT3B pathway is completely unknown (Figure 1-6).

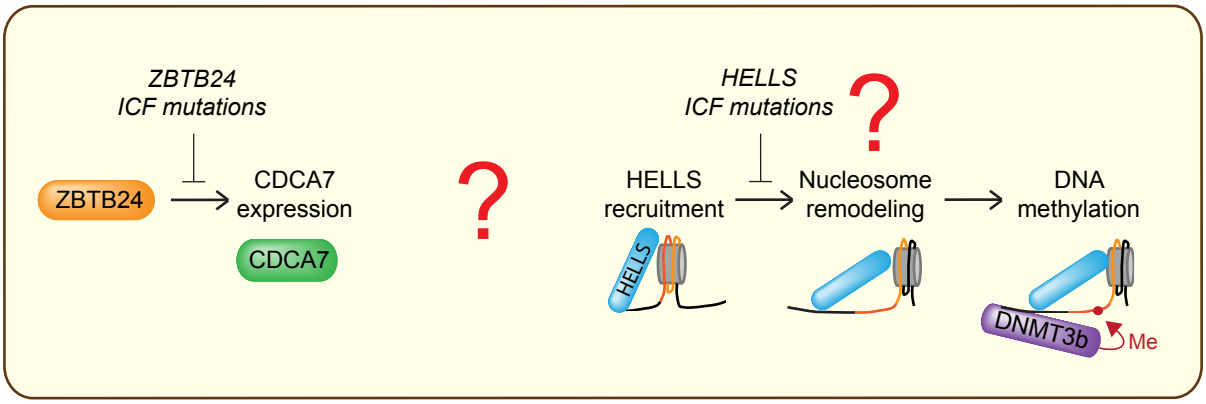

Figure 1-6. The understanding of the proteins involved in ICF syndrome at the onset of this thesis. The connection between ZBTB24-CDCA7 and HELLS-DNMT3B pathways was unresolved. Also, HELLS was a putative remodeling enzyme, but was shown to not possess nucleosome remodeling activity in vitro.

HELLS and CDCA7

HELLS

Helicase Lymphoid Specific (HELLS, also LSH, PASG, or SMARCA6) was initially cloned from thymus tissue(Jarvis et al., 1996), and is an SNF2-like nucleosome remodeler due to sequence similarity to the family. Although HELLS has no chromatin binding domains common to nucleosome remodelers, it contains a conserved DExx-HELICc ATPase domain, suggesting it may still possess nucleosome remodeling activity (Figure 1-7). Purified recombinant *Arabidopsis* DDM1 (HELLS homolog), has been shown to remodel nucleosomes in vitro(Zemach et al., 2013), and many of HELLS functions in mammals (discussed below) have been shown to depend on a functional ATPase domain(Ren et al., 2015; Termanis et al., 2016), which is consistent with the notion that HELLS is a nucleosome remodeler. However, purified murine HELLS cannot remodel nucleosomes in vitro(Zemach et al., 2013), opening the possibility that nucleosome remodeling is not a conserved function of HELLS.

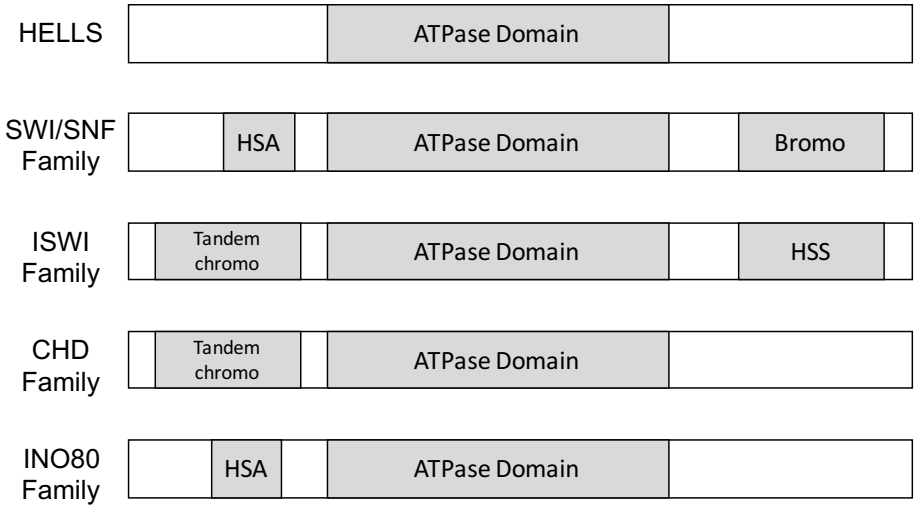

Figure 1-7. HELLS possess a conserved ATPase domain but lacks chromatin binding domains common to nucleosome remodeling complexes. Nucleosome remodeling proteins typically contain additional chromatin binding domains including Helicase-SANT (HAS), bromo, tandem chromo, and HAND-SANT-SLIDE (HSS) domains. Adapted from (Clapier and Cairns, 2009).

The role of HELLS in facilitating DNA methylation is well studied. A primary function of DNA methylation is the silencing of repeat elements, and upon knockout of HELLS in mouse embryonic fibroblasts ($Lsh^{-/-}$), repeat elements including long terminal repeats and satellites are hypomethylated concurrent with their expression(Yu et al., 2014). HELLS interacts with DNMT3B(Zhu et al., 2006) and facilitates DNMT3B targeting throughout the genome(Xi et al., 2009). Although no remodeling activity has been shown for HELLS(Burrage et al., 2012) (discussed above), the ability of HELLS to establish DNA methylation at repeat elements requires the ATPase activity of HELLS in fibroblasts(Termanis et al., 2016) and stem cells(Ren et al., 2015), leading the field to assume that HELLS facilitates DNA methylation by remodeling chromatin. Nucleosomes are refractory to DNA methylation by DNA methyltransferase(Felle et al., 2011) so it is hypothesized that nucleosome remodeling by HELLS could facilitate DNMT3B access to the underlying DNA. In *Arabidopsis*, where HELLS has been extensively studied, heterochromatic H1-containing nucleosomes are a barrier to DNA methylation, which is overcome by HELLS remodeling(Zemach et al., 2013).

CDCA7

CDCA7 is a relatively uncharacterized protein containing a conserved C-terminal CXXC zinc finger domain (Figure 1-8). The CXXC zinc finger motif is a common domain found in proteins including DNMT1, Tet1 and MLL1 and has DNA binding activity on non-methylated DNA(Frauer et al., 2011). However, the 4X CXXC zinc finger domain of CDCA7 is an atypical member of the family, having little sequence similarity.

Specifically, DNMT1 and other canonical CXXC zinc finger proteins harbor two CXXCXXC motifs, while CDCA7 harbors 4 split CXXC motifs. CDCA7 was originally classified as a direct downstream target of c-Myc(Prescott et al., 2001). Upon expression, CDCA7 is thought to interact with Myc to induce cell transformation(Gill et al., 2013). In zebrafish where CDCA7 is best characterized, CDCA7 is required for hematopoietic stem cell formation(Guiu et al., 2014), however, the precise physiological and biochemical role of CDCA7 in each of these processes is not defined.

Figure 1-8. The zinc finger domain of CDCA7 is conserved between species and paralogs. The zinc finger domains from the indicated CDCA7 species (top) and paralogs (bottom) were aligned with ClustalW. The CXXC zinc finger motif is indicated with black bars.

Vertebrates possess two paralogs of CDCA7 (CDCA7 and CDCA7L), which share about 50% sequence identity. The zinc finger domain of CDCA7 is highly conserved between species and between paralogs (Figure 1-8), however, the N-terminus is more divergent (Figure A-2). Although the c-MYC interaction is conserved between CDCA7 paralogs(Gill et al., 2013; Hartwell et al., 1970; Huang et al., 2005), the functional overlap between the two proteins is unknown. As CDCA7L is upregulated in response to CDCA7 knockout in mammalian cells (Motoko Unoki, personal communication), there may be compensation between paralogs, complicating the study of CDCA7. In addition to CDCA7L, frogs possess a third CDCA7 found in the embryo(Peshkin et al., 2015), which I name CDCA7e.

Open questions and significance

Cell cycle regulation of chromatin composition

Although the major components (by mass) of mitotic chromosomes were determined decades ago(Hirano and Mitchison, 1994), proteins scarcely detected on chromosomes can have dramatic mitotic functions (e.g. (Funabiki and Murray, 2000)). Because of this, studies have attempted to catalog the entire set of proteins found on interphase(Kustatscher et al., 2014) and mitotic chromatin(Ohta et al., 2010). However, no study has systematically identified how the chromatin composition changes throughout the cell cycle and how these changes are regulated. Through studying individual proteins, it has been shown that many proteins are evicted from mitotic chromosomes(Gottesfeld and Forbes, 1997; John and Workman, 1998; Martinez-

Balbas et al., 1995; Rizkallah and Hurt, 2009), but these findings have been called into question(Teves et al., 2016). Recently, it was shown that standard fixation protocols used during immunofluorescence cause many proteins to appear to have been evicted from mitotic chromatin, even though endogenous tagging and live imaging shows they are indeed still bound to mitotic chromatin(Teves et al., 2016). It is therefore important to determine the regulation of the mitotic chromatin proteome in the absence of these in vivo artefacts.

Molecular basis of ICF syndrome

At the onset of this project, there was no known connection between CDCA7-HELLS and ICF syndrome. As I began studying these proteins, it was reported that mutations in CDCA7 and HELLS cause ICF syndome(Thijssen et al., 2015), but it was difficult to reconcile how a variety of proteins (DNMT3B, HELLS, CDCA7, ZBTB24) each lead to the ICF phenotype. Phenotypic connections between DNMT3B-HELLS(Myant and Stancheva, 2008; Zhu et al., 2006) and CDCA7-ZBTB24(Wu et al., 2016) have been documented, but a unifying hypothesis for the molecular defect underlying ICF syndrome is absent. Specifically, since biochemical information about each of these proteins is lacking (except for DNMT3B), only speculative hypotheses can be proposed for how they are unified.

CHAPTER 2: CELL CYCLE REGULATION OF CHROMATIN COMPOSTION

Results

An assay to systematically determine the cell cycle and nucleosome regulation of chromatin composition

For a variety of reasons (discussed in Chapter 1), manipulating chromatin under physiological conditions has been challenging. To circumvent these issues, I used *Xenopus* egg extracts, which recapitulate cell cycle events on exogenously added chromatin. When added to interphase extract, demembranated sperm DNA will replicate and chromatinize with high efficiency(Blow and Laskey, 1986). When the extract is cycled into mitosis the chromatin will condense into paired mitotic chromatids, and a mitotic spindle will form around the chromatin(Sawin and Mitchison, 1991). Analogously, plasmid DNA can be coupled to magnetic beads and will chromatinize when added to *Xenopus* egg extract. When DNA coated beads are added to interphase extract they assemble nuclear envelopes and when added to mitotic extract they nucleate microtubules, forming bipolar mitotic spindles(Heald et al., 1996). These experiments highlight how DNA beads incubated in *Xenopus* egg extracts resemble physiological chromatin more so than in traditional tissue culture extracts.

Typically, when adding naked DNA to *Xenopus* egg extract, histones stored in the extract are loaded onto the DNA by HIRA, the canonical replicated-independent nucleosome assembly chaperone(Ray-Gallet et al., 2002). To facilitate manipulation and study of histones, I preloaded in vitro purified histones onto a tandem array of 19 nucleosome positioning sequences (Widom's 601 sequence (Lowary and Widom,

1998)) separated by 53 bp of linker DNA. These nucleosome arrays were coupled to magnetic beads, and when incubated in *Xenopus* egg extract, chromatin binding proteins associate with the beads. Similar to the physiologically loaded endogenous histones, these pre-loaded nucleosome beads can form nuclear envelopes in interphase and mitotic spindles in M phase(Zierhut et al., 2014). To identify chromatin binding proteins, beads can be recovered from the extract, washed, and the chromatin associated proteins are analyzed by Western blotting or mass spectrometry. By manipulating the underlying histones or the extract in which the chromatin is incubated, I can systematically assess how a variety of factors affect the composition of chromatin by Western blotting, immunofluorescence and mass spectrometry. In the paragraphs that immediately follow, I describe the method and rational of all experimental perturbations I performed to study how the composition of chromatin is regulated (summarized in Figure 2-1).

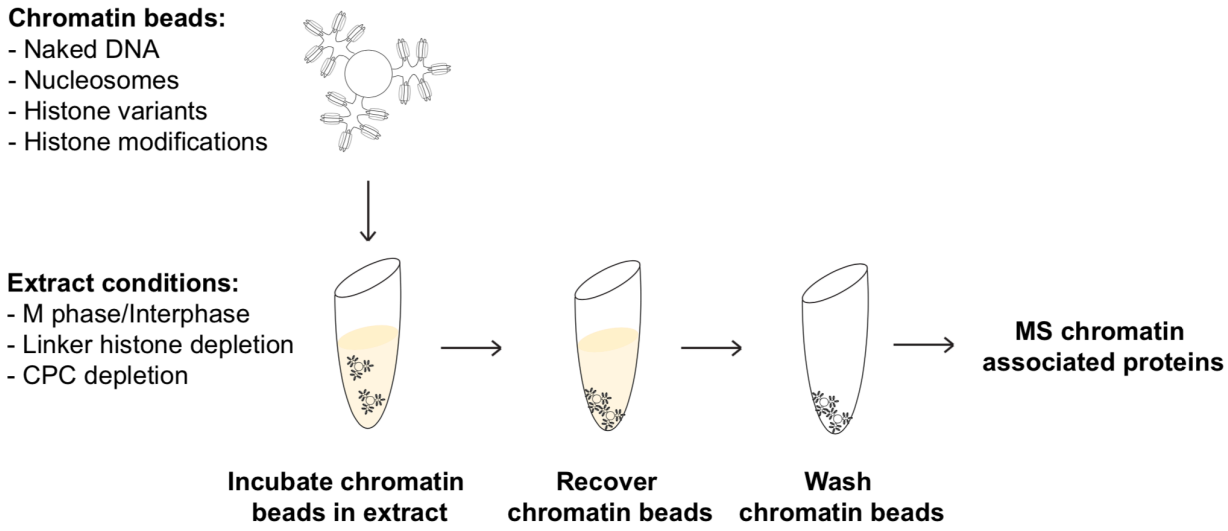

Figure 2-1. Schematic of mass spectrometry experiments to determine the regulation of chromatin associated proteins. Chromatin beads are incubated in *Xenopus* egg extract, allowing chromatin assocaited proteins to bind. Beads are recovered, washed, and chromatin associated proteins are determined by mass spectrometry.

Histones are fundamental in nearly all chromatin processes; completely depleting histones from cellular chromatin results in gene expression dysfunction(Wyrick et al., 1999) and lethality(Roberts et al., 2002), which makes assessing their contribution to the chromosome composition difficult in cellular systems. To overcome these limitations, Christian Zierhut established a strategy to deplete and complement histones from *Xenopus* egg extract. Specifically, Christian Zierhut immunodepleted endogenous H3/H4 from *Xenopus* egg extracts with an H4K12Ac monoclonal antibody and added back either naked DNA arrays or nucleosomal DNA arrays coupled to magnetic beads to study the role of nucleosomes in physiological processes. Although many histone antibodies were tested for H3/H4 immunodepletion, anti-H4K12Ac was most effective(Zierhut et al., 2014), consistent with H4 stored in the egg being marked with K12Ac(Shechter et al., 2009). Using this methodology, I could query which chromatin binding proteins depend on nucleosomes under physiological conditions. Additionally, as most nucleosomes are bound by H1(Van Holde, 1989), I could deplete H1 from the extract to determine the specific contributions of the linker histone within the nucleosome.

Histone variants are important contributors to cellular processes with well documented roles in transcription(Talbert and Henikoff, 2017). As histones are purified from bacteria in my assay, I can incorporate histone variants into the nucleosomal arrays with ease. Therefore, I tested the contribution of H3.2 nucleosomes and H3.3 nucleosomes, which differ in only 4 amino acids. While H3.3, loaded independently of DNA replication, is thought to play important roles in transcriptional regulation(Sakai et

al., 2009), transcription is generally repressed in *Xenopus* eggs(Newport and Kirschner, 1982), allowing us to specifically study the transcription-independent roles of histone variants in affecting the chromatin landscape.

In addition to individual contributions of chromatin factors, I was interested in the interaction between multiple factors. Therefore, in the same experiment I assayed the combinatorial effect of the cell cycle (interphase vs. mitotic extract), Aurora B (mock vs. CPC depletion), and the heterochromatin mark H3K9me3 (H3 vs. H3K9me3 nucleosomes) on the chromatin composition. These perturbations are expected to have connected effects(Fischle et al., 2005). since Aurora B phosphorylates H3S10, which is adjacent to H3K9me3 and the cell cycle causes a large array of modifications to the H3 N-terminal tail and elsewhere on chromatin. Indeed, previous studies have documented the combinatorial effects of these histone tail marks, such as the H3K9me3 interactor HP1 being evicted by neighboring H3S10ph(Fischle et al., 2005; Hirota et al., 2005), providing a precedent for these experiments.

Major and minor determinants of chromosome composition

As outlined above, I purified chromatin beads from *Xenopus* egg extract and using mass spectrometry, quantified how chromatin binding proteins were regulated by the underlying chromatin and extract conditions. Although I tested the contribution of many factors to the proteomic composition of chromatin, the presence or absence of nucleosomes had the broadest effect (Figure 2-1A-B, Figure A-3, Figure A-4). I defined the cutoff as being enriched greater than 4-fold by the presence or absence of

nucleosomes, and observed that only 57.3% of proteins are unaffected by chromatin with or without nucleosomes. These proteins, including DNA damage proteins RPA and Ku70-80, are likely proteins that bind DNA, but can still interact with DNA in the nucleosomal context. 30.5% of proteins exclusively associate with non-nucleosomal DNA. Proteins in this class, such as tRNA synthases, are nucleic acid binding proteins, which likely are inhibited by nucleosomes. Finally, 12.2% of identified proteins exclusively associate with nucleosomes, including core histones and the linker histone H1. These proteins are either specifically recruited to nucleosomes (such as RCC1 (Makde et al., 2010)), or bind DNA in a nucleosome dependent manner. Similarly, the cell cycle had a strong effect on how proteins interact with chromatin; 34.9% of proteins are affected by the cell cycle (Figure 2-1C). Notably, I detected known mitotic proteins (condensin) only on mitotic chromatin and known interphase proteins (MCM complex and nuclear pore complex proteins) only on interphase chromatin (Figure A-5), supporting effective cell cycle manipulation of the extract.

Figure 2-2. Nucleosomes and the cell cycle are the major determinants of chromosome composition. Histograms of the number of chromatin associated proteins affected by each experimental perturbation. For all proteins identified on chromatin, their enrichment on Nucleosomal vs Naked DNA mitotic (A) and interphase (B) chromatin, M phase vs interphase nucleosomal chromatin (C), H3.3 vs H3.2 mitotic chromatin (D), H3 vs H3K9me3 mitotic chromatin (E), mock depleted vs CPC depleted mitotic chromatin (F), and mock depleted vs H1 depleted chromatin (G) are plotted.

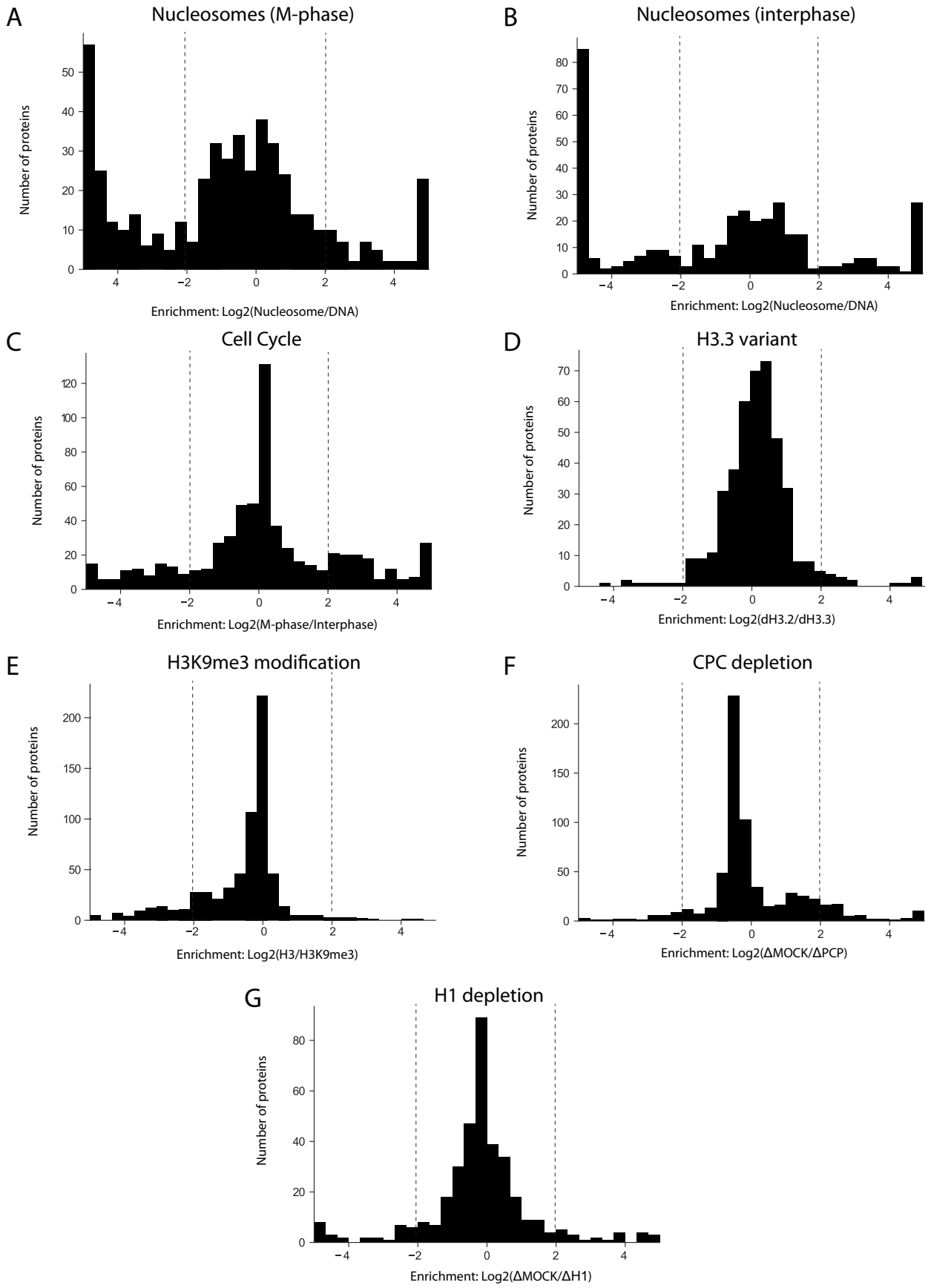
A
Nucleosomes (M-phase)
Number of proteins
Enrichment: Log2(Nucleosome/DNA)
B
Nucleosomes (interphase)
Number of proteins
Enrichment: Log2(Nucleosome/DNA)
C
Cell Cycle
Number of proteins
Enrichment: Log2(M-phase/Interphase)
D
H3.3 variant
Number of proteins
Enrichment: Log2(dH3.2/dH3.3)
E
H3K9me3 modification
Number of proteins
Enrichment: Log2(H3/H3K9me3)
F
CPC depletion
Number of proteins
Enrichment: Log2(ΔMOCK/ΔPCP)
G
H1 depletion
Number of proteins
Enrichment: Log2(ΔMOCK/ΔH1)

The overarching effect of nucleosomes and the cell cycle is in sharp contrast with the effect of the histone variant H3.3, which had little effect on the composition of chromatin. Only 5.4% of proteins were affected by more than four-fold in the presence of H3.3 (Figure 2-2D). Of the few proteins that were affected, none could be reproducibly verified (Christian Zierhut, personal communication). These data are consistent with H3.3 only modifying four amino acids on a 262 kiladalton nucleosome particle, which is not expected to largely affect the composition of chromatin.

Similarly, 85.2% of proteins were unaffected by the heterochromatin mark H3K9me3 (Figure 2-2E), indicating that this has little effect on the chromatin composition. Although only 12.8% of proteins are specifically recruited to H3K9me3 chromatin (Figure A-6), these proteins include factors known to be critically important for heterochromatin structure such as HP1(Nakayama et al., 2001), which organizes heterochromatin into a phase-separated liquid droplet(Larson et al., 2017). This dataset provides a rich set of novel candidate proteins which may bind H3K9me3 and play important roles in heterochromatin structure and function (Figure A-6). For example, ZNF850 (an uncharacterized protein) and ASAP3 (an ADP-ribosylation factor implicated in cancer cell invasion(Ha et al., 2008)) have no reported link to heterochromatin. My data suggest that these proteins may either bind H3K9me3 directly or interact with other H3K9me3 interactors and warrant follow up studies. The predictive power of this data set is well illustrated with CHD3, which was one of the most abundant proteins binding H3K9me3 chromatin. CHD3 is known to be involved in heterochromatin organization(Klement et al., 2014), and my data suggest it may be through direct

interaction with H3K9me3. Indeed, following my study, a recent biochemical studied showed that CHD3 has enhanced affinity for H3K9me3(Tencer et al., 2017).

Depletion of the CPC (Figure A-7) and linker histone H1 (Figure A-8) only affect 14.4% and 14.8% of the chromatin proteome, respectively, indicative of a relatively minor and specialized effect on chromatin (Figure 2-2F,G). Combined with the previous results, these data show that nucleosomes and the cell cle are the key determinants of global chromatin composition, while other perturbations like histone variants, histone modifications, linker histones, and regulatory kinases impart cellular functions only by modulating specific proteins.

Nucleosomal and cell cycle regulation of chromatin

To uncover insights into the regulation of mitotic chromosome assembly, I specifically focused on nucleosome-dependent chromatin binding proteins and how chromatin is regulated by the cell cycle, since these are the major determinants of chromatin composition (Figure 2-2) and have been relatively unstudied.

Unexpectedly, many proteins that possess DNA binding activity in vitro show nucleosome dependent chromatin association in physiological egg extracts (summarized in Figure 2-3A). For example, the linker histone H1 has well established DNA binding activity in vitro(Ura et al., 1996), but requires nucleosomes for chromatin recruitment. While conducting these experiments, it was shown that in vitro H1 binds to the dyad of the nucleosome and constrict dynamics of the DNA entering and exiting the nucleosome(Bednar et al., 2017). My data suggest that H1 may be specifically recruited

to this position in cells and avoids non-specific interactions with non-nucleosomal DNA. Similarly, many other DNA binding proteins are highly abundant exclusively on nucleosomal chromatin including the histone chaperone complex FACT and RCC1, a guanine nucleotide exchange factor required for mitotic spindle assembly (Figure 2-3B). I was surprised to see topoisomerase II exclusively on nucleosomal DNA as it is known to act on naked DNA (Figure 2-3A,C). However, as expected, purified topoisomerase II preferentially associated with naked DNA over nucleosomal DNA (Figure 2-3D). Collectively, these data show that proteins with in vitro DNA may still require nucleosomes to associate with chromatin in vivo. I envision that regulation by chaperones or other signaling methods restricts these proteins to nucleosomal DNA (see Chapter 4).

Figure 2-3. Proteins with DNA binding activity require nucleosomes to associate with physiological chromatin. (A) Summary of most abundant nucleosome-dependent, chromatin associated proteins. Naked DNA or chromatin beads were incubated in mitotic *Xenopus* egg extract, recovered, washed, and the chromatin associated proteins were analyzed by mass spectrometry. The most abundant proteins that were at least 5-fold enriched on nucleosome beads over naked DNA are summarized. (B, C) Western blot analysis of nucleosome dependent, chromatin associated proteins. Chromatin beads were treated as in (A). (D) Purified topoisomerase II interacts with naked DNA and nucleosomes in vitro. Purified topoisomerase II was incubated with DNA or nucleosome beads. Beads were recovered, washed, and chromatin bound topoisomerase II was visualized by coomassie staining.

A

Protein	Abundance on chromatin (a.u.)	Reported DNA binding activity?	Reference
H4	5.6×10^9	-	
H2B	4.3×10^9	-	
H3	3.2×10^9	-	
H2A	1.1×10^9	-	
H1	4.0×10^8	Yes	Ura et al., 1996
Spt16 (FACT)	1.1×10^8	Yes	Li et al., 2005
SSRP1 (FACT)	7.2×10^7	Yes	Li et al., 2005
RCC1	5.3×10^7	Yes	Seino et al., 1992
Ran	3.5×10^7	No	
DDB1	2.9×10^7	Yes	Chu et al., 1988
Topoisomerase II	2.4×10^7	Yes	This study
Aurora B (CPC)	2.2×10^7	No	
Dasra	1.9×10^7	No	
Shugoshin I	1.8×10^7	No	
INCENP	1.6×10^7	No	

B

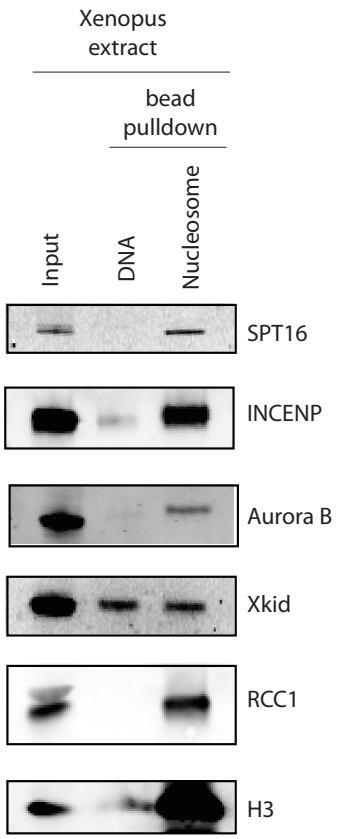

C

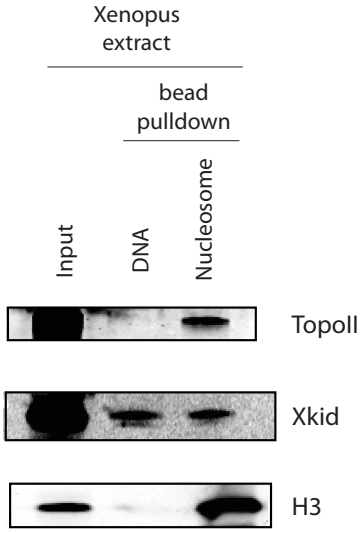

D

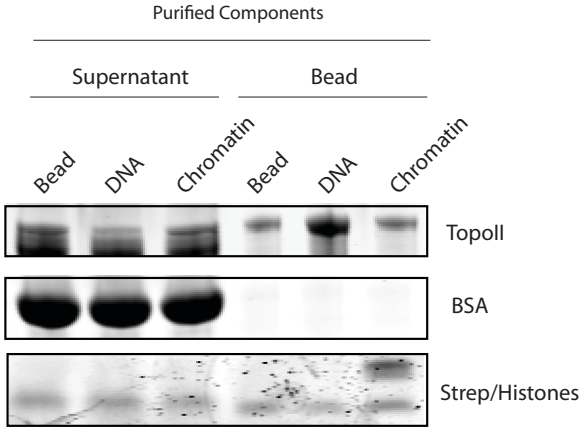

A catalog of how a variety of chromatin binding proteins are regulated throughout the cell cycle is shown in Figure 2-4. Of the proteins enriched on mitotic chromatin (Figure 2-4B), many have known functions in mitosis including RCC1, which is required for mitotic spindle formation(Carazo-Salas et al., 1999) and H1, which is required for mitotic chromosome condensation(Maresca et al., 2005). The mitotic specific-proteins also include relatively unstudied proteins such as CIP2A, an inhibitor of PP2A, and C1QPB, a novel interactor of the CPC (Michael Wheelock, personal communication). These data point to a mitotic role for these proteins, and warrants follow up studies.

65.1% of proteins are found on chromatin in interphase as well as M phase, and likely function throughout the cell cycle (Figure 2-4C). Interestingly, many proteins involved in repairing DNA damage (ATM, MRE11, BLM, WRN, RPA) are found on chromatin throughout the cell cycle (Figure 2-4C). Although the DNA damage response is largely attenuated in mitosis(Giunta et al., 2010), these results suggest a primary DNA damage response (including ATM and MRE11) still occurs throughout the cell cycle in the frog egg. Finally, I see a large fraction of proteins (14.7%) that bind specifically to interphase specific chromatin and are evicted from mitotic chromatin (Figure 2-4D). Although the mitotic eviction of many proteins has been individually documented (e.g. (Rizkallah and Hurt, 2009) and reviewed in (Gottesfeld and Forbes, 1997)), this is the first global assessment of how the proteome is regulated in mitosis. Of the proteins specific to interphase chromatin, I found proteins involved in DNA replication (MCM2-7), nuclear envelope structure (Lamin A), DNA repair (MSH2-6), and nucleosome assembly and remodeling. The functional consequences of the global

eviction of chromatin binding proteins during mitosis is unknown, however, I speculate that their removal may facilitate the loading of mitosis-specific proteins required to condense and segregate chromosomes accurately (see below).

Figure 2-4. Summary of the cell cycle regulation of chromatin associated proteins. (A) Abundance of all proteins on M phase and interphase chromatin. Nucleosome beads were incubated in M phase or interphase extract, recovered, washed and the chromatin associated proteins were analyzed by mass spectrometry. The abundance of each identified protein is plotted. Proteins identified only on a single sample are plotted along the axes. (B-D) Individual proteins from (A). For each mitosis specific (B), cell cycle independent (C), or interphase specific (D) protein, the abundance on chromatin, the enrichment on M phase over interphase chromatin, and the nucleosome dependency are reported.

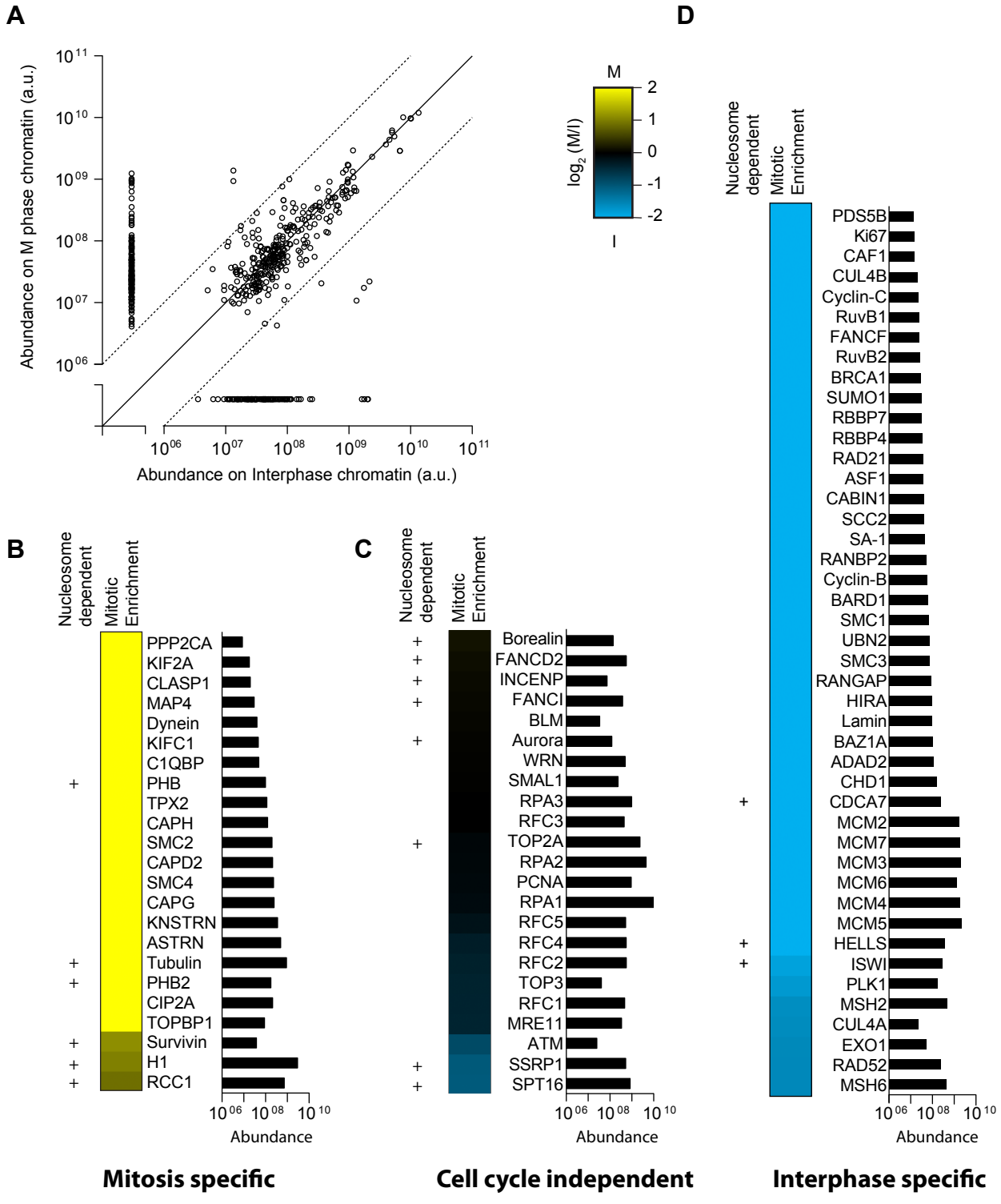
A
Abundance on M phase chromatin (a.u.)
Abundance on Interphase chromatin (a.u.)
log2 (M/I)
M
I
B
Nucleosome dependent
Mitotic Enrichment
PPP2CA
KIF2A
CLASP1
MAP4
Dynein
KIFC1
C1QBP
PHB
TPX2
CAPH
SMC2
CAPD2
SMC4
CAPG
KNSTRN
ASTRN
Tubulin
PHB2
CIP2A
TOPBP1
Survivin
H1
RCC1
Abundance
Mitosis specific
C
Borealin
FANCD2
INCENP
FANCI
BLM
Aurora
WRN
SMAL1
RPA3
RFC3
TOP2A
RPA2
PCNA
RPA1
RFC5
RFC4
RFC2
TOP3
RFC1
MRE11
ATM
SSRP1
SPT16
Cell cycle independent
D
PDS5B
Ki67
CAF1
CUL4B
Cyclin-C
RuvB1
FANCF
RuvB2
BRCA1
SUMO1
RBBP7
RBBP4
RAD21
ASF1
CABIN1
SCC2
SA-1
RANBP2
Cyclin-B
BARD1
SMC1
UBN2
SMC3
RANGAP
HIRA
Lamin
BAZ1A
ADAD2
CHD1
CDCA7
MCM2
MCM7
MCM3
MCM6
MCM4
MCM5
HELLS
ISWI
PLK1
MSH2
CUL4A
EXO1
RAD52
MSH6
Interphase specific

Nucleosomal and cell cycle regulation of mitotic chromosome structural proteins

As discussed in Chapter 1, topoisomerase II and condensin are the two primary molecules involved in shaping mitotic chromosomes. In my mass spectrometry experiments, I uncovered an interesting divergent regulation of these two factors.

Consistent with condensin's primary function occurring during mitosis, I saw all subunits of condensin I specifically recruited to mitotic chromatin (Figure 2-5A). Although purified condensin harbors DNA binding activity, I saw an exclusion of condensin from interphase chromatin (Figure 2-5A), suggesting that additional cell cycle regulations are imparted on its DNA binding activity. Combined with published data that shows condensin's ATPase activity is activated in mitosis(Kimura et al., 1998), these data show that condensin acts specifically during mitosis via enhanced chromatin targeting and activity. Surprisingly, I saw that condensin preferred naked DNA beads over nucleosome beads (Figure 2-5B,C). At the time of these experiments, this result was in direct contradiction to a published study showing that condensin is recruited to nucleosomes in mitosis(Tada et al., 2011). Since condensin is thought to condense mitotic chromosomes through its positive DNA supercoiling activity, this result suggests that nucleosomes may be refractory to condensin mediated chromosome shaping. Following these experiments, condensin's exclusion from nucleosomal DNA was independently verified by multiple labs(Kinoshita et al., 2015; Shintomi et al., 2017; Toselli-Mollereau et al., 2016). Although reduced, condensin could be detected on nucleosomal chromatin, which I interpret as condensin still having affinity for nucleosomal DNA or that it can bind the linker region between nucleosomes, however,

the canonical condensin-DNA structure requires ~190 base pairs of free DNA(Bazett-Jones et al., 2002). As mitotic chromosomes are largely composed of nucleosomes, the ability of condensin to act in the context of nucleosomes is likely required for its function.

Figure 2-5. Differential regulation of condensin and topoisomerase II. Abundance of condensin (A, B, C) and topoisomerase II (C, D, E) on the indicated chromatin measured by mass spectrometry (A, B, D, E) or Western blotting (C).

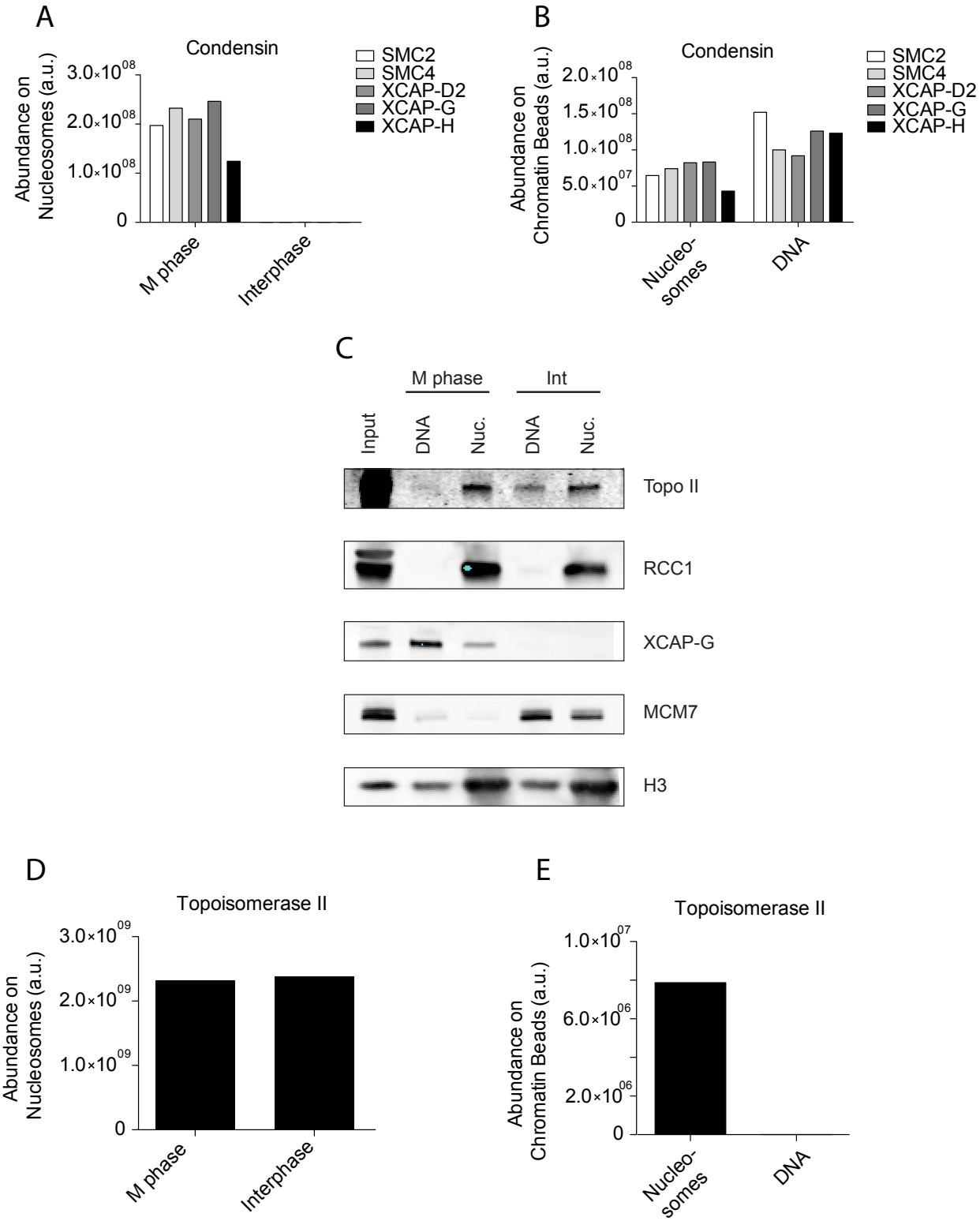
A
Condensin
Abundance on Nucleosomes (a.u.)
3.0×10^08
2.0×10^08
1.0×10^08
0
M phase
Interphase
SMC2
SMC4
XCAP-D2
XCAP-G
XCAP-H
B
Condensin
Abundance on Chromatin Beads (a.u.)
2.0×10^08
1.5×10^08
1.0×10^08
5.0×10^07
0
Nucleo-somes
DNA
SMC2
SMC4
XCAP-D2
XCAP-G
XCAP-H
C
M phase
Int
Input
DNA
Nuc.
DNA
Nuc.
Topo II
RCC1
XCAP-G
MCM7
H3
D
Topoisomerase II
Abundance on Nucleosomes (a.u.)
3.0×10^09
2.0×10^09
1.0×10^09
0
M phase
Interphase
E
Topoisomerase II
Abundance on Chromatin Beads (a.u.)
1.0×10^07
6.0×10^06
2.0×10^06
0
Nucleo-somes
DNA

In contrast to condensin, topoisomerase II is recruited to chromatin independently of cell cycle phase (Figure 2-5C,D). Unexpectedly, although topoisomerase II is well documented to enzymatically act on naked DNA(Berger et al., 1996), I find that the association of topoisomerase II with chromatin requires nucleosomes in mitosis, and has a strong preference for nucleosomes in interphase (Figure 2-5 C,E). This indicates that although topoisomerase II acts on naked DNA, its interaction with the DNA substrate is transient and requires nucleosomes for stable association. While carrying out this study, an independent group verified that topoisomerase II interacts with histones to associate with chromatin and further identified the H3 tail as important in the recruitment(Lane et al., 2013).

If topoisomerase II is associated with chromatin throughout the cell cycle, how does it exclusively shape mitotic chromosomes during M phase? To address this question, I assayed topoisomerase II's enzymatic activity by monitoring decatenation of kinetoplast DNA. Kinetoplast DNA, mitochondrial DNA isolated from *Crithidia, fasciculate*, is highly catenated circular DNA but when added to *Xenopus* egg extract topoisomerase II decatenates the DNA resulting in individual circles, which can be resolved by gel electrophoresis (Figure 2-6A). I find that topoisomerase II decatenation activity is exclusively activated during mitosis (Figure 2-6B). However, my previous experiments were done on naked DNA. Although nucleosomes have been suggested inhibit topoisomerase II activity(Capranico et al., 1990), the mitotic chromosome is coated with nucleosomes, which raises the possibility that topoisomerase II is largely inactive on mitotic chromatin. However, by making nucleosomal kinetoplast DNA by salt

dialysis (Figure 2-6C) I saw that topoisomerase II has only slightly reduced activity on nucleosomes, indicating that topoisomerase II is still enzymatically functional within the context of nucleosomal chromatin. Collectively, these results show that although topoisomerase II associates with nucleosomal DNA throughout the cell cycle, topoisomerase II enzymatic activity is activated in mitosis where it is can facilitate decatenation of sister chromatids even in the presence of nucleosomes. Furthermore, I propose that topoisomerase II has enhanced binding affinity to nucleosomes that overcomes its slightly reduced activity on the nucleosomal substrate.

Figure 2-6. Topoisomerase II decatenation activity is stimulated in mitosis and can decatenate a nucleosomal substrate. (A) Kinetoplast DNA (kDNA) decatenation to assay topoisomerase II activity. kDNA was added to mock depleted or topoisomerase II depleted mitotic *Xenopus* extract. At the indicated time point, the DNA was extracted and resolved by agarose gel electrophoresis. kDNA is highly catenated and remains in the well while topoisomerase II dependent decatenation results in circular DNA that enters the gel. (B) Topoisomerase II is stimulated in mitosis. kDNA was added to mitotic or interphase *Xenopus* extract. At the indicated time point, the DNA was extracted and resolved by agarose gel electrophoresis. (C) Topoisomerase II can act on a nucleosomal substrate. kDNA or nucleosomal kDNA, generated by salt dialysis with histones, was added to mitotic *Xenopus* extract. At the indicated time point, the DNA was extracted and resolved by agarose gel electrophoresis (right). To verify the kDNA chromatinization, the nucleosomal kDNA was digested with MNase (right).

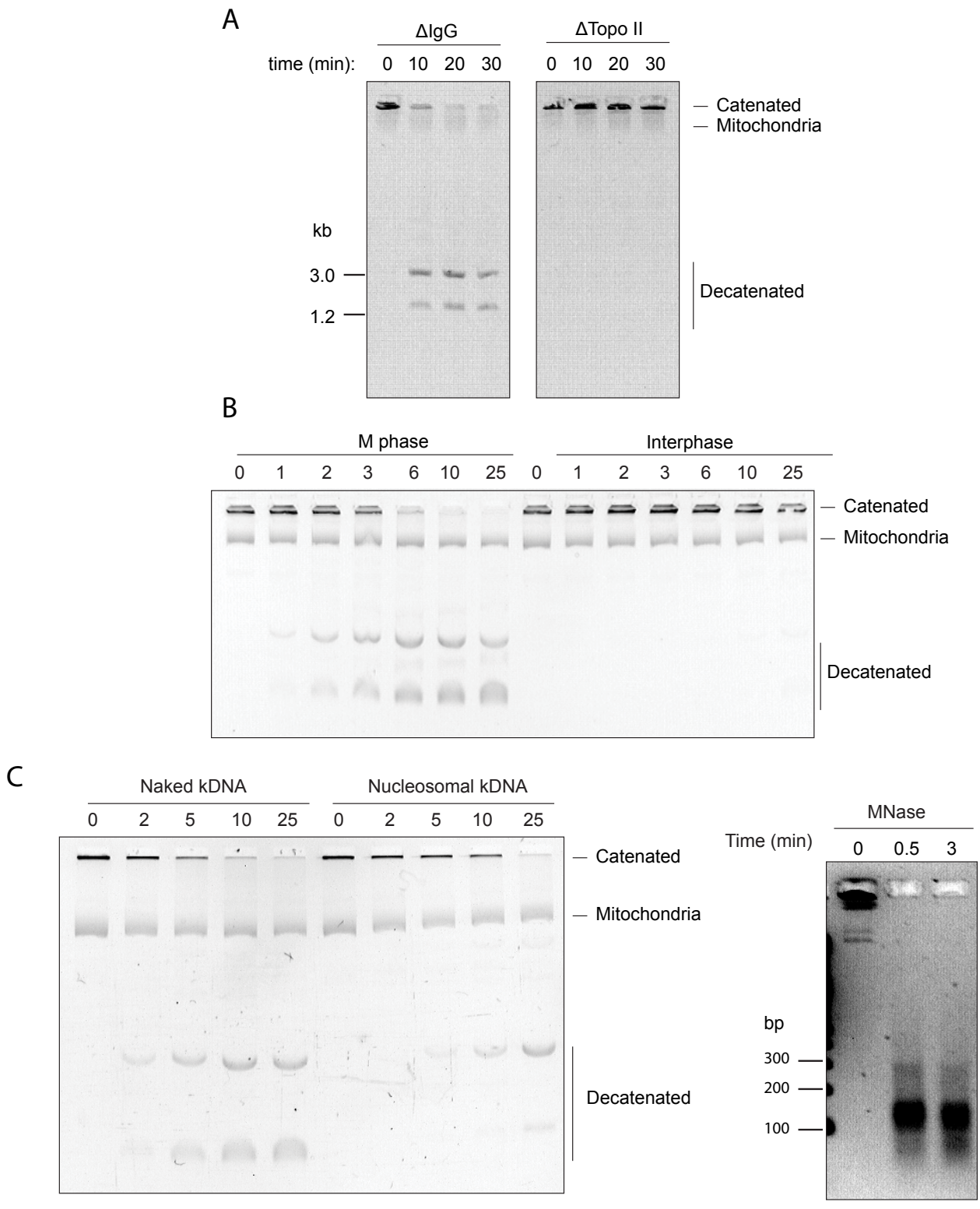
A
ΔIgG
ΔTopo II
time (min):
0 10 20 30
0 10 20 30
Catenated
Mitochondria
kb
3.0
1.2
Decatenated
B
M phase
Interphase
0 1 2 3 6 10 25 0 1 2 3 6 10 25
Catenated
Mitochondria
Decatenated
C
Naked kDNA
Nucleosomal kDNA
0 2 5 10 25 0 2 5 10 25
Catenated
Mitochondria
Decatenated
MNase
Time (min)
0 0.5 3
bp
300
200
100

Except for nucleosomes and the cell cycle, the chromatin recruitment of condensin and topoisomerase II is largely unaffected by experimental perturbations (Figure 2-7). Their association with chromatin in not affected by the heterochromatin mark H3K9me3 (Figure 2-7A), the mitotic kinase Aurora B (Figure 2-7B), the linker histone H1 (Figure 2-7C) or the histone variant H3.3 (Figure 2-7D). As condensin and topoisomerase II play pivotal roles in mitosis, this data is consistent with the function of these proteins needing to act globally and be immune to the specific chromatin context.

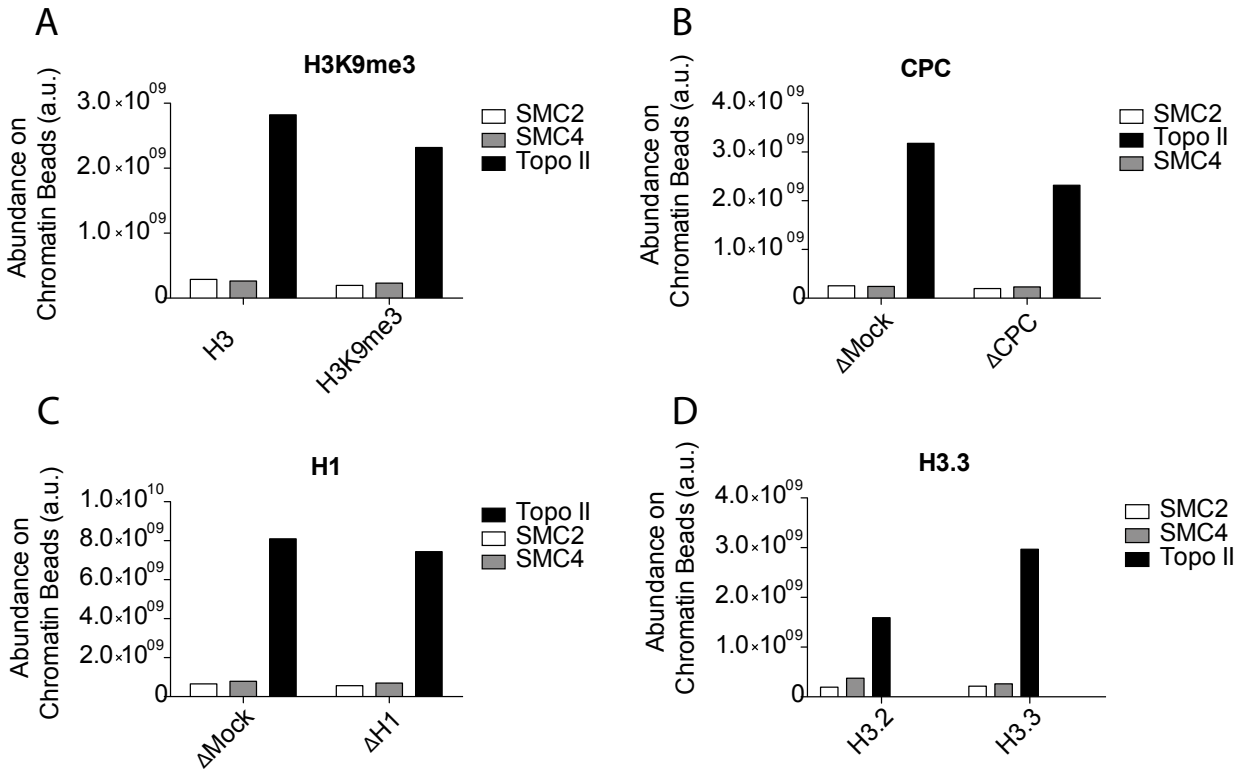

Figure 2-7. Condensin and topoisomerase II are largely unaffected by the underlying chromatin. The abundance of SMC2-SMC4 (condensin) and topoisomerase II on H3 and H3K9me3 (A), mock depleted and CPC depleted (B), mock depleted and H1 depleted (C), and H3.2 and H3.3 nucleosome beads incubated in mitotic *Xenopus* egg extract, determined by mass spectrometry.

Cell cycle regulation of nucleosome remodeling and assembly complexes

Among the proteins that are evicted from mitotic chromatin are nucleosome remodelers. Nearly all proteins found in nucleosome remodeling complexes are evicted from mitotic chromatin including components of ISWI, NURD, INO80, among others (Figure 2-8A). The main exception to this is the FACT complex, which is only slightly enriched on interphase chromatin relative to mitotic chromatin (Figure 2-8A,B). In addition to being evicted from mitotic chromatin, most nucleosome remodelers are dependent on nucleosomes for chromatin association, consistent with the nucleosome being the substrate of their enzymatic reaction. As both FACT and ISWI depend on nucleosomes (Figure 2-8C, E), but are differentially regulated by the cell cycle, it is likely that not all nucleosomal remodelers are under control of the same regulatory module. Indeed, the mechanism of mitotic eviction appears to be different between remodeling complexes; ISWI is evicted from mitotic chromatin in an Aurora B dependent manner (Figure 2-8D) while other remodeling/assembly complexes such as NURD and HIRA are evicted from mitotic chromatin independently of Aurora B (Figure 2-8F).

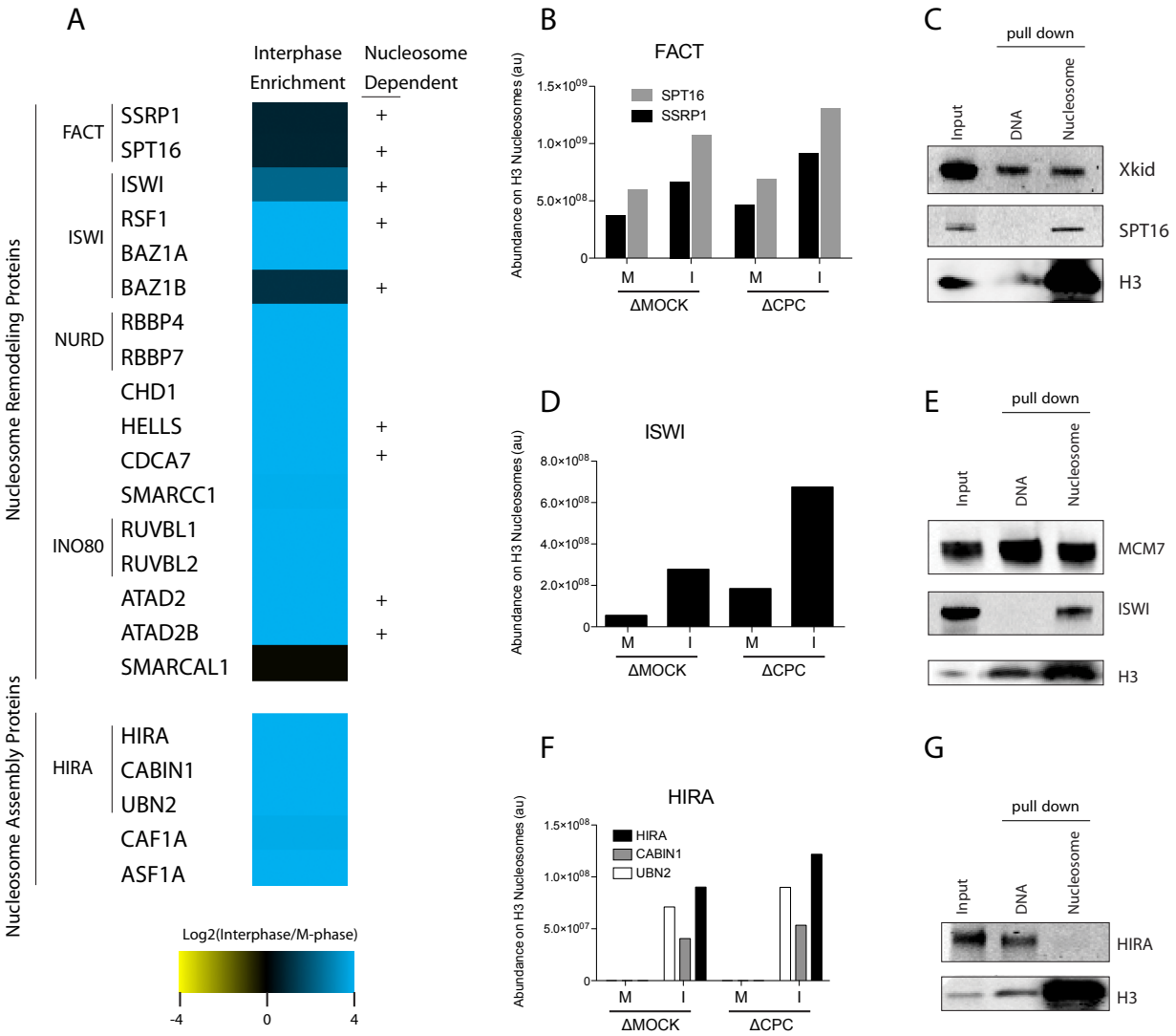

Figure 2-8. Nucleosome remodeling and assembly proteins are evicted from mitotic chromatin. (A) The enrichment of each nucleosome remodeling and assembly protein on interphase relative to mitotic nucleosome beads was determined by mass spectrometry. Whether the proteins are dependent on nucleosomes for chromatin association is also indicated. Quantification of the amount of FACT (B, C), ISWI (D, E), and HIRA (F, G) bound to the indicated chromatin beads measured by mass spectrometry (B, D, E) or Western blotting (C, E, G).

Similar to nucleosome remodelers, the main proteins involved in nucleosome assembly are evicted from mitotic chromatin (Figure 2-8A). This includes the histone chaperones required nucleosome assembly Asf1, HIRA, and CAF1. As opposed to nucleosome remodelers, which largely require nucleosomes, HIRA is specifically recruited to naked DNA in interphase (Figure 2-8G). This suggests a temporally segregated model whereby histone chaperones are recruited to sites of naked DNA to deposit histones in interphase, followed by recruitment of nucleosome remodelers, which properly position the nucleosomes.

Cell cycle regulation of nucleosome assembly

Due to the striking mitotic eviction of proteins involved in nucleosome assembly and remodeling, I hypothesized that mitotic eviction of nucleosome remodelers and histone chaperones would result in diminished nucleosome assembly during mitosis. To test this, I used a supercoiling assay, whereby relaxed plasmid DNA is added to *Xenopus* egg extract, and nucleosome incorporation is monitored by measuring the supercoiling state of the plasmid (every incorporated nucleosome increases the linkage number by -1, which migrates faster by gel electrophoresis). As expected, interphase extract possesses robust nucleosome assembly activity (Figure 2-9A). Surprisingly, concomitant with eviction of HIRA and other nucleosome remodeling complexes, mitotic extract showed markedly reduced nucleosome assembly activity (Figure 2-9A). While interphase extract completely chromatinized a plasmid in 90 minutes, very few histones had been deposited on mitotic plasmids after 180 minutes.

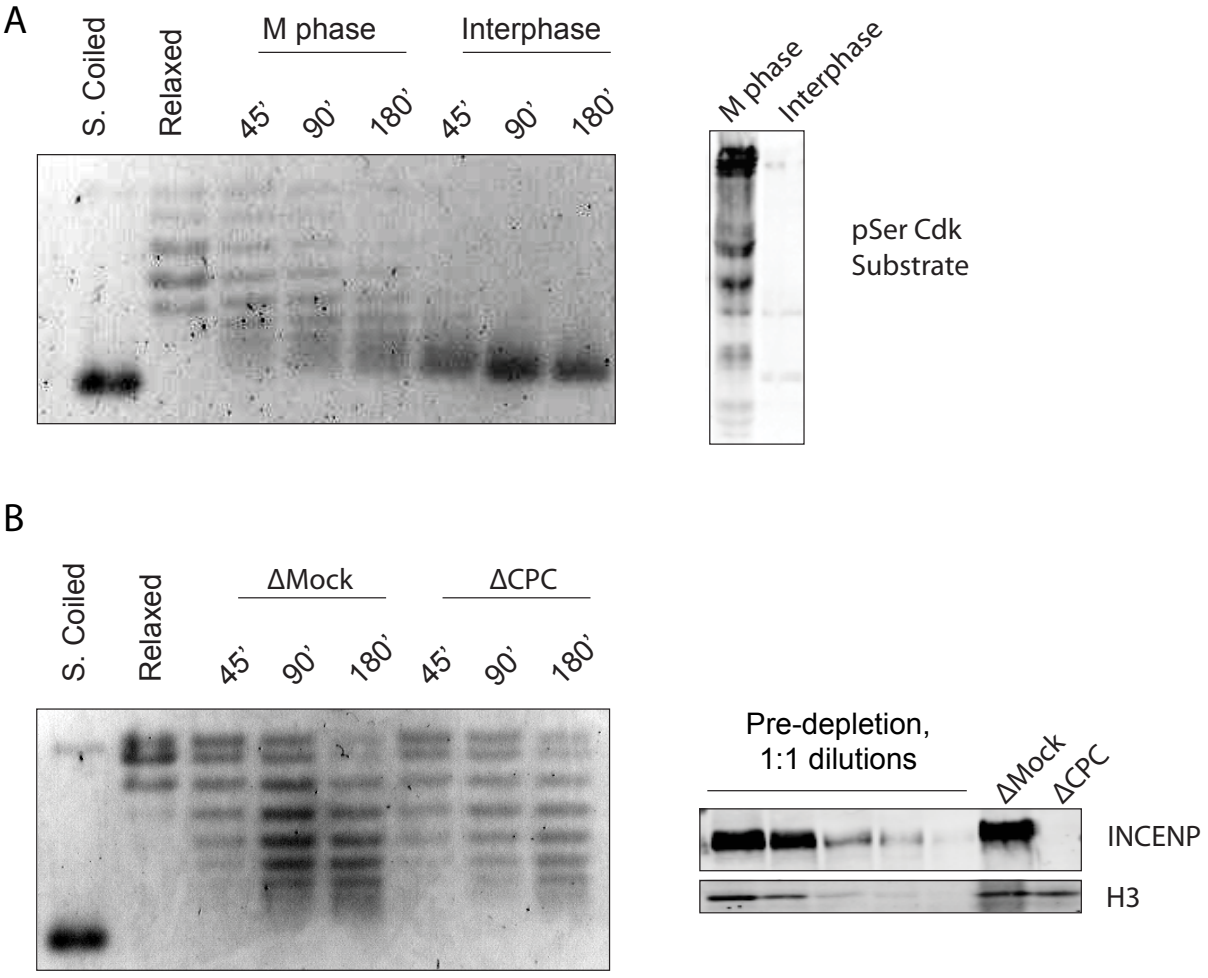

Figure 2-9. Nucleosome assembly is suppressed in mitosis independent of the CPC. (A) Agarose gel analysis of relaxed plasmid chromatinized in mitotic and interphase *Xenopus* egg extract. At the indicated times, the plasmid was purified from the extract, and the supercoiling state was determined. Nucleosome loading results in a supercoiled plasmid, which migrates faster than relaxed plasmid. The cell cycle manipulation was verified by Western blotting the cell lysate using an antibody that recognizes phosphorylated Cdk1 substrates (right). (B) Agarose gel analysis of relaxed plasmid chromatinized in mock and CPC depleted mitotic *Xenopus* egg extract, processed as in (A). The CPC depletion was verified by Western blot analysis of INCENP (right).

Since some remodelers including ISWI and HELLS are evicted by mitotic chromatin by Aurora B, I wondered if reduced nucleosome assembly was downstream of Aurora B activity. However, depleting Aurora B had no effect on nucleosome assembly kinetics (Figure 2-9B). Although purified ISWI can catalyze nucleosome assembly activity in vitro(Ito et al., 1999), this result is consistent with ISWI depletion having no effect on nucleosome assembly kinetics in *Xenopus* egg extract(MacCallum et al., 2002).

Since Aurora B does not affect nucleosome assembly and is only responsible for a fraction of nucleosome remodelers and assembly proteins being evicted from mitotic chromatin, I sought to identify how other factors might be regulated. Specifically, I focused on HIRA, the histone chaperone required for replication-independent nucleosome assembly(Ray-Gallet et al., 2002). As discussed above, HIRA is evicted from mitotic chromatin in a manner independent of Aurora B (Figure 2-8F), and specifically, the protein is recruited to naked DNA (Figure 2-8G). HIRA deposits the histone variant H3.3 onto naked DNA(Ricketts et al., 2015), however, since my chromatin was made with H3.2, it is possible that HIRA was excluded from H3.2 nucleosomes but could still interact with H3.3 nucleosomal chromatin. Nevertheless, HIRA did not bind chromatin beads containing H3.2 nor H3.3 chromatin, showing that indeed, HIRA only interacts with naked DNA regardless of histone variant (Figure 2-10A).

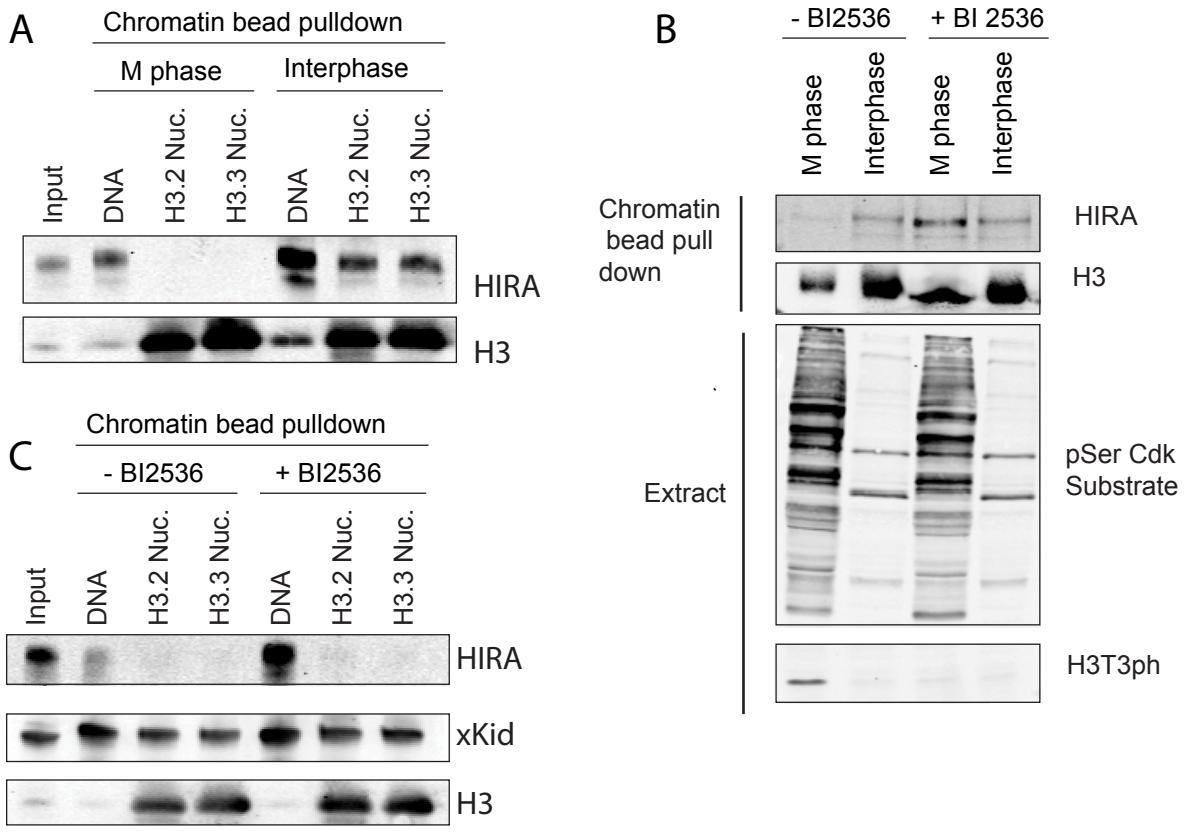

Figure 2-10. Plx1 mediated eviction of HIRA from DNA beads in mitosis. (A) Western blot analysis of naked DNA, H3.2 nucleosome or H3.3 nucleosome beads isolated from M phase or interphase extract depleted of H3/H4. (B) Western blot analysis of DNA beads isolated from M phase or interphase extract (+/- BI2536). (C) Western blot analysis of Naked DNA, H3.2 nucleosome or H3.3 nucleosome beads isolated from M phase extract depleted of H3/H4 (+/- BI2536).

Through testing a variety of possible causes of the mitotic eviction of HIRA, I identified the mitotic kinase Plx1 as being responsible for the mitotic eviction of HIRA (Figure 2-10B, C). HIRA mitotic eviction from chromatin beads (Figure 2-10B, C) and sperm chromatin (Figure 2-11A) was completely abolished when adding the Plx1 inhibitor BI5236(Steegmaier et al., 2007). Interestingly, even following Plx1 inhibition, HIRA only interacted with naked DNA and could still not bind H3.2 or H3.3 nucleosomes (Figure 2-10C). In contrast, HIRA chromatin localization to sperm (Figure 2-11B) or DNA beads (Figure 2-10B) was not affected by BI5236 in interphase extract, consistent with Plx1 being auto-inhibited in interphase(Ghenoiu et al., 2013).

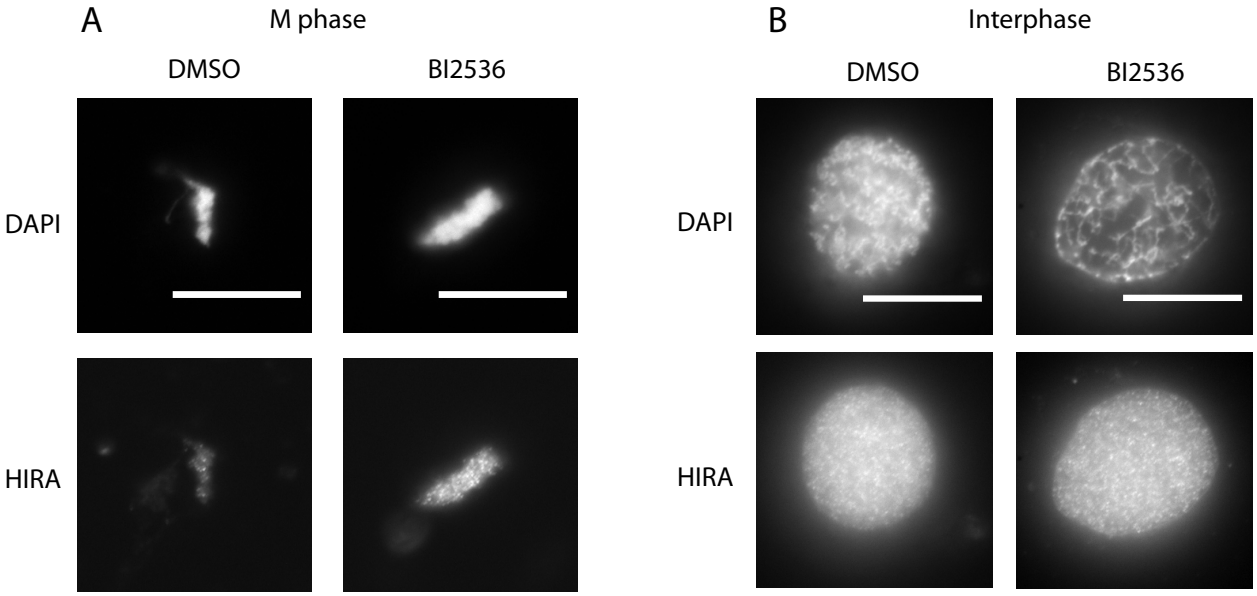

Figure 2-11. Plx1 mediated eviction of HIRA from sperm chromatin in mitosis. (A-B) Immunofluorescence of HIRA on replicated interphase (A) or mitotic (B) sperm chromatin chromatinized in *Xenopus* egg extract. Scale bar 15 μm.

Plx1 targets can be identified by the presence of a phosphorylated Polo box domain binding motif, S[S/T], which recruits Plx1 to its substrate for further phosphorylation(Elia et al., 2003a; Elia et al., 2003b). Since chromatin localization of HIRA is regulated by Plx1, I wondered if it was a direct target of the kinase. Indeed, HIRA harbors a Polo Box domain binding motif (Figure 2-12A), and is gel-shifted in mitosis in a Plx1 dependent manner (Figure 2-12B), suggesting that HIRA may be a direct target of Plx1. In agreement with this hypothesis, HIRA is a reported interactor of Plk1(Kettenbach et al., 2011).

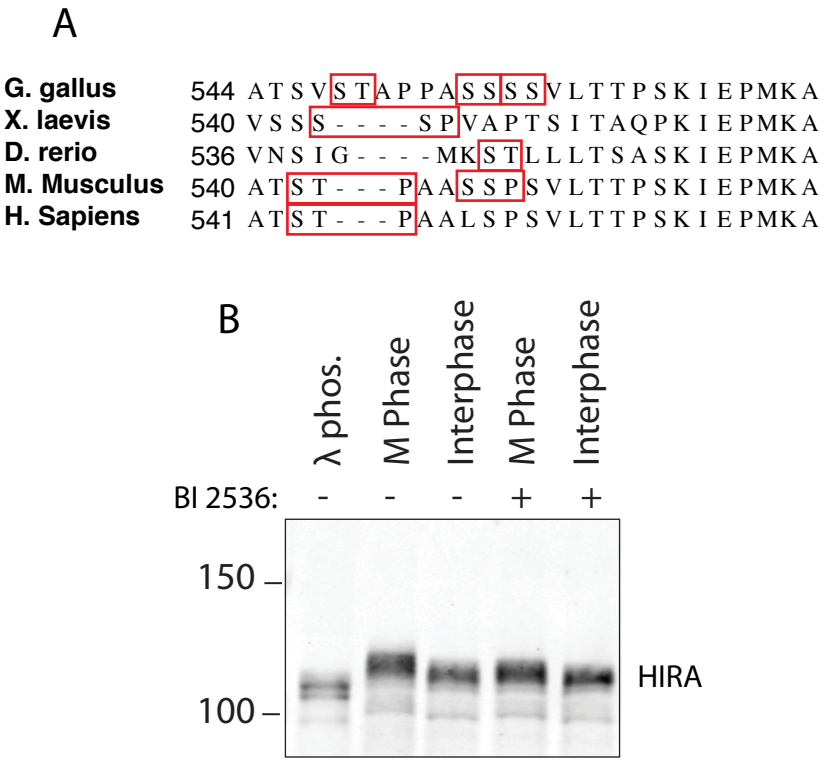

Figure 2-12. HIRA harbors a Polo box binding motif and displays a phospho-dependent gel shift in mitosis. (A) Alignment of HIRA from the indicated species. The Polobox binding motif is highlighted in red. If followed by Proline, the Polo box binding motif is also a Cdk1 phosphorylation consensus site. (B) Western blot analysis HIRA in mitotic or interphase *Xenopus* extract (+/- BI2536). Where indicated, the extract was treated with lambda phosphatase.

As HIRA is the major histone chaperone required for replication-independent nucleosome assembly, I wondered if Plx1 mediated eviction of HIRA is responsible for the previously-identified mitotic suppression of nucleosome assembly (Figure 2-9A). By monitoring plasmid nucleosome assembly kinetics, upon Plx1 inhibition by BI2532, I saw a dramatic increase in nucleosome assembly kinetics in mitosis to near interphase levels (Figure 2-13A). Although BI2532 is reportedly specific for Polo-like kinase 1, it also has off-target inhibitory activity on Polo-like kinase 2 and 3(Steegmaier et al., 2007). The *Xenopus* egg has no detectable Plk2, but contains Plk3 (23 nM)(Wuhr et al., 2014), making the previous results inconclusive. Importantly, immunodepleting Plx1 from *Xenopus* egg extracts results in a similar increase in mitotic nucleosome assembly kinetics (Figure 2-13B), indicating that the results are not due to off-target effects of BI5236. As expected, neither BI2532 nor Plx1 depletion had any effect on nucleosome assembly in interphase extracts, since Plx1 inhibition has no effect on HIRA in interphase.

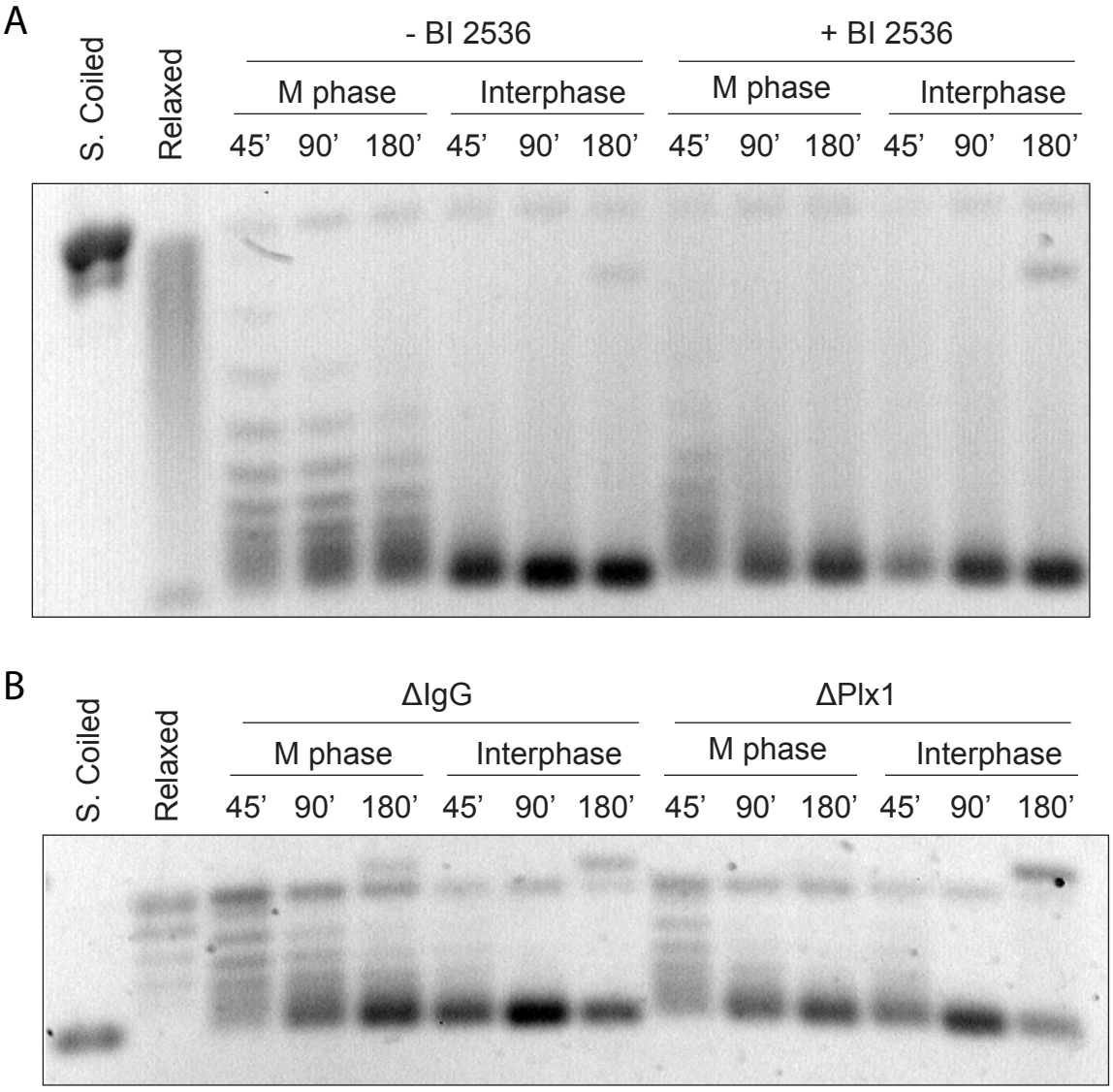

Figure 2-13. Plx1 mediated suppression of nucleosome assembly in mitosis. (A) Agarose gel analysis of relaxed plasmid chromatinized in mitotic or interphase *Xenopus* egg extract (+/- BI 2536). At the indicated times, the plasmid was purified from the extract, and the supercoiling state was determined by agarose gel electrophoresis. (B) As in (A) except mock or Plx1 depleted *Xenopus* egg extract was used.

Collectively, these data show that the action of multiple mitotic kinases are responsible for evicting nearly all nucleosome remodeling proteins, at least in part to suppress mitotic nucleosome assembly. Specifically, Plx1 regulates the association of HIRA with chromatin and ultimately suppresses nucleosome assembly in mitosis. The physiological implications of this regulation are discussed in the following section.

Discussion and perspective

The global landscape of cell cycle regulated chromatin proteins

Previous studies have looked at the chromatin proteome in interphase(Kustatscher et al., 2014) and mitosis(Ohta et al., 2010) individually but have not looked directly at how the cell cycle controls the chromatin proteome. However, countless studies have tracked individual proteins by immunofluorescence and have noted cell cycle regulation.

Recently, immunofluorescence studies that report the mitotic eviction of chromatin proteins have been called into question(Teves et al., 2016). Apparently, a large number of proteins that are shown to be evicted from mitotic chromatin by immunofluorescence such as Sox2, Oct4, Essrb, Klf4, Sp1, Foxo1, and Foxo3a do not show similar behavior when endogenously tagged GFP constructs are monitored. The authors reason that formaldehyde gradients that naturally occur as the fixative enters the cell, coupled with high off-rates of DNA binding proteins, may “extract” the protein off chromatin as the sample is fixed. This mechanism would apply to all antibodies and challenges all previous reports of proteins being evicted from mitotic chromatin

determined by immunofluorescence. A second group has independently verified this phenomenon(Lerner et al., 2016). Interestingly, it is reported that methanol fixation may not have this problem(Lerner et al., 2016), at least in one tested case.

In the work presented here, since no fixation is involved, I avoid the complications associated with fixation-based methods and get a proteome-wide view of how the cell cycle regulates chromatin binding proteins. This allowed me to unambiguously determine the mitotic eviction of a variety of proteins including HIRA, Asf1, ISWI, and HELLS-CDCA7. Although some of these proteins are confirmatory, such as HIRA(De Lucia et al., 2001), these confirmations are required considering the artefacts involved in formaldehyde based fixation methods.

Additionally, I was able to identify known and novel mitotic binding proteins. As discussed previously, the mitotic chromatin beads are highly coated with condensin, in agreement with condensin being a major chromatin associated protein complex(Hirano and Mitchison, 1994). I also identified several proteins that have previously unknown functions in mitosis, which warrant further study. For example, CIP2A was exclusively enriched on mitotic chromatin and clustered with condensin Figure 3-3B). CIP2A is a phosphatase inhibitor (PP2A) with a known role in centrosome separation(Jeong et al., 2014), however, my results suggest that it may have another mitotic function on chromatin. Similarly, GEN1, is a nuclease known to be required for resolution of anaphase ultrafine bridges(Chan et al., 2018) was found exclusively on mitotic chromatin. This finding suggests that GEN1 specifically acts during mitotic to resolve

recombination intermediates and may be inactive in the preceding interphase, as has previously been hypothesized(Chan and West, 2014).

Through these experiments, I identified an interesting regulation of condensin and topoisomerase II, major components of mitotic chromosomes. Specifically, both proteins are activated in mitosis, but by different mechanisms. Topoisomerase II associates with chromatin throughout the cell cycle, while it is enzymatically activated in mitosis. Alternatively, condensin cannot interact with chromatin in interphase, and only associates with mitotis. Interestingly, I find that although both components prefer naked DNA, they can work in the context of nucleosomes, and are robust against a variety of chromatin conditions.

Since I depleted Aurora B, I could determine which mitotic chromatin associated proteins depend on the mitotic kinase for localization. However, results from this experiment highlighted an important caveat: I noticed that tubulin and many microtubule binding proteins co-purified with mitotic chromatin beads in a manner dependent on Aurora B. These include alpha tubulin, beta tubulin, RHAMM and MAP4 among others. Unfortunately, in *Xenopus* egg extract, microtubules are locally polymerized near chromatin in an Aurora B dependent manner, raising the possibility that microtubules (and microtubule binding proteins) are co-purifying with the beads. Because of this, it is unclear which of these proteins are bona fide chromatin binders and which are MT binders. To parse microtubule interactors from chromatin interactors, the experiments need to be repeated in nocodazole, a drug that effectively depolymerizes microtubules in *Xenopus* egg extract.

Mitotic eviction of nucleosome assembly and remodeling proteins

One of the most striking findings while studying the cell cycle regulation of chromatin binding proteins was the global eviction of proteins involved in nucleosome assembly and remodeling during mitosis. This includes remodelers ISWI, CHD1, INO80, and HELLS-CDCA7, as well as assembly factors such as Asf1, CAF, and HIRA. Although mitotic eviction has been previously reported for some of these proteins such as HIRA(De Lucia et al., 2001) and CHD1(Stokes and Perry, 1995), these findings warrant revisiting due to the previously discussed fixation artifacts. Additionally, I found that mitotic eviction of nucleosome assembly/remodeling proteins, including the histone chaperone HIRA was concomitant with a decrease in nucleosome assembly rate in mitosis.

Because nucleosomes are required for mitotic chromosome compaction(Shintomi et al., 2017), the finding that nucleosome assembly is repressed in mitosis is counterintuitive. These results suggest that if interphase nucleosome assembly is incomplete when the cell enters mitosis, the cell has no mechanism to complete nucleosome assembly, which could result in de-compacted chromosomes and chromosome segregation errors. This could be especially problematic during the early embryonic cell cycles, where interphase only lasts 30 minutes(Morgan, 2007) and may not have time to completely chromatinize during interphase. However, in the following paragraph I detail a hypothesis to reconcile this counter-intuition.

Other than nucleosomes, the major components involved in shaping mitotic chromosomes are condensin and topoisomerase II. Interestingly, the action of both components is refractory to nucleosomes. Although I show that topoisomerase II is specifically recruited to nucleosomes (Figure 2-5C), enzymatic decatenation activity prefers non-nucleosomal DNA (Figure 2-6C). Since the enzymatic activity of topoisomerase II is important for shaping mitotic chromosomes(Sakaguchi and Kikuchi, 2004; Samejima et al., 2012), mitotic chromatin containing excess nucleosomes could inhibit topoisomerase II mediated chromosome shaping. Similarly, I showed that condensin prefers naked DNA over nucleosomal DNA for mitotic chromatin association (Figure 2-5C). While this has been independently verified by other groups(Kinoshita et al., 2015; Shintomi et al., 2017; Toselli-Mollereau et al., 2016), one report goes as far as to say that nucleosomes must be evicted during mitosis in order to facilitate condensin loading, and identify Gcn5 and RSC as the factors required for the mitotic eviction of nucleosomes(Toselli-Mollereau et al., 2016). As HIRA is very efficient in binding naked DNA (Figure 2-8G) and assembling nucleosomes(Ray-Gallet et al., 2002), HIRA activity would need to be suppressed to prevent nucleosome re-assembly on recently evicted nucleosomes. This would prevent futile nucleosome eviction-reassembly cycles. For these collective reasons, mitotic nucleosome assembly may need to be dampened to facilitate chromosome shaping.

To test this hypothesis, the deleterious effects of increased nucleosome assembly in mitosis would need to be determined. One way to achieve this would be to determine condensin/topoisomerase II activity on mitotic chromosomes formed in Plx1

inhibited extracts, which have increased nucleosome assembly kinetics in mitosis. My hypothesis would predict decreased condensin/topoisomerase II loading under this condition, as well as improper mitotic chromatin compaction. Unfortunately, Plx1 is required to remove most cohesin from mitotic chromosomes via the “prophase pathway”, causing Plx1 inhibition to result in major mitotic chromosome structural defects independent of its role in nucleosome assembly(Sumara et al., 2002). Further complicating this experiment, Plk1 was shown to directly interact with condensin to facilitate chromosome condensation(Abe et al., 2011). However, my data suggest that Plx1-dependent nucleosome assembly suppression is mediated by HIRA phosphorylation. Therefore, finding point mutations in HIRA that inhibit its Plx1 dependent phosphorylation could increase mitotic nucleosome assembly and allow me to specifically determine the contribution of nucleosome assembly in mitotic chromosome compaction independent of other Plx1 functions.

The hypothesis that reduced nucleosome assembly facilitates condensin and topoisomerase II activity does not explain the mitotic eviction of nucleosome remodelers including ISWI, CHD1, INO80, HELLS, and others. A recent study(Nocetti and Whitehouse, 2016) in budding yeast may shed light on the biology behind this phenomenon. In interphase, nucleosome remodelers precisely position nucleosomes often into dense arrays, but in mitosis nucleosome spacing is much more homogenous than in interphase. This could alleviate densely packed nucleosomes, exposing free DNA, which is required for condensin binding and topoisomerase II activity. Therefore, to achieve maximal condensin/topoisomerase II dependent chromosome shaping,

reduced nucleosome assembly may need to be coupled to reduced remodeler mediated nucleosome packing. However, I note that mitosis specific remodelers (currently not identified) may be required to homogenously space nucleosomes.

CHAPTER 3: HELLS-CDCA7, A BIPARTITE NUCLEOSOME REMODELING COMPLEX

Results

Co-regulation of chromatin complexes

Subunits of stable protein complexes are expected to biochemically co-fractionate. When combined with mass spectrometry, this principle has been used to identify hundreds of soluble protein complexes, many of which were previously unknown(Havugimana et al., 2012; Wan et al., 2015). Analogously, I reasoned that subunits of chromatin bound complexes would be co-regulated on chromatin. Therefore, I used a combination of three different perturbations (cell cycle, ±CPC, ±H3K9me3), to determine if protein complexes were co-regulated over eight different chromatin conditions. Indeed, manual inspection of known chromatin bound complexes showed that subunits are similarly regulated within conditions, even if their absolute amounts change dramatically between conditions (Figure 3-1A-I). For example, Ku70 and Ku80 (Figure 3-1A) have near identical levels on various chromatin conditions, consistent with them forming a stoichiometric complex on chromatin. Drastic examples include condensin, a five subunit complex, which only appears on M phase chromatin (Figure 3-1F) and MCM2-7, a six subunit complex, which only appears on interphase chromatin (Figure 3-1D).

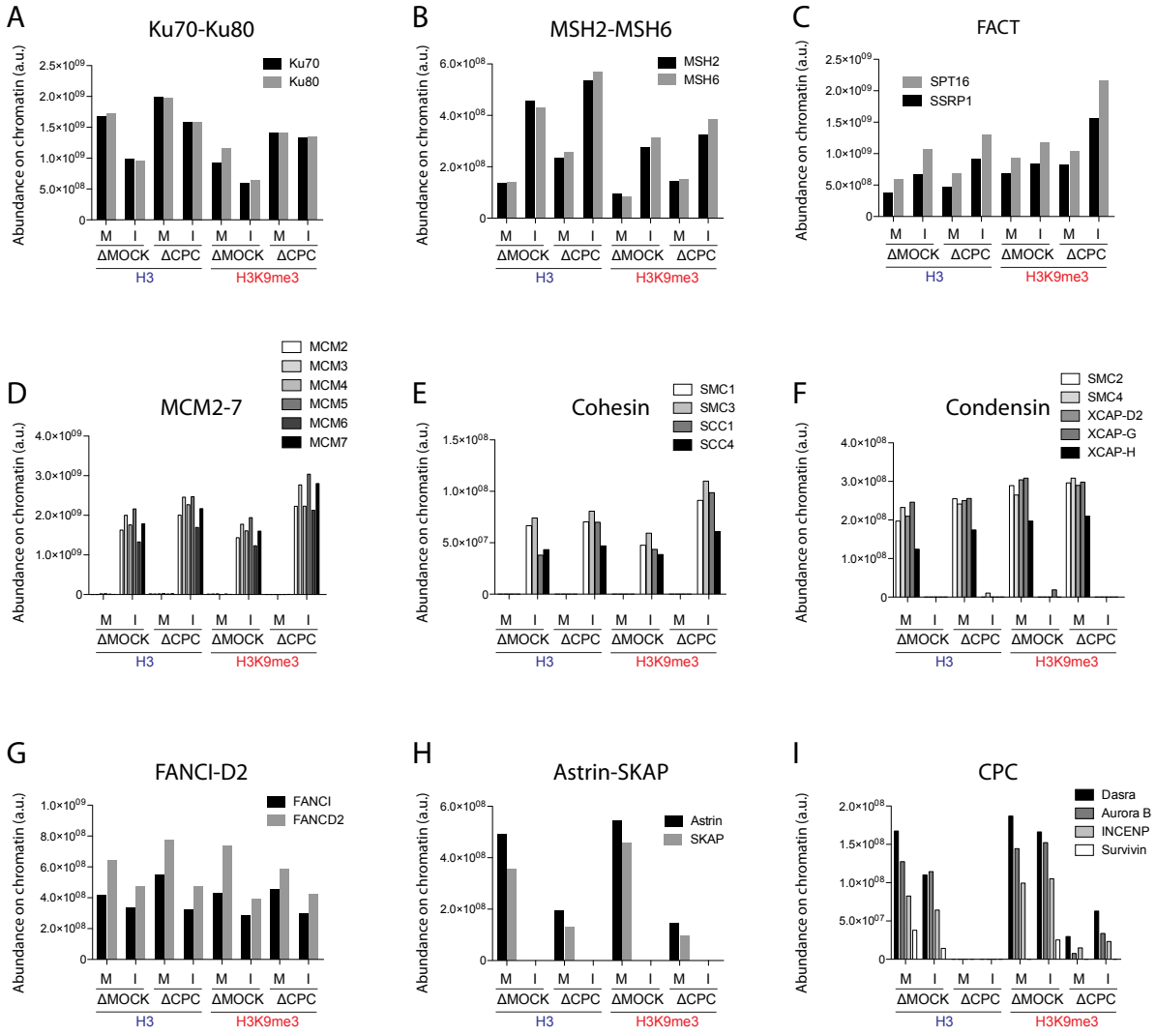

Figure 3-1. Subunits of 1:1 stoichiometric protein complexes are co-regulated on chromatin. (A-I) Abundance of individual subunits for each protein complex on eight different types of chromatin (cell cycle, ±CPC, ±H3K9me3). M: M phase, I: interphase.

Although many 1:1 stoichiometric complexes can be identified, I also identified non-1:1 co-regulated complexes on chromatin (Figure 3-2A-C) such as ATRX-DAXX, which binds H3K9me3 chromatin. However, ATRX is ~10 fold more abundant than DAXX on chromatin. Consistent with ATRX directly binding H3K9me3(Noh et al., 2015), these data suggest that approximately 90% of ATRX associates with chromatin independently of DAXX. Similarly, ATR-ATRIP (Figure 3-2B) and Topoisomerase II-TOPBP1, two complexes known to interact (Figure 3-2C) showed non-1:1 stoichiometries on chromatin.

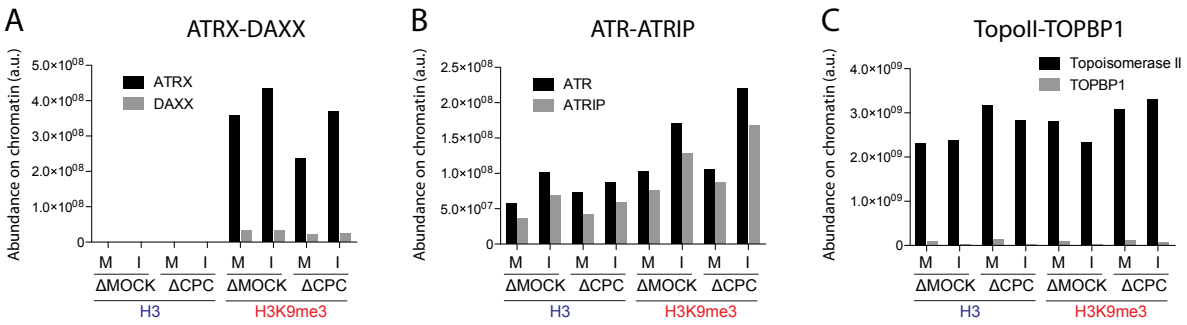

Figure 3-2. Subunits of non-1:1 stoichiometric protein complexes are co-regualted on chromatin. (A-C) Abundance of individual subunits for each protein complex on the indicated chromatin.

In an attempt to identify novel chromatin associated complexes, I used an unsupervised hierarchical clustering and ordering algorithm that identifies similarity between the proteomic profiles of different proteins (Van der Laan and Pollard, 2003)(Figure 3-3A). The algorithm is hierarchical; it first partitioned the data into broad categories mostly dependent on the cell cycle: M phase exclusive, M phase enriched, interphase exclusive, interphase enriched, and non-discriminant chromatin binding proteins. After broad characterization, the algorithm further partitioned the clusters until proteins of stable complexes were clustered together. For example, the five subunits of condensin cluster within the M phase exclusive cluster (Figure 3-3B). Even protein complexes that are only subtly affected by experimental conditions are clustered, such as FACT and ATR-ATRIP, which cluster within the interphase enriched cluster (Figure 3-3C) or Ku70-80, which clusters within the M phase enriched cluster (Figure 3-3D).

Figure 3-3. Hierarchical clustering of mass spectrometry data identifies known protein complexes. (A) Unsupervised clustering of chromatin associated proteins. A heat map of each protein's abundance on each indicated chromatin condition is displayed, with proteins enriched on a given chromatin sample colored yellow. Examples of known stoichiometric chromatin associated complexes cluster together and are indicated. Fine-grained protein complex clusters (left) and coarse-grained cell-cycle clusters (right) are labelled. (B-D) Close-up of individual clusters from (A). The dendrogram and individual proteins are labelled from the M phase specific (B), general (C) and M phase enriched (D) branches, with the indicated protein complexes highlighted in red.

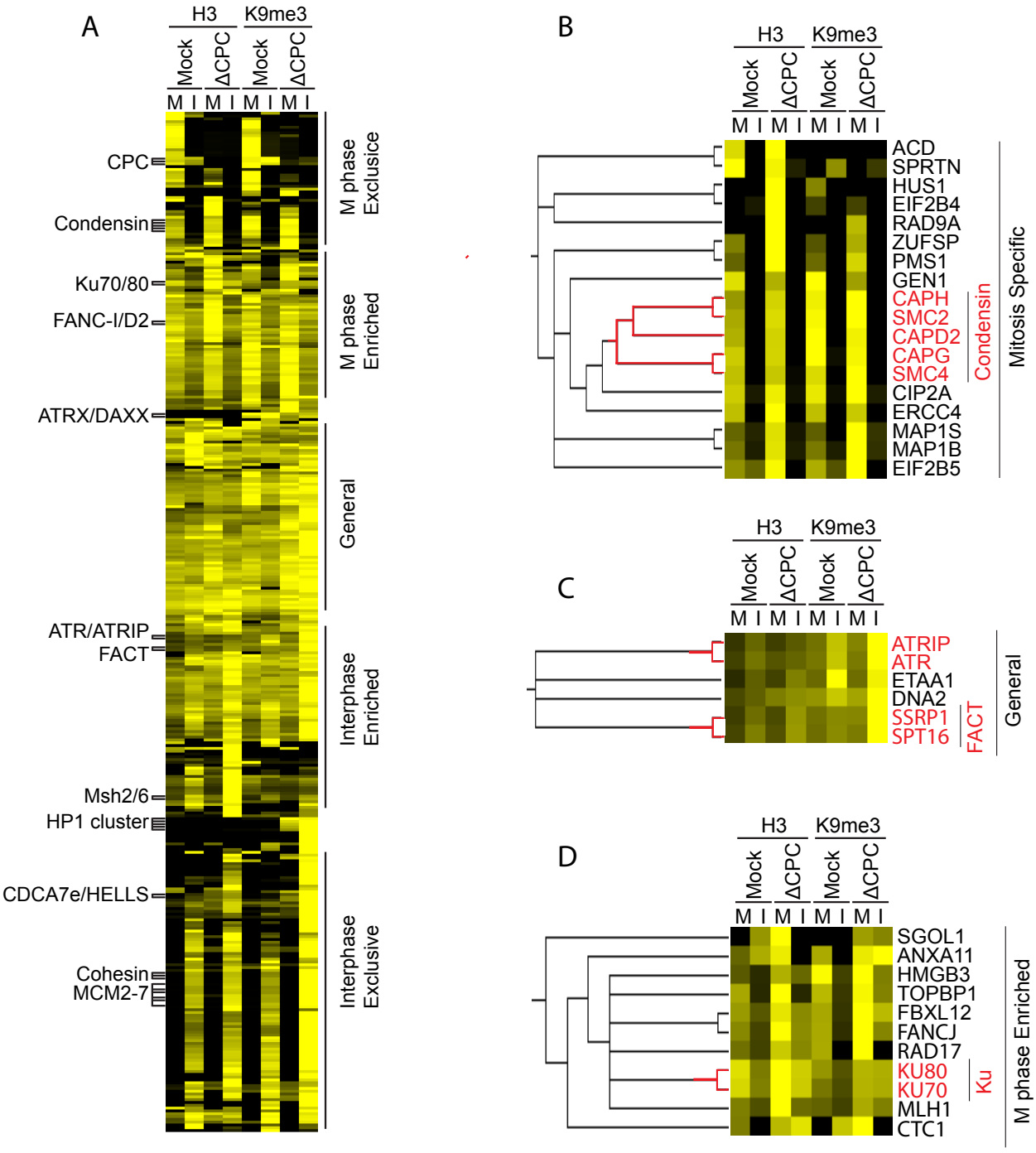
A
H3
K9me3
Mock
ΔCPC
Mock
ΔCPC
M I M I M I M I
CPC
Condensin
Ku70/80
FANC-I/D2
ATRX/DAXX
ATR/ATRIP
FACT
Msh2/6
HP1 cluster
CDCA7e/HELLS
Cohesin
MCM2-7
M phase Exclusice
M phase Enriched
General
Interphase Enriched
Interphase Exclusive
B
H3
K9me3
Mock
ΔCPC
Mock
ΔCPC
M I M I M I M I
ACD
SPRTN
HUS1
EIF2B4
RAD9A
ZUFSP
PMS1
GEN1
CAPH
SMC2
CAPD2
CAPG
SMC4
CIP2A
ERCC4
MAP1S
MAP1B
EIF2B5
Condensin
Mitosis Specific
C
H3
K9me3
Mock
ΔCPC
Mock
ΔCPC
M I M I M I M I
ATRIP
ATR
ETAA1
DNA2
SSRP1
SPT16
FACT
General
D
H3
K9me3
Mock
ΔCPC
Mock
ΔCPC
M I M I M I M I
SGOL1
ANXA11
HMGB3
TOPBP1
FBXL12
FANCJ
RAD17
KU80
KU70
MLH1
CTC1
Ku
M phase Enriched

HELLS-CDCA7 are co-regulated on chromatin

Based on my observation that subunits of protein complexes have similar proteomic profiles and cluster together, I sought to identify novel chromatin associated protein complexes. Intriguingly, HELLS, a putative nucleosome remodeler, clustered with a relatively uncharacterized protein, CDCA7 (introduced in chapter 1) (Figure 3-4A). HELLS-CDCA7 clustered within the interphase enriched cluster, specifically within a branch of the cluster that is modulated by the CPC (Figure 3-4A). As discussed in Chapter 1, the *Xenopus* egg only contains an embryonic paralog of CDCA7(Wuhr et al., 2014), which I name CDCA7e. Accordingly, I only detected CDCA7e and not CDCA7 or CDCA7L peptides on chromatin beads isolated from egg extract.

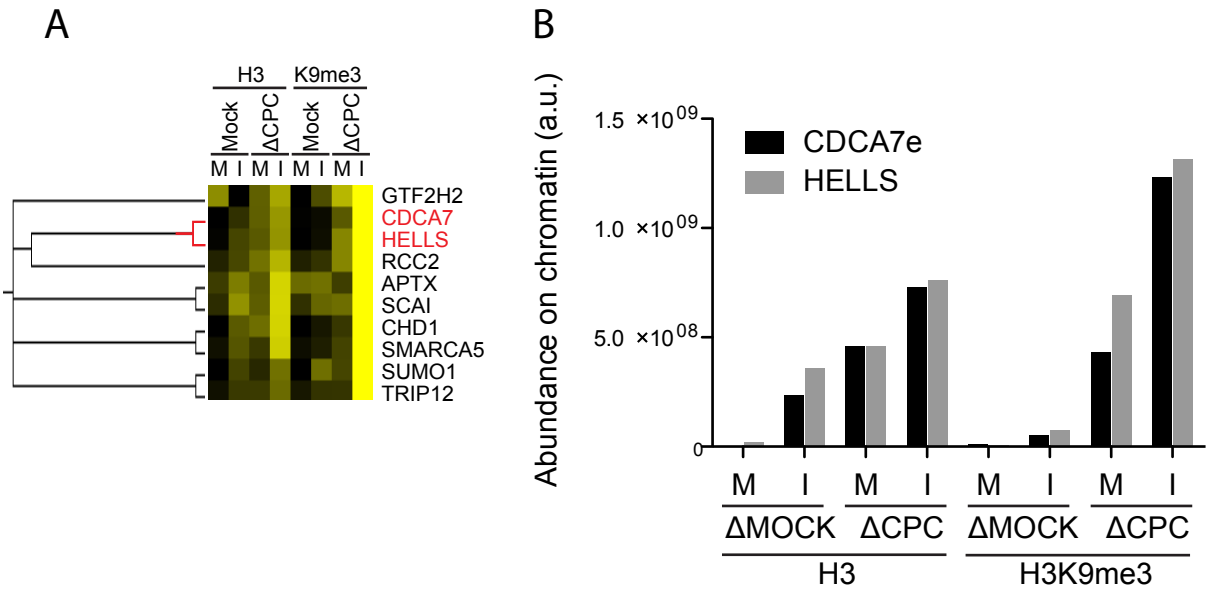

Figure 3-4. HELLS and CDCA7e are co-regulated on chromatin. (A) Close up of dendrogram containing HELLS and CDCA7e (red). (B) Abundance of HELLS and CDCA7e identified by LC-MS/MS on the indicated chromatin beads.

HELLS and CDCA7e showed a strikingly similar profile on chromatin, where both proteins were evicted from mitotic chromatin in a manner dependent on Aurora B, and both proteins showed little preference for H3 or H3K9me3 chromatin (Figure 3-4B). Western blotting confirmed the Aurora B-mediated cell cycle regulation of HELLS-CDCA7e (Figure 3-5A) on chromatin beads and immunofluorescence showed that HELLS was similarly regulated by Aurora B on sperm chromatin (Figure 3-5B). As H3S10 and H3S28 are major mitotic phosphorylation targets of the CPC, I wondered if these sites were important in the mitotic eviction of HELLS-CDCA7e. Therefore, I generated chromatin beads harboring alanine or aspartic acid to block or mimic phosphorylation at these residues, respectively. Interestingly, the CPC mediated eviction of HELLS-CDCA7e was entirely unaffected by mutations at these residues (Figure 3-5C). ISWI, another chromatin protein known to be evicted from mitotic chromatin by the CPC(MacCallum et al., 2002) was similarly unaffected by H3S10 and H3S28 phosphorylation (Figure 3-5C). Additionally, HELLS and CDCA7e do not bind H3 tail peptides incubated in *Xenopus* extracts (Figure 3-5D), consistent with Aurora B mediated regulation of HELLS-CDCA7 occurring independently of histone tail phosphorylation. Collectively, these data suggest that the Aurora B mediated mitotic regulation of HELLS-CDCA7 may occur by direct phosphorylation of HELLS-CDCA7 or through other chromatin phosphorylation events.

Figure 3-5. HELLS-CDCA7e is evicted from mitotic chromatin by the CPC.
(A) Western blot analyses of HELLS and CDCA7e co-purified with nucleosome beads recovered from M phase or interphase mock or CPC depleted extracts. (B) Immunofluorescence of HELLS and DAPI staining on mitotic sperm chromatin in mock or CPC depleted extract. Scale bar 15 μm. (C) Western blot analyses of proteins co-purified with nucleosome beads recovered from M phase mock or CPC depleted extracts. Nucleosomes containing wild-type H3 (SS), H3S10AS28A (SS), or H3S10DS28D (DD) were used. (D). Western blot analysis of proteins co-purified with peptide pulldown from mitotic extract and interphase extract. Scrambled H3 peptides were used to control for non-specific binding.

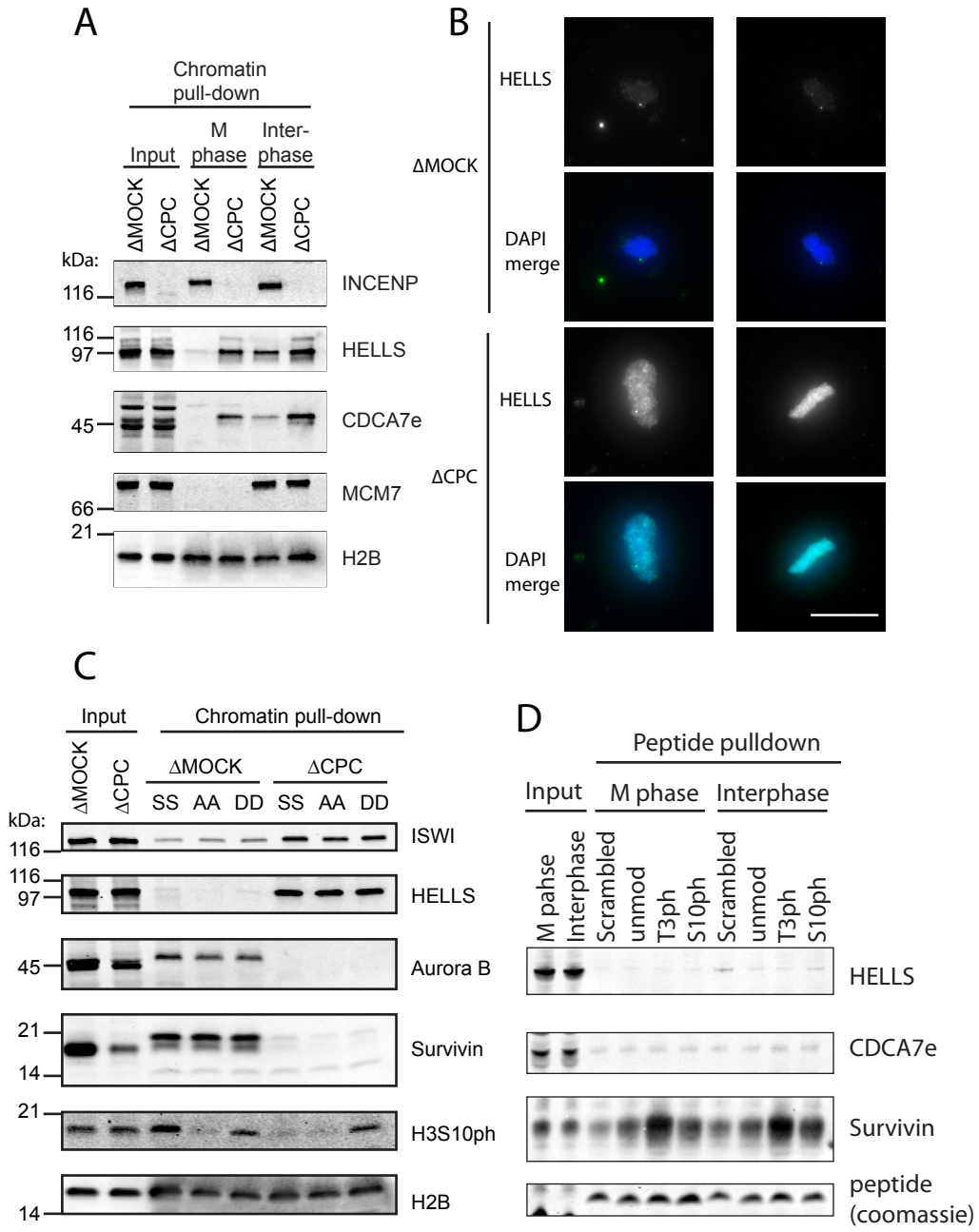
A
Chromatin pull-down
Input
M phase
Inter-phase
ΔMOCK
ΔCPC
ΔMOCK
ΔCPC
ΔMOCK
ΔCPC
kDa:
116
INCENP
116
97
HELLS
45
CDCA7e
66
MCM7
21
H2B
B
ΔMOCK
HELLS
DAPI merge
ΔCPC
HELLS
DAPI merge
C
Input
Chromatin pull-down
ΔMOCK
ΔCPC
ΔMOCK
ΔCPC
SS AA DD SS AA DD
kDa:
116
ISWI
116
97
HELLS
45
Aurora B
21
14
Survivin
21
H3S10ph
14
H2B
D
Peptide pulldown
Input
M phase
Interphase
M pahse
Interphase
Scrambled
unmod
T3ph
S10ph
Scrambled
unmod
T3ph
S10ph
HELLS
CDCA7e
Survivin
peptide (coomassie)

HELLS-CDCA7 require nucleosomes for chromatin association

Similar to many nucleosome remodelers, mass spectrometry analysis determined that HELLS-CDCA7e depends on nucleosomes to associate with chromatin beads in extract (Figure 3-6A). This dependency was verified by Western blotting and occurs in both interphase and M phase (Figure 3-6B). The linker histone only associates with nucleosomes (Figure 3-6B) and HELLS has been hypothesized to remodel H1 nucleosomes(Brzeski and Jerzmanowski, 2003{Zemach, 2013 #286), therefore I wondered if HELLS-CDCA7e depends on the linker histone for chromatin association. By immunodepleting embryonic H1 and performing mass spectrometry on nucleosome beads as before, I observed H1 dependent chromatin association of HELLS on mitotic chromatin beads (Figure 3-6C), however, by Western blotting this dependency was not seen on interphase chromatin (Figure 3-6D). Parsing this regulation will require further studies.

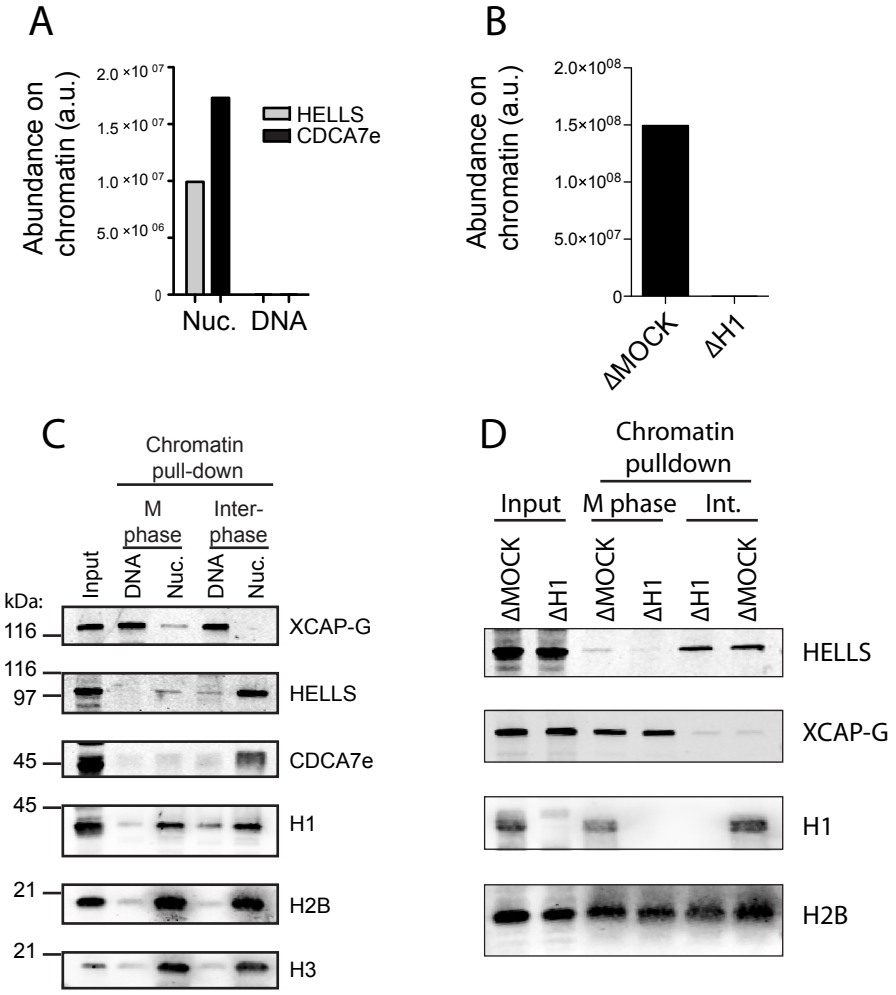

Figure 3-6. Histone regulation of HELLS and CDCA7e. (A) HELLS-CDCA7e requires nucleosomes to associate with chromatin in M phase. Abundance of HELLS and CDCA7e co-purified with nucleosome or DNA beads recovered from H3-H4 depleted M phase extracts determined by LC-MS/MS. (B) HELLS and CDCA7e require nucleosomes to associate with chromatin in interphase and M phase. Western blot analyses of proteins co-purified with nucleosome or DNA beads recovered from M phase or interphase H3-H4 depleted extracts. (C) HELLS requires H1 to associate with mitotic chromatin. MS analysis of proteins co-purified with nucleosome beads recovered from mock or H1 depleted M phase extracts. (D) Abundance of HELLS co-purified with nucleosome or DNA beads recovered from H3-H4 depleted M phase or interphase extracts determined by Western blotting.

Many nucleosome dependent chromatin binding proteins in physiological cytoplasmic extract(Zierhut et al., 2014) possess DNA binding activity in isolation, including H1(Nightingale et al., 1996), RCC1(Ohtsubo et al., 1989), topoisomerase II(Zierhut et al., 2014), and FACT(Winkler et al., 2011). To determine if HELLS and CDCA7e also possessed DNA binding activity, I purified maltose binding protein-CDCA7e (MBP-CDCA7e) from *E. coli*. Initial attempts at purifying HELLS from *E. coli* were unsuccessful, so HELLS-calmodulin binding peptide (HELLS-CBP) was purified from *S. cerevisiae*. Indeed, purified HELLS-CBP and MBP-CDCA7e also possess DNA binding activity (Figure 3-7) despite their nucleosome-dependency in egg extracts. I attempted to determine if their dependency could be recapitulated in vitro on mononucleosomes lacking linker DNA, however, HELLS-CBP binding to uncoupled beads complicated the results (Figure A-10). These results suggest that under physiological conditions, CDCA7e-HELLS is either outcompeted by other endogenous DNA binding proteins for binding to naked DNA, or that there is nucleosome dependent regulation of HELLS-CDCA7e, for example by RCC1 (discussed below).

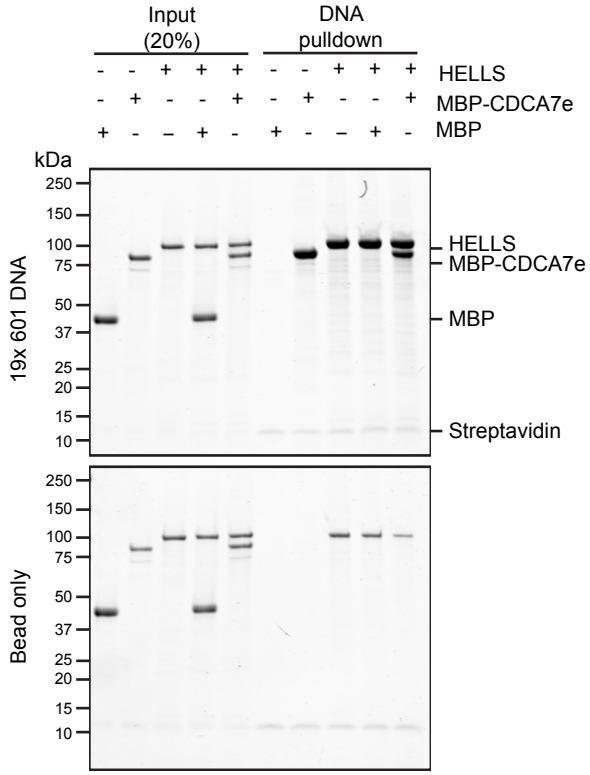

Figure 3-7. HELLS and CDCA7e have DNA binding activity in vitro. Coomassie stained gel of a pulldown of 19x601 DNA beads incubated with MBP, MBP-CDCA7e or HELLS-CBP. Uncoupled beads were used to control for non-specific binding.

HELLS-CDCA7e form a stoichiometric complex on chromatin

As HELLS-CDCA7e showed similar chromatin binding profiles, I hypothesized that they form a complex. Endogenous HELLS and CDCA7e interact in reciprocal co-immunoprecipitation experiments in mitotic *Xenopus* egg extract (Figure 3-8A-B). Exogenously expressed MYC-CDCA7e and HELLS-GFP co-immunoprecipitated in both interphase and M phase extract (Figure 3-8C), indicating that the interaction is not cell cycle regulated. By comparing the amount of HELLS-CDCA7 in the extract to the amount co-immunoprecipitated, I note that very little co-immunoprecipitation occurs, indicating that they do not form a stable 1:1 cytoplasmic complex. However, their interaction is likely direct since purified HELLS-CBP and MBP-CDCA7e co-immunoprecipitate in vitro (Figure 3-8D).

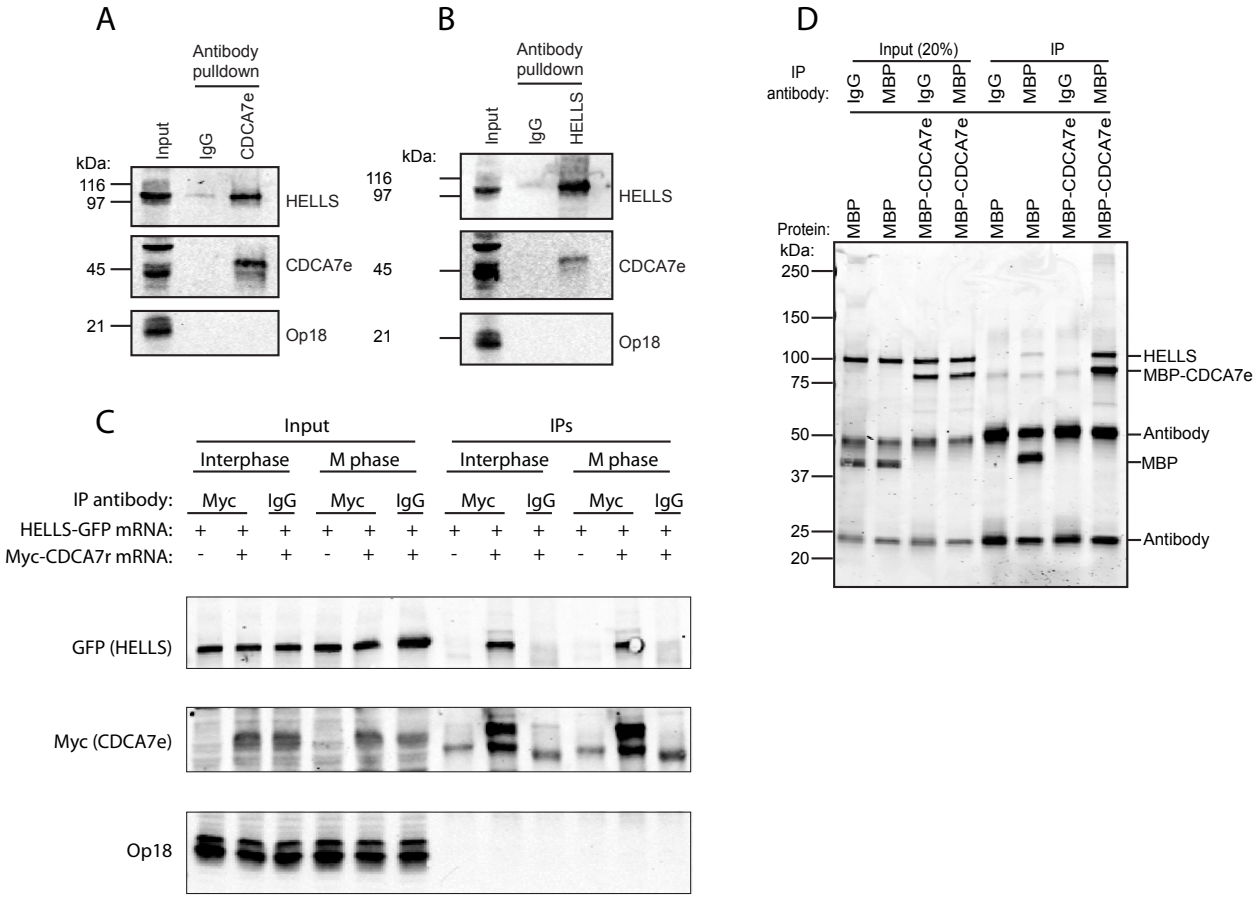

Figure 3-8. HELLS and CDCA7e interact in extract and in isolation. (A-B) Western blot analysis of CDCA7e (A) and HELLS (B) immunoprecipitation from M phase *Xenopus* extracts. Preimmune rabbit IgG was used to control for non-specific binding. (C) Western blot analysis of Myc-CDCA7e immunoprecipitations from M phase and interphase *Xenopus* extracts expressing HELLS-GFP and Myc-CDCA7e from mRNA. Preimmune rabbit IgG was used to control for non-specific binding. (D) Coomassie stained gel of purified HELLS-CBP co-immunoprecipitation with MBP-CDCA7e. Purified HELLS-CBP was incubated with MBP-CDCA7e or MBP and immunoisolation was performed using beads coupled with anti-MBP antibodies or control IgG.

Since HELLS-CDCA7e are co-regulated on chromatin and interact in vitro, I tested whether they were co-dependently recruited to chromatin. Depleting HELLS from *Xenopus* egg extract had no effect on CDCA7e recruitment to interphase chromatin beads, however CDCA7e depletion resulted in near-abolishment of HELLS chromatin association (Figure 3-9A). Mass spectrometry independently verified that CDCA7e recruits HELLS to chromatin, and further showed that this dependency persists on mitotic chromatin (Figure 3-9B). Importantly, exogenous addition of purified MBP-CDCA7e could rescue HELLS recruitment in CDCA7e depleted extracts in a dose-dependent manner (Figure 3-9C). Combined with the observation that CDCA7e can bind naked DNA and nucleosome arrays (Figure 3-9D), these results show that CDCA7e is the chromatin binding component of the HELLS-CDCA7e complex. Importantly, purified CDCA7e can also bind mononucleosomes lacking linker DNA (Figure 3-9E), indicating that CDCA7e can be recruited directly to nucleosomal DNA or to nucleosomes themselves.

Figure 3-9. CDCA7e is the DNA-binding module of the HELLS-CDCA7e chromatin associated complex. (A) Western blot analysis of proteins co-purified with nucleosome beads recovered from interphase extracts mock depleted or depleted of HELLS or CDCA7e. (B) Abundance of HELLS and CDCA7e on interphase and M phase chromatin mock depleted or depleted of HELLS or CDCA7e, determined by LC-MS/MS. (C) Western blot analysis of proteins co-purified with nucleosome beads purified from CDCA7e depleted interphase extract complemented with the indicated concentration of MBP-CDCA7e. (D) Coomassie stained gel of a pulldown of nucleosome array or DNA beads incubated with MBP-CDCA7e. Uncoupled beads were used to control for non-specific binding. (E) Coomassie stained gel of a pulldown of mononucleosome beads without linker DNA or naked DNA beads incubated with MBP-CDCA7e. Uncoupled beads were used to control for non-specific binding. (F) Abundance of HELLS and CDCA7e on chromatin beads purified from interphase extracts (top), determined by quantitative Western blotting (bottom) (n=6 replicates, SEM is shown).

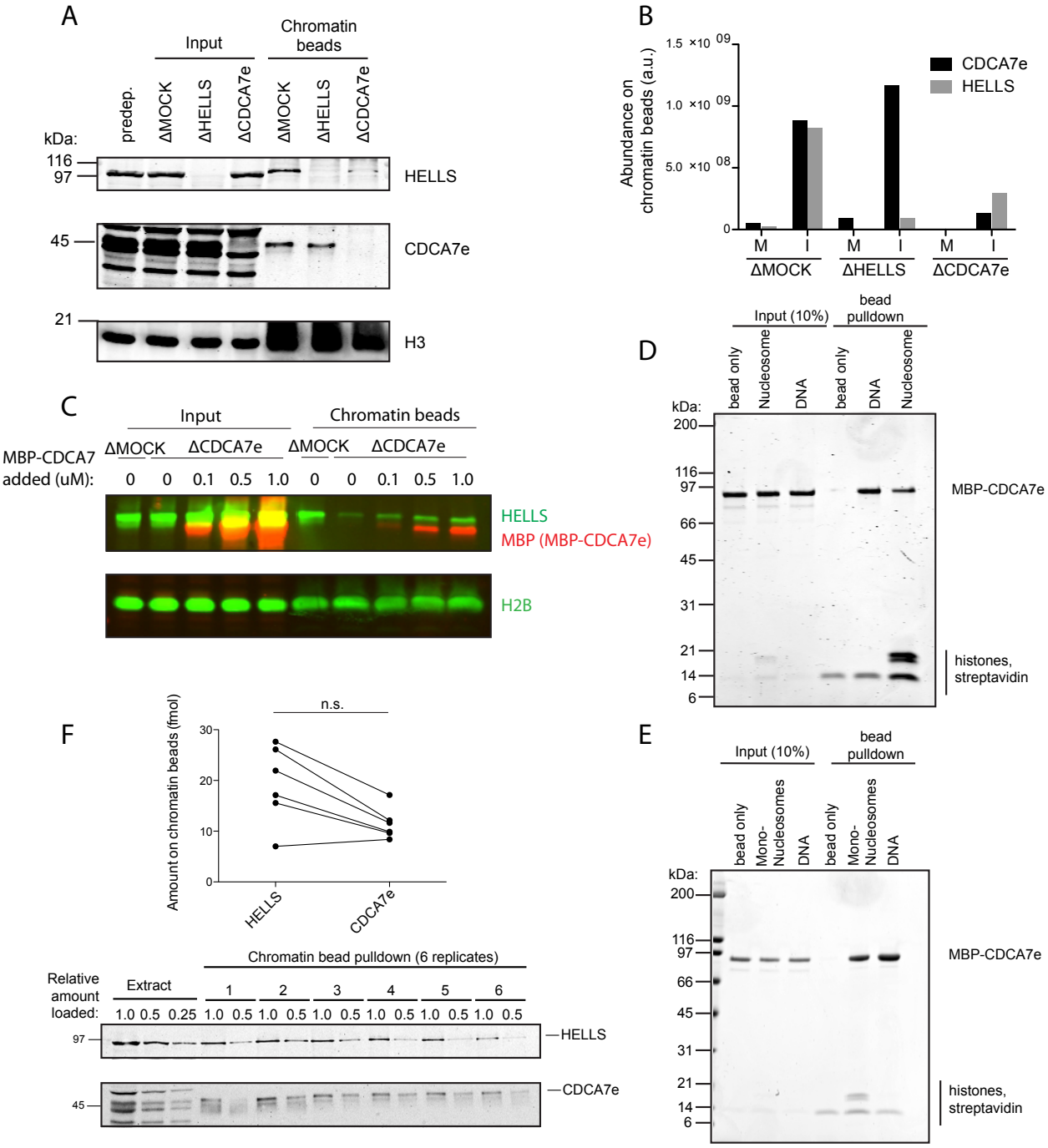
A
Input
Chromatin beads
predep.
ΔMOCK
ΔHELLS
ΔCDCA7e
ΔMOCK
ΔHELLS
ΔCDCA7e
kDa:
116
97
HELLS
45
CDCA7e
21
H3
B
Abundance on chromatin beads (a.u.)
1.5 ×10 09
1.0 ×10 09
5.0 ×10 08
0
CDCA7e
HELLS
M
I
M
I
M
I
ΔMOCK
ΔHELLS
ΔCDCA7e
C
Input
Chromatin beads
MBP-CDCA7 added (uM):
ΔMOCK
ΔCDCA7e
ΔMOCK
ΔCDCA7e
0 0 0.1 0.5 1.0 0 0 0.1 0.5 1.0
HELLS
MBP (MBP-CDCA7e)
H2B
D
Input (10%)
bead pulldown
bead only
Nucleosome
DNA
bead only
DNA
Nucleosome
kDa:
200
116
97
66
45
31
21
14
6
MBP-CDCA7e
histones, streptavidin
F
n.s.
Amount on chromatin beads (fmol)
30
20
10
0
HELLS
CDCA7e
Chromatin bead pulldown (6 replicates)
Relative amount loaded:
Extract
1
2
3
4
5
6
1.0 0.5 0.25 1.0 0.5 1.0 0.5 1.0 0.5 1.0 0.5 1.0 0.5 1.0 0.5
97
HELLS
45
CDCA7e
E
Input (10%)
bead pulldown
bead only
Mono-Nucleosomes
DNA
bead only
Mono-Nucleosomes
DNA
kDa:
200
116
97
66
45
31
21
14
6
MBP-CDCA7e
histones, streptavidin

Stable cytoplasmic complexes typically co-deplete all subunits when immunoprecipitated from egg extract (e.g. (Okuhara et al., 1999; Sampath et al., 2004)). Since neither HELLS nor CDCA7e depletion fail to reproducibly co-deplete the other component (Figure 3-9A), I hypothesize that they do not form a stable cytoplasmic complex. Instead, they likely only form a stoichiometric complex on chromatin, since equimolar amounts of HELLS and CDCA7e were detected across a variety of mass spectrometry experiments (Figure 3-4), which was independently verified by quantitative Western blotting (Figure 3-9F).

HELLS-CDCA7e is a nucleosome remodeling complex

As introduced in Chapter 1, HELLS is a putative nucleosome remodeling complex, however, mouse HELLS has no nucleosome remodeling activity in isolation(Burrage et al., 2012). I hypothesized that HELLS-CDCA7e forms a functional nucleosome remodeling complex. To assay for nucleosome remodeling, I used mononucleosome engineered to contain a restriction enzyme site that is protected by histones (Figure 3-10A). Upon nucleosome sliding, the restriction site is exposed and can be cleaved. Using this assay, I verified that purified HELLS-CBP alone has nearly non-detectable nucleosome remodeling activity. However, HELLS-CDCA7e has robust nucleosome sliding activity that is dependent on ATP. As expected, purified MBP-CDCA7e alone has no nucleosome sliding activity (Figure 3-10).

Figure 3-10. HELLS and CDCA7e comprise a nucleosome remodeling complex. (A) Restriction enzyme accessibility nucleosome remodeling assay with HELLS-CBP and MBP-CDCA7e. 601-positioned mononucleosomes with a *Pst*I site engineered 15 bp into the nucleosome with 20 bp flanking DNA on each end were incubated with the indicated remodeling proteins and *Pst*I. Productive nucleosome sliding exposes the *Pst*I site, resulting in cleaved DNA (arrow). Following the reaction, DNA was purified and resolved on a 10% polyacrylamide gel and visualized with SYBR gold. (B) Native gel nucleosome remodeling assay with HELLS-CBP and MBP-CDCA7e. Center-positioned mononucleosomes (same as A) were incubated with the indicated remodeling proteins. Reactions were stopped, resolved on a 5% polyacrylamide gel, and visualized with SYBR gold. Sliding results in end positioned nucleosomes, which migrate faster. (C) Native gel nucleosome remodeling assay. End-positioned (left) or center-positioned mononucleosomes (right) were incubated with the indicated remodeling proteins. Reactions were stopped, resolved on a 5% polyacrylamide gel, and visualized with SYBR gold. (D) Restriction enzyme accessibility nucleosome remodeling assay. 601-positioned mononucleosomes with a HaeIII site 11 bp into the nucleosome with 60 bp flanking DNA on the 3' end were incubated with the indicated remodeling proteins and HaeIII. Productive nucleosome sliding exposes the HaeIII site, resulting in cleaved DNA (arrow). DNA was resolved on a 10% polyacrylamide gel and visualized with SYBR gold.

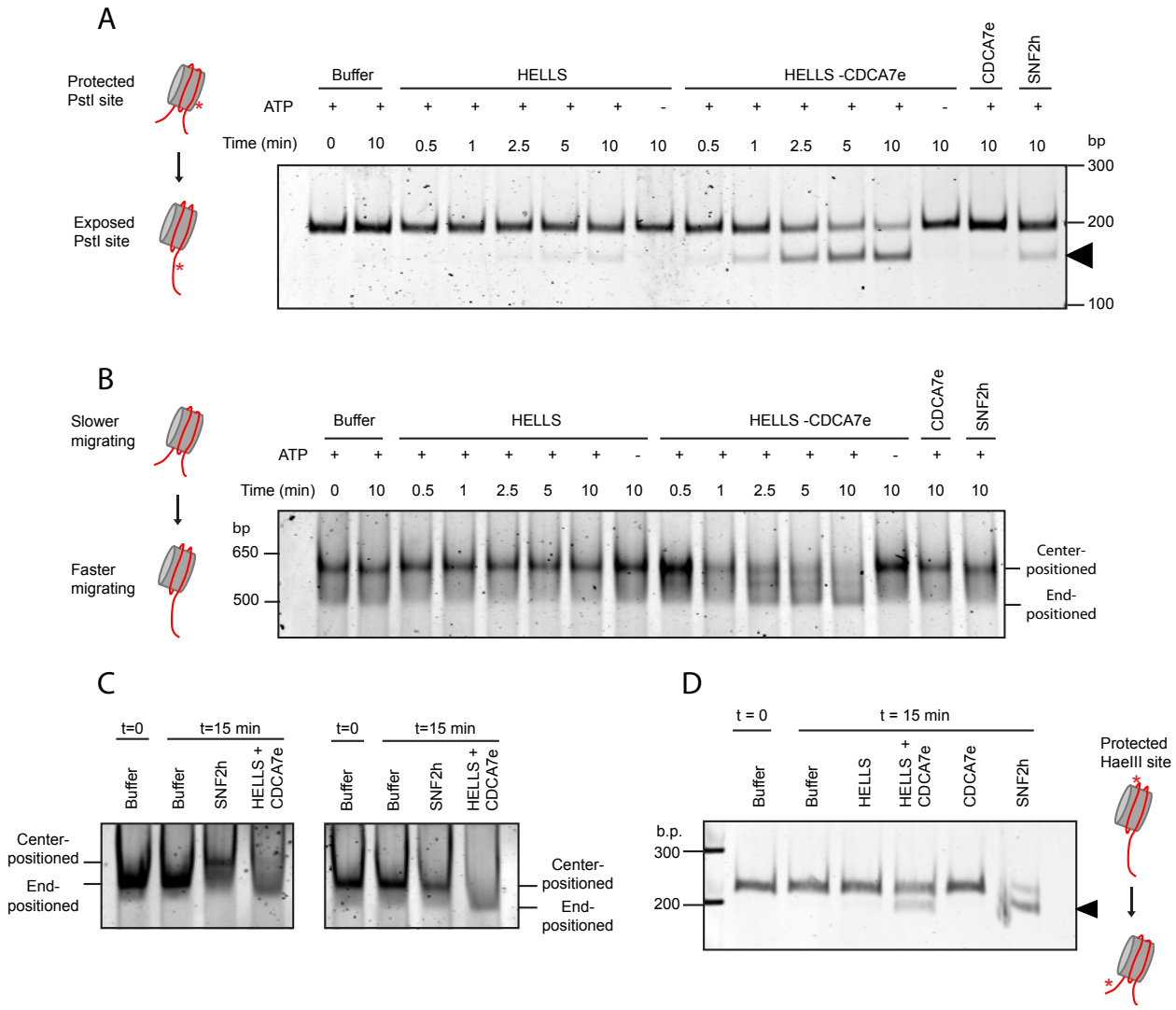
A
Protected PstI site
Exposed PstI site
Buffer
HELLS
HELLS -CDCA7e
CDCA7e
SNF2h
ATP
Time (min)
bp
300
200
100
B
Slower migrating
Faster migrating
650
500
Center-positioned
End-positioned
C
t=0
t=15 min
Buffer
SNF2h
HELLS + CDCA7e
D
t = 0
t = 15 min
HELLS
CDCA7e
b.p.
Protected HaeIII site

Nucleosome remodelers can slide nucleosomes to the end or middle of DNA fragments, which can be distinguished by native gel electrophoresis. Using this principle, I saw that HELLS-CDCA7e can robustly slide a center-positioned nucleosome to the end of a DNA fragment, but has no effect on an end-positioned nucleosome (Figure 3-10B). As expected, SNF2h, which slides nucleosomes from the end to the center of DNA fragments(He et al., 2006), shows the reciprocal activity (Figure 3-10C). Interestingly, in a restriction enzyme-based assay starting with an end-positioned nucleosome, I still see sliding activity (Figure 3-11D), indicating that although HELLS-CDCA7e prefers to end-position nucleosomes, the complex can still mobilize these nucleosomes. These results show that indeed HELLS-CDCA7e is a nucleosome remodeling complex that requires both components for remodeling activity.

Nucleosome remodelers utilize energy from ATP hydrolysis to mobilize nucleosomes. As was previously shown(Burrage et al., 2012), HELLS possesses DNA-dependent ATPase activity (Figure 3-11A,B), even in the absence of CDCA7e. Interestingly, CDCA7e increases the ATPase activity of HELLS ~2 fold. Collectively, these results show that CDCA7e stimulates HELLS ATPase activity, and couples its ATPase activity to productive remodeling. As HELLS-CDCA7e is a bona fide nucleosome remodeling complex, these results reconcile previous studies that have assumed HELLS is a nucleosome remodeler(Burrage et al., 2012; Ren et al., 2015), even though it possesses no nucleosome remodeling activity in isolation.

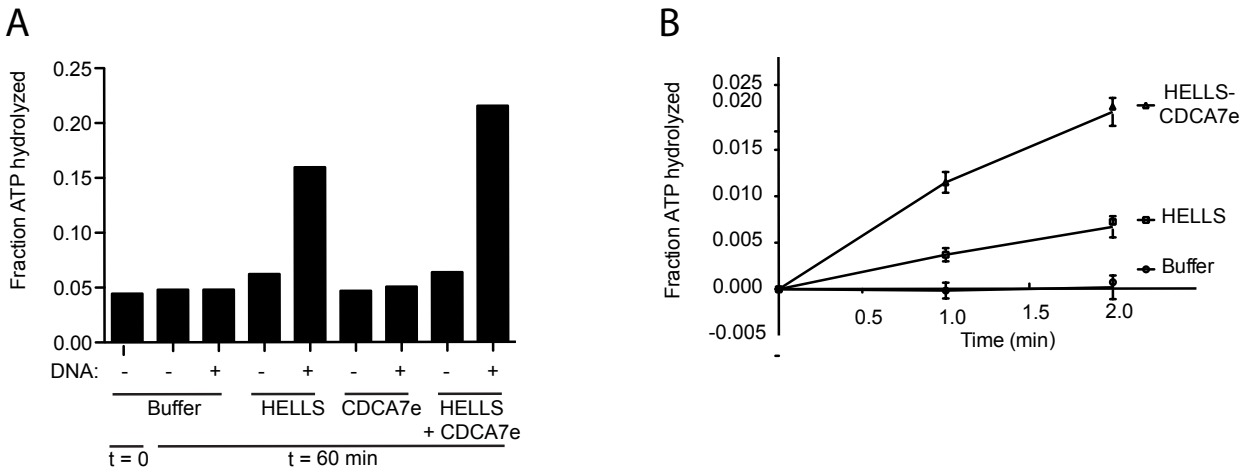

Figure 3-11. (A-B) Quantification of ATPase activity. The indicated proteins were incubated with gamma-33P ATP for the indicated times at 37 ˚C (A) or 16 ˚C (B) for the indicated time. Reaction was separated by TLC, exposed to a PhosphorStorage screen, and the fraction of hydrolyzed ATP was quantified. In (B), mean and standard deviation from n = 3 distinct replicates are displayed.

HELLS-CDCA7e is required for mitotic chromatin structure

HELLS has a reported role in facilitating DNA methylation(Myant and Stancheva, 2008; Zhu et al., 2006), therefore, I tested whether HELLS-CDCA7e depletion had an effect on DNA methylation in *Xenopus* egg extract. Using a radiolabeled nucleotide incorporation assay, I saw no defect in replication-coupled DNA methylation following HELLS depletion (Figure 3-12A). DNA methylation can also be monitored indirectly in *Xenopus* egg extract. As nuclei replicate, the resulting hemi-methylated chromatin acquires H3K23 ubiquitylation, an important transient intermediate in DNMT1 mediated DNA methylation(Nishiyama et al., 2013). Disruption of DNA methylation (by depleting DNMT1, for example) results in an accumulation of H3K23 ubiquitylation, which can be monitored by a slower migrating H3 species. While I saw robust H3 ubiquitylation upon DNMT1 depletion, I hardly see an effect following HELLS-CDCA7e depletion, in agreement with a functional maintenance DNA methylation pathway in the absence of HELLS-CDCA7e (Figure 3-12B). These results contradict the reported role of HELLS in DNMT1-mediated DNA methylation in *Xenopus*(Dunican et al., 2015). However, these results are consistent with HELLS-independent DNMT1targeting to chromatin(Yan et al., 2003) and no detectable de novo DNA methyltransferases in the *Xenopus* egg(Wuhr et al., 2014). As these are both bulk DNA methylation assays, I note that HELLS-CDCA7 may still facilitate site-specific methylation in a small portion of the genome that I may have missed.

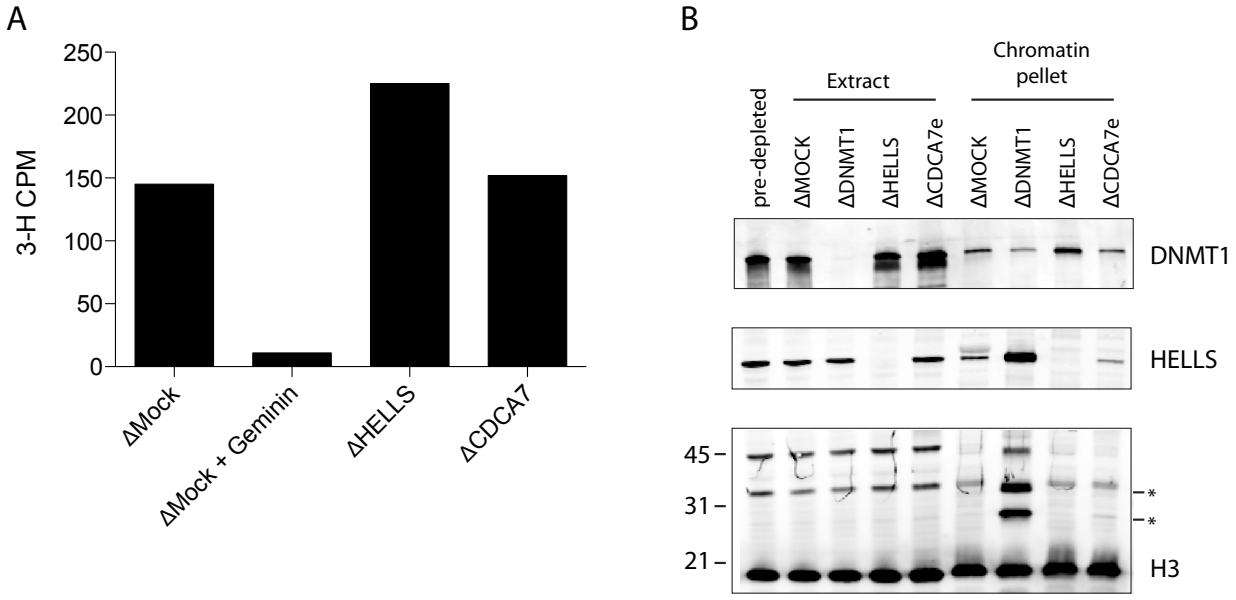

Figure 3-12. HELLS and CDCA7e are not required for replication dependent DNA methylation maintenance. (A) 3-H SAM incorporation into interphase nuclei replicated in mock depleted extract or extract depleted of HELLS or CDCA7e. Geminin was used where indicated to inhibit DNA replication. (B) Western blot analysis of *Xenopus* extract and sperm nuclei replicated in *Xenopus* extract and pelleted. Disruption in DNA methylation results in H3 ubiquitylation, indicated by asterisks.

A dramatic phenotype seen in ICF patients is the stretching of juxtacentromeric heterochromatin(Smeets et al., 1994). I wondered if this phenotype could be recapitulated and studied in *Xenopus* egg extracts. Replicated, paired chromosomes can be visualized in *Xenopus* egg extracts by diluting mitotic spindles formed in the extract, which dissolves the spindle and yields individualized chromosomes(Funabiki and Murray, 2000). However, depletion of HELLS-CDCA7e resulted in chromosomes with primary constrictions that were indistinguishable from wild type chromosomes.

While inspecting mitotic chromosomes, I noticed that at a low frequency, entire CDCA7e depleted chromosomes were axially stretched and thin, which were term “fragile” (Figure 3-13A,B). In some experiments, all chromosomes were longer, with a less noticeable fragile phenotype (Figure 3-13C). This phenotype was also seen upon HELLS depletion, but not consistently (compare Figures 3-13 and 3-17, for example). Although the exact molecular nature of the mitotic chromosome defect is unknown, chromosome length can be rescued by adding exogenous recombinant CDCA7e to CDCA7e depleted extract, indicating that the defect is not due to co-depletion of other proteins (Figure 3-13D,E). Proper chromosome morphology can be rescued by adding back CDCA7e at the start of the experiment, or only after chromosomes have replicated during the subsequent M phase, showing that M phase activity of CDCA7e is sufficient for its chromosome formation activity (Figure 3-13D,E). However, this experiment does not definitively show that HELLS-CDCA7e acts during mitosis under normally conditions, since it is possible that HELLS-CDCA7e typically acts only during interphase, but if needed, could fulfill its function in M phase.

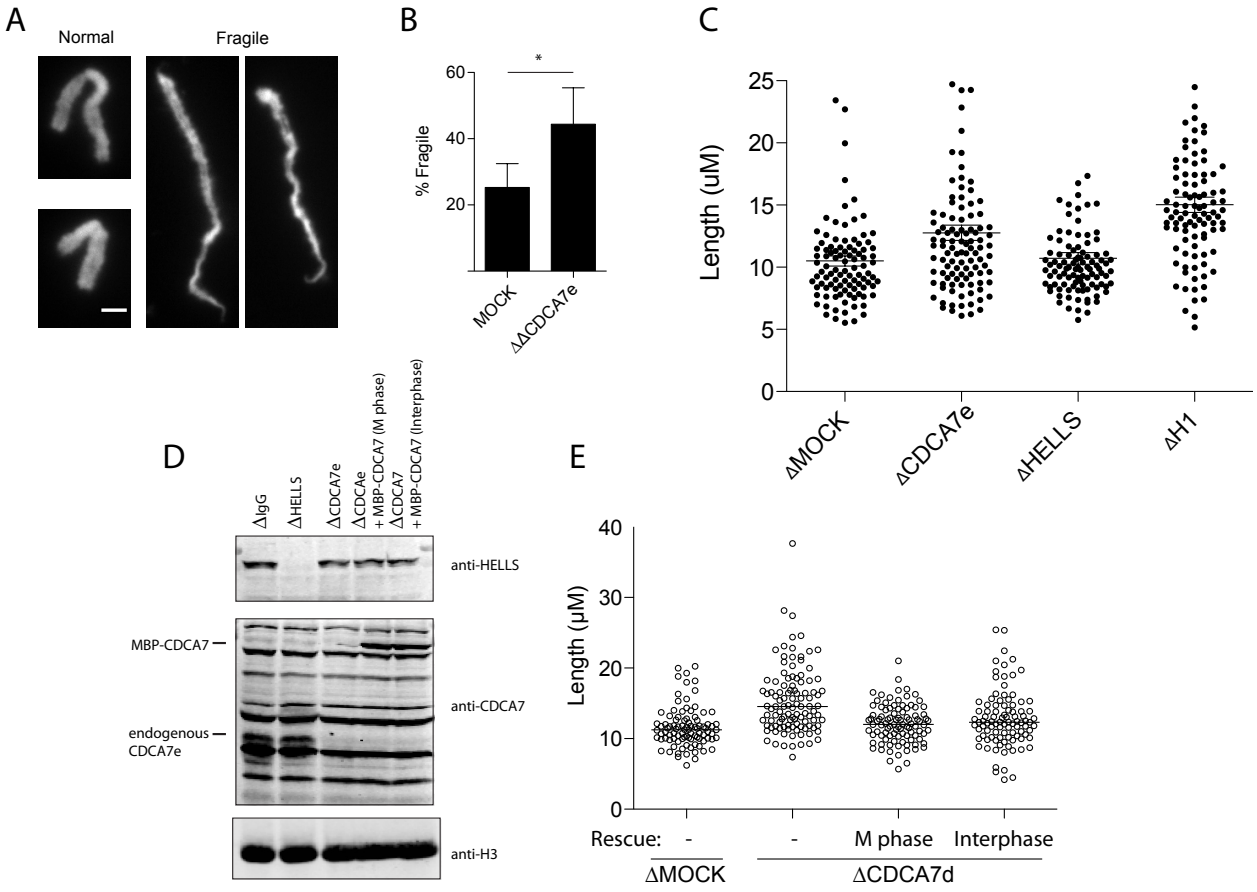

Figure 3-13. CDCA7e is required for proper mitotic chromosome morphology. (A-B) Chromosomes (examples in A) were formed in mock or CDCA7e depleted extract, stained with DAPI and then manually scored for fragility (quantified in B). (C) Chromosomes were formed in mock, CDCA7, HELLS or H1 depleted extract, stained with DAPI, and the axial length was measured. Each point is the length of an individual chromosome. (D-E) Exogenously added MBP-CDCA7e can rescue the chromosome morphology defect in interphase or mitosis. Western blot analysis (D) of CDCA7e depletion and add-back, and chromosome length measurements (E) from chromosomes formed in mock or CDCA7 extract. Where indicated, CDCA7e depleted extract was complimented with CDCA7 either during interphase, or after replication in the following mitosis.

To better understand the mitotic chromosome morphological defect, I stained chromosomes with PicoGreen. PicoGreen quantitatively stains DNA, allowing me to overcome the confounding effect that *Xenopus laevis* chromosomes naturally vary in length by 3-fold(Session et al., 2016). As expected, there is a linear relationship between the total H2B staining and the total PicoGreen staining on chromosomes (Figure 3-14A). Using PicoGreen as an estimate for DNA amount, I saw that fragile chromosomes are longer than expected for their quantity of DNA (Figure 3-14B,C). Additionally, fragile chromosomes have less PicoGreen staining per unit area (Figure 3-14D). Collectively, these data show that in the absence of CDCA7e, chromosomes tend to decompact and become axially elongated, reminiscent of H1 and condensin II depletion. Further experiments are required to determine the precise molecular defect.

Figure 3-14. CDCA7e depleted fragile chromosomes are decompacted and axially elongated. (A) PicoGreen and H2B intensity on individual chromosomes formed in *Xenopus* egg extract. (B) PicoGreen intensity and length measurements for individual chromosomes formed in untreated (top) or CDCA7 depleted (bottom) extract. Fragile chromosomes are labeled in red. Note that the fragile chromosomes are longer than expected for their DNA content. (C) Images of chromosomes from (B). Scale bar 1μm. (D) Measurement of average PicoGreen intensity, a surrogate for DNA compaction, on fragile and normal chromosomes formed in mock or CDCA7 depleted extract. Each dot is a measurement for a single chromosome.

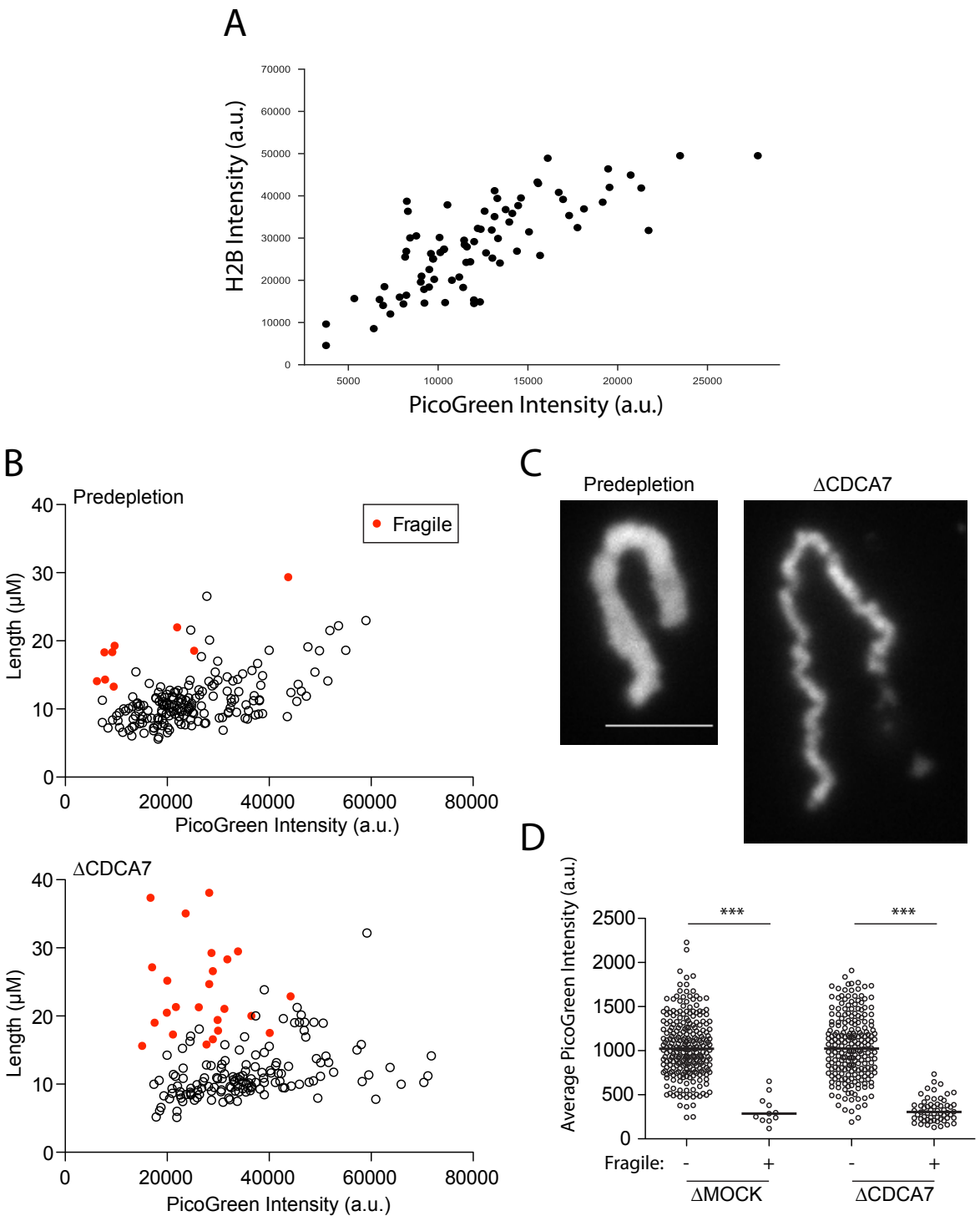
A
H2B Intensity (a.u.)
PicoGreen Intensity (a.u.)
B
Predepletion
Fragile
Length (μM)
PicoGreen Intensity (a.u.)
ΔCDCA7
C
Predepletion
ΔCDCA7
D
Average PicoGreen Intensity (a.u.)
***
***
Fragile:
ΔMOCK
ΔCDCA7

ICF patient mutations reveal functions of CDCA7

Thus far, four CDCA7 mutations have been identified in ICF patients, which each map to the conserved zinc finger domain(Thijssen et al., 2015). Interestingly, they are all adjacent to a CXXC motif, raising the possibility that the ICF mutations disrupt the zinc finger domain (Figure 3-15A). To determine the molecular defect that these CDCA7 mutations cause, I purified recombinant CDCA7e engineered with three separate corresponding patient mutations (R232C, R232H, or R262H). All three tested ICF mutants could robustly interact with HELLS, indicating that the HELLS-CDCA7 complex can still form in ICF patients (Figure 3-15B,C). In an in vitro DNA binding assay, CDCA7e-R232C/H mutations greatly disrupted DNA binding of the protein (Figure 3-15D). Similarly, these mutations failed to bind sperm chromatin in *Xenopus* egg extract and failed to recruit HELLS to chromatin. Interestingly, CDCA7e-R262H showed robust DNA-binding activity in vitro, but could not associate with sperm chromatin in egg extract, suggesting that it may have a problem binding nucleosomal DNA (Figure 3-15E). Collectively, these data indicate that a primary defect of CDCA7 ICF mutations is a failure to recruit the HELLS-CDCA7 complex to chromatin under physiological conditions.

Figure 3-15. CDCA7 ICF patient mutations disrupt DNA binding and fail to recruit the HELLS-CDCA7 complex to chromatin. (A) Alignment of CDCA7 zinc finger domains from the indicated species. The CXXC motifs are underlined, and residues with identified ICF mutations are highlighted in red. (B) Coomassie staining (top) and autography (bottom) of HELLS-CDCA7e ICF mutant immunoprecipitation. Recombinant MBP-CDCA7e harboring the indicated ICF mutations was immunoprecipitated from reticulocyte lysate expressing 35S-labeled HELLS-GFP or GFP. (C) Quantification of (B). Mean and range from two independent experiments are plotted. (D) Coomassie stained gel of a pulldown of DNA beads incubated with MBP-CDCA7e harboring the indicated ICF mutations. Uncoupled beads (bottom) were used to control for non-specific binding. (E) Western blot analyses of proteins co-purified with chromatin beads recovered from interphase extracts mock depleted or depleted of CDCA7e. Beads coated with 19x601 naked DNA were chromatinized in interphase extract for 90 min prior to addition of 1 μM recombinant MBP-CDCA7e harboring the indicated ICF mutations. Following an additional 60 min incubation, chromatin beads were recovered.

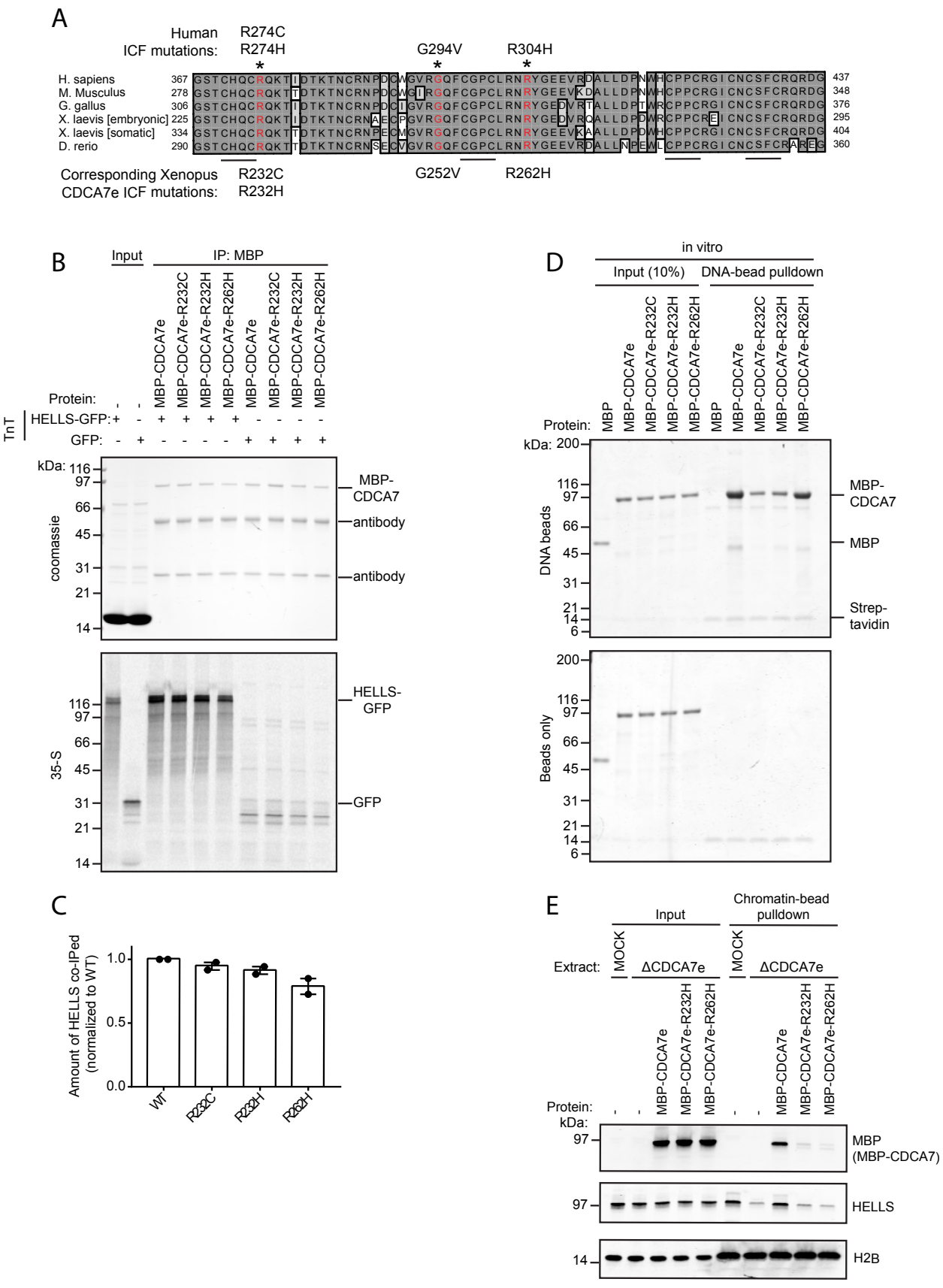
A
Human ICF mutations:
R274C
R274H
G294V
R304H
H. sapiens 367 GSTCHQCRQKTIDTKTNCRNPDCWGVRGQFCGPCLRNRYGEEVRDALLDPNWHCPPCRGICNCSFCRQRDG 437
M. Musculus 278 GSTCHQCRQKTTDTKTNCRNPDCWGIRGQFCGPCLRNRYGEEVKDALLDPNWHCPPCRGICNCSFCRQRDG 348
G. gallus 306 GSTCHQCRQKTIDTKTNCRNPDCIGVRGQFCGPCLRNRYGEDVRTALLDPTWRCPPCRGICNCSFCRQRDG 376
X. laevis [embryonic] 225 GSTCHQCRQKTIDTKTNCRNAECPGVRGQFCGPCLRNRYGEDVRQALLDPDWRCPPCREICNCSFCRQRDG 295
X. laevis [somatic] 334 GSTCHQCRQKTTDTKTNCRNPECMGVRGQFCGPCLRNRYGEEVKAALLDPDWHCPPCRGICNCSFCRQRDG 404
D. rerio 290 GSTCHQCRQKTTDTKTNCRNSECVGVRGQFCGPCLRNRYGEEVRDALLNPEWLCPPCRGICNCSFCRARDG 360
Corresponding Xenopus CDCA7e ICF mutations:
R232C
R232H
G252V
R262H
B
Input
IP: MBP
MBP-CDCA7e
MBP-CDCA7e-R232C
MBP-CDCA7e-R232H
MBP-CDCA7e-R262H
Protein:
TnT
HELLS-GFP:
GFP:
kDa:
coomassie
MBP-CDCA7
antibody
antibody
35-S
HELLS-GFP
GFP
C
Amount of HELLS co-IPed (normalized to WT)
WT
R232C
R232H
R262H
D
in vitro
Input (10%)
DNA-bead pulldown
Protein:
kDa:
DNA beads
Beads only
MBP-CDCA7
MBP
Strep-tavidin
E
Input
Chromatin-bead pulldown
Extract:
MOCK
ΔCDCA7e
Protein:
kDa:
MBP (MBP-CDCA7)
HELLS
H2B

I next tested whether the CDCA7 ICF patient mutations disrupt chromatin remodeling by the complex. Surprisingly, HELLS-CDCA7 harboring ICF patient mutations remodeled nucleosomes at a rate similar to wild type HELLS-CDCA7 (Figure 3-15A). Since the previous remodeling experiments were done with HELLS-CDCA7 in excess, it is possible that the ICF mutations have a remodeling defect that is masked by having excess protein. I therefore performed the same experiment with equimolar remodeler:nucleosome and with nucleosomes in excess. Under these conditions, HELLS-CDCA7 harboring ICF patient mutations still remodeled nucleosomes as effectively as the wildtype counterpart (Figure 3-15B,C). Collectively, these data suggest that in vivo CDCA7e serves two separable functions whereby CDCA7e is required to recruit HELLS to chromatin, and once there, CDCA7e activates HELLS remodeling activity. The CDCA7 ICF mutations tested here retain the ability to activate HELLS remodeling activity, however, they are deficient for chromatin targeting of the complex.

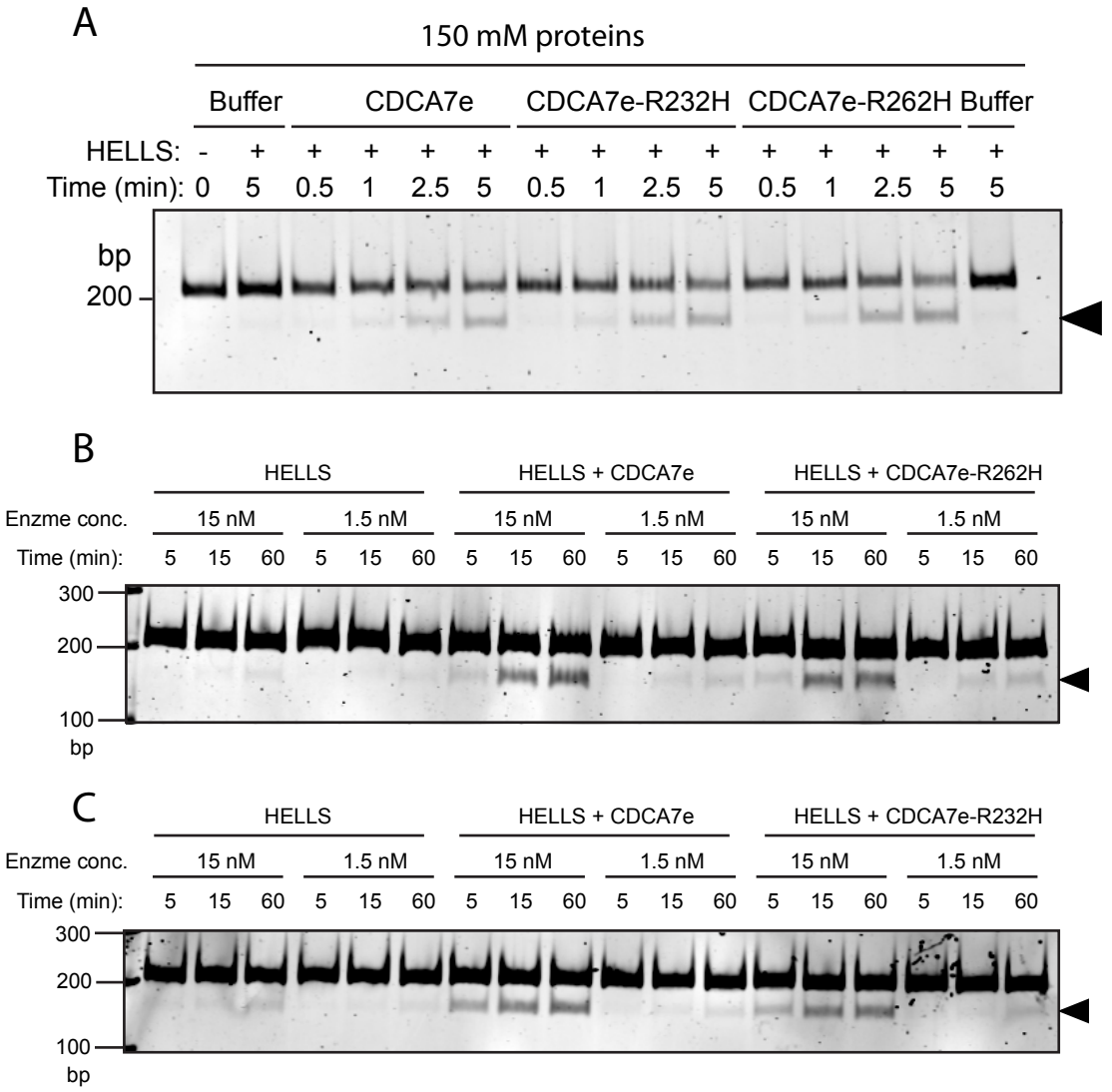

Figure 3-16. CDCA7 ICF patient mutations still stimulate HELLS remodeling activity. (A-C) Restriction enzyme accessibility nucleosome remodeling assay. 601-positioned mononucleosomes (15 nM) with a 34 and 15 bp flanking DNA on the 5' and 3' end, respectively, incubated with the indicated remodeling proteins at their indicated concentration and *MspI* endonuclease. Productive nucleosome sliding exposes an *Msp*I site, resulting in cleaved DNA (arrow). After reaction, DNA was purified and resolved on a 10% polyacrylamide gel and visualized with SYBR gold. Reactions were performed with remodeling proteins in excess (A) or limiting (B-C).

Expectedly, CDCA7 ICF mutations that cannot bind chromatin in *Xenopus* egg extract, and cannot recruit HELLS, also could not rescue the chromosome morphology defect of CDCA7 depleted chromosomes. Complementation with CDCA7 ICF mutations still caused axial elongation of mitotic chromosomes, similar to CDCA7 depletion (Figure 3-16A, B). At present, I am unsure if this phenotype is at all connected to the stretched juxtacentromeric chromatin phenotype seen in ICF patients (discussed in Chapter 5). Collectively, these data show that the DNA binding of CDCA7 and HELLS recruitment is required for proper mitotic chromosome structure.

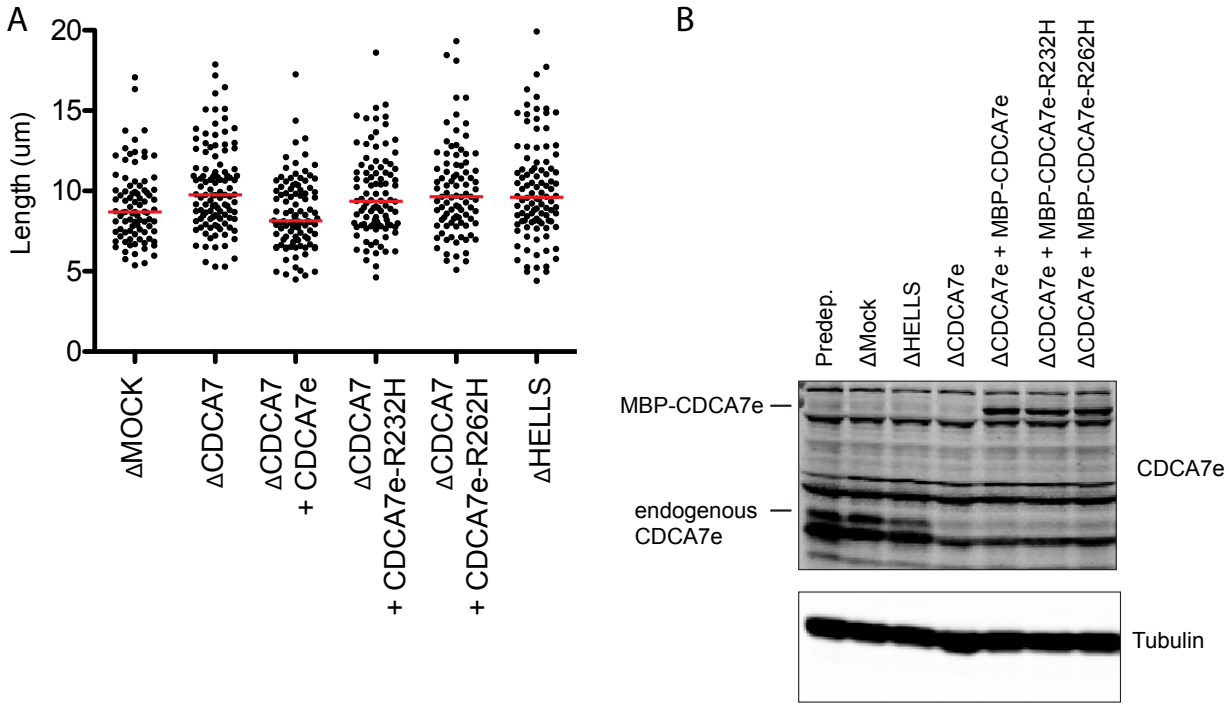

Figure 3-17. CDCA7 ICF patient mutations do not rescue the CDCA7 depletion chromosome morphology defect. (A) Chromosome length measurements for chromosomes formed in mock, CDCA7e, or HELLS depleted extract. Where indicated, CDCA7e depleted extract was complimented with MBP-CDCA7 or MBP-CDCA7 harboring the indicated ICF patient mutations. Each point is the length of a single chromosome. (B) Western blot of extract from (A).

Discussion and perspective

A streamlined comparative proteomics method for chromatin-associated protein complex identification

Combining affinity purification of target proteins and MS has long been used to identify the composition of protein complexes(Gingras et al., 2007) and has recently been performed on over 8,000 bait proteins(Huttlin et al., 2017). This method has the advantage of detecting multiple major and minor interactors of the protein of interest (approximately 7 interactors per protein on average(Huttlin et al., 2017)). More recently, unbiased approaches to identifying soluble protein complexes have been developed by combining biochemical fractionation with MS(Wan et al., 2015). Similar to the reasoning used in this chapter to identify protein complexes, this method assumes that cytoplasmic complexes will biochemically co-fractionate. While providing a rich set of potential protein complexes, these methods have required 1,163(Havugimana et al., 2012) and 6,387(Wan et al., 2015) LC-MS/MS runs, making it infeasible for smaller studies. Additionally, it may miss protein complexes that only form in certain contexts, such as on chromatin. For example, these methods did not identify HELLS-CDCA7 as a complex because HELLS-CDCA7 only forms a stable complex on chromatin and likely do not biochemically co-fractionate in the cytoplasm.

Here I identified known and novel protein complexes from an experiment of only 8 LC-MS/MS samples, greatly reducing time and cost. Several advances made this possible. Most importantly, filtering out proteins that are highly abundant in the cytoplasm, but only scarcely detected on chromatin was required. By only using the top

70th percentile of enriched proteins, a few bona fide chromatin associated proteins such as RUVBL1-2(Magalska et al., 2014) were omitted, but common chromatin contaminants such as mitochondria and proteasome proteins were successfully filtered. The 70th percentile filter will likely need to be manually adjusted from experiment to experiment based on the degree of non-specific co-purifying proteins. I found that a combination of highly similar (mock vs. CPC depletion and H3K9me3 vs. unmodified) and disparate (Interphase vs. M phase) conditions was important for identifying complexes.

Disparate conditions (such as the cell cycle) allow the identification of complexes that are specifically affected by the manipulation, for example, the mitotic eviction of HELLS and CDCA7. The principle is to find conditions that affect the largest number of proteins possible, thereby partitioning the complexes. Alternatively, highly similar conditions serve as an internal control whereby protein complex subunits co-vary across different samples due to biological variance. This is exemplified by Ku70-80, which largely binds chromatin regardless of the cell cycle stage, Aurora B, or H3K9me3, but Ku70 and Ku80 show identical fluctuations between conditions (Figure 3-1). In this regard, it would be useful to have biological replicates of the same condition, but refrain from averaging the results. By keeping biological replicates separate, one could identify co-fluctuations of complexes between replicates.

Additionally, focusing on a single subcellular location (chromatin) decreased the total number of identified proteins, simplifying the analysis. By simply repeating the experiment with more perturbations, for example, by other histone modifications,

depleting more chromatin proteins, DNA modifications, and the source of extracts, I envision that hierarchical clustering analysis will provide a more comprehensive picture of protein complexes that associate with chromatin.

The role of HELLS-CDCA7 in shaping mitotic chromosomes

Using the previously described approach to identify novel chromatin bound complexes, I identified the HELLS-CDCA7 remodeling complex, and classified its biochemical activity. To determine the biological function of HELLS-CDCA7, I generated antibodies to facilitate immunodepletion from *Xenopus* egg extracts. Although I was originally looking for ICF-like stretched centromeres in CDCA7 depleted *Xenopus* extracts, I mainly observed whole chromosome axial stretching at a low frequency. We are far from understanding how HELLS-CDCA7 contributes to mitotic chromosome structure, but here I speculate two different mechanisms by which HELLS-CDCA7 could affect chromosome structure: by having a direct effect on the organization of mitotic chromatin or indirectly by affecting chromosome structural proteins.

As cells enter mitosis, large arrays of regularly spaced nucleosomes form(Nocetti and Whitehouse, 2016), which may facilitate the polymer melt structure formation of condensed mitotic chromosomes(Nozaki et al., 2013). Therefore, HELLS-CDCA7 mediated chromatin compaction may be a direct result of the nucleosome positioning that occurs during mitosis. HELLS-CDCA7 depleted chromosomes may still form rod like structures due to the action of condensin and topoisomerase II, which can form mitotic rods in the absence of chromatin compaction(Shintomi et al., 2017), but may

remain decondensed due to an interphase-like nucleosome positioning. In this regard, it will be insightful to determine how HELLS-CDCA7 behaves on nucleosome arrays in vitro; although I show that HELLS-CDCA7 slides mononucleosomes to the end of DNA fragments, this model predicts that HELLS-CDCA7 might precisely space nucleosome arrays in vitro. Additionally, MNase digestion of mitotic chromosomes depleted of HELLS-CDCA7 could determine if nucleosome spacing is affected in the fragile chromosomes.

Alternatively to this direct model, HELLS-CDCA7 may indirectly compact mitotic chromosomes by facilitating the action of mitotic chromosomal proteins such as condensin and topoisomerase II. In chapter 2, I showed that condensin preferentially associates with naked DNA and topoisomerase II preferentially acts on naked DNA although both can act in the context of nucleosomes. Therefore, by sliding nucleosomes, HELLS-CDCA7 may act to expose naked DNA for condensin and topoisomerase II action, facilitating that shaping of mitotic chromosomes. This mechanism would be reminiscent of the RSC remodeling complex, which has been shown to evict nucleosomes to allow condensin to bind mitotic chromosomes(Toselli-Mollereau et al., 2016). However, since excess condensin I action is thought to result in radially thinner and axially elongated mitotic chromosomes, my results are consistent with an increase of condensin I. Therefore, HELLS-CDCA7 may slide nucleosomes to prevent the erroneous excess association of condensin. Indeed, preliminary results showed that CDCA7 depleted stretched chromosomes had abnormally high amounts of

condensin I, however, these results were not entirely reproducible and warrant further clarification.

As chromosomes depleted of CDCA7 resemble H1 depletion (Figure 3-13C), HELLS-CDCA7 may be in the same functional pathway as H1 to shape mitotic chromosomes. Therefore, the connection between HELLS-CDCA7 and H1 requires further elucidation. For example, HELLS-CDCA7 may be required to remodel H1-containing nucleosomes to facilitate condensin loading as described above. Although it has been proposed that HELLS preferentially remodels H1 containing nucleosomes(Lyons and Zilberman, 2017; Zemach et al., 2013), this has not been tested biochemically, and preliminary results indicate that HELLS-CDCA7 remodeling is unaffected by H1. However, since I found that HELLS interacts with H1 in soluble *Xenopus* egg extract, follow up studies are required.

Regardless of whether HELLS-CDCA7 acts directly or indirectly to shape mitotic chromosomes, there may be other nucleosome remodelers involved in the process. It has been shown that drosophila ISWI mutants have misshaped, thin polytene chromosomes(Deuring et al., 2000), somewhat similar to CDCA7 depleted *Xenopus* chromosomes. Therefore, it will be important to look at the role of other remodelers alone or in combination with HELLS-CDCA7 in shaping chromosomes.

At present, it is unclear if the ICF chromosomal stretching defect is related to the fragile chromosome defect seen on CDCA7 depleted *Xenopus* chromosomes. On one hand, microscopically the chromosomes appear very similar, even if the defect is confined to juxtacentromeric heterochromatin in ICF patients. On the other hand, my

results indicate that HELLS-CDCA7 affects chromosome structure in a DNA methylation independent manner (Figure 3-11). This is contradictory to the hypothesis that ICF fragile chromosomes are caused in a DNA methylation dependent manner. For this reason, I imagine that the two defects are caused by similar, but distinct mechanisms. Although the chromosomal main defect associated with CDCA7 depletion in egg extract is whole chromosome stretching, I did see local centromeric stretching extremely rarely (Figure 3-18). Unfortunately, since these events were so infrequent and also observed in mock depleted extracts, I was unable to determine if this event was due to CDCA7 depletion. Interestingly, these internally stretched regions had an excess of condensin I, supporting the hypothesis that excess condensin may cause the stretching phenotype associated with ICF syndrome. To study this hypothesis in a more controlled setting, condensin immunofluorescence on ICF patient mitotic chromosomes would need to be performed. Other than stretching, I was unable to identify other chromosomal defects present in ICF patients. There was no indication of rearrangements or multiradial chromosomes, however, these events may have been too infrequent to notice.

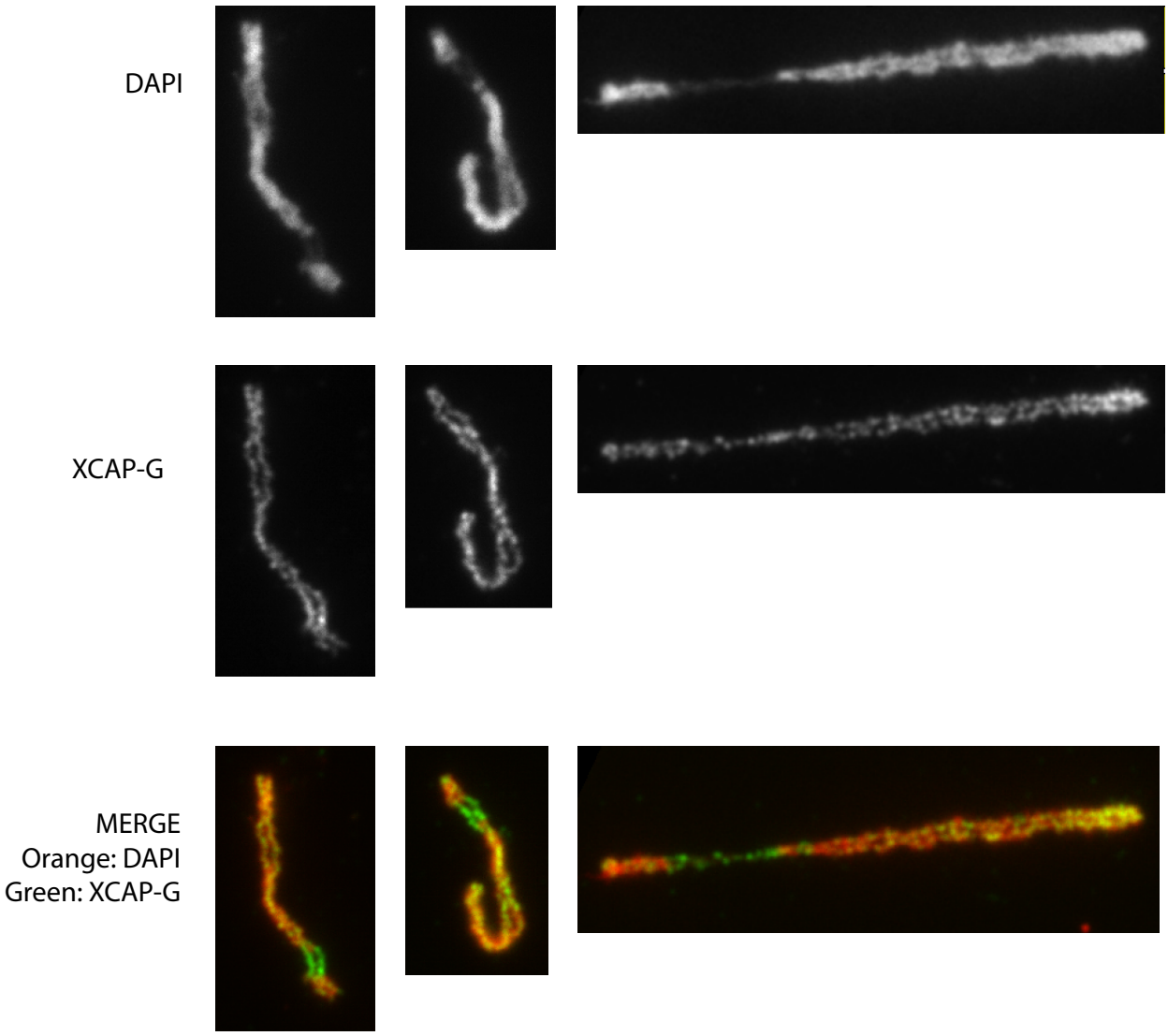

Figure 3-18. Stretched chromosomal regions contain excess condensin.

Immunofluorescence was performed on chromosomes isolated from *Xenopus* extracts.

Nucleosome dependent DNA binding proteins

One of the most unexpected findings from Chapter 2 was that many DNA binding proteins require nucleosomes to associate with chromatin in physiological extracts. For example, the linker histone(Ura et al., 1996) and FACT complex(Li et al., 2005) both have reported naked DNA binding activity in vitro, but require nucleosomes in *Xenopus* extract for stable chromatin association. In this chapter, I further studied this discrepancy in the context of HELLS-CDCA7. Here I discuss two theories to explain the discrepancy.

Chaperones can inhibit non-specific interactions of proteins with their substrate. For example, core histones are typically chaperoned in the cytoplasm, to prevent their non-specific and deleterious interaction with DNA(Laskey et al., 1978). I envision a similar mechanism may be occurring to prevent DNA binding proteins from non-specifically interacting with non-nucleosomal DNA. For example, H1 affects local chromatin structure by docking on the nucleosome and restricting the dynamics of neighboring linker DNA(Bednar et al., 2017). Although it can also interact with naked DNA alone, I envision that it's cytoplasmic chaperone, Nap1(Shintomi et al., 2005), may prevent these non-specific interactions and direct H1 specifically to nucleosomes. Indeed, in the absence of Nap1, erroneous H1-chromatin aggregates form(Shintomi et al., 2005). I speculate other nucleosome-dependent DNA binders may act in a similar manner.

Alternatively to chaperones, RCC1 mediated Ran-GTP signaling may be required for DNA binding proteins to associate with chromatin. Many proteins are sequestered in

the cytoplasm by importins. Chromatin bound RCC1 generates Ran-GTP, which releases the cargo from sequestration. Importantly, RCC1 requires nucleosomes for chromatin association(Makde et al., 2010; Zierhut et al., 2014) and full catalytic activity(Nemergut et al., 2001). The role of RCC1 in releasing sequestered proteins is well studied in microtubule assembly. Proteins involved in microtubule nucleation, including NuMA and TPX2, are sequestered by importins. Upon release by RCC1-generated Ran-GTP, these and other proteins stabilize microtubules to form the mitotic spindle(Gruss et al., 2001; Nachury et al., 2001; Wiese et al., 2001). Although well documented in microtubule assembly, RCC1 mediated regulation of chromatin binding proteins is less well established. However, it was shown that a chromatin binding protein Kid is sequestered in the cytoplasm by importins and can only load onto mitotic chromatin following RCC1 mediated release(Tahara et al., 2008). In agreement with this model, HELLS contains a bipartite NLS, which could sequester the HELLS-CDCA7 complex by importins until nucleosome dependent RCC1 signaling releases the complex. In the absence of nucleosomes, although HELLS-CDCA7 possesses DNA binding activity, importins would inhibit its DNA interaction. It is possible that other nucleosome dependent signaling pathways may be acting in an analogous manner.

CHAPTER 4: DISCUSSION AND PERSPECTIVE

A unifying model for ICF syndrome

At the onset of this project, there was no connection between HELLS and CDCA7 to ICF syndrome. Only mutations in DNMT3B and ZBTB24 were known to cause the disease, and the 30% of remaining patients had unidentified genetic causes. The generally accepted model was that DNMT3B mediated DNA methylation was defective in ICF due to reduced activity in DNMT3B enzymatic activity(Gowher and Jeltsch, 2002), however the role of ZBTB24 was entirely unknown. As the project progressed, it was reported that mutations in either HELLS or CDCA7 lead to ICF syndrome(Thijssen et al., 2015), but just like ZBTB24, the molecular function of these proteins was entirely unclear. Importantly, HELLS had previously been shown to direct the DNA methylation activity of DNMT3B to repress transcription(Myant and Stancheva, 2008), which naturally led to the hypothesis that HELLS (and potentially CDCA7 and ZBTB24) ICF mutations inhibit DNA methylation in a manner similar to DNMT3B ICF mutations. Indeed, somehow, HELLS, ZBTB24, and CDCA7 knockdown all lead to reduced DNA methylation in fibroblasts(Thijssen et al., 2015). Finally, it was shown that ZBTB24 is required for the expression of CDCA7(Wu et al., 2016), but how ZBTB24, CDCA7, and HELLS are functionally and molecularly related to DNMT3B was not established.

The data presented in Chapter 3 lead to a unifying model for ICF syndrome, which relates all known proteins involved in the disease (DNMT3B, HELLS, CDCA7, and ZBTB24) (Figure 4-1). In my preferred model, all ICF patient mutations converge on

defects in DNA methylation. Specifically, I fill in the missing link between the ZBTB24-CDCA7 and HELLS-DNMT3B axes. As HELLS requires CDCA7 for in vitro remodeling activity, I propose that the concerted action of HELLS-CDCA7 nucleosome remodeling at juxtacentromeric heterochromatin facilitates DNMT3B mediated DNA methylation. Combined with the knowledge that ZBTB24 is required for CDCA7 expression(Wu et al., 2016), I now provide a model for ICF syndrome, which explains all known ICF patient mutations at a high level. Furthermore, I specifically uncovered how CDCA7 ICF patient mutations inhibit recruitment of the HELLS-CDCA7 complex to chromatin, which would disrupt the DNA methylation pathway. Although this model explains how all known ICF causative proteins lead to defects in DNA methylation, the largest gap in the model is how reduced DNA methylation leads to the various ICF syndrome symptoms.

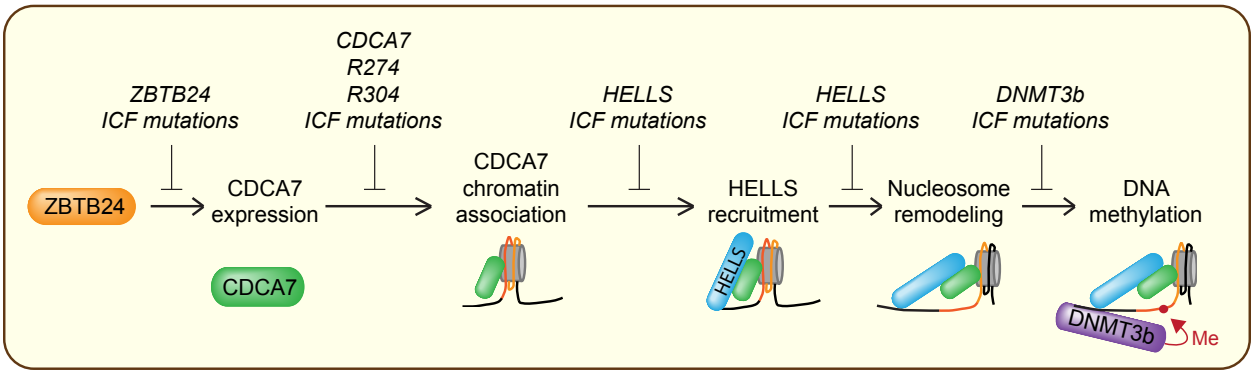

Figure 4-1. A unified model for ICF syndrome that converges on DNA methylation defects.

Consistent with my model, many HELLS ICF patient mutations are predicted to create a null protein, either by frameshift or by point mutation in the conserved ATPase domain, which is expected to abrogate its remodeling activity. However, two mutations have been identified that map to the C-terminal domain downstream of the ATPase domain(Thijssen et al., 2015). These mutations may indicate that this domain plays an important unknown role in mediating DNA methylation. As the core ATPase domain of nucleosome remodeler proteins is thought to be able to remodel nucleosomes even in the absence of the flanking domains(Clapier and Cairns, 2012), HELLS C-terminal domain may be required for auxiliary functions. For example, mutations in this domain may abrogate CDCA7 or DNMT3B interaction. Alternatively, this domain may be important for targeting HELLS-CDCA7 to specific genomic loci such as juxtacentromeric heterochromatin. Therefore, engineering these C-terminal mutations into HELLS could be useful for dissecting the mechanism of HELLS activity.

In this model, the sole role of ZBTB24 is to provide CDCA7 to the cell. Unlike the other ICF proteins that mostly contain patient mutations in a single domain, ICF mutations have been found throughout ZBTB24. At present, only the deletion of a large domain within ZBTB24 (containing the BTB domain, AT hook, and a portion of the zinc finger domain) has been shown to result in reduced CDCA7 expression. As nothing is known about the function and mechanism of ZBTB24 action, studying individual ICF patient mutations within ZBTB24 could be a useful way to access the function of each domain within ZBTB24 and parse its various activities. For example, the BTB domain is speculated to facilitate dimerization of the protein, however this has not been

experimentally tested. Engineering ICF patient mutation V68 or H132, which maps to the BTB domain of ZBTB24 could be used to test this hypothesis. Similar approaches could be used to study the AT-hook and zinc finger domains, both of which have unknown functions with corresponding ICF patient mutations.

An alternative model for ICF syndrome

Here, I propose an alternative model for ICF syndrome. In contrast to my previous model (Figure 4-1) which converged on defects in DNA methylation, this model converges on defective remodeling of juxtacentromeric nucleosomes (Figure 4-2).

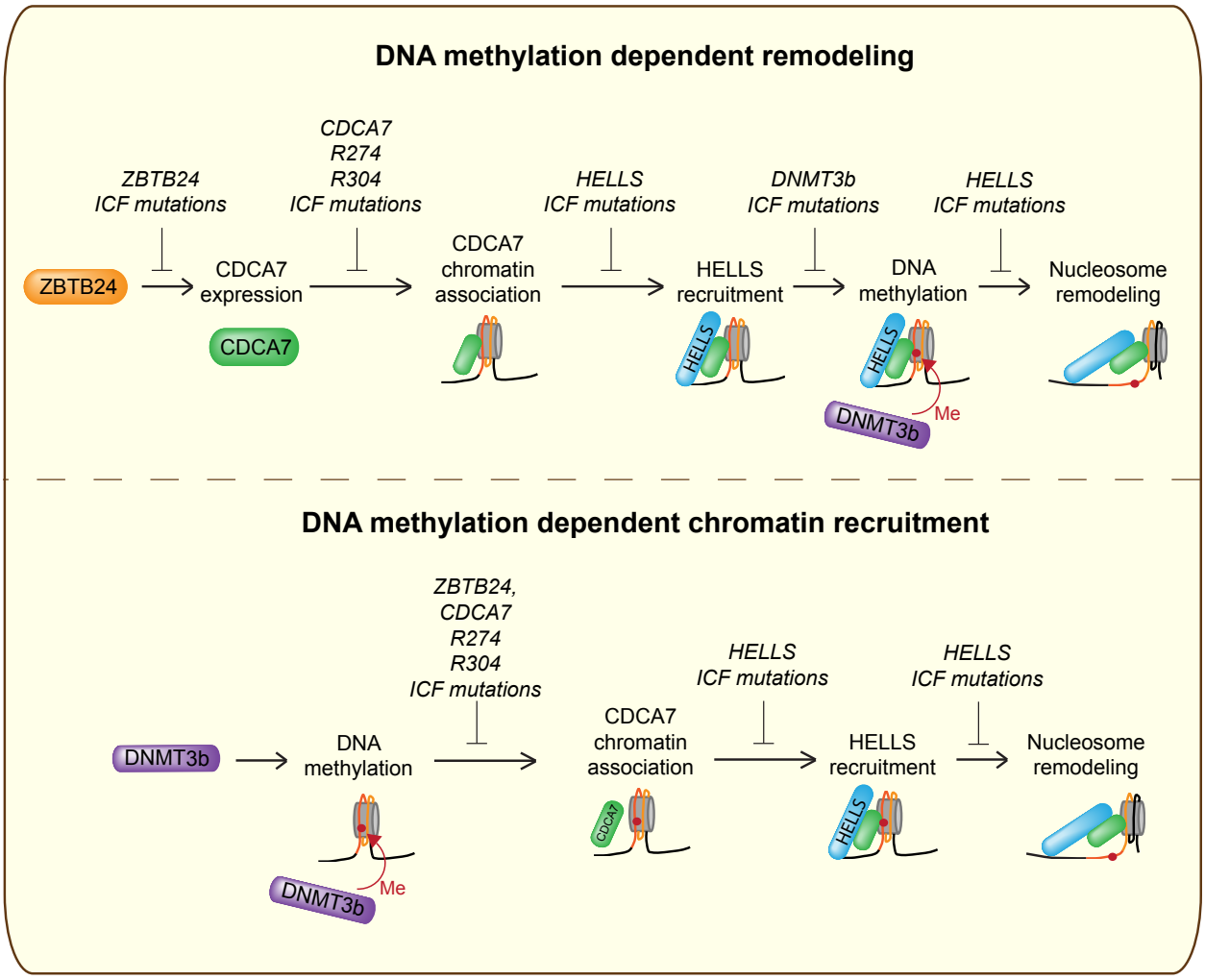

Figure 4-2. An alternative model for ICF syndrome that converges on nucleosome remodeling. The HELLS-CDCA7 remodeling complex can either require DNA methylation for remodeling activity (top) or chromatin recruitment (bottom).

Nucleosome remodelers make multiple contacts with DNA within the nucleosome(Farnung et al., 2017), therefore it is conceivable that the HELLS-CDCA7 remodeling complex is regulated by DNA methylation. Perhaps DNA methylation enhances the remodeling activity of HELLS-CDCA7, or facilitates the physiological targeting of the complex to juxtacentromeric heterochromatin. Therefore, defective DNMT3B mediated DNA methylation could result in reduced HELLS-CDCA7 mediated nucleosome remodeling directly, or indirectly via reduced chromatin localization. Likewise, ZBTB24 mutations would result in decreased CDCA7 expression, and reduced targeting of the complex to methylated loci. Analogous to the previous model, this model does not explain how defective juxtacentromeric nucleosome remodeling results in ICF syndrome symptoms.

There is precedence for nucleosome remodeling to be affected by DNA methylation. In the most well studied case, the nucleosome remodeler Mi-2 associates with MBD2(Le Guezennec et al., 2006), which specifically recognizes methylated DNA(Hendrich and Bird, 1998). It is thought that MBD2 directs the remodeling activity of Mi-2 to methylated promoters to facilitate gene silencing(Becker and Workman, 2013). Interestingly, Mi-2 can be alternatively associated with MBD3(Le Guezennec et al., 2006), which only binds unmethylated DNA. These data suggest that the complex is differently target to genomic context by auxiliary subunits that recognize DNA methylation, or lack thereof. This precedence supports that CDCA7-HELLS may be specifically targeted to and remodel methylated juxtacentromeric heterochromatin.

Multiple lines of evidence favor the “DNA methylation defect” (Figure 4-1) model over this “nucleosome remodeling defect” (Figure 4-2) model for ICF syndrome. The biochemical properties of HELLS and DDM1 (*A. thaliana* HELLS) are similar (see below) and the ATPase activity of DDM1 is unaffected by DNA methylation(Brzeski and Jerzmanowski, 2003). However, the nucleosome sliding activity has not been explicitly tested. Additionally, in my remodeling experiments (Figure 3-10), HELLS-CDCA7 shows robust sliding activity on unmethylated DNA, while the proposed model converging on nucleosome remodeling defects would be consistent with minimal sliding activity on unmethylated DNA. A direct comparison of the nucleosome sliding kinetics on unmethylated vs. methylated DNA would be required to cleanly address this discrepancy though. Moreover, this nucleosome remodeling defect model is inconsistent with the observations that patients with defective ZBTB24, HELLS, and CDCA7 also show reduced DNA methylation at juxtacentromeric heterochromatin, which would not be expected if HELLS-CDCA7 remodeling is downstream of DNMT3B mediated DNA methylation. Although, it is possible that a methylation-remodeling feedback loop could result in these methylation defect. Finally, this model contradicts preliminary experiments that HELLS-CDCA7 is specifically recruited to DNA beads coated with unmethylated DNA instead of methylated DNA in *Xenopus* extracts, whereas the model predicts the opposite (J. Xue, personal communication). Because of these inconsistencies, I favor the original model where all ICF mutations converge on DNA methylation, however, more experiments are required to definitively test this.

HELLS regulation by CDCA7, CDCA7L and CDCA7e

Given that Arabidopsis HELLS can remodel nucleosomes in vitro without any accessory factors, it raises the question of why vertebrate HELLS requires CDCA7. Here, I propose that CDCA7 paralogs act as a mechanism to differentially regulate HELLS.

Auxiliary proteins are well known to alter the biochemical directionality of nucleosome remodeling enzymes. In the most thoroughly studied example, Snf2h was shown to end-position nucleosomes when in complex with RSF, but center-position nucleosomes when in complex with BAZ1A(Oppikofer et al., 2017). In a similar manner, while CDCA7e efficiently slides nucleosomes to the end of DNA fragments (Figure 3-10), HELLS-CDCA7 or HELLS-CDCA7L could center-position or randomize nucleosomes on DNA fragments. In contrast to HELLS-CDCA7e, DDM1 effectively center-positions mononucleosome substrates, highlighting the potential plasticity in the biochemical functionality of HELLS. Unfortunately, no convincing hypothesis has been proposed to explain how these biochemical differences could manifest into different biological functions.

In addition to enzymatic regulation, CDCA7 paralogs may differentially target HELLS to different genomic loci. I hypothesize that the CDCA7 paralogs recruit HELLS to juxtacentromeric heterochromatin, since CDCA7 ICF mutations result in reduced juxtacentromeric DNA methylation. However, HELLS is localized to other loci throughout the genome including LINE-1 elements(Ren et al., 2015) and promoters(von Eyss et al., 2012), which could be due to either CDCA7 or CDCA7L mediated targeting.

This targeting specialization is in agreement with CDCA7 being the chromatin-binding module of the HELLS-CDCA7 complex. By recognizing different DNA sequences, DNA methylation states, or nucleosome modifications, CDCA7 and CDCA7L could functionally specialize to recruit HELLS to different genomic loci. This would be analogous to ISWI, which uses auxiliary proteins to target the complex to differentially modified nucleosomes. Alternatively, CDCA7 may be a specificity factor that recruits HELLS to specific histone variants, similarly to DAXX within the ATRX-DAXX complex. To get a complete picture, a recently developed high-throughput assay(Dann et al., 2017) could be used to determine how HELLS-CDCA7, CDCA7L and CDCA7e are affected by the underlying chromatin modifications.

By specifically knocking out CDCA7 or CDCA7L and performing ChIP-seq on HELLS, the individual contribution of each CDCA7 paralog could be determined. Based on RNA-seq analysis, CDCA7 and CDCA7L are differentially expressed in a tissue-dependent manner. Therefore, it may be required to perform these CDCA7/CDCA7L knockdown HELLS ChIP-seq experiments in a variety of cell lines to get a complete understanding of the differences between paralogs.

The similarities and differences between DDM1 and HELLS-CDCA7

Comparing and contrasting DDM1 and HELLS-CDCA7 may lead to important insights into the function and regulation of these proteins. In many regards, DDM1 and HELLS are biochemically and functionally similar. Although HELLS requires nucleosomes and CDCA7 for chromatin interaction in physiological extracts, purified

HELLS and DDM1 both interact with naked DNA and nucleosomes in vitro (Figure 3-7 and (Brzeski and Jerzmanowski, 2003)). In addition to binding DNA, purified HELLS and DDM1 possess naked DNA and nucleosome dependent ATPase activity in the absence of any auxiliary proteins (Figure 3-11 and (Brzeski and Jerzmanowski, 2003)). One striking difference between their nucleosome remodeling activities is that DDM1 prefers to mobilize end-positioned nucleosomes to the center of DNA fragments, while HELLS-CDCA7 does the opposite (Figure 3-10 and (Brzeski and Jerzmanowski, 2003)). Finally, DDM1 and HELLS are functionally similar as both are required for facilitating cytosine methylation(Lyons and Zilberman, 2017).

Since vertebrate HELLS and *A. thaliana* DDM1 are well conserved (in sequence and function), it is surprising that DDM1 itself can remodel nucleosomes while HELLS requires CDCA7 for remodeling. While examining the sequence structure, I noticed that vertebrate HELLS contains a 59 amino acid insert between its two ATPase domains, not present in DDM1. Interestingly, this insert is conserved in opisthokonts, but is lacking in plants (Figure 4-3). This “split-ATPase” structure in vertebrate HELLS is reminiscent of a distantly related nucleosome remodeler INO80. INO80 has a 281 amino acid insertion between its ATPase domains, and similar to HELLS, is thought to be unable to remodel nucleosomes on its own. Instead INO80 is proposed to require actin, Arp4, Arp5, Arp8, Ies2, Ies6, RUVBL1, and RUVBL2 for remodeling(Willhoft et al., 2016). Perhaps insertions between the ATPase domains are a common mechanism to render nucleosome remodelers dependent on auxiliary proteins.

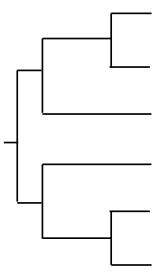

Species		Contains Insert?	Remodels?	GenBank Accession
A. thaliana	Plant	No	Yes	OAO91248.1
C. sativa	Plant	No	?	XP_010444738.1
C. eustigma	Algae	No	?	GAX75958.1
S. cerevisiae	Yeast	Yes	?	AJU35866.1
M. musculus	Animal	Yes	No	AAI00395.1
X. laevis	Animal	Yes	No	AAH97562.1

Figure 4-3. Phylogeny of HELLS. Dendrogram, whether HELLS remodels and contains a “split-ATPase” insert is shown for the indicated species.

I wondered if perhaps DDM1 possesses intrinsic nucleosome sliding activity because it is a hybrid of HELLS-CDCA7 in a single polypeptide. Indeed, Arabidopsis DDM1 contains a 116 amino acid stretch with low homology to CDCA7 (24% identity) (Figure 4-4). This homologous stretch maps to the zinc finger domain of CDCA7, and occurs between the two ATPase domains of DDM1. Although the homology maps to the zinc finger domain of CDCA7, the CXXC motifs are largely divergent between CDCA7 and DDM1, suggesting that the domain is not a bona fide zinc finger domain in DDM1. Interestingly, vertebrate HELLS also contains the homology to CDCA7, but the CDCA7 homology domain is disrupted by the previously described 59 amino acid insertion (Figure 4-4). I speculate that by disrupting the CDCA7 homology domain in vertebrate HELLS, the remodeler became dependent on an external CDCA7, which could allow specialization by different CDCA7 paralogs (CDCA7, CDCA7L, CDCA7e). It would be interesting to test if vertebrate HELLS remodeling activity could be rescued by removing the 59 amino acid disruption within its CDCA7 homology domain. Alternatively, it would be interesting to test if Arabidopsis HELLS could be made dependent on external CDCA7 by disrupting its CDCA7 homology domain with the vertebrate HELLS insert.

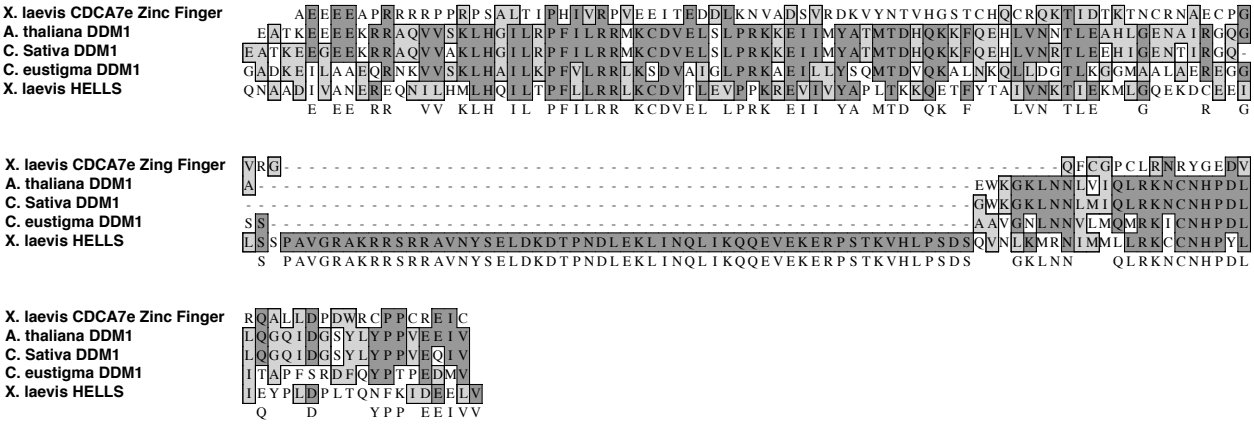

Figure 4-4. DDM1 contains homology to the CDCA7 zinc finger. Note how *X. laevis* HELLS also contains homology to CDCA7, however, it is interrupted by an insertion.

As DDM1 can remodel nucleosomes in the absence of CDCA7, I was surprised to find that the *A. thaliana* genome contains proteins harboring homology to the CDCA7 zinc finger (identified by reciprocal blast search). I speculate that DDM1 with the CDCA7 zinc finger homology domain may be able to remodel nucleosomes in vitro, but may not be targeted to correct genomic loci in vivo. This would be reminiscent of HELLS-CDCA7 with CDCA7 harboring ICF mutations (Figure 3-16), has remodeling activity comparable to wild type CDCA7 but cannot associate with chromatin under physiological conditions. DDM1 could likewise utilize CDCA7 like proteins for genomic targeting and chromatin association. As there are at least four proteins in the *A. thaliana* genome that contain the CDCA7 zinc finger domain (Figure 4-5), these proteins may differentially target DDM1 to different genomic loci in distinct contexts. This could be tested by performing ChIP-seq on DDM1 in the absence of the various CDCA7 paralogs.

Alternatively, DDM1 was initially noted as a relatively weak remodeler, only able to mobilize 50% of nucleosomes in a remodeling assay(Brzeski and Jerzmanowski, 2003). Therefore, DDM1 may be reliant on CDCA7 like proteins for robust remodeling activity in vitro and in vivo.

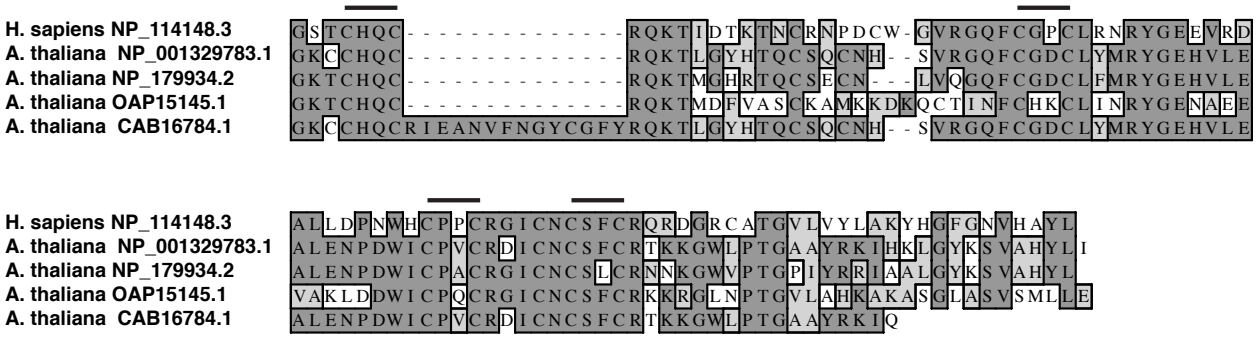

Figure 4-5. Arabidopsis proteins containing the CDCA7 CXXC zinc finger motif.

The CXXC motifs are underlined.

Outlook: Open Questions in ICF syndrome

In the previous paragraphs, I outlined how all known ICF mutations may lead to defects in DNA methylation. Currently, the major question regarding ICF syndrome is how the patient symptoms, including immunodeficiency and centromere instability, are caused by defects in DNA methylation. Here I speculate that the causes of ICF patient symptoms may arise from unresolved DNA damage.

As previously discussed, ICF patients have stretched juxtacentromeric heterochromatin on chromosomes 1, 9, and 16 in lymphocytes. However, ICF patients do not have reported chromosomal abnormalities in fibroblasts(Maraschio et al., 1989), suggesting that the chromosomal defect may be specific to lymphocytes and may be causative to the immunodeficiency symptoms. As CDCA7 ICF mutations caused mitotic chromosomal abnormalities in *Xenopus* egg extracts (Figure 3-17), I looked for similarities between the *Xenopus* egg and lymphocytes. Two similarities were apparent: shortened cell cycle length and suppressed DNA damage response. Both the frog egg (30-80 min (Morgan, 2007)) and stimulated lymphocytes (10.5 hr (Auf der Maur and Berlincourt-Bohni, 1979)) have relatively short cell cycles. Additionally, the ATR-mediated DNA damage response is attenuated in the frog egg prior to the mid-blastula transition(Peng et al., 2008) as well as in lymphocytes(Jones et al., 2004). These unique similarities lead me to a model whereby the chromosome defects associated with ICF arise from DNA damage in the shortened cell cycle that remains unresolved as the cells enter mitosis. Accelerated cell cycles coupled to suppressed resolution of DNA damage could lead to accumulation of genetic defects and ultimately lead to cell death.

While highly speculative, a few lines of evidence support this hypothesis. First, although most ICF patients have agammaglobulinaemia, all ICF patients have B cells, suggesting that late stage lymphocyte differentiation is defective, which is consistent with the hypothesized accumulating DNA damage leading to cell death. Similarly, ICF patients have an increased frequency of mitotic defects such as anaphase bridges in their cultured lymphoblastoid cell lines(Gisselsson et al., 2005), suggests that there may be unresolved DNA damage in these cells. Furthermore, ICF proteins have been shown to be involved in the DNA damage response. HELLS has previously been shown to be required for efficient repair of DNA double strand breaks via promoting gamma-H2AX phosphorylation(Burrage et al., 2012). Additionally, although not understood why, global genomic DNA demethylation results in a variety of DNA damage associated with chromosomal defects including increased mutation rates(Chen et al., 1998), chromosome instability(Chen et al., 2007), chromosome duplications(Gaudet et al., 2003) and apoptosis(Jackson-Grusby et al., 2001). These reports highlight how ICF patients may be susceptible to DNA damage, and unresolved DNA damage ultimately leading to cell death in lymphocytes could manifest with symptoms associated with ICF such as agammaglobulinaemia and immunodeficiency.

To test this hypothesis, it would be useful to know if ATR depletion could recapitulate ICF-like chromosomal defects in non-lymphocytes. In agreement with this idea, ATR inhibition with caffeine can cause chromosomal abnormalities in ICF patient fibroblasts(Maraschio et al., 1989), however, a more specific ATR deletion/inhibition will need to be performed to confirm the role of ATR in the process. Additionally, it would be

interesting to see if reintroducing ATR in lymphocytes could suppress the chromosomal abnormalities in ICF patient cells. As an alternative approach, since ATR is suppressed in the *Xenopus* egg prior to the mid-blastula transition, it would be interesting to compare chromosomes in CDCA7 depleted extract made from pre- and post-MBT *Xenopus* embryos. The prediction would be that post-MBT, activated ATR would resolve the DNA damage resulting in phenotypically normal chromosomes, while pre-MBT extract would show stretched and fragile chromosomes.

In summary, this work connects many previously disparate observations about ICF syndrome into a unified theory, and points a way forward in studying the rare disease. Much of this work was published in (Jenness et al., 2018; Zierhut et al., 2014)

CHAPTER 5: MATERIALS AND METHODS

Biochemistry

Cloning

Codon optimized *Xenopus* HELLS-TEV-CBP (Thermo GeneArt Strings) was Gibson assembled into pRS306G(Devbhandari et al., 2017) yeast expression plasmid containing PGK1 3' UTR. *Xenopus* embryonic CDCA7e (GE EXL1051-205982802) was Gibson assembled into pMAL (NEB). CDCA7 (accession no. BC130191), CDCA7L (accession no. BC126014), and CDCA7e were Gibson assembled with an N-terminal 6x MYC tag into pCS2. HELLS (accession no. NM_001092973.1) was Gibson assembled with a C-terminal GFP tag into pCS2.

Protein purification

MBP-CDCA7-HIS was expressed in *E. coli* at 16 °C overnight. Cells were centrifuged, resuspended in lysis buffer (1X PBS, 150 mM NaCl, 4 mM 2-mercaptoethanol, 20 mM imidazole, 0.1% Triton X-100, 100 μM $ZnSO_4$, 1 mM PMSF, 0.25 mg/ml lysozyme, 5 μg/ml DNaseI, 10 μg/ml leupeptin, 10 g/ml pepstatin and 10 μg/ml chymostatin, pH 7.8), and lysed by sonication. Lysate was centrifuged (Sorvall SS34 rotor, 14,000 r.p.m.) for 30 min at 4 °C, and supernatant was incubated with 2 ml Ni-NTA agarose (Qiagen) for 1 h at 4 °C. Resin was washed 3 times with 20 ml wash buffer (1X PBS, 150 mM NaCl, 4 mM 2-mercaptoethanol, 100 μM $ZnSO_4$, pH 7.8) supplemented with 20 mM imidazole, 10 mM ATP, and 2.5 mM $MgCl_2$. Protein was

eluted with wash buffer containing 400 mM imidazole. Eluate was incubated with 5 ml amylose resin (New England BioLabs) for 1 h at 4 °C. Amylose resin was washed 3 times with 20 ml wash buffer, and MBP-CDCA7e was eluted with wash containing 20 mM maltose. Purifed MBP-CDCA7e was dialyzed in buffer (1X PBS, 150 mM NaCl, 4 mM 2-mercaptoethanol, 100 μM ZnSO4, pH 7.8) and concentrated via spin column (Amicon).

To purify HELLS-CBP, *S. cerevisiae* containing pRS306G(Devbhandari et al., 2017) containing HELLS-CBP were grown in YP-raffinose at 30 °C to 1.3 x 10^7 cells/ml. Protein expression was induced by adding galactose (2% final) and incubating for 4 h. Cells were centrifuged, washed once with buffer A (25 mM HEPES, 1 M sorbitol, pH 7.6), and once with buffer B (45 mM HEPES, 0.02% Triton X-100, 10% glycerol, 5 mM Mg $(OAc)_2$, 0.1 M K-glutamate, pH 7.6). Cells were resuspended in 0.5 volumes buffer B with supplemented with 1 mM DTT, 10 μg/ml leupeptin, 10 μg/ml pepstatin and 10 μg/ml chymostatin. Cells were frozen dropwise in liquid N_2 and ground in a cryogenic grinding mill (SPEX). Cell powder was resuspended in buffer C (10 mM HEPES, 300 mM KCl, 10 mM 2-mercaptoethanol, pH 8.0) containing 2 mM $CaCl_2$, and centrifuged (SS-34 rotor, 19,000 r.p.m.) for 30 min at 4 °C. Supernatant was incubated with 5 ml calmodulin resin for 1 h at 4 °C. Resin was washed 5 times with 20 ml buffer C containing 2 mM $CaCl_2$, and protein was eluted with buffer C, supplemented with 10 mM EDTA. Eluate was loaded on a heparin column (GE), washed with buffer C, and eluted with buffer C containing 500 mM KCl. Purified HELLS-CBP was concentrated by covering HELLS-containing dialysis membrane with sucrose for 1 h at 4 °C.

Histones were purified as described(Zierhut et al., 2014). H2B, H2A, H3.2 and H4 were individually expressed in *E. coli* for 4 h at 37 °C. Cells were centrifuged, washed once with lysis buffer (50 mM Tris-Cl, 100 mM NaCl, 10 mM imidazole, 10 mM 2-mercaptoethanol, 0.25 mg/ml lysozyme, 5 μg/ml DNaseI, 10 μg/ml leupeptin, 10 μg/ml pepstatin and 10 μg/ml chymostatin, pH 8.0) and resuspended in 30 ml lysis buffer. Cells were lysed by sonication and centrifuged (SS34, 20,000 g) for 15 min at 4 °C. Inclusion bodies were rinsed with wash buffer (50 mM Tris-Cl, 100 mM NaCl, 10 mM imidazole, 10 mM 2-mercaptoethanol, pH 8.0), and resuspended in 15 ml wash buffer with 1% Triton X-100. Inclusion bodies were centrifuged (SS34, 13,000 r.p.m.), washed twice with wash buffer, and centrifuged again. Pellets were resuspended in 1 ml DMSO, diluted in 25 ml D500 buffer (6 M Guanidine HCl, 500 mM NaCl, 50 mM Tric-Cl, 5 mM 2-mercaptoethanol, 7.5 mM imidazole, pH 8.0), and rotated overnight at room temperature. Mixture was centrifuged (SS34, 30,000 r.p.m.) for 20 min at 4 °C. H2B, H3, and H4 were further purified by incubation with 1.5 ml Ni-NTA agarose resin for 90 min at room temperature. Resin was washed 5 times with 20 ml D500 and 3 times with 20 ml D1000 (6 M Guanidine HCl, 1 M NaCl, 50 mM Tric-Cl, 5 mM 2-mercaptoethanol, 7.5 mM imidazole, pH 8.0). Proteins were eluted with 5 ml elution buffer (6 M Guanidine HCl, 1 M NaCl, 50 mM Tric-Cl, 5 mM 2-mercaptoethanol, 300 mM imidazole, pH 7.5). H3 harboring K9 trimethylation was generated by protein semisynthesis as described(Muller et al., 2016)

H3-H4 tetramers and H2A-H2B dimers were refolded as described(Zierhut et al., 2014). Each histone (45 μM) was added to 4.5 ml final volume D500. Histones were

dialyzed stepwise in dialysis buffer (20 mM MOPS, 500 mM EDTA, 1 mM EDTA, 4 mM DTT, pH 7.0) containing 10%, 5%, and 2.5% glycerol each for 4 h. Refolded histones were centrifuged, and the supernatant was incubated with 0.02 mg/ml TEV protease overnight at 16 °C. Refolded histones were purified by size exclusion chromatography (GE Healthcare HiLoad 16/60 Superdex 75).

SNF2h was a gift of N. Gamarra and G. Narlikar.

Nucleosome array and mononucleosome purification

19x601 Nucleosome arrays were prepared as described(Zierhut et al., 2014). Nineteen 601-positioning sequences separated by 53 bp linking DNA were digested from pAS696 with HaeII, DraI, EcoRI and XbaI. The array was purified by PEG precipitation, and both ends were biotinylated by Klenow (NEB) fill-in with biotin-16-dUTP (ChemCyte). 19x601 arrays were purified from free nucleotides by Illustra Nick columns (GE Healthcare). 19x601 nucleosome arrays were prepared by gradient salt dialysis of H3-H4 tetramers, H2A-H2B dimers onto the DNA array. The quality of the array was verified by AvaI digest, which cuts between 601 monomers, resulting in pure mono-nucleosomes when resolved on a native polyacrylamide gel. Nucleosome arrays (900 ng) were coupled to 3 μL M-280 streptavidin Dynabeads (ThermoFisher) in bead coupling buffer (2.5% polyvinyl alcohol, 150 mM NaCl, 50 mM Tris-Cl, 0.25 mM EDTA, 0.05% Triton X-100, pH 8.0) at room temperature for 3 h. When coupling naked 19x601 DNA to Dynabeads, bead-coupling buffer contained 1.5 M NaCl. Mononucleosomes

were prepared as above, but with digesting AvaI arrays and PEG purification prior to salt dialysis.

Antibodies

A summary of all custom antibodies generated in this study is summarized (Table 5-1). For antibody production, C-terminal or N-terminal peptides of *Xenopus* proteins were synthesized (Rockefeller University Proteomics Resource Center). Peptides were coupled to keyhole limpet hemocyanin according to manufactures' protocol (ThermoFisher) and used for rabbit immunization (Cocalico Biologicals). Antibodies were affinity purified from serum using the same peptides coupled to SulfoLink resin (ThermoFisher) according to manufacturers' protocol. All other antibodies used throughout this study and their sources are listed (Table 5-2).

Table 5-1. Custom antibodies generated in this study.

Protein	Antigen	Western Blot	Immuno-depletion	IF	Identifier
xHELLS	CQGVFKVVDSTEVTVS	Yes	Yes	Yes	RU1995
xHELLS	MPVGQSSAEQVSPAPC	Yes	Yes	No	RU1996
xCDCA7e	CLNSLRNTKDEDSDGS	Yes	Yes	No	RU1998
xH1M	CGAPVKAGKKGKKVTN	Yes	Yes	Yes	RU1974
xHP1-gamma	MGKKQNGKSKKVEEAC	Yes	Yes	?	RU1985
xSPT16	CKGHAPLPNPSKKRKK	Yes	Yes	?	RU1983

Custom antibodies generated in this study and whether they have specific reactivity by Western blot, immunodepletion, or immunofluorescence (IF).

Table 5-2. Published antibodies used in this study

Antibody	Reference
Aurora B	(Kelly et al., 2007)
CDCA7	RU1998
Dasra	(Sampath et al., 2004)
DNMT1	(Nishiyama et al., 2013)
GFP	Thermo A11122
H1M	RU1974
H2B	Abcam Ab1790
H3	Abcam Ab1791
H3T3ph	Millipore 07-424
H3K9me3**	(Chandra et al., 2012)
H3S10ph*	H. Kimura gift, unpublished
H4K12Ac	(Hayashi-Takanaka et al., 2015)
HELLS	RU1995
HIRA	(Ray-Gallet et al., 2002)
INCENP	(Sampath et al., 2004)
ISWI	(MacCallum et al., 2002)
MBP	NEB E8032
MCM7	(Walter and Newport, 2000)
MYC	Millipore 4A6
Op18	(Budde et al., 2001)

Phospho-Aurora B	Cell signaling 2914
Phospho-CDK substrate	Cell signaling 2324
Plx1	(Kelly et al., 2007)
RCC1	(Nachury et al., 2001)
Spt16	Cell signaling mAB 12191
Survivin	(Tseng et al., 2010)
Topoisomerase II	(Hirano and Mitchison, 1993)
XCAP-G	(Zierhut et al., 2014)
Xkid	(Funabiki and Murray, 2000)

Antibodies used in this study and their associated references.

* H3S10 antibody (3-7C4) allows H3K9 mono-, di-, tri-methylation and H3K9 acetylation

** H3K9me3 antibody (2F3) is occluded by H3S10ph.

Immunoprecipitations

For in vitro co-immunoprecipitation experiments, 2.5 μg anti-MBP (NEB E8032) or preimmune mouse IgG (Sigma-Aldrich) were coupled to 10 ul Protein A Dynabeads for 1 h at room temperature. Beads were recovered on a magnet and washed extensively in sperm dilution buffer. Beads were resuspended in sperm dilution buffer with 0.05% Triton X-100 and 200 nM indicated proteins. Samples were agitated for 30 min at 20 °C. Beads were recovered on a magnet, washed three times with sperm dilution buffer with 0.05% Triton X-100. Beads were resuspended in SDS-PAGE buffer, resolved by gel electrophoresis, and stained with GelCode Blue (ThermoFisher).

To test MBP-CDCA7e ICF mutant binding to HELLS-GFP, HELLS-GFP or GFP was expressed in the TnT Coupled Reticulocyte Lysate System (Promega) according to the manufacturer's instructions. TnT reaction was diluted 1:5 in binding buffer (10 mM HEPES, 100 mM NaCl, 0.025% Triton X-100, 0.25 mM TCEP, pH 7.8) containing 100 nM CDCA7e, and incubated for 20 min at 20 °C. To each sample, 10 μl anti-MBP coated protein A beads were added, and the sample incubated for 20 min at 20 °C. Beads were recovered, washed and resolved by gel electrophoresis as before. Gel was stained with GelCode Blue (Thermo Fisher), dried, and exposed on a PhosphorImager screen.

Chromatin interactions

To assay CDCA7e chromatin binding in vitro, 3 μl 19x601 DNA or nucleosome beads were incubated in 50 μl binding buffer (20 mM HEPES, 200 mM NaCl, 0.05%

Triton X-100, 0.5 mM TCEP, pH 7.8) containing 1 μM of MBP-CDCA7e for 30 min at 20 °C. Beads were collected on a magnet and washed 3 times with binding buffer. Beads were resuspended in SDS-PAGE buffer, boiled, and collected on a magnet. The supernatant resolved by gel electrophoresis and stained with GelCode Blue. To assay HELLS DNA binding, 3 μl DNA beads were incubated in 20 μl sperm dilution buffer with 0.05% Triton X-100 and 1 μM protein for 45 min at room temperature. Beads were collected on a magnet and washed 3 times with sperm dilution buffer with 0.05% Triton X-100. Beads were resuspended in SDS-PAGE buffer, boiled, and collected on a magnet. The supernatant resolved by gel electrophoresis and stained with GelCode Blue. To assay recombinant topoisomerase II chromatin binding in vitro, nucleosome beads, DNA beads or uncoupled beads were incubated in binding buffer (10 mM Tris, pH 7.5, 150 mM NaCl, 0.05% Triton X-100) containing 1.6 μM recombinant *Xenopus* topoisomerase II (a gift from Y. Azuma) and 1 ng/μl BSA for 60 min at 20 °C with vigorous agitation. Beads were recovered on a magnet and washed three times in binding buffer. Bound proteins were eluted from the beads by incubation with SDS sample buffer.

ATPase assays

For ATPase assays, 100 nM protein was added to 10 μl ATPase buffer (25 mM HEPES, 60 mM KCl, 4% glycerol, 4 mM $MgCl_2$, 1 mM cold ATP, 0.1 μCi/μL γ-33P ATP, pH 7.6) containing 40 ng/μl DNA or nucleosomes, and incubated at 16 °C. At the indicated times, 1 μl reaction was spotted on PEI a cellulose TLC plate and dried. Plates

were separated in 1.2 M KH_2PO_4, pH 3.8. Plates were dried and exposed on a PhosphorImager screen.

Nucleosome remodeling assays

To assay nucleosome remodeling by restriction enzyme accessibility, mononucleosomes were positioned on a 601 sequence with a *Pst*I site engineered 15 bp into the nucleosome and 20 bp flanking DNA on each end (a gift of N. Gamarra and G. Narlikar). Nucleosomes (15 nM) were added to remodeling buffer (6.5 mM HEPES, 2 mM ATP-Mg, 5 mM $MgCl_2$, 70 mM KCl, 0.02% Triton X-100, 3 U/μl *Pst*I (NEB), pH 7.5) containing 100 nM HELLS, CDCA7e or SNF2h (a gift of N. Gamarra and G. Narlikar). Where indicated, 15 or 1.5 mM remodeling proteins were substituted. Reactions incubated at 25 °C. At the indicated times, 5 μl remodeling reaction was added to 5 μl stop buffer (20 mM Tris, 70 mM EDTA, 2% SDS, 20% glycerol, 0.2 mg/ml bromophenol blue, 3.3 mg/ml Proteinase K, pH 7.5) and incubated at 50 °C for 20 min. 5 μl of each sample was resolved on a 10% polyacrylamide gel in 1X TBE at 150 V for 3 h and stained with SYBR gold for 30 min. Where indicated, a similar procedure was performed using a mononucleosome on a 601 sequence containing 34 bp and 23 bp flanking DNA on the 5' and 3' ends respectively and *Msp*I restriction enzyme (NEB). To assay mobility of end positioned nucleosomes, mononucleosomes were positioned on a 601 sequence containing 60 bp 3' flanking DNA, and the protocol was repeated using *Hae*III in place of *PstI*.

To assay nucleosome remodeling by native gel, aforementioned center-positioned or end-positioned mononucleosomes (20 nM) were added to remodeling buffer (12 mM HEPES, 2 mM ATP-Mg, 3 mM $MgCl_2$, 0.02% Triton X-100, 70 mM KCl, 11% glycerol, pH 7.5) containing 100 nM HELLS-CBP, MBP-CDCA7e or SNF2h (100 nM), and incubated at room temperature. At the indicated times, 5 μl remodeling reaction was added to 5 μL stop solution (0.7 mg/ml plasmid DNA, 30 mM ADP, 20% glycerol). 5 μl of each sample was resolved on a 5% polyacrylamide gel in 0.5X TBE at 80V for 3 h and stained with SYBR gold.

Western blotting and immunofluorescence

All Western blotting and immunofluorescence was performed at room temperature. For all Western blots, proteins were transferred to a nitrocellulose membrane (GE) and blocked in Blocking Buffer (4% milk, 1x PBS, 0.1% azide) for 30 min. Membranes were coated in primary antibodies diluted in Abdil (10 mM Tris, 150 mM NaCl, 2 % BSA, 0.1 % Triton X-100, 0.1% azide, pH 7.4) and rocked for 1 h. All primary antibodies were used at 1 μg/mL except for anti-phospho-Aurora B (1:200), anti-MCM7 (1:9000), anti-survivin (12 μg/ml), Plx1 (0.2 μg/mL) and anti-Aurora B (5 μg/ml). Membranes were washed three times with PBS-T (1X PBS, 0.05% Tween-20). Primary antibodies were detected by coating membranes with LI-COR IRDye secondary antibody (1:15,000 in Abdil) for an hour. Membranes were washed as before three times with PBS-T, once with PBS, and subsequently imaged and quantified on an Odyssey Infrared Imaging System.

For all immunofluorescence experiments, coverslips were blocked in 500 μL Abdil overnight. Coverslips were incubated in primary antibody (50 μL) diluted in Abdil for 1 h. All primary antibodies were used at 1 μg/mL. Coverslips were washed three times with Abdil and incubated in secondary antibody (50 μL) diluted in Abdil. Secondary used were conjugated with Alexa Fluor 555 or Alexa Fluor 488 (Life Technologies) diluted 1:1000 in Abdil. Coverslips were washed three times in Abdil. For staining DNA, coverslips were incubated in Hoechst (0.5 μg/mL) or PicoGreen (1:500) diluted in Abdil for 30 min, and washed once with Abdil. Coverslips were mounted in 2 μL Mounting Buffer (90% glycerol, 1xPBS) and sealed with nail polish.

All microscopy was performed on a Delta Vision Spectris (Applied Precision) microscope. For maximum and average projections, Z-sections of 200 nM were collected over the entire depth of the sample. All image analysis was performed with ImageJ. To measure chromosome lengths, dashed lines were drawn down the center of each chromosome axis, and the distance was recorded.

Protein alignment

Protein alignment was performed with MacVector. Proteins were aligned using ClustalW with an open gap penalty of 10 and an extended gap penalty of 0.2.

Xenopus egg extracts

Extract preparation and depletions

CSF-arrested *Xenopus laevis* egg crude extracts were prepared as described(Murray, 1991). Extracts were kept on ice, and all extract experiments were performed at 20 °C unless specified. For experiments in interphase extract, $CaCl_2$ was added (0.3 mM final). Where indicated, Plx1 inhibitor BI2536 was used at 10 μM, and geminin was used at 200 nM.

To immunodeplete HELLS, CDCA7e, Plx1, or the CPC in 50 μl extract, 25 μg anti-HELLS, anti-CDCA7e, or anti-INCENP antibody was coupled to 100 μl Protein A Dynabeads (ThermoFisher). INCENP antibody was crosslinked to the beads with BS_3 (ThermoFisher), following manufacture's protocol. Antibody beads were washed extensively in sperm dilution buffer (5 mM HEPES, 100 mM KCl, 150 mM sucrose, 1 mM $MgCl_2$, pH 8.0), split in half, and extract was depleted in two rounds at 4 °C, each 45 min. Beads were removed on a magnet. To deplete H1M, the previous depletion protocol was performed twice. To deplete DNMT1, 85 μL serum was coupled to 25 μL protein A beads as before and used to deplete 33 μL extract in three separate rounds. For all experiments, mock depletion was performed using purified preimmune rabbit IgG (Sigma-Aldrich).

Histones H3-H4 were depleted as described(Zierhut et al., 2014). To deplete 50 μl extract, 130 μg anti-H4K12ac antibody was coupled to 12.5 ul rProtein A sepharose (GE Healthcare). Extract was rotated with beads for 60 min at 4 °C and recovered.

Depleted extract was incubated with 8.5 μl fresh rProtein A sepharose to recover leached antibody for 35 min at 4 °C and recovered.

Analysis of chromatin associated proteins

Analysis of chromatin associated proteins was carried out as described(Zierhut et al., 2014). Nucleosome beads (0.15 μl/μl extract) were incubated in *Xenopus* egg extract for 2 h at 16 °C for MS experiments or 80 min at 20 °C for all other experiments, with flicking every 20 minutes. The extract was diluted with 10 volumes CSF-XB (10 mM HEPES, 100 mM KCl, 1 mM $MgCl_2$, 50 mM sucrose, 5 mM EGTA, pH 8), and recovered on a magnet for 5 min at 4 °C. Beads were washed and recovered 3 times with 150 μl CSF-XB with 0.05% Triton X-100. Beads were resuspended in SDS-PAGE buffer and boiled. The beads were collected on a magnet and the supernatant resolved by gel electrophoresis. For mass spectrometry experiments, samples were run 1 cm into the gel.

Mass spectrometry

For MS analysis, standard trypsin digestion was performed followed by LC-MS/MS on a Finnigan Orbitrap XL (Thermo Scientific) mass spectrometer. MS/MS data were extracted with Proteome Discoverer (Thermo Scientific) and queried against an mRNA derived *X. laevis* reference database(Wuhr et al., 2014) with Mascot (Matrixscience). This database was crucial, since the previously used NCBI database did not contain embryonic CDCA7e at the time. Mass tolerance of 20 p.p.m. peptide

precursor and 0.5 Da peptide fragments were used. Oxidized methionine, N-terminal acetylation and up to three missed cleavage sites were allowed. Proteome Discoverer (Thermo Scientific) was used to quantify protein abundance on chromatin. LC-MS peaks of each identified peptide were integrated, and isotope peaks for each peptide were summed to give the total peptide area. Protein abundance was calculated by averaging of the three greatest peptide signals for each protein. Experimental reproducibility of this procedure has been reported(Zierhut et al., 2014).

Unsupervised clustering of mass spectrometry data was performed on the top 70th percentile of chromatin associated proteins enriched over their extract concentration(Wuhr et al., 2014). Clustering was performed using the default HOPACH algorithm(Van der Laan and Pollard, 2003) using cosine angle as the distance metric. Entire clustering is shown in Figure A-11.

Immunoprecipitation

For co-immunoprecipitation from *Xenopus* egg extracts, anti-HELLS and anti-CDCA7e antibodies (25 μg) were coupled to 100 μl Protein A Dynabeads for 1 h at room temperature. Antibodies were crosslinked to the beads with BS_3, following manufacture's protocol. Antibody-beads were washed extensively in sperm dilution buffer (5 mM HEPES, 100 mM KCl, 150 mM sucrose, 1 mM $MgCl_2$, pH 8.0). 50 μl extract was added to the beads and incubated on ice for 1 h with flicking every 20 min. The extract was diluted with 10 volumes CSF-XB (100 mM KCl, 1 mM $MgCl_2$, 50 mM sucrose, 5 mM EGTA and 10 mM HEPES, pH 8), and recovered on a magnet for 5

min. Beads were washed and recovered 3 times with 150 μl CSF-XB with 0.05% Triton X-100. Beads were resuspended in SDS-PAGE buffer and boiled. Control immunoprecipitation was performed using purified preimmune rabbit IgG (Sigma-Aldrich).

To test somatic CDCA7 and CDCA7L binding to HELLS, MYC-CDCA7, MYC-CDCA7L, and MYC-CDCA7e mRNA were generated with an mMESSAGE mMACHINE SP6 kit (Life Technologies) according to manufacturer's instructions. mRNA was added to interphase *Xenopus* egg extract (100 μg/ml final) and incubated for 90 min, prior to immunoprecipitation experiment as described previously.

For immunoprecipitation of exogenously expressed Myc-CDCA7e and HELLS-GFP, the indicated mRNAs were generated with an mMESSAGE mMACHINE SP6 kit (Life Technologies) according to manufacturer's instructions. mRNA was added to interphase *Xenopus* egg extract (100 μg/ml final) and incubated for 90 min. Cycloheximide was added to stop translation (100 μg/mL), and half of the sample was cycled to M phase by addition of cyclin-B Δ90 (24 μg/mL) prior to immunoprecipitation experiment as described previously.

Nucleosome assembly on plasmids

pBlueScript plasmid was incubated in interphase or mitotic *Xenopus* extract (20 ng/uL final) at 20 °C. At the indicated time points, 25 μL extract was removed and diluted 1:10 in Stop Buffer (20 mM Tris, 20 mM EDTA, 0.5% SDS, 0.05 mg/ml RNase A, pH 8.0 @ 22 °C) and incubated for 25 min at 37 °C. The solution was diluted 1:1 in Stop

Buffer supplemented with 1 mg/mL Proteinase K instead of RNase A and incubated for 30 min at 37 °C. DNA was phenol-chloroform extract twice, chloroform extract once, and ethanol precipitated. DNA pellets were resuspended in TE (10 mM Tris, 1 mM EDTA, pH 8.0 @ 22 °C) containing 0.05 mg/mL RNase A, and incubated 37 °C for 15 minutes. Samples were resolved on 1% agarose gel for 36 h at 0.75 V/cm. Gel was stained with SybrSafe (Thermo Fisher) and imaged.

Chromosome and spindle assembly

To assemble mitotic spindles, demembranated *Xenopus* sperm (1,000 sperm/μL extract) was replicated in interphase *Xenopus* egg extract for 90 min at 20 °C. To cycle the extract into mitosis, two volumes of fresh CSF extract and cycle B Δ90 (24 μg/mL) was added. Where indicated, nocodazole was added to 32 μM to depolymerize microtubules. The extract was mixed and incubated for 45-60 min at 20 °C. Extract (20 μL) was diluted 1:100 in Spindle Fix (1X BRB80 (80 mM PIPES, 1 mM $MgCl_2$, 1 mM EGTA pH 6.9), 30% glycerol, 2% formaldehyde), mixed by inversion, and incubated for 5 min at room temperature. The sample was layer on top of 5 mL Spindle Cushion (1X BRB80, 40% glycerol) and centrifuged onto a coverslip (Sorvall HB6, 5500 rpm, 18 °C for 15 min). The cushion interface was washed twice in 1X BRB80 and the cushion was removed by aspiration. The cover slip was removed and fixed in ice cold methanol (300 μL) for 5 min. Spindles were visualized by processing the coverslips for immunofluorescence (above).

To assemble mitotic chromosomes, demembranated *Xenopus* sperm (1,000 sperm/μL extract) was replicated in interphase *Xenopus* egg extract for 90 min at 20 °C. To cycle the extract into mitosis, two volumes of fresh CSF extract and cyclin B Δ90 (24 μg/mL) was added. Where indicated, nocaodazole was added to 32 μM to depolymerize microtubules. The extract was mixed and incubated for 45-60 min at 20 °C. Extract was dilute 1:4 in Chromosome Dilution Buffer (10 mM HEPES, 250 mM Sucrose, 5mM EGTA, 200 mM KCl, 0.5 mM $MgCl_2$, pH 8.0), and incubated 10 min at room temperature. Mixture was dilute 1:4 in Chromosome Fix (1X MMR (5 mM HEPES, 100 mM NaCl, 2 mM KCl, 1mM $MgCl_2$, 2 mM $CaCl_2$, 0.1 mM EDTA, pH 7.8), 0.5% Triton X-100, 20% glycerol, 2.664% formaldehyde) and incubated 5 min at room temperature. The sample was layer on top of X mL Chromosome Cushion (1X MMR, 40% glycerol) and centrifuged onto a coverslip (Sorvall HB6, 8000 rpm, 30min at 18°C). The cushion interface was washed twice in 1X BRB80 and the cushion was removed by aspiration. Chromosomes were visualized by processing the coverslips for immunofluorescence (above).

DNA methylation assays

To directly assay for DNA methylation, 1 μL ^{3}H-SAM (Perkin Elmer, NET155H) was added to 50 μL interphase extract containing sperm chromatin (1000 sperm/μL) and incubated for 22 °C for 1 hr. The extract was diluted with 250 μL CPB (50 mM KCl, 5 mM MgCl2, 20 mM HEPEK-KOH, 2% sucrose, pH 7.7), and mixed by flicking. Nuclei

were isolated with the Wizard Genomic DNA Purification Kit (Promega, A1120), and ^{3}H incorporation was determined by scintillation counting.

To indirectly assay for DNA methylation, *Xenopus* sperm (3000/μL) was added to interphase extract and incubated for 3 hr at 22 °C. Extract was diluted five-fold in CPB + 0.1% NP-40, and layered onto a CPB-30% sucrose cushion. Chromatin was pelleted by centrifugation, 15,000g for 10 minutes. The sample-cushion interface was washed twice with TBS + 0.5% Triton X-100, and the cushion was removed. The chromatin pellet was recovered in 20 μL SDS-PAGE buffer, resolved by gel electrophoresis, and Western blotting was performed against the indicated proteins. Abrogation in DNA methylation results in the accumulation of H3-ubiquitylation, monitored by a slower migrating H3 band.

Kinetoplast DNA decatenation assay

Kinetoplast DNA (Topogen) (10 ng/μL) was added to *Xenopus* egg extract, and the mixture was incubated on ice. At the indicated time, 15 μL extract was removed, diluted 1:10 in Stop Buffer (20 mM Tris, 20 mM EDTA, 0.5% SDS, 0.05 mg/ml RNase A, pH 8.0 @ 22 °C) and incubated for 25 min at 37 °C. The solution was diluted 1:1 in Stop Buffer supplemented with 1 mg/mL Proteinase K instead of RNase A and incubated for 30 min at 37 °C. DNA was phenol-chloroform extract twice, chloroform extract once, and ethanol precipitated. DNA pellets were resuspended in TE (10 mM Tris, 1 mM EDTA, pH 8.0 @ 22 °C) containing 0.05 mg/mL RNase A, and incubated 37 °C for 15 minutes. Samples were resolved on 1% agarose. Gel was stained with SybrSafe and

imaged. For the indicated experiments, nucleosomal kinetoplast chromatin was assembled by salt dialysis, and verified by MNase digestion.

CHAPTER 6: APPENDIX

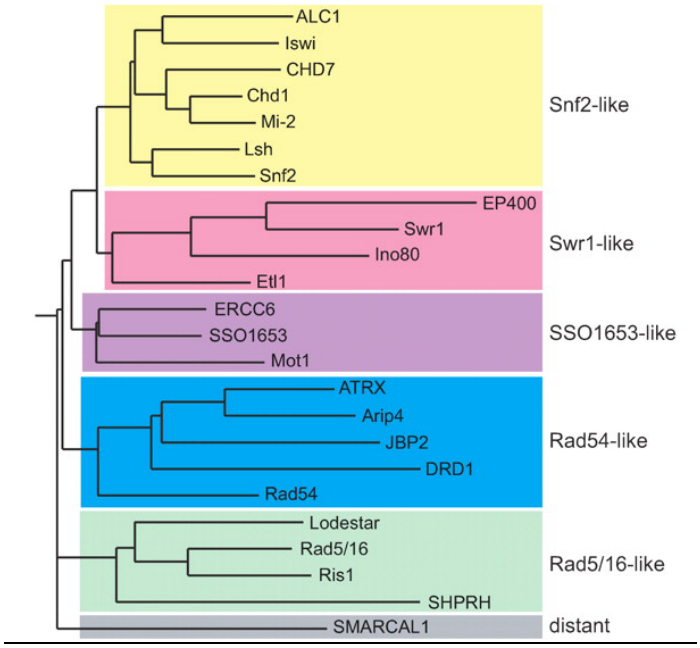

Figure A-1. Phylogeny of SNF2 family remodeling proteins. Rooted tree of SNF family proteins, taken from (Flaus et al., 2006).

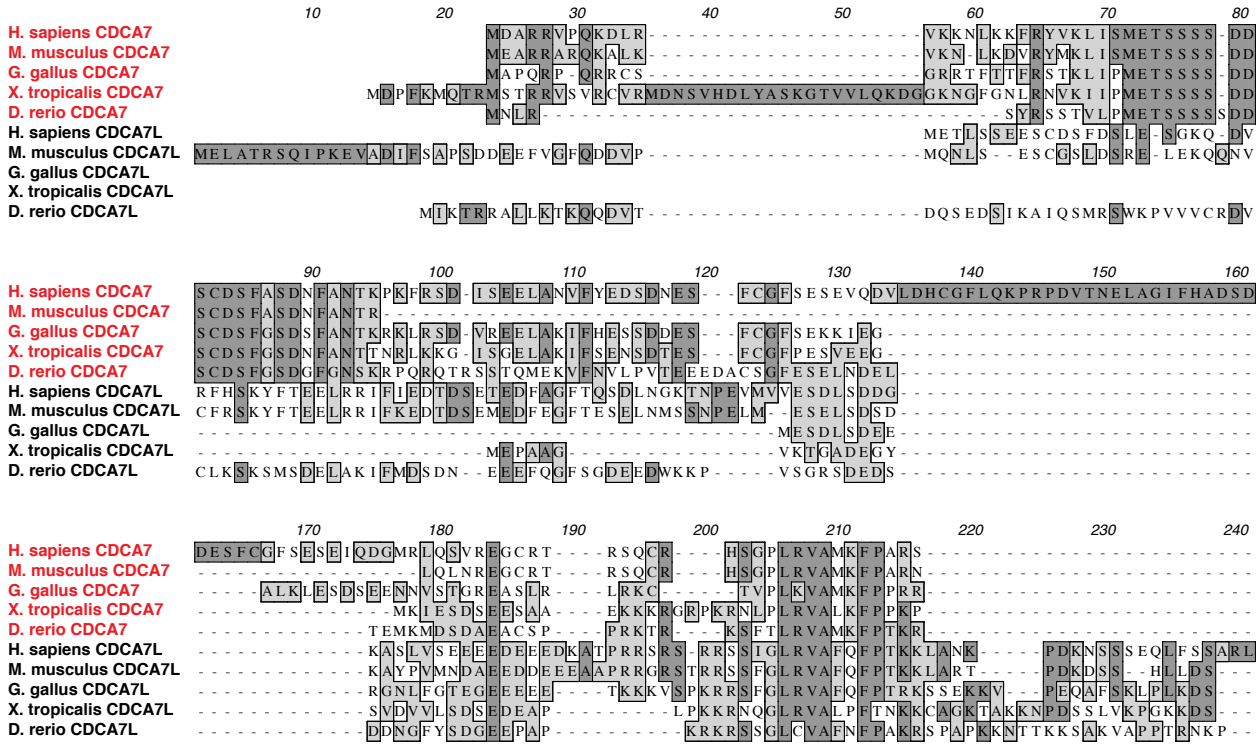
H. sapiens CDCA7
M. musculus CDCA7
G. gallus CDCA7
X. tropicalis CDCA7
D. rerio CDCA7
H. sapiens CDCA7L
M. musculus CDCA7L
G. gallus CDCA7L
X. tropicalis CDCA7L
D. rerio CDCA7L

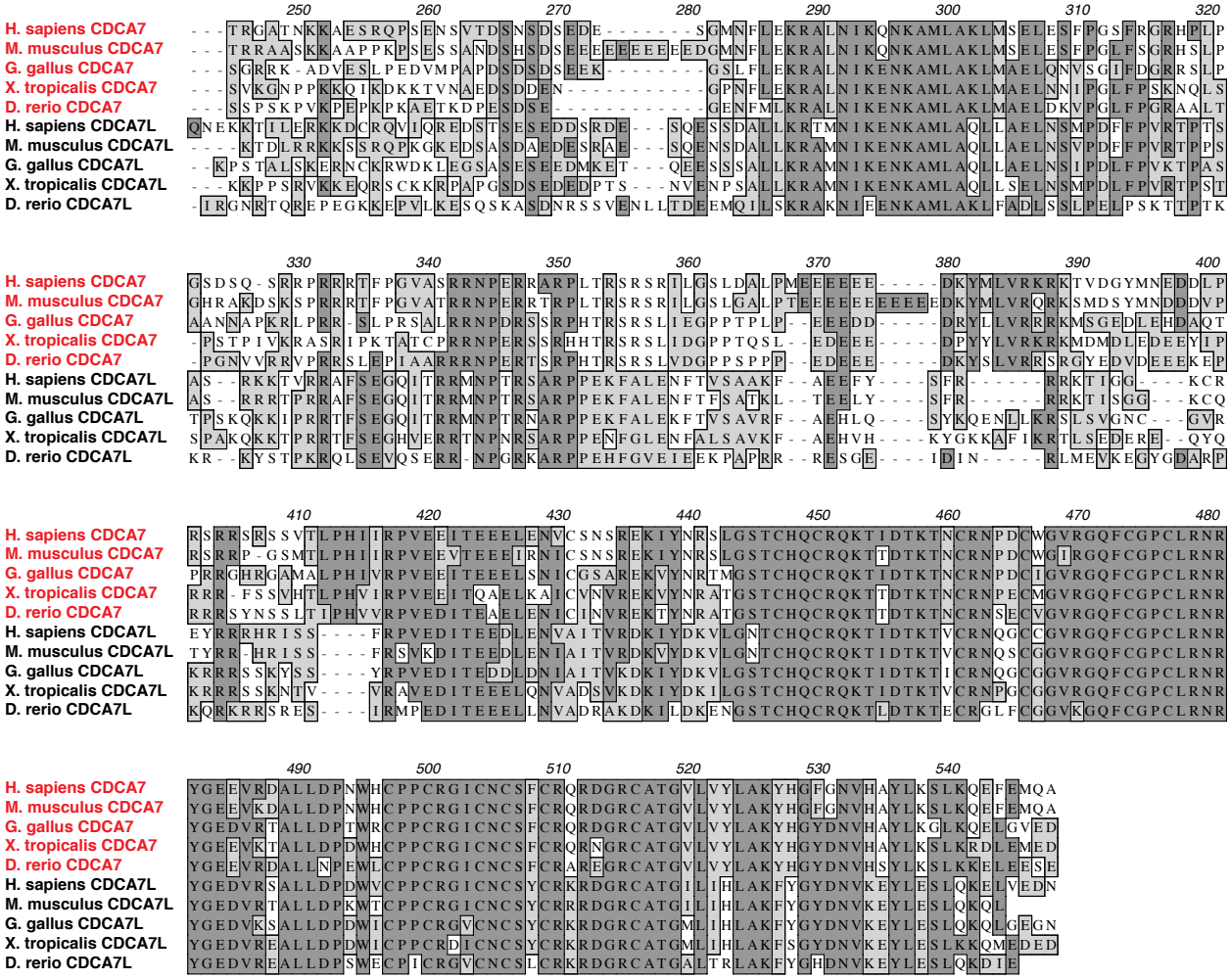

Figure A-2. Alignment of CDCA7 (red) and CDCA7L (black) from the indicated species.

Gene Symbol	Protein	Abundance on Nucleosomes	Abundance on Naked DNA
YBX2	Y-box-binding protein 2	n.d.	4.88×10^7
CL19415Contig1	Uncharacterized Protein	n.d.	3.36×10^7
FARSB	Phenylalanine--tRNA ligase beta subunit	n.d.	2.64×10^7
KARS	Lysine--tRNA ligase	n.d.	2.57×10^7
AIMP1	Aminoacyl tRNA synthase complex-interacting multifunctional protein 1	n.d.	2.46×10^7
KARS	Lysine--tRNA ligase	n.d.	2.42×10^7
EPRS	Bifunctional glutamate/proline--tRNA ligase	n.d.	2.32×10^7
DARS	Aspartate--tRNA ligase, cytoplasmic	n.d.	2.04×10^7
QARS	Glutamine--tRNA ligase	n.d.	1.91×10^7
AIMP1	Aminoacyl tRNA synthase complex-interacting multifunctional protein 1	n.d.	1.69×10^7

Figure A-3. Most abundant proteins binding mitotic naked DNA. Proteins with >10 fold enrichment on naked DNA over nucleosome beads isolated from mitotic extract, quantified by mass spectrometry.

Gene Symbol	Protein	Abundance on Naked DNA	Abundance on Nucleosomes
HIST1H4A	Histone H4	2.07×10^{10}	6.08×10^{8}
HIST2H2BF	Histone H2B	1.91×10^{10}	4.25×10^{8}
HIST2H3A	Histone H3.2	1.40×10^{10}	1.33×10^{8}
H2AFX	Histone H2A.x	1.19×10^{10}	3.58×10^{8}
HIST2H2AB	Histone H2A type 2-B	1.13×10^{10}	3.58×10^{8}
H1FOO	Histone H1oo	1.24×10^{10}	7.22×10^{7}
AURKB	Aurora kinase B	8.01×10^{9}	1.43×10^{7}
H1FOO	Histone H1oo	7.77×10^{9}	6.45×10^{7}
RCC1	Regulator of chromosome condensation	2.54×10^{9}	n.d.
SUPT16H	FACT complex subunit SPT16	1.36×10^{9}	n.d.
RAN	GTP-binding nuclear protein Ran	1.23×10^{9}	n.d.
SSRP1	FACT complex subunit SSRP1	8.30×10^{8}	n.d.
PI4KA	Phosphatidylinositol 4-kinase alpha	n.d.	3.49×10^{9}
DARS	Aspartate--tRNA ligase, cytoplasmic	n.d.	1.77×10^{9}
HMGB2	High mobility group protein B2	2.30×10^{7}	1.72×10^{9}
KARS	Lysine--tRNA ligase	n.d.	1.32×10^{9}
AIMP1	Aminoacyl tRNA synthase complex-interacting multifunctional protein 1	n.d.	1.23×10^{9}
EPRS	Bifunctional glutamate/proline--tRNA ligase	n.d.	1.03×10^{9}
QARS	Glutamine--tRNA ligase	n.d.	8.44×10^{8}
FARSB	Phenylalanine--tRNA ligase beta subunit	n.d.	7.25×10^{8}
IARS	Isoleucine--tRNA ligase, cytoplasmic	n.d.	7.12×10^{8}
LARS	Leucine--tRNA ligase, cytoplasmic	n.d.	7.04×10^{8}

Figure A-4. Most abundant interphase proteins affected by nucleosomes. Proteins with >10 fold enrichment on nucleosome beads (top) or naked DNA beads (bottom) isolated from interphase extract, quantified by mass spectrometry

Gene Symbol	Protein	Abundance on Interphase chromatin	Abundance on Interphase Chromatin
TUBB4B	Tubulin beta	1.34×10^{7}	1.38×10^{9}
TUBA1B	Tubulin alpha	n.d.	1.02×10^{9}
SPAG5	Sperm-associated antigen 5	n.d.	4.92×10^{8}
KNSTRN	Small kinetochore-associated protein	n.d.	3.56×10^{8}
ACTG1	Actin, cytoplasmic 2	5.76×10^{7}	2.94×10^{8}
NCAPG	Condensin complex subunit 3	n.d.	2.46×10^{8}
SMC4	Structural maintenance of chromosomes protein 4	n.d.	2.32×10^{8}
KIAA1524	CIP2A	2.71×10^{7}	2.10×10^{8}
NCAPD2	Condensin complex subunit 1	n.d.	2.10×10^{8}
SMC2	Structural maintenance of chromosomes protein 2	n.d.	1.97×10^{8}
DDX3X	ATP-dependent RNA helicase DDX3X	2.10×10^{10}	n.d.
MCM5	DNA replication licensing factor MCM5	2.16×10^{9}	2.21×10^{7}
MCM3	MCM3 minichromosome maintenance deficient 3	2.00×10^{9}	n.d.
MCM7	DNA replication licensing factor MCM7	1.78×10^{9}	n.d.
MCM4	DNA replication licensing factor MCM4	1.76×10^{9}	1.74×10^{7}
MCM2	DNA replication licensing factor MCM2	1.63×10^{9}	n.d.
MCM6	DNA replication licensing factor MCM6	1.33×10^{9}	1.08×10^{7}
HELLS	Lymphoid-specific helicase	3.58×10^{8}	2.06×10^{7}
NUP214	Nuclear pore complex protein Nup214	2.53×10^{8}	n.d.
CDCA7	Cell division cycle-associated protein 7	2.35×10^{8}	n.d.

.

Figure A-5. Most abundant proteins affected by the cell cycle. Proteins with >10 fold enrichment on either M phase (top) or interphase (bottom) chromatin, quantified by mass spectrometry.

Gene Symbol	Protein	Abundance on H3K9me3 chromatin	Abundance on H3 unmodified chromatin
EMC4	ER membrane protein complex subunit 4	1.11×10^{10}	n.d.
CHD3	Chromodomain-helicase-DNA-binding protein 3	2.28×10^{9}	n.d.
CBX3	Chromobox protein homolog 3	4.27×10^{9}	1.27×10^{7}
ATRX	Transcriptional regulator ATRX	3.69×10^{9}	n.d.
TATDN1	Putative deoxyribonuclease TATDN1	3.47×10^{9}	n.d.
SUV39H1	Histone-lysine N-methyltransferase SUV39H1	2.15×10^{9}	n.d.
ERBB2IP	Protein LAP2	1.79×10^{9}	n.d.
RBPJ	Recombining binding protein suppressor of hairless	1.11×10^{9}	n.d.
CDCA8	Borealin	6.30×10^{8}	n.d.
CBX5	Chromobox homolog 5 (HP1 alpha homolog, Drosophila), isoform CRA_a	5.53×10^{8}	n.d.
FANCL	E3 ubiquitin-protein ligase FANCL	4.98×10^{8}	n.d.
ASAP3	Arf-GAP with SH3 domain, ANK repeat and PH domain-containing protein 3	4.97×10^{8}	n.d.
SUV39H2	Histone-lysine N-methyltransferase SUV39H2	4.86×10^{8}	n.d.
IRS1	Insulin receptor substrate 1	4.37×10^{8}	n.d.
ZNF850	Zinc finger protein 850	4.24×10^{8}	n.d.

Figure A-6. Most abundant proteins binding H3K9me3. Proteins with >10 fold enrichment on H3K9me3 nucleosome beads over H3 unmodified isolated from interphase CPC depleted extract, quantified by mass spectrometry.

Gene Symbol	Protein	Abundance on △CPC chromatin	Abundance on △MOCK chromatin
CDCA7	Cell division cycle-associated protein 7	4.62×10^8	n.d.
HELLS	Lymphoid-specific helicase	4.62×10^8	2.06×10^7
CHD1	Chromodomain-helicase-DNA-binding protein 1	1.89×10^8	n.d.
EIF2B3	Translation initiation factor eIF-2B subunit gamma	1.64×10^8	n.d.
CCDC39	Coiled-coil domain-containing protein 39	1.43×10^8	n.d.
UBE3C	Ubiquitin-protein ligase E3C	1.42×10^8	n.d.
CUL9	Cullin-9	1.32×10^8	n.d.
PLCH2	1-phosphatidylinositol 4,5-bisphosphate phosphodiesterase eta-2	1.01×10^8	n.d.
CDH23	Cadherin 23 isoform B2	9.49×10^7	n.d.
BAZ1A	Bromodomain adjacent to zinc finger domain protein 1A	6.59×10^7	n.d.
TUBB4B	Tubulin beta	4.16×10^7	1.38×10^9
TUBA1B	Tubulin alpha	2.20×10^7	1.02×10^9
CCNB2	Cyclin B2	n.d.	1.81×10^9
CDCA8	Borealin	n.d.	1.67×10^9
AURKB	Aurora kinase B	n.d.	1.27×10^9
ZFP161	Zinc finger protein 161 homolog	n.d.	1.14×10^6
ZMYM4	Zinc finger MYM-type protein 4	n.d.	1.09×10^9
ENO1	Alpha-enolase	9.50×10^6	1.01×10^9
GAPDH	Glyceraldehyde-3-phosphate dehydrogenase	n.d.	9.89×10^8
INCENP	Inner centromere protein	n.d.	8.26×10^8

Figure A-7. Most abundant proteins affected by the CPC. Proteins with >10 fold enrichment on CPC depleted (top) or mock depleted (bottom) nucleosome beads isolated from M phase extract, quantified by mass spectrometry.

Gene Symbol	Protein	Abundance on △H1 chromatin	Abundance on △MOCK chromatin
DOK6	Docking protein 6	4.65×10^{10}	n.d.
C11ORF16	Uncharacterized protein C11orf16	1.55×10^{10}	n.d.
HIST2H2AB	Histone H2A type 2-B	1.22×10^{10}	n.d.
H2AFX	Histone H2A.x	1.07×10^{10}	8.73×10^{8}
HIST2H2AB	Histone H2A type 2-B	1.06×10^{10}	7.08×10^{7}
RPA3	Replication protein A 14 kDa subunit	3.21×10^{9}	6.13×10^{7}
MFN2	Mitofusin-2	2.037×10^{9}	n.d.
WDR35	WD repeat-containing protein 35	7.61×10^{8}	n.d.
DPPA2	Developmental Pluripotency Associated 2	6.28×10^{8}	1.50×10^{7}
EIF2S2	Eukaryotic translation initiation factor 2 subunit 2	3.41×10^{8}	n.d.
PRPF8	Pre-mRNA-processing-splicing factor 8	n.d.	2.41×10^{10}
SUMO3	Small ubiquitin-related modifier 3	n.d.	2.47×10^{9}
SUMO2	Small ubiquitin-related modifier 2	n.d.	2.43×10^{9}
H1FOO	Histone H1oo		2.38×10^{9}
TBL3	Transducin beta-like protein 3	n.d.	1.61×10^{9}
DC015933	Uncharacterized Protein	n.d.	9.73×10^{8}
HMGB1	High mobility group protein B1		4.41×10^{8}
DSP	Desmoplakin	n.d.	4.25×10^{8}
ACTB	Actin, cytoplasmic 1		3.67×10^{8}
ANXA7	Annexin A7	n.d.	3.55×10^{8}

Figure A-8. Most abundant proteins affected by H1. Proteins with >10 fold enrichment on H1 depleted (top) or mock depleted (bottom) nucleosome beads isolated from M phase extract, quantified by mass spectrometry.

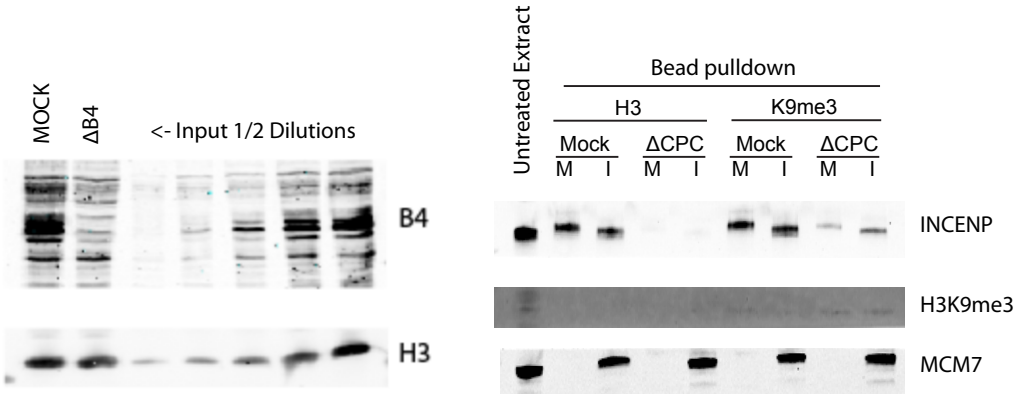

Figure A-9. Depletions associated with Figure 2-7. Extract from the experiments associated with Figure 2-7 were analyzed by Western blotting for the indicated proteins to assess depletion level.

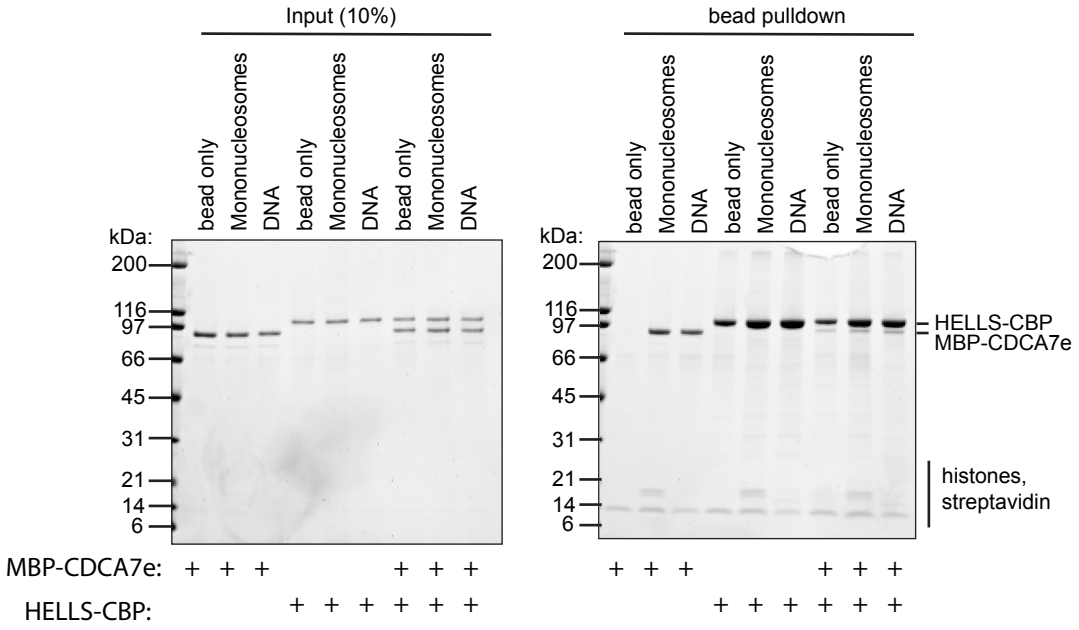

Figure A-10. HELLS and CDCA7 bind mononucleosomes independently of each other in vitro. Coomassie stained gel of a pulldown of mononucleosome beads without linker DNA or naked DNA beads incubated with the indicated proteins. Uncoupled beads were used to control for non-specific binding. Note the strong non-specific binding of HELLS to the bead only control.

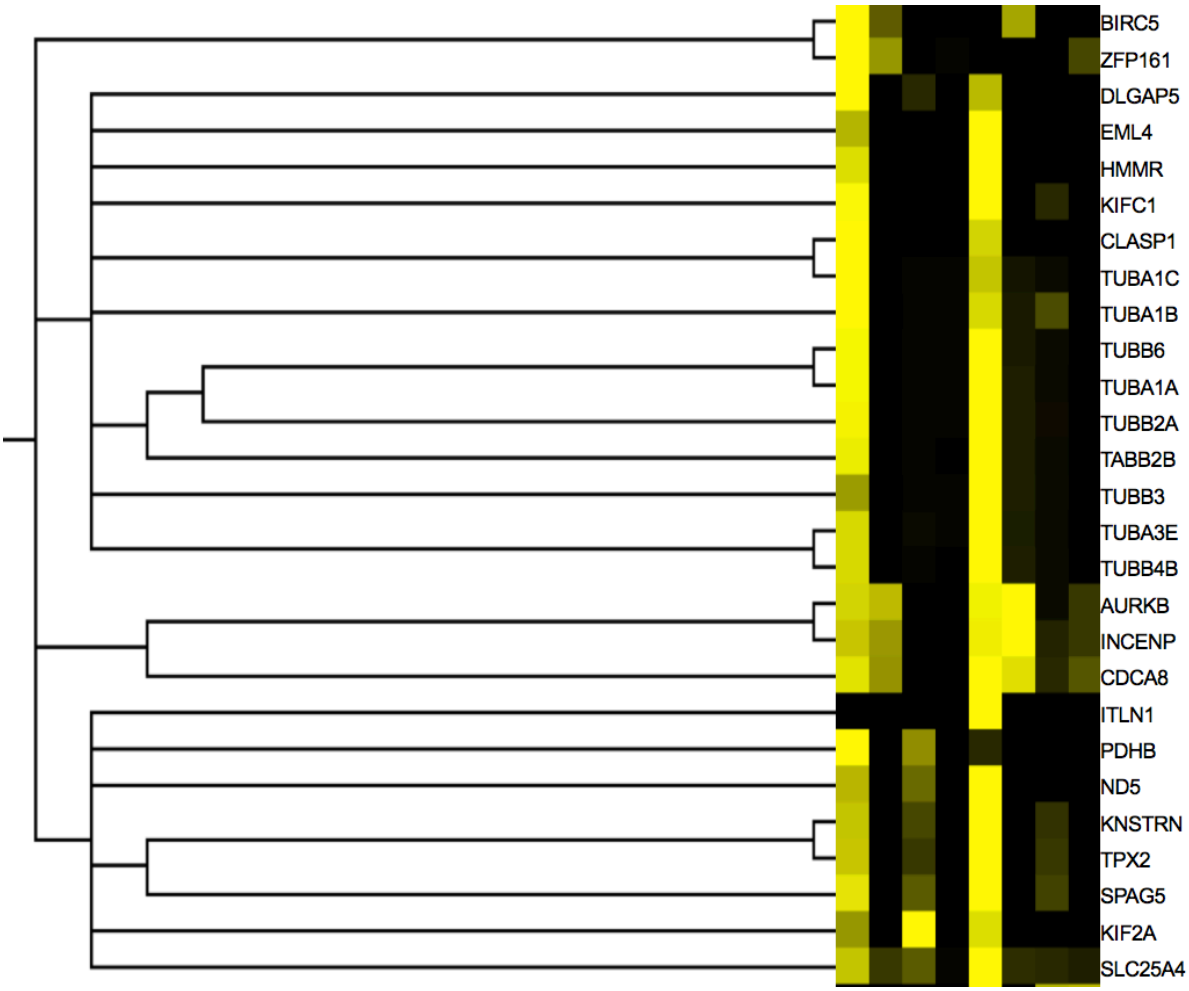
BIRC5
ZFP161
DLGAP5
EML4
HMMR
KIFC1
CLASP1
TUBA1C
TUBA1B
TUBB6
TUBA1A
TUBB2A
TABB2B
TUBB3
TUBA3E
TUBB4B
AURKB
INCENP
CDCA8
ITLN1
PDHB
ND5
KNSTRN
TPX2
SPAG5
KIF2A
SLC25A4

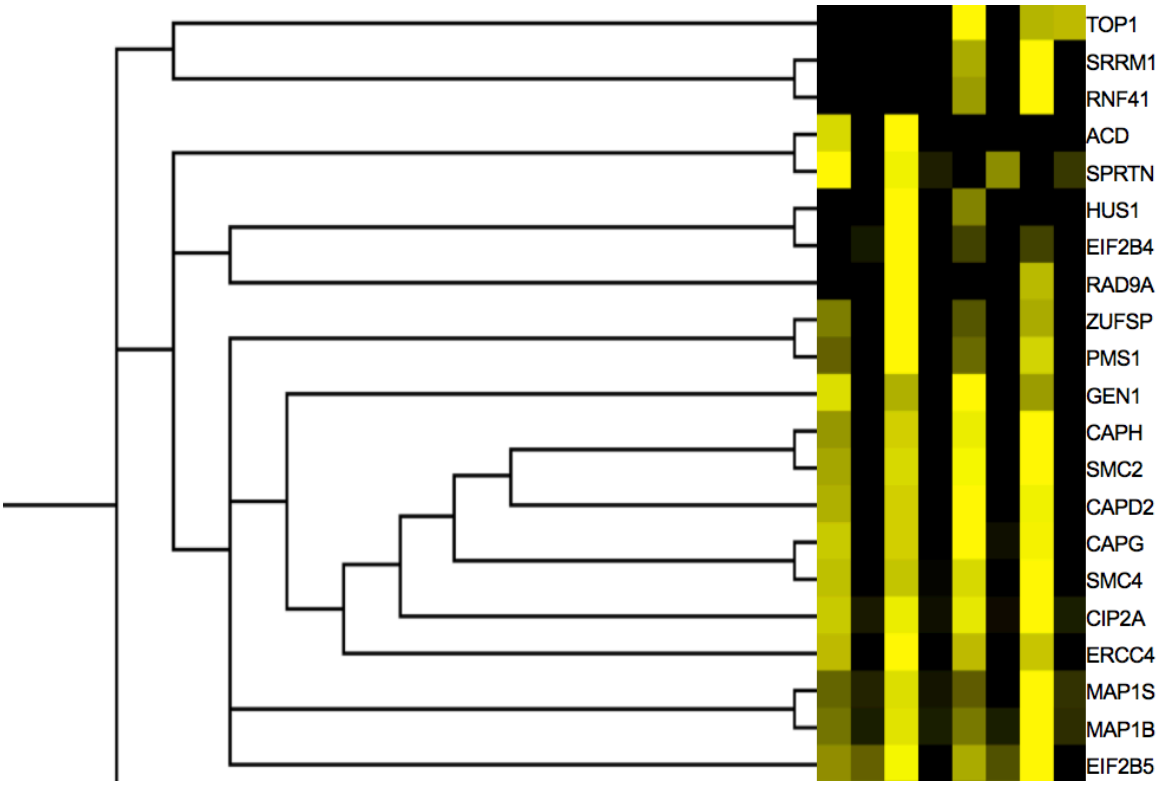
TOP1
SRRM1
RNF41
ACD
SPRTN
HUS1
EIF2B4
RAD9A
ZUFSP
PMS1
GEN1
CAPH
SMC2
CAPD2
CAPG
SMC4
CIP2A
ERCC4
MAP1S
MAP1B
EIF2B5

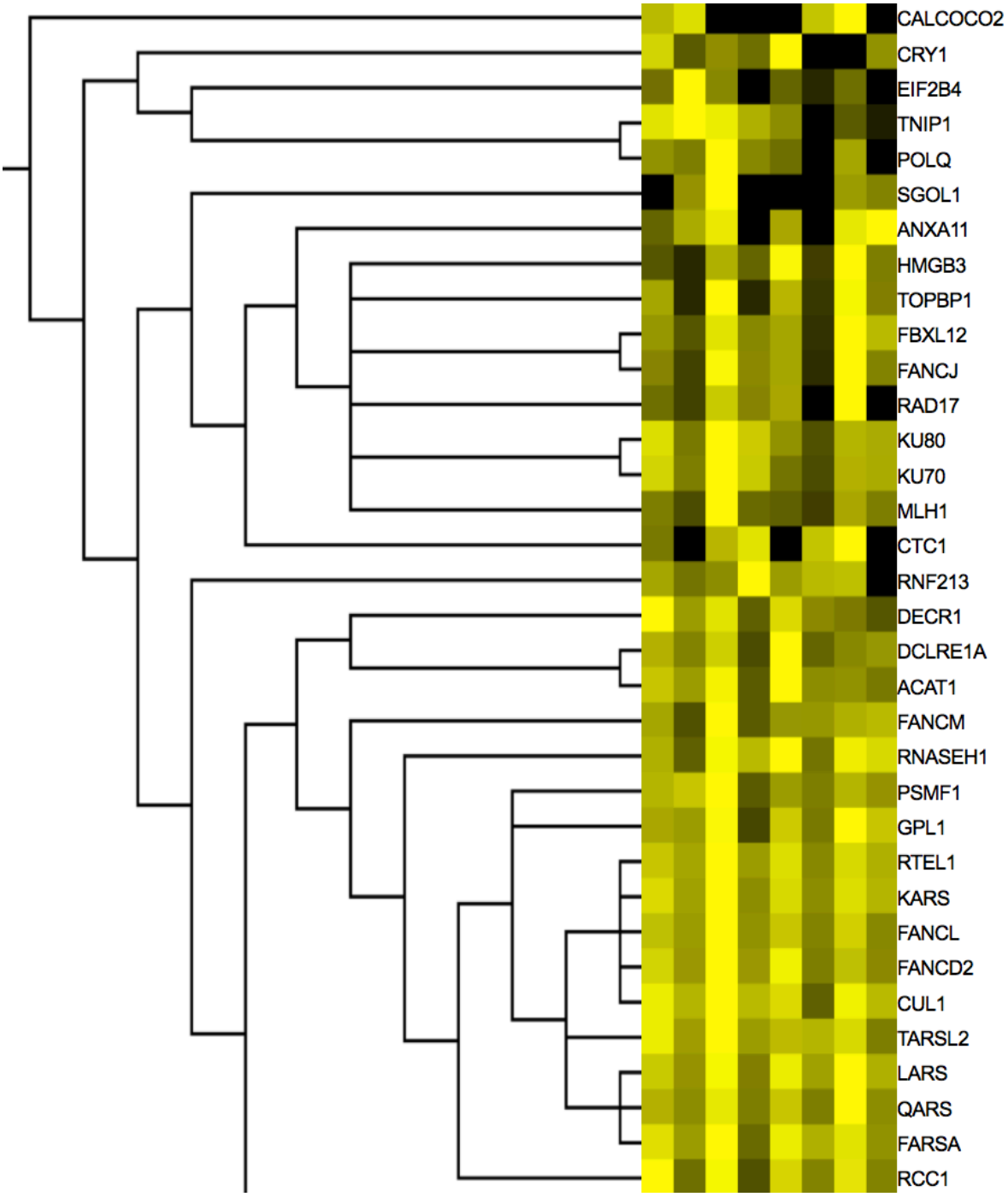
CALCOCO2
CRY1
EIF2B4
TNIP1
POLQ
SGOL1
ANXA11
HMGB3
TOPBP1
FBXL12
FANCJ
RAD17
KU80
KU70
MLH1
CTC1
RNF213
DECR1
DCLRE1A
ACAT1
FANCM
RNASEH1
PSMF1
GPL1
RTEL1
KARS
FANCL
FANCD2
CUL1
TARSL2
LARS
QARS
FARSA
RCC1

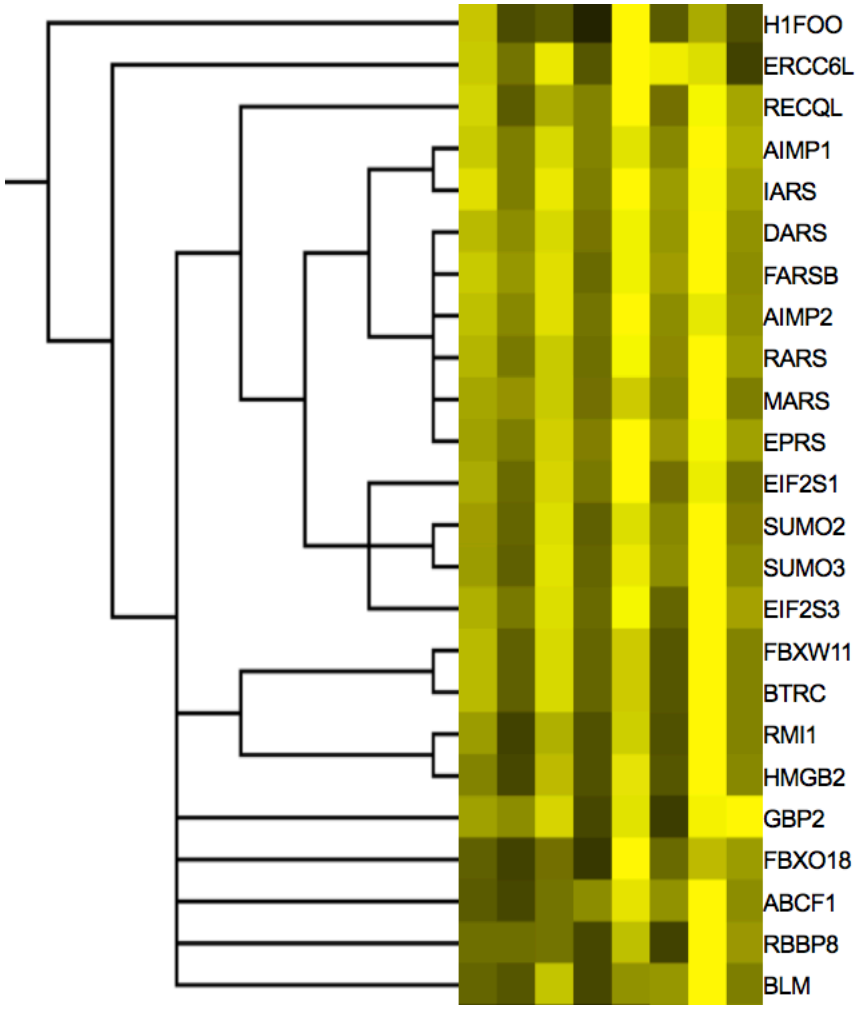
H1FOO
ERCC6L
RECQL
AIMP1
IARS
DARS
FARSB
AIMP2
RARS
MARS
EPRS
EIF2S1
SUMO2
SUMO3
EIF2S3
FBXW11
BTRC
RMI1
HMGB2
GBP2
FBXO18
ABCF1
RBBP8
BLM

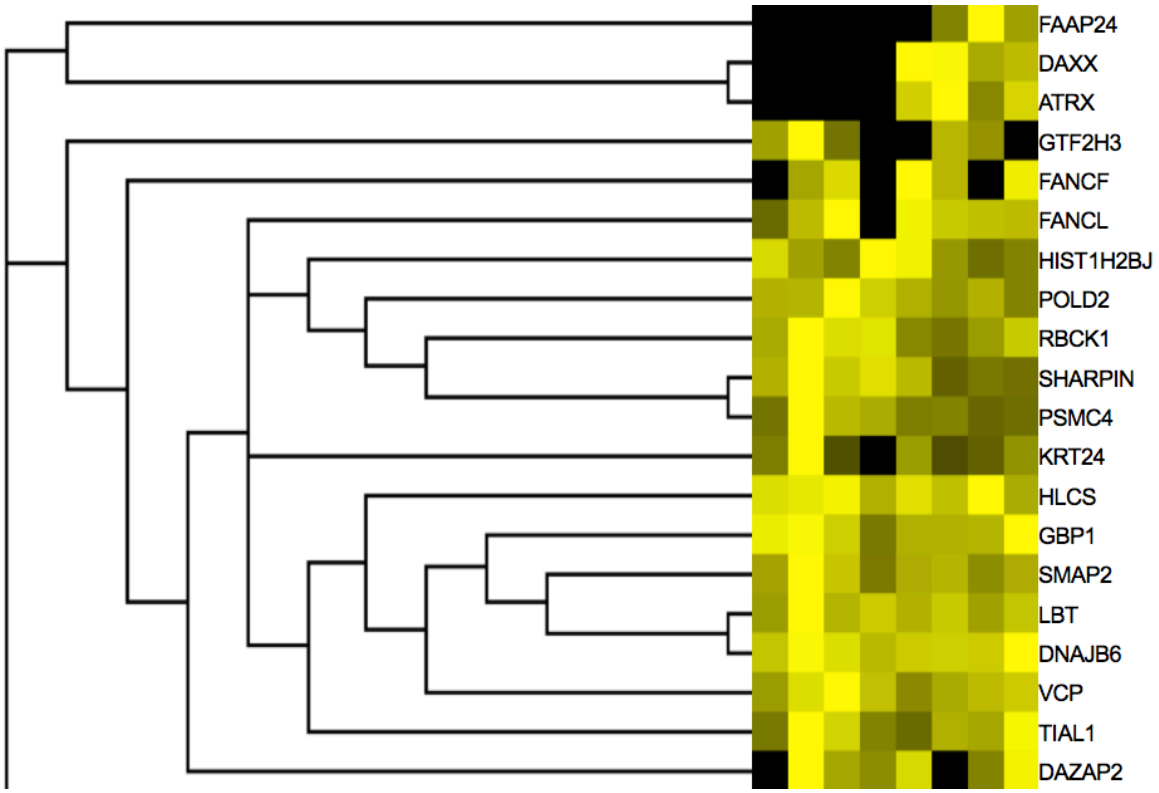
FAAP24
DAXX
ATRX
GTF2H3
FANCF
FANCL
HIST1H2BJ
POLD2
RBCK1
SHARPIN
PSMC4
KRT24
HLCS
GBP1
SMAP2
LBT
DNAJB6
VCP
TIAL1
DAZAP2

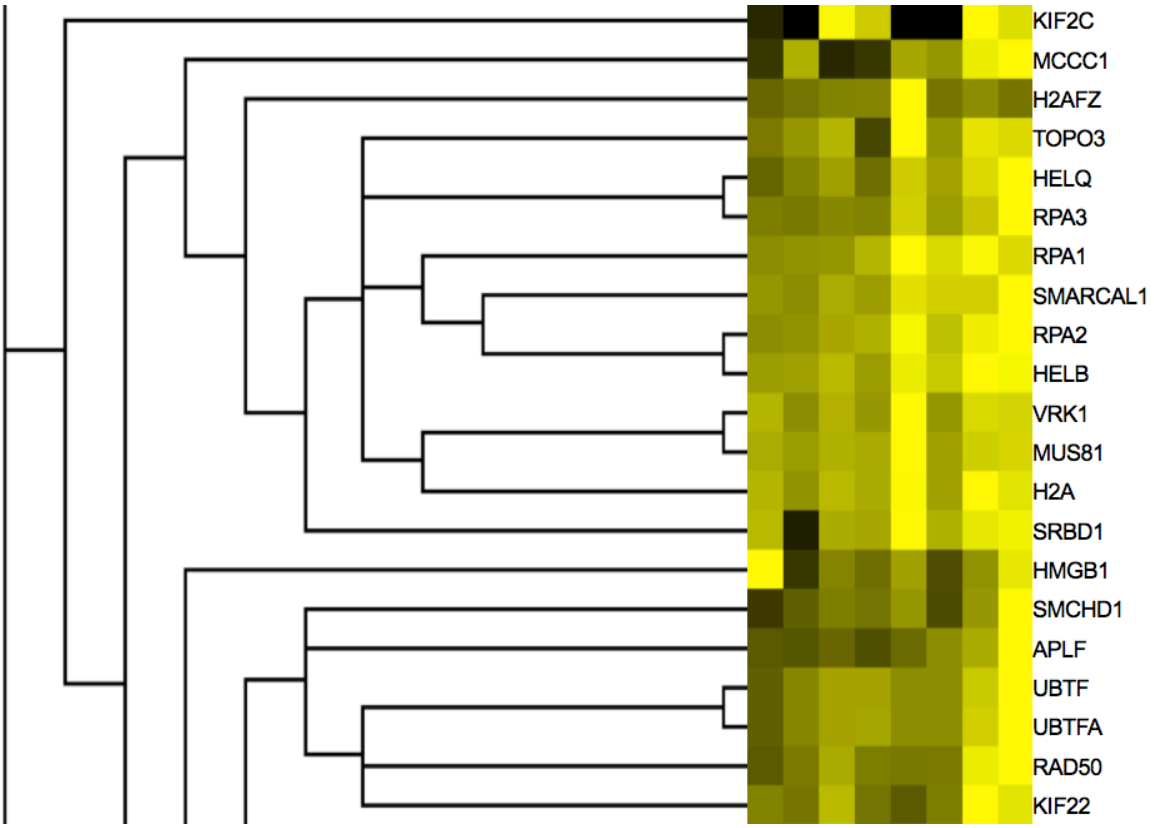
KIF2C
MCCC1
H2AFZ
TOPO3
HELQ
RPA3
RPA1
SMARCAL1
RPA2
HELB
VRK1
MUS81
H2A
SRBD1
HMGB1
SMCHD1
APLF
UBTF
UBTFA
RAD50
KIF22

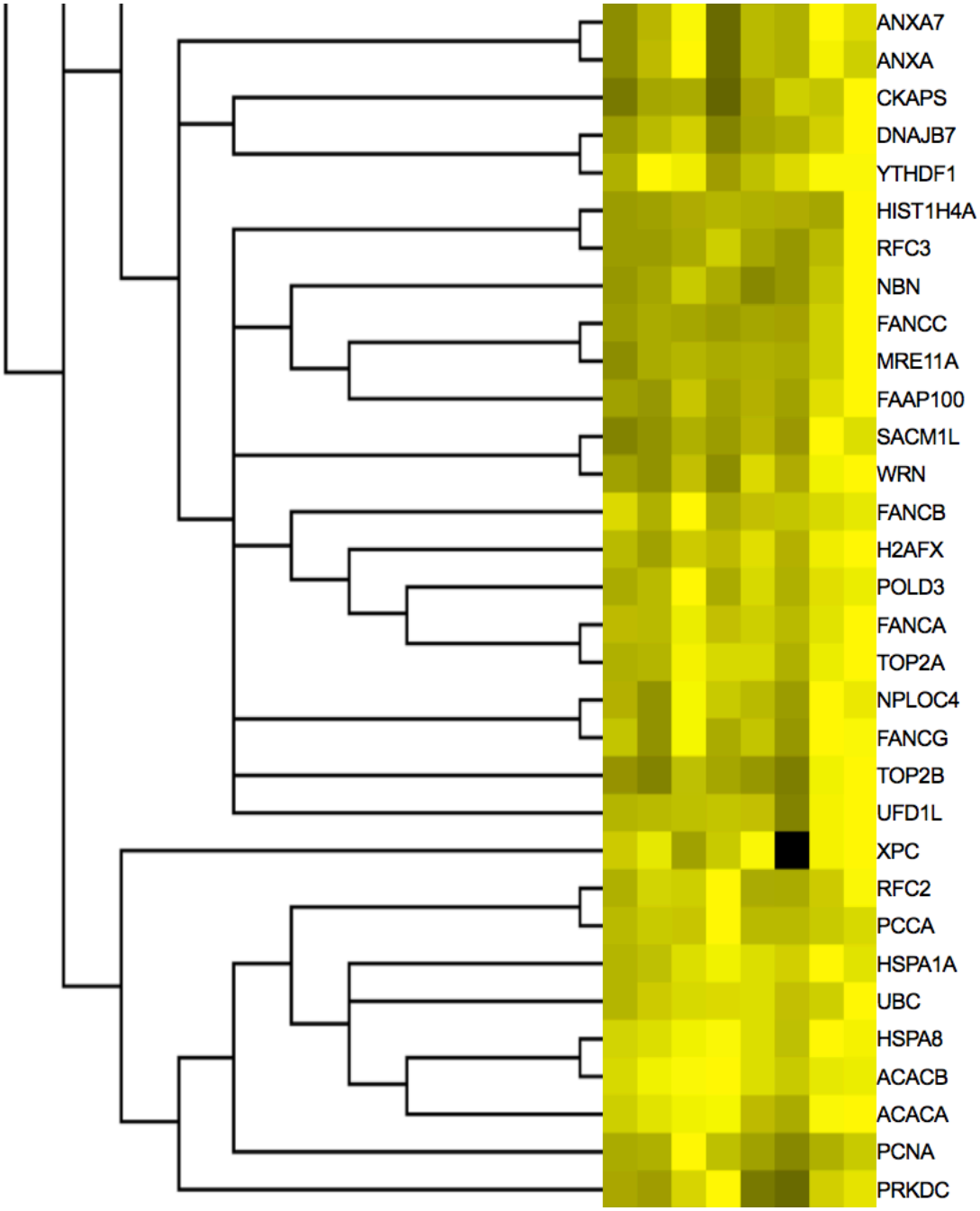
ANXA7
ANXA
CKAPS
DNAJB7
YTHDF1
HIST1H4A
RFC3
NBN
FANCC
MRE11A
FAAP100
SACM1L
WRN
FANCB
H2AFX
POLD3
FANCA
TOP2A
NPLOC4
FANCG
TOP2B
UFD1L
XPC
RFC2
PCCA
HSPA1A
UBC
HSPA8
ACACB
ACACA
PCNA
PRKDC

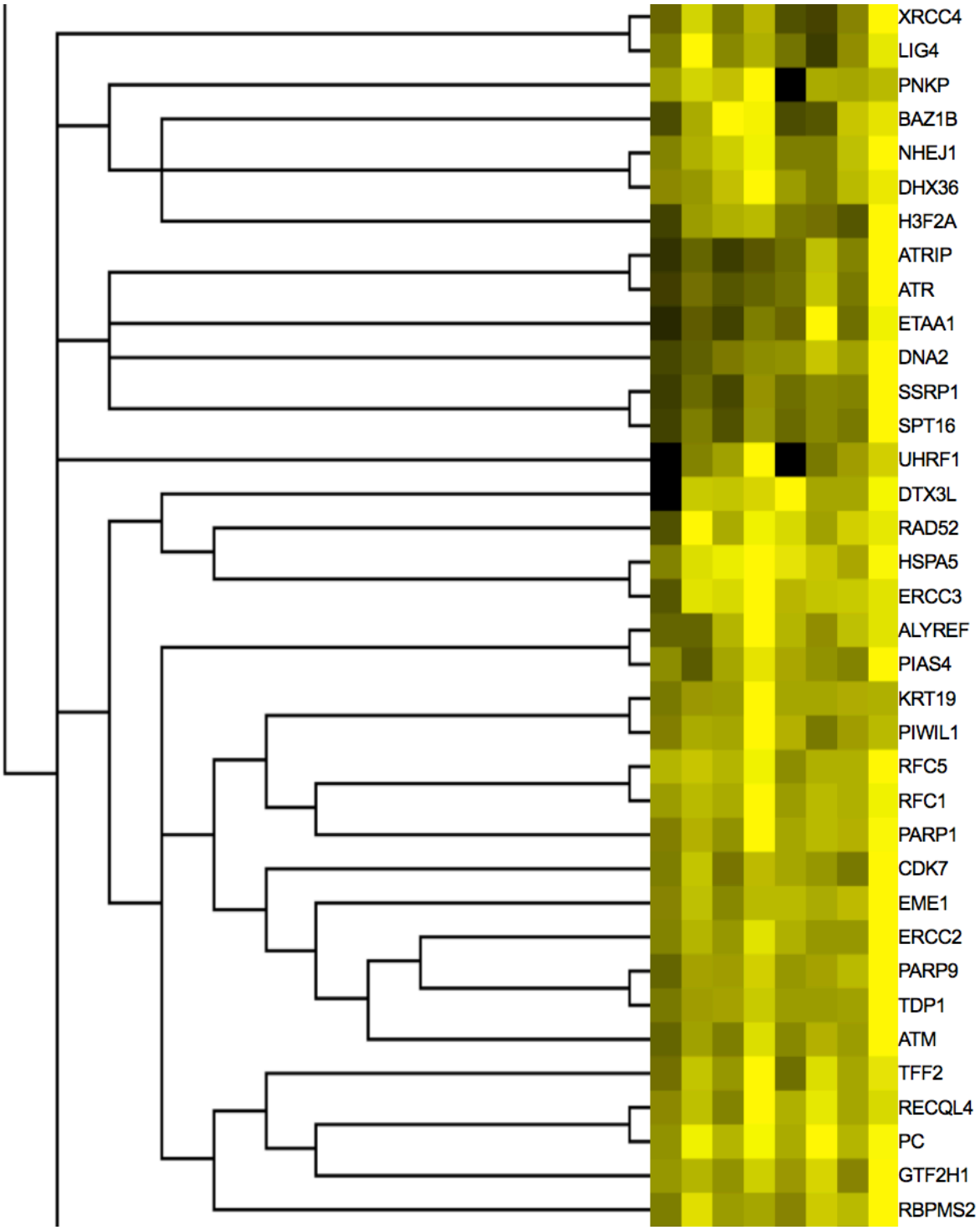
XRCC4
LIG4
PNKP
BAZ1B
NHEJ1
DHX36
H3F2A
ATRIP
ATR
ETAA1
DNA2
SSRP1
SPT16
UHRF1
DTX3L
RAD52
HSPA5
ERCC3
ALYREF
PIAS4
KRT19
PIWIL1
RFC5
RFC1
PARP1
CDK7
EME1
ERCC2
PARP9
TDP1
ATM
TFF2
RECQL4
PC
GTF2H1
RBPMS2

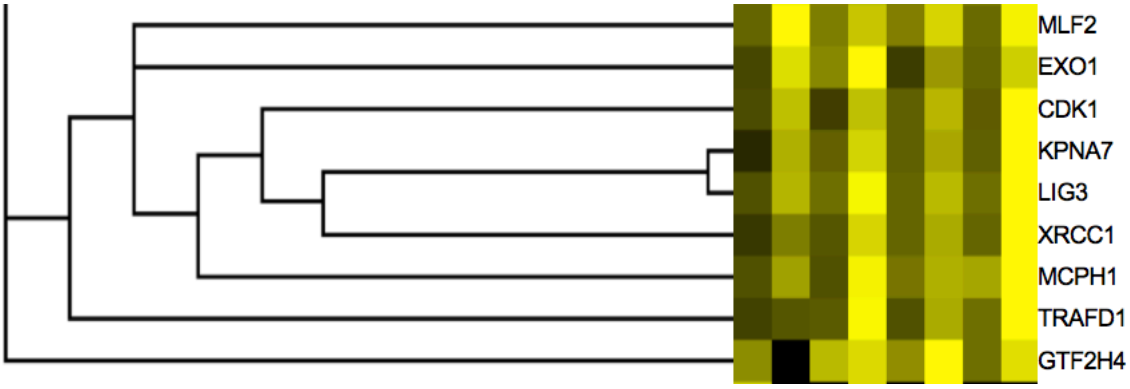
MLF2
EXO1
CDK1
KPNA7
LIG3
XRCC1
MCPH1
TRAFD1
GTF2H4

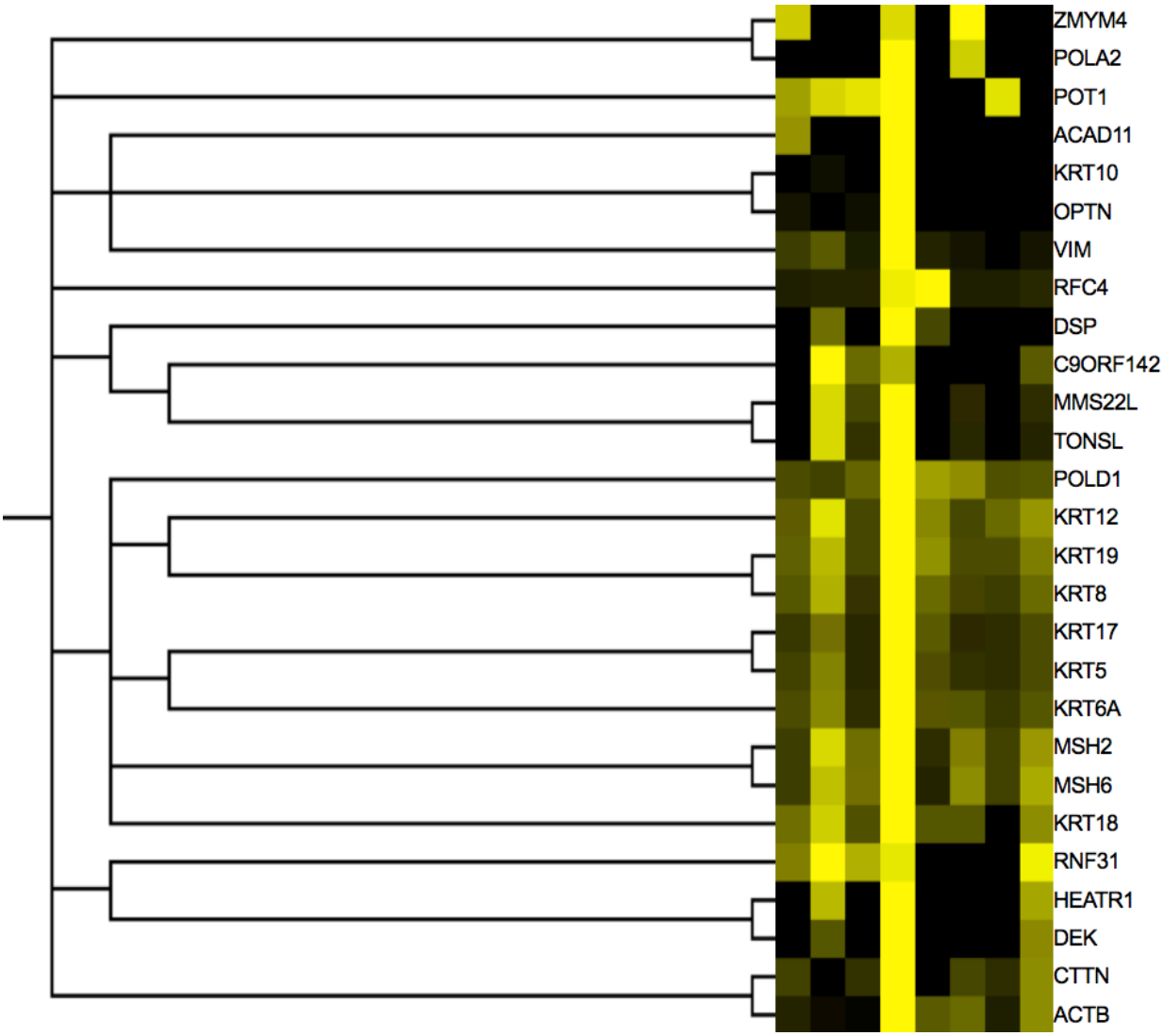
ZMYM4
POLA2
POT1
ACAD11
KRT10
OPTN
VIM
RFC4
DSP
C9ORF142
MMS22L
TONSL
POLD1
KRT12
KRT19
KRT8
KRT17
KRT5
KRT6A
MSH2
MSH6
KRT18
RNF31
HEATR1
DEK
CTTN
ACTB

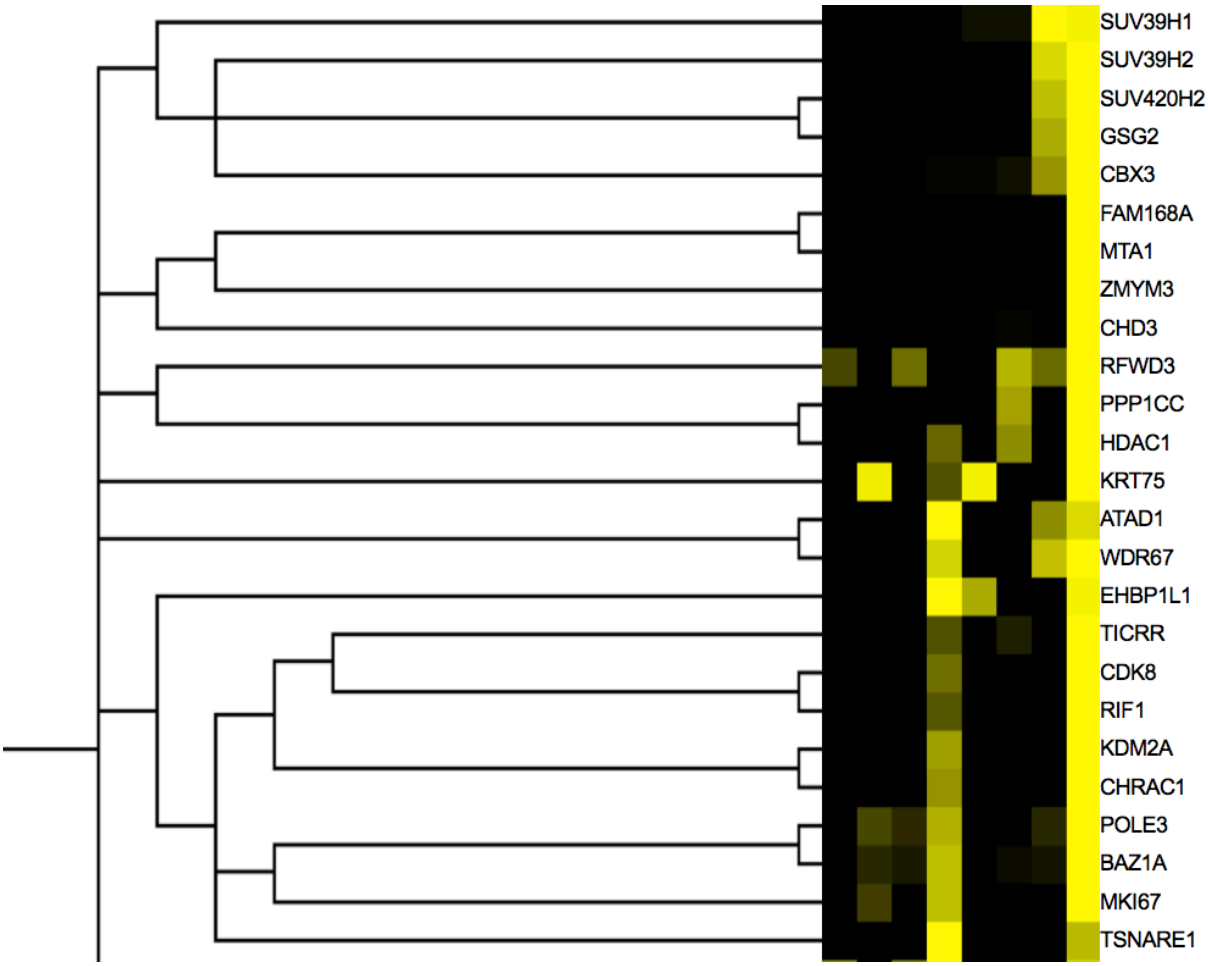
SUV39H1
SUV39H2
SUV420H2
GSG2
CBX3
FAM168A
MTA1
ZMYM3
CHD3
RFWD3
PPP1CC
HDAC1
KRT75
ATAD1
WDR67
EHBP1L1
TICRR
CDK8
RIF1
KDM2A
CHRAC1
POLE3
BAZ1A
MKI67
TSNARE1

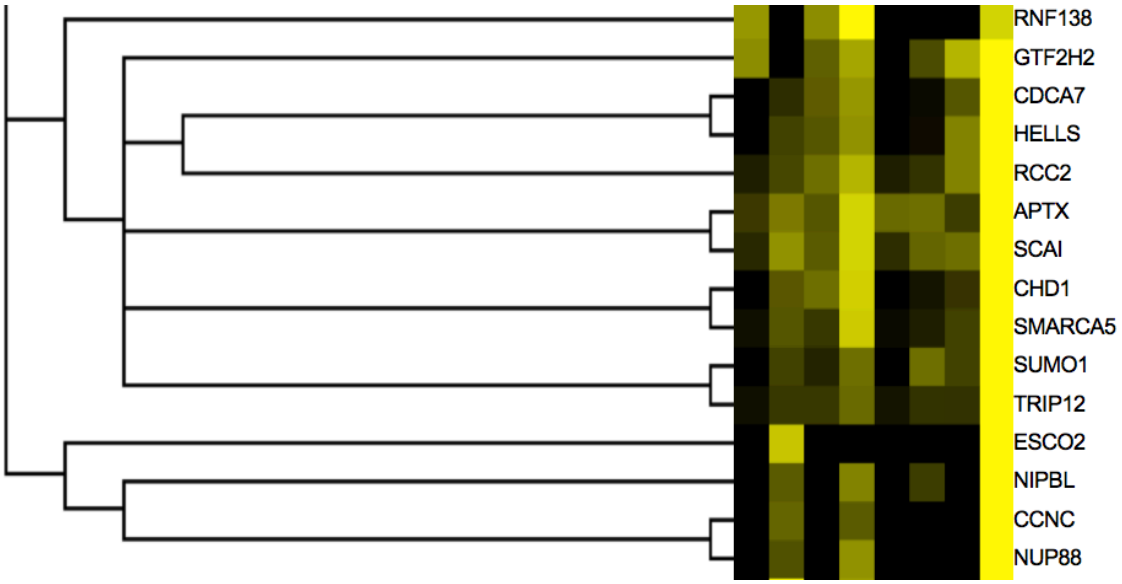
RNF138
GTF2H2
CDCA7
HELLS
RCC2
APTX
SCAI
CHD1
SMARCA5
SUMO1
TRIP12
ESCO2
NIPBL
CCNC
NUP88

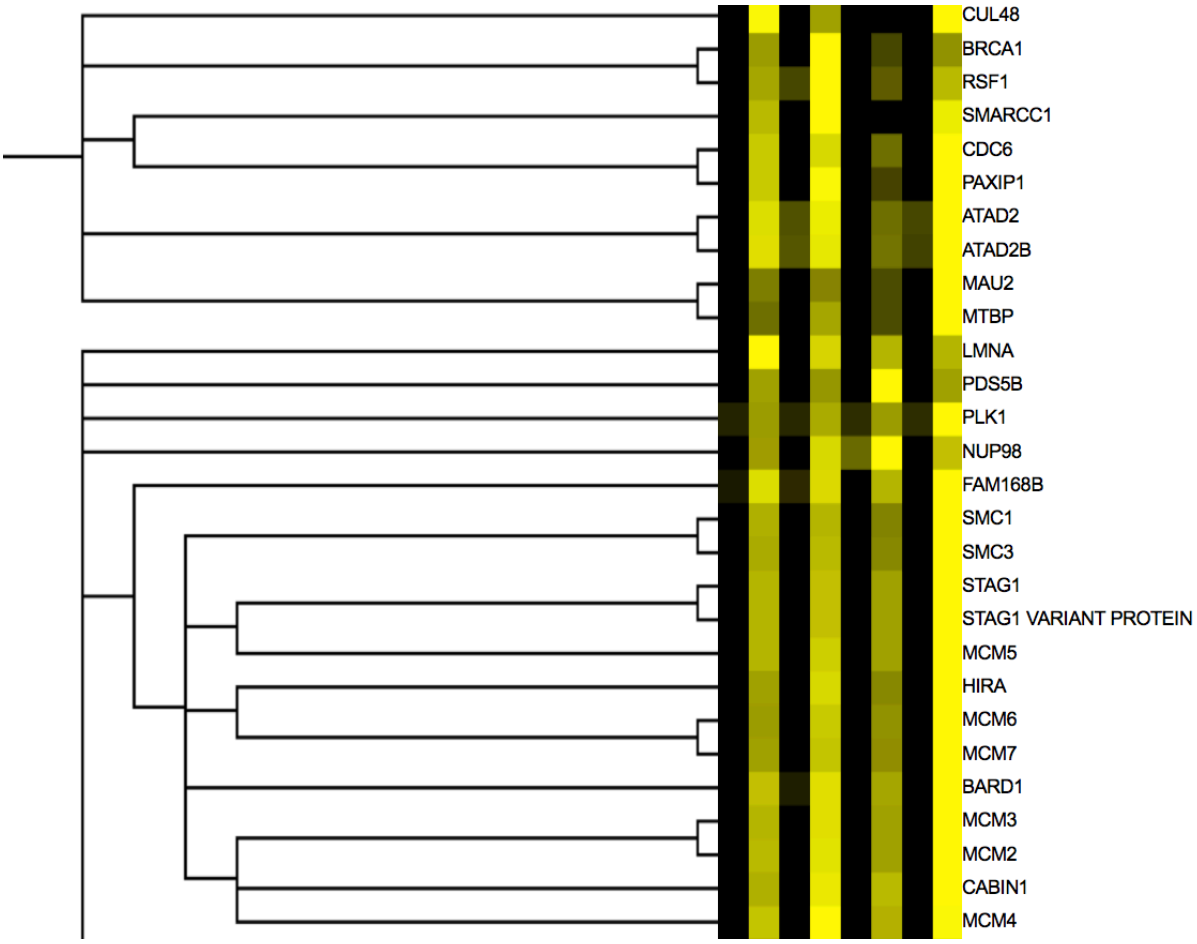
CUL48
BRCA1
RSF1
SMARCC1
CDC6
PAXIP1
ATAD2
ATAD2B
MAU2
MTBP
LMNA
PDS5B
PLK1
NUP98
FAM168B
SMC1
SMC3
STAG1
STAG1 VARIANT PROTEIN
MCM5
HIRA
MCM6
MCM7
BARD1
MCM3
MCM2
CABIN1
MCM4

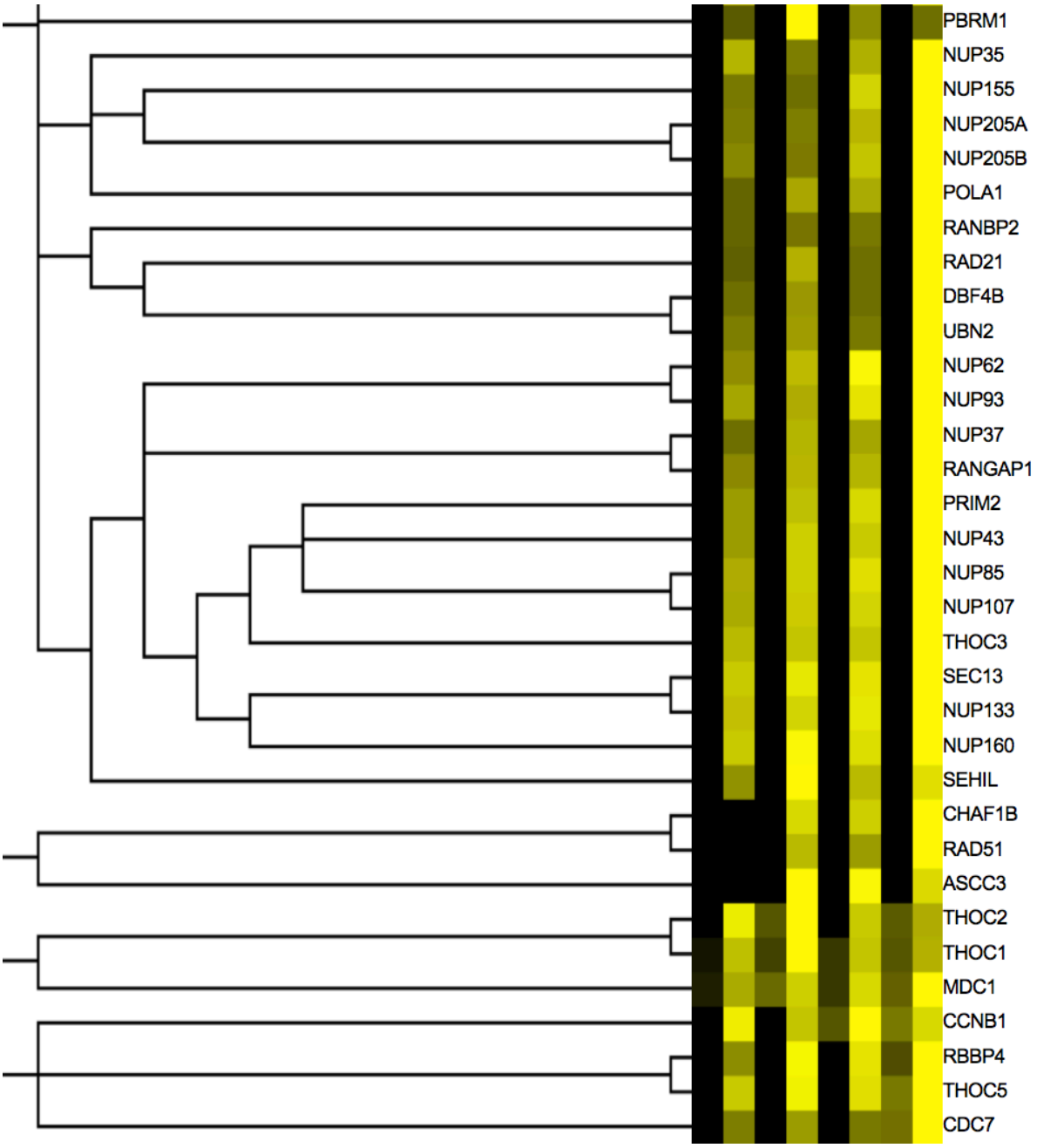
PBRM1
NUP35
NUP155
NUP205A
NUP205B
POLA1
RANBP2
RAD21
DBF4B
UBN2
NUP62
NUP93
NUP37
RANGAP1
PRIM2
NUP43
NUP85
NUP107
THOC3
SEC13
NUP133
NUP160
SEHIL
CHAF1B
RAD51
ASCC3
THOC2
THOC1
MDC1
CCNB1
RBBP4
THOC5
CDC7

Figure A-11. Hierarchical clustering of chromatin associated proteins. Each column is the abundance of the indicated protein detected on chromatin under a given condition. Columns 1, 2, 3, 4 are H3 nucleosome chromatin and columns 5, 6, 7, 8 are H3K9me3 chromatin. Columns 1, 3, 5, 7, are M phase extract and columns 2, 4, 6, 8 are interphase extract. Columns 1, 2, 5, 6 are mock depleted extract and columns 3, 4, 7, 8 are CPC depleted extract.

REFERENCES

Abe, S., K. Nagasaka, Y. Hirayama, H. Kozuka-Hata, M. Oyama, Y. Aoyagi, C. Obuse, and T. Hirota. 2011. The initial phase of chromosome condensation requires Cdk1-mediated phosphorylation of the CAP-D3 subunit of condensin II. *Genes Dev*. 25:863-874.

Adams, C.C., and J.L. Workman. 1995. Binding of disparate transcriptional activators to nucleosomal DNA is inherently cooperative. *Mol Cell Biol*. 15:1405-1421.

Ahel, D., Z. Horejsi, N. Wiechens, S.E. Polo, E. Garcia-Wilson, I. Ahel, H. Flynn, M. Skehel, S.C. West, S.P. Jackson, T. Owen-Hughes, and S.J. Boulton. 2009. Poly(ADP-ribose)-dependent regulation of DNA repair by the chromatin remodeling enzyme ALC1. *Science*. 325:1240-1243.

Auf der Maur, P., and K. Berlincourt-Bohni. 1979. Human lymphocyte cell cycle: studies with the use of BrUdR. *Hum Genet*. 49:209-215.

Bachman, K.E., M.R. Rountree, and S.B. Baylin. 2001. Dnmt3a and Dnmt3b are transcriptional repressors that exhibit unique localization properties to heterochromatin. *J Biol Chem*. 276:32282-32287.

Baxter, J., N. Sen, V.L. Martinez, M.E. De Carandini, J.B. Schvartzman, J.F. Diffley, and L. Aragon. 2011. Positive supercoiling of mitotic DNA drives decatenation by topoisomerase II in eukaryotes. *Science*. 331:1328-1332.

Bazett-Jones, D.P., K. Kimura, and T. Hirano. 2002. Efficient supercoiling of DNA by a single condensin complex as revealed by electron spectroscopic imaging. *Mol Cell*. 9:1183-1190.

Becker, P.B., and J.L. Workman. 2013. Nucleosome remodeling and epigenetics. *Cold Spring Harb Perspect Biol*. 5.

Bednar, J., I. Garcia-Saez, R. Boopathi, A.R. Cutter, G. Papai, A. Reymer, S.H. Syed, I.N. Lone, O. Tonchev, C. Crucifix, H. Menoni, C. Papin, D.A. Skoufias, H.

Kurumizaka, R. Lavery, A. Hamiche, J.J. Hayes, P. Schultz, D. Angelov, C. Petosa, and S. Dimitrov. 2017. Structure and Dynamics of a 197 bp Nucleosome in Complex with Linker Histone H1. *Mol Cell*. 66:384-397 e388.

Berger, J.M., S.J. Gamblin, S.C. Harrison, and J.C. Wang. 1996. Structure and mechanism of DNA topoisomerase II. *Nature*. 379:225-232.

Blow, J.J., and R.A. Laskey. 1986. Initiation of DNA replication in nuclei and purified DNA by a cell-free extract of Xenopus eggs. *Cell*. 47:577-587.

Bouazoune, K., and R.E. Kingston. 2012. Chromatin remodeling by the CHD7 protein is impaired by mutations that cause human developmental disorders. *Proc Natl Acad Sci U S A*. 109:19238-19243.

Brahma, S., M.I. Udugama, J. Kim, A. Hada, S.K. Bhardwaj, S.G. Hailu, T.H. Lee, and B. Bartholomew. 2017. INO80 exchanges H2A.Z for H2A by translocating on DNA proximal to histone dimers. *Nat Commun*. 8:15616.

Bruno, M., A. Flaus, C. Stockdale, C. Rencurel, H. Ferreira, and T. Owen-Hughes. 2003. Histone H2A/H2B dimer exchange by ATP-dependent chromatin remodeling activities. *Mol Cell*. 12:1599-1606.

Brzeski, J., and A. Jerzmanowski. 2003. Deficient in DNA methylation 1 (DDM1) defines a novel family of chromatin-remodeling factors. *J Biol Chem*. 278:823-828.

Budde, P.P., A. Kumagai, W.G. Dunphy, and R. Heald. 2001. Regulation of Op18 during spindle assembly in Xenopus egg extracts. *J Cell Biol*. 153:149-158.

Burrage, J., A. Termanis, A. Geissner, K. Myant, K. Gordon, and I. Stancheva. 2012. The SNF2 family ATPase LSH promotes phosphorylation of H2AX and efficient repair of DNA double-strand breaks in mammalian cells. *J Cell Sci*. 125:5524-5534.

Capranico, G., C. Jaxel, M. Roberge, K.W. Kohn, and Y. Pommier. 1990. Nucleosome positioning as a critical determinant for the DNA cleavage sites of mammalian DNA topoisomerase II in reconstituted simian virus 40 chromatin. *Nucleic Acids Res*. 18:4553-4559.

Carazo-Salas, R.E., G. Guarguaglini, O.J. Gruss, A. Segref, E. Karsenti, and I.W. Mattaj. 1999. Generation of GTP-bound Ran by RCC1 is required for chromatin-induced mitotic spindle formation. *Nature*. 400:178-181.

Carmena, M., M. Wheelock, H. Funabiki, and W.C. Earnshaw. 2012. The chromosomal passenger complex (CPC): from easy rider to the godfather of mitosis. *Nat Rev Mol Cell Biol*. 13:789-803.

Chan, Y.W., K. Fugger, and S.C. West. 2018. Unresolved recombination intermediates lead to ultra-fine anaphase bridges, chromosome breaks and aberrations. *Nat Cell Biol*. 20:92-103.

Chan, Y.W., and S.C. West. 2014. Spatial control of the GEN1 Holliday junction resolvase ensures genome stability. *Nat Commun*. 5:4844.

Chandra, T., K. Kirschner, J.Y. Thuret, B.D. Pope, T. Ryba, S. Newman, K. Ahmed, S.A. Samarajiwa, R. Salama, T. Carroll, R. Stark, R. Janky, M. Narita, L. Xue, A. Chicas, S. Nunez, R. Janknecht, Y. Hayashi-Takanaka, M.D. Wilson, A. Marshall, D.T. Odom, M.M. Babu, D.P. Bazett-Jones, S. Tavare, P.A. Edwards, S.W. Lowe, H. Kimura, D.M. Gilbert, and M. Narita. 2012. Independence of repressive histone marks and chromatin compaction during senescent heterochromatic layer formation. *Mol Cell*. 47:203-214.

Chen, P., and G. Li. 2017. Structure and Epigenetic Regulation of Chromatin Fibers. *Cold Spring Harb Symp Quant Biol*.

Chen, R.Z., U. Pettersson, C. Beard, L. Jackson-Grusby, and R. Jaenisch. 1998. DNA hypomethylation leads to elevated mutation rates. *Nature*. 395:89-93.

Chen, T., S. Hevi, F. Gay, N. Tsujimoto, T. He, B. Zhang, Y. Ueda, and E. Li. 2007. Complete inactivation of DNMT1 leads to mitotic catastrophe in human cancer cells. *Nat Genet*. 39:391-396.

Ciosk, R., W. Zachariae, C. Michaelis, A. Shevchenko, M. Mann, and K. Nasmyth. 1998. An ESP1/PDS1 complex regulates loss of sister chromatid cohesion at the metaphase to anaphase transition in yeast. *Cell*. 93:1067-1076.

Clapier, C.R., and B.R. Cairns. 2009. The biology of chromatin remodeling complexes. *Annu Rev Biochem*. 78:273-304.

Clapier, C.R., and B.R. Cairns. 2012. Regulation of ISWI involves inhibitory modules antagonized by nucleosomal epitopes. *Nature*. 492:280-284.

Corona, D.F., G. Langst, C.R. Clapier, E.J. Bonte, S. Ferrari, J.W. Tamkun, and P.B. Becker. 1999. ISWI is an ATP-dependent nucleosome remodeling factor. *Mol Cell*. 3:239-245.

Coudreuse, D., and P. Nurse. 2010. Driving the cell cycle with a minimal CDK control network. *Nature*. 468:1074-1079.

Cowell, I.G., N.J. Sunter, P.B. Singh, C.A. Austin, B.W. Durkacz, and M.J. Tilby. 2007. gammaH2AX foci form preferentially in euchromatin after ionising-radiation. *PLoS One*. 2:e1057.

Cuvier, O., and T. Hirano. 2003. A role of topoisomerase II in linking DNA replication to chromosome condensation. *J Cell Biol*. 160:645-655.

Dann, G.P., G.P. Liszczak, J.D. Bagert, M.M. Muller, U.T.T. Nguyen, F. Wojcik, Z.Z. Brown, J. Bos, T. Panchenko, R. Pihl, S.B. Pollock, K.L. Diehl, C.D. Allis, and T.W. Muir. 2017. ISWI chromatin remodellers sense nucleosome modifications to determine substrate preference. *Nature*. 548:607-611.

de Greef, J.C., J. Wang, J. Balog, J.T. den Dunnen, R.R. Frants, K.R. Straasheijm, C. Aytekin, M. van der Burg, L. Duprez, A. Ferster, A.R. Gennery, G. Gimelli, I. Reisli, C. Schuetz, A. Schulz, D.F. Smeets, Y. Sznajer, C. Wijmenga, M.C. van Eggermond, M.M. van Ostaijen-Ten Dam, A.C. Lankester, M.J. van Tol, P.J. van den Elsen, C.M. Weemaes, and S.M. van der Maarel. 2011. Mutations in ZBTB24 are associated with immunodeficiency, centromeric instability, and facial anomalies syndrome type 2. *Am J Hum Genet*. 88:796-804.

De Lucia, F., S. Lorain, C. Scamps, F. Galisson, J. MacHold, and M. Lipinski. 2001. Subnuclear localization and mitotic phosphorylation of HIRA, the human homologue of Saccharomyces cerevisiae transcriptional regulators Hir1p/Hir2p. *Biochem J*. 358:447-455.

Dechassa, M.L., A. Sabri, S. Pondugula, S.R. Kassabov, N. Chatterjee, M.P. Kladde, and B. Bartholomew. 2010. SWI/SNF has intrinsic nucleosome disassembly activity that is dependent on adjacent nucleosomes. *Mol Cell*. 38:590-602.

Deindl, S., W.L. Hwang, S.K. Hota, T.R. Blosser, P. Prasad, B. Bartholomew, and X. Zhuang. 2013. ISWI remodelers slide nucleosomes with coordinated multi-base-pair entry steps and single-base-pair exit steps. *Cell*. 152:442-452.

Deuring, R., L. Fanti, J.A. Armstrong, M. Sarte, O. Papoulas, M. Prestel, G. Daubresse, M. Verardo, S.L. Moseley, M. Berloco, T. Tsukiyama, C. Wu, S. Pimpinelli, and J.W. Tamkun. 2000. The ISWI chromatin-remodeling protein is required for gene expression and the maintenance of higher order chromatin structure in vivo. *Mol Cell*. 5:355-365.

Devbhandari, S., J. Jiang, C. Kumar, I. Whitehouse, and D. Remus. 2017. Chromatin Constrains the Initiation and Elongation of DNA Replication. *Mol Cell*. 65:131-141.

Dimitrov, S., M.C. Dasso, and A.P. Wolffe. 1994. Remodeling sperm chromatin in Xenopus laevis egg extracts: the role of core histone phosphorylation and linker histone B4 in chromatin assembly. *J Cell Biol*. 126:591-601.

Dixon, J.R., D.U. Gorkin, and B. Ren. 2016. Chromatin Domains: The Unit of Chromosome Organization. *Mol Cell*. 62:668-680.

Dixon, J.R., S. Selvaraj, F. Yue, A. Kim, Y. Li, Y. Shen, M. Hu, J.S. Liu, and B. Ren. 2012. Topological domains in mammalian genomes identified by analysis of chromatin interactions. *Nature*. 485:376-380.

Dunican, D.S., S. Pennings, and R.R. Meehan. 2015. Lsh Is Essential for Maintaining Global DNA Methylation Levels in Amphibia and Fish and Interacts Directly with Dnmt1. *Biomed Res Int*. 2015:740637.

Dworkin-Rastl, E., H. Kandolf, and R.C. Smith. 1994. The maternal histone H1 variant, H1M (B4 protein), is the predominant H1 histone in Xenopus pregastrula embryos. *Dev Biol*. 161:425-439.

Eeftens, J.M., S. Bisht, J. Kerssemakers, M. Kschonsak, C.H. Haering, and C. Dekker. 2017. Real-time detection of condensin-driven DNA compaction reveals a multistep binding mechanism. *EMBO J*. 36:3448-3457.

Ehrlich, M., K. Jackson, and C. Weemaes. 2006. Immunodeficiency, centromeric region instability, facial anomalies syndrome (ICF). *Orphanet J Rare Dis*. 1:2.

Elia, A.E., L.C. Cantley, and M.B. Yaffe. 2003a. Proteomic screen finds pSer/pThr-binding domain localizing Plk1 to mitotic substrates. *Science*. 299:1228-1231.

Elia, A.E., P. Rellos, L.F. Haire, J.W. Chao, F.J. Ivins, K. Hoepker, D. Mohammad, L.C. Cantley, S.J. Smerdon, and M.B. Yaffe. 2003b. The molecular basis for phosphodependent substrate targeting and regulation of Plks by the Polo-box domain. *Cell*. 115:83-95.

Eltsov, M., K.M. Maclellan, K. Maeshima, A.S. Frangakis, and J. Dubochet. 2008. Analysis of cryo-electron microscopy images does not support the existence of 30-nm chromatin fibers in mitotic chromosomes in situ. *Proc Natl Acad Sci U S A*. 105:19732-19737.

Fan, Y., T. Nikitina, E.M. Morin-Kensicki, J. Zhao, T.R. Magnuson, C.L. Woodcock, and A.I. Skoultchi. 2003. H1 linker histones are essential for mouse development and affect nucleosome spacing in vivo. *Mol Cell Biol*. 23:4559-4572.

Farnung, L., S.M. Vos, C. Wigge, and P. Cramer. 2017. Nucleosome-Chd1 structure and implications for chromatin remodelling. *Nature*.

Felle, M., H. Hoffmeister, J. Rothammer, A. Fuchs, J.H. Exler, and G. Langst. 2011. Nucleosomes protect DNA from DNA methylation in vivo and in vitro. *Nucleic Acids Res*. 39:6956-6969.

Fischle, W., B.S. Tseng, H.L. Dormann, B.M. Ueberheide, B.A. Garcia, J. Shabanowitz, D.F. Hunt, H. Funabiki, and C.D. Allis. 2005. Regulation of HP1-chromatin binding by histone H3 methylation and phosphorylation. *Nature*. 438:1116-1122.

Flaus, A., D.M. Martin, G.J. Barton, and T. Owen-Hughes. 2006. Identification of multiple distinct Snf2 subfamilies with conserved structural motifs. *Nucleic Acids Res*. 34:2887-2905.

Frauer, C., A. Rottach, D. Meilinger, S. Bultmann, K. Fellinger, S. Hasenoder, M. Wang, W. Qin, J. Soding, F. Spada, and H. Leonhardt. 2011. Different binding properties and function of CXXC zinc finger domains in Dnmt1 and Tet1. *PLoS One*. 6:e16627.

Funabiki, H., and A.W. Murray. 2000. The Xenopus chromokinesin Xkid is essential for metaphase chromosome alignment and must be degraded to allow anaphase chromosome movement. *Cell*. 102:411-424.

Fyodorov, D.V., B.R. Zhou, A.I. Skoultchi, and Y. Bai. 2017. Emerging roles of linker histones in regulating chromatin structure and function. *Nat Rev Mol Cell Biol*.

Gasser, R., T. Koller, and J.M. Sogo. 1996. The stability of nucleosomes at the replication fork. *J Mol Biol*. 258:224-239.

Gaudet, F., J.G. Hodgson, A. Eden, L. Jackson-Grusby, J. Dausman, J.W. Gray, H. Leonhardt, and R. Jaenisch. 2003. Induction of tumors in mice by genomic hypomethylation. *Science*. 300:489-492.

Ghenoiu, C., M.S. Wheelock, and H. Funabiki. 2013. Autoinhibition and Polo-dependent multisite phosphorylation restrict activity of the histone H3 kinase Haspin to mitosis. *Mol Cell*. 52:734-745.

Gill, R.M., T.V. Gabor, A.L. Couzens, and M.P. Scheid. 2013. The MYC-associated protein CDCA7 is phosphorylated by AKT to regulate MYC-dependent apoptosis and transformation. *Mol Cell Biol*. 33:498-513.

Gingras, A.C., M. Gstaiger, B. Raught, and R. Aebersold. 2007. Analysis of protein complexes using mass spectrometry. *Nat Rev Mol Cell Biol*. 8:645-654.

Gisselsson, D., C. Shao, C.M. Tuck-Muller, S. Sogorovic, E. Palsson, D. Smeets, and M. Ehrlich. 2005. Interphase chromosomal abnormalities and mitotic missegregation of hypomethylated sequences in ICF syndrome cells. *Chromosoma*. 114:118-126.

Giunta, S., R. Belotserkovskaya, and S.P. Jackson. 2010. DNA damage signaling in response to double-strand breaks during mitosis. *J Cell Biol*. 190:197-207.

Goloborodko, A., J.F. Marko, and L.A. Mirny. 2016. Chromosome Compaction by Active Loop Extrusion. *Biophys J*. 110:2162-2168.

Gottesfeld, J.M., and D.J. Forbes. 1997. Mitotic repression of the transcriptional machinery. *Trends Biochem Sci*. 22:197-202.

Gottschalk, A.J., R.D. Trivedi, J.W. Conaway, and R.C. Conaway. 2012. Activation of the SNF2 family ATPase ALC1 by poly(ADP-ribose) in a stable ALC1.PARP1.nucleosome intermediate. *J Biol Chem*. 287:43527-43532.

Gowher, H., and A. Jeltsch. 2002. Molecular enzymology of the catalytic domains of the Dnmt3a and Dnmt3b DNA methyltransferases. *J Biol Chem*. 277:20409-20414.

Green, L.C., P. Kalitsis, T.M. Chang, M. Cipetic, J.H. Kim, O. Marshall, L. Turnbull, C.B. Whitchurch, P. Vagnarelli, K. Samejima, W.C. Earnshaw, K.H. Choo, and D.F. Hudson. 2012. Contrasting roles of condensin I and condensin II in mitotic chromosome formation. *J Cell Sci*. 125:1591-1604.

Gruss, O.J., R.E. Carazo-Salas, C.A. Schatz, G. Guarguaglini, J. Kast, M. Wilm, N. Le Bot, I. Vernos, E. Karsenti, and I.W. Mattaj. 2001. Ran induces spindle assembly by reversing the inhibitory effect of importin alpha on TPX2 activity. *Cell*. 104:83-93.

Guiu, J., D.J. Bergen, E. De Pater, A.B. Islam, V. Ayllon, L. Gama-Norton, C. Ruiz-Herguido, J. Gonzalez, N. Lopez-Bigas, P. Menendez, E. Dzierzak, L. Espinosa, and A. Bigas. 2014. Identification of Cdca7 as a novel Notch transcriptional target involved in hematopoietic stem cell emergence. *J Exp Med*. 211:2411-2423.

Ha, V.L., S. Bharti, H. Inoue, W.C. Vass, F. Campa, Z. Nie, A. de Gramont, Y. Ward, and P.A. Randazzo. 2008. ASAP3 is a focal adhesion-associated Arf GAP that functions in cell migration and invasion. *J Biol Chem*. 283:14915-14926.

Hansen, R.S., C. Wijmenga, P. Luo, A.M. Stanek, T.K. Canfield, C.M. Weemaes, and S.M. Gartler. 1999. The DNMT3B DNA methyltransferase gene is mutated in the ICF immunodeficiency syndrome. *Proc Natl Acad Sci U S A*. 96:14412-14417.

Hara, R., J. Mo, and A. Sancar. 2000. DNA damage in the nucleosome core is refractory to repair by human excision nuclease. *Mol Cell Biol*. 20:9173-9181.

Hartwell, L.H., J. Culotti, and B. Reid. 1970. Genetic control of the cell-division cycle in yeast. I. Detection of mutants. *Proc Natl Acad Sci U S A*. 66:352-359.

Havugimana, P.C., G.T. Hart, T. Nepusz, H. Yang, A.L. Turinsky, Z. Li, P.I. Wang, D.R. Boutz, V. Fong, S. Phanse, M. Babu, S.A. Craig, P. Hu, C. Wan, J. Vlasblom, V.U. Dar, A. Bezginov, G.W. Clark, G.C. Wu, S.J. Wodak, E.R. Tillier, A. Paccanaro, E.M. Marcotte, and A. Emili. 2012. A census of human soluble protein complexes. *Cell*. 150:1068-1081.

Hayashi-Takanaka, Y., K. Maehara, A. Harada, T. Umehara, S. Yokoyama, C. Obuse, Y. Ohkawa, N. Nozaki, and H. Kimura. 2015. Distribution of histone H4 modifications as revealed by a panel of specific monoclonal antibodies. *Chromosome Res*. 23:753-766.

He, X., H.Y. Fan, G.J. Narlikar, and R.E. Kingston. 2006. Human ACF1 alters the remodeling strategy of SNF2h. *J Biol Chem*. 281:28636-28647.

Heald, R., R. Tournebize, T. Blank, R. Sandaltzopoulos, P. Becker, A. Hyman, and E. Karsenti. 1996. Self-organization of microtubules into bipolar spindles around artificial chromosomes in Xenopus egg extracts. *Nature*. 382:420-425.

Hendrich, B., and A. Bird. 1998. Identification and characterization of a family of mammalian methyl-CpG binding proteins. *Mol Cell Biol*. 18:6538-6547.

Hirano, T., and T.J. Mitchison. 1993. Topoisomerase II does not play a scaffolding role in the organization of mitotic chromosomes assembled in Xenopus egg extracts. *J Cell Biol*. 120:601-612.

Hirano, T., and T.J. Mitchison. 1994. A heterodimeric coiled-coil protein required for mitotic chromosome condensation in vitro. *Cell*. 79:449-458.

Hirota, T., J.J. Lipp, B.H. Toh, and J.M. Peters. 2005. Histone H3 serine 10 phosphorylation by Aurora B causes HP1 dissociation from heterochromatin. *Nature*. 438:1176-1180.

Huang, A., C.S. Ho, R. Ponzielli, D. Barsyte-Lovejoy, E. Bouffet, D. Picard, C.E. Hawkins, and L.Z. Penn. 2005. Identification of a novel c-Myc protein interactor,

JPO2, with transforming activity in medulloblastoma cells. *Cancer Res*. 65:5607-5619.

Hur, S.K., E.J. Park, J.E. Han, Y.A. Kim, J.D. Kim, D. Kang, and J. Kwon. 2010. Roles of human INO80 chromatin remodeling enzyme in DNA replication and chromosome segregation suppress genome instability. *Cell Mol Life Sci*. 67:2283-2296.

Huttlin, E.L., R.J. Bruckner, J.A. Paulo, J.R. Cannon, L. Ting, K. Baltier, G. Colby, F. Gebreab, M.P. Gygi, H. Parzen, J. Szpyt, S. Tam, G. Zarraga, L. Pontano-Vaites, S. Swarup, A.E. White, D.K. Schweppe, R. Rad, B.K. Erickson, R.A. Obar, K.G. Guruharsha, K. Li, S. Artavanis-Tsakonas, S.P. Gygi, and J.W. Harper. 2017. Architecture of the human interactome defines protein communities and disease networks. *Nature*.

Irniger, S., S. Piatti, C. Michaelis, and K. Nasmyth. 1995. Genes involved in sister chromatid separation are needed for B-type cyclin proteolysis in budding yeast. *Cell*. 81:269-278.

Ito, T., M.E. Levenstein, D.V. Fyodorov, A.K. Kutach, R. Kobayashi, and J.T. Kadonaga. 1999. ACF consists of two subunits, Acf1 and ISWI, that function cooperatively in the ATP-dependent catalysis of chromatin assembly. *Genes Dev*. 13:1529-1539.

Jackson-Grusby, L., C. Beard, R. Possemato, M. Tudor, D. Fambrough, G. Csankovszki, J. Dausman, P. Lee, C. Wilson, E. Lander, and R. Jaenisch. 2001. Loss of genomic methylation causes p53-dependent apoptosis and epigenetic deregulation. *Nat Genet*. 27:31-39.

Jarvis, C.D., T. Geiman, M.P. Vila-Storm, O. Osipovich, U. Akella, S. Candeias, I. Nathan, S.K. Durum, and K. Muegge. 1996. A novel putative helicase produced in early murine lymphocytes. *Gene*. 169:203-207.

Jeffrey, P.D., A.A. Russo, K. Polyak, E. Gibbs, J. Hurwitz, J. Massague, and N.P. Pavletich. 1995. Mechanism of CDK activation revealed by the structure of a cyclinA-CDK2 complex. *Nature*. 376:313-320.

Jenness, C., S. Giunta, M.M. Muller, H. Kimura, T.W. Muir, and H. Funabiki. 2018. HELLS and CDCA7 comprise a bipartite nucleosome remodeling complex defective in ICF syndrome. *Proc Natl Acad Sci U S A*. 115:E876-E885.

Jeong, A.L., S. Lee, J.S. Park, S. Han, C.Y. Jang, J.S. Lim, M.S. Lee, and Y. Yang. 2014. Cancerous inhibitor of protein phosphatase 2A (CIP2A) protein is involved in centrosome separation through the regulation of NIMA (never in mitosis gene A)-related kinase 2 (NEK2) protein activity. *J Biol Chem*. 289:28-40.

John, S., and J.L. Workman. 1998. Bookmarking genes for activation in condensed mitotic chromosomes. *Bioessays*. 20:275-279.

Jones, G.G., P.M. Reaper, A.R. Pettitt, and P.D. Sherrington. 2004. The ATR-p53 pathway is suppressed in noncycling normal and malignant lymphocytes. *Oncogene*. 23:1911-1921.

Kakui, Y., A. Rabinowitz, D.J. Barry, and F. Uhlmann. 2017. Condensin-mediated remodeling of the mitotic chromatin landscape in fission yeast. *Nat Genet*. 49:1553-1557.

Kato, D., A. Osakabe, Y. Arimura, Y. Mizukami, N. Horikoshi, K. Saikusa, S. Akashi, Y. Nishimura, S.Y. Park, J. Nogami, K. Maehara, Y. Ohkawa, A. Matsumoto, H. Kono, R. Inoue, M. Sugiyama, and H. Kurumizaka. 2017. Crystal structure of the overlapping dinucleosome composed of hexasome and octasome. *Science*. 356:205-208.

Kelly, A.E., C. Ghenoiu, J.Z. Xue, C. Zierhut, H. Kimura, and H. Funabiki. 2010. Survivin reads phosphorylated histone H3 threonine 3 to activate the mitotic kinase Aurora B. *Science*. 330:235-239.

Kelly, A.E., S.C. Sampath, T.A. Maniar, E.M. Woo, B.T. Chait, and H. Funabiki. 2007. Chromosomal enrichment and activation of the aurora B pathway are coupled to spatially regulate spindle assembly. *Dev Cell*. 12:31-43.

Kettenbach, A.N., D.K. Schweppe, B.K. Faherty, D. Pechenick, A.A. Pletnev, and S.A. Gerber. 2011. Quantitative phosphoproteomics identifies substrates and functional modules of Aurora and Polo-like kinase activities in mitotic cells. *Sci Signal*. 4:rs5.

Kimura, H., and P.R. Cook. 2001. Kinetics of core histones in living human cells: little exchange of H3 and H4 and some rapid exchange of H2B. *J Cell Biol*. 153:1341-1353.

Kimura, K., M. Hirano, R. Kobayashi, and T. Hirano. 1998. Phosphorylation and activation of 13S condensin by Cdc2 in vitro. *Science*. 282:487-490.

Kimura, K., and T. Hirano. 1997. ATP-dependent positive supercoiling of DNA by 13S condensin: a biochemical implication for chromosome condensation. *Cell*. 90:625-634.

Kinoshita, K., T.J. Kobayashi, and T. Hirano. 2015. Balancing acts of two HEAT subunits of condensin I support dynamic assembly of chromosome axes. *Dev Cell*. 33:94-106.

Klement, K., M.S. Luijsterburg, J.B. Pinder, C.S. Cena, V. Del Nero, C.M. Wintersinger, G. Dellaire, H. van Attikum, and A.A. Goodarzi. 2014. Opposing ISWI- and CHD-class chromatin remodeling activities orchestrate heterochromatic DNA repair. *J Cell Biol*. 207:717-733.

Komura, J., and T. Ono. 2005. Disappearance of nucleosome positioning in mitotic chromatin in vivo. *J Biol Chem*. 280:14530-14535.

Krebs, J.E., C.J. Fry, M.L. Samuels, and C.L. Peterson. 2000. Global role for chromatin remodeling enzymes in mitotic gene expression. *Cell*. 102:587-598.

Kustatscher, G., N. Hegarat, K.L. Wills, C. Furlan, J.C. Bukowski-Wills, H. Hochegger, and J. Rappsilber. 2014. Proteomics of a fuzzy organelle: interphase chromatin. *EMBO J*. 33:648-664.

Lane, A.B., J.F. Gimenez-Abian, and D.J. Clarke. 2013. A novel chromatin tether domain controls topoisomerase IIalpha dynamics and mitotic chromosome formation. *J Cell Biol*. 203:471-486.

Langmore, J.P., and C. Schutt. 1980. The higher order structure of chicken erythrocyte chromosomes in vivo. *Nature*. 288:620-622.

Larson, A.G., D. Elnatan, M.M. Keenen, M.J. Trnka, J.B. Johnston, A.L. Burlingame, D.A. Agard, S. Redding, and G.J. Narlikar. 2017. Liquid droplet formation by HP1alpha suggests a role for phase separation in heterochromatin. *Nature*. 547:236-240.

Laskey, R.A., B.M. Honda, A.D. Mills, and J.T. Finch. 1978. Nucleosomes are assembled by an acidic protein which binds histones and transfers them to DNA. *Nature*. 275:416-420.

Le Dily, F., D. Bau, A. Pohl, G.P. Vicent, F. Serra, D. Soronellas, G. Castellano, R.H. Wright, C. Ballare, G. Filion, M.A. Marti-Renom, and M. Beato. 2014. Distinct structural transitions of chromatin topological domains correlate with coordinated hormone-induced gene regulation. *Genes Dev*. 28:2151-2162.

Le Guezennec, X., M. Vermeulen, A.B. Brinkman, W.A. Hoeijmakers, A. Cohen, E. Lasonder, and H.G. Stunnenberg. 2006. MBD2/NuRD and MBD3/NuRD, two distinct complexes with different biochemical and functional properties. *Mol Cell Biol*. 26:843-851.

Lerner, J., A. Bagattin, F. Verdeguer, M.P. Makinistoglu, S. Garbay, T. Felix, L. Heidet, and M. Pontoglio. 2016. Human mutations affect the epigenetic/bookmarking function of HNF1B. *Nucleic Acids Res*. 44:8097-8111.

Li, Y., D.M. Keller, J.D. Scott, and H. Lu. 2005. CK2 phosphorylates SSRP1 and inhibits its DNA-binding activity. *J Biol Chem*. 280:11869-11875.

Lieberman-Aiden, E., N.L. van Berkum, L. Williams, M. Imakaev, T. Ragoczy, A. Telling, I. Amit, B.R. Lajoie, P.J. Sabo, M.O. Dorschner, R. Sandstrom, B. Bernstein, M.A. Bender, M. Groudine, A. Gnirke, J. Stamatoyannopoulos, L.A. Mirny, E.S. Lander, and J. Dekker. 2009. Comprehensive mapping of long-range interactions reveals folding principles of the human genome. *Science*. 326:289-293.

Lorentz, A., L. Heim, and H. Schmidt. 1992. The switching gene swi6 affects recombination and gene expression in the mating-type region of Schizosaccharomyces pombe. *Mol Gen Genet*. 233:436-442.

Lowary, P.T., and J. Widom. 1998. New DNA sequence rules for high affinity binding to histone octamer and sequence-directed nucleosome positioning. *J Mol Biol*. 276:19-42.

Luger, K., A.W. Mader, R.K. Richmond, D.F. Sargent, and T.J. Richmond. 1997. Crystal structure of the nucleosome core particle at 2.8 A resolution. *Nature*. 389:251-260.

Lusser, A., D.L. Urwin, and J.T. Kadonaga. 2005. Distinct activities of CHD1 and ACF in ATP-dependent chromatin assembly. *Nat Struct Mol Biol*. 12:160-166.

Lyons, D.B., and D. Zilberman. 2017. DDM1 and Lsh remodelers allow methylation of DNA wrapped in nucleosomes. *Elife*. 6.

MacCallum, D.E., A. Losada, R. Kobayashi, and T. Hirano. 2002. ISWI remodeling complexes in Xenopus egg extracts: identification as major chromosomal components that are regulated by INCENP-aurora B. *Mol Biol Cell*. 13:25-39.

Magalska, A., A.K. Schellhaus, D. Moreno-Andres, F. Zanini, A. Schooley, R. Sachdev, H. Schwarz, J. Madlung, and W. Antonin. 2014. RuvB-like ATPases function in chromatin decondensation at the end of mitosis. *Dev Cell*. 31:305-318.

Makde, R.D., J.R. England, H.P. Yennawar, and S. Tan. 2010. Structure of RCC1 chromatin factor bound to the nucleosome core particle. *Nature*. 467:562-566.

Maraschio, P., R. Tupler, E. Dainotti, M. Piantanida, G. Cazzola, and L. Tiepolo. 1989. Differential expression of the ICF (immunodeficiency, centromeric heterochromatin, facial anomalies) mutation in lymphocytes and fibroblasts. *J Med Genet*. 26:452-456.

Maresca, T.J., B.S. Freedman, and R. Heald. 2005. Histone H1 is essential for mitotic chromosome architecture and segregation in Xenopus laevis egg extracts. *J Cell Biol*. 169:859-869.

Martinez-Balbas, M.A., A. Dey, S.K. Rabindran, K. Ozato, and C. Wu. 1995. Displacement of sequence-specific transcription factors from mitotic chromatin. *Cell*. 83:29-38.

Mazumdar, M., S. Sundareshan, and T. Misteli. 2004. Human chromokinesin KIF4A functions in chromosome condensation and segregation. *J Cell Biol*. 166:613-620.

Miniou, P., D. Bourc'his, D. Molina Gomes, M. Jeanpierre, and E. Viegas-Pequignot. 1997a. Undermethylation of Alu sequences in ICF syndrome: molecular and in situ analysis. *Cytogenet Cell Genet*. 77:308-313.

Miniou, P., M. Jeanpierre, D. Bourc'his, A.C. Coutinho Barbosa, V. Blanquet, and E. Viegas-Pequignot. 1997b. alpha-satellite DNA methylation in normal individuals and in ICF patients: heterogeneous methylation of constitutive heterochromatin in adult and fetal tissues. *Hum Genet*. 99:738-745.

Mizuguchi, G., X. Shen, J. Landry, W.H. Wu, S. Sen, and C. Wu. 2004. ATP-driven exchange of histone H2AZ variant catalyzed by SWR1 chromatin remodeling complex. *Science*. 303:343-348.

Mora-Bermudez, F., D. Gerlich, and J. Ellenberg. 2007. Maximal chromosome compaction occurs by axial shortening in anaphase and depends on Aurora kinase. *Nat Cell Biol*. 9:822-831.

Morgan, D.O. 2007. The cell cycle : principles of control. New Science Press ; Sinauer Associates, London
Sunderland, MA. xxvii, 297 p. pp.

Muller, M.M., B. Fierz, L. Bittova, G. Liszczak, and T.W. Muir. 2016. A two-state activation mechanism controls the histone methyltransferase Suv39h1. *Nat Chem Biol*. 12:188-193.

Murray, A.W. 1991. Cell cycle extracts. *Methods Cell Biol*. 36:581-605.

Murray, A.W., and M.W. Kirschner. 1989. Cyclin synthesis drives the early embryonic cell cycle. *Nature*. 339:275-280.

Murray, A.W., M.J. Solomon, and M.W. Kirschner. 1989. The role of cyclin synthesis and degradation in the control of maturation promoting factor activity. *Nature*. 339:280-286.

Myant, K., and I. Stancheva. 2008. LSH cooperates with DNA methyltransferases to repress transcription. *Mol Cell Biol*. 28:215-226.

Nachury, M.V., T.J. Maresca, W.C. Salmon, C.M. Waterman-Storer, R. Heald, and K. Weis. 2001. Importin beta is a mitotic target of the small GTPase Ran in spindle assembly. *Cell*. 104:95-106.

Nagasaka, K., M.J. Hossain, M.J. Roberti, J. Ellenberg, and T. Hirota. 2016. Sister chromatid resolution is an intrinsic part of chromosome organization in prophase. *Nat Cell Biol*. 18:692-699.

Nakayama, J., J.C. Rice, B.D. Strahl, C.D. Allis, and S.I. Grewal. 2001. Role of histone H3 lysine 9 methylation in epigenetic control of heterochromatin assembly. *Science*. 292:110-113.

Nasmyth, K. 2001. Disseminating the genome: joining, resolving, and separating sister chromatids during mitosis and meiosis. *Annu Rev Genet*. 35:673-745.

Naumova, N., M. Imakaev, G. Fudenberg, Y. Zhan, B.R. Lajoie, L.A. Mirny, and J. Dekker. 2013. Organization of the mitotic chromosome. *Science*. 342:948-953.

Nemergut, M.E., C.A. Mizzen, T. Stukenberg, C.D. Allis, and I.G. Macara. 2001. Chromatin docking and exchange activity enhancement of RCC1 by histones H2A and H2B. *Science*. 292:1540-1543.

Newport, J., and M. Kirschner. 1982. A major developmental transition in early Xenopus embryos: I. characterization and timing of cellular changes at the midblastula stage. *Cell*. 30:675-686.

Nightingale, K.P., D. Pruss, and A.P. Wolffe. 1996. A single high affinity binding site for histone H1 in a nucleosome containing the Xenopus borealis 5 S ribosomal RNA gene. *J Biol Chem*. 271:7090-7094.

Nishino, Y., M. Eltsov, Y. Joti, K. Ito, H. Takata, Y. Takahashi, S. Hihara, A.S. Frangakis, N. Imamoto, T. Ishikawa, and K. Maeshima. 2012. Human mitotic chromosomes consist predominantly of irregularly folded nucleosome fibres without a 30-nm chromatin structure. *EMBO J*. 31:1644-1653.

Nishiyama, A., L. Yamaguchi, J. Sharif, Y. Johmura, T. Kawamura, K. Nakanishi, S. Shimamura, K. Arita, T. Kodama, F. Ishikawa, H. Koseki, and M. Nakanishi. 2013. Uhrf1-dependent H3K23 ubiquitylation couples maintenance DNA methylation and replication. *Nature*. 502:249-253.

Nitta, H., M. Unoki, K. Ichiyanagi, T. Kosho, T. Shigemura, H. Takahashi, G. Velasco, C. Francastel, C. Picard, T. Kubota, and H. Sasaki. 2013. Three novel ZBTB24

mutations identified in Japanese and Cape Verdean type 2 ICF syndrome patients. *J Hum Genet*. 58:455-460.

Nocetti, N., and I. Whitehouse. 2016. Nucleosome repositioning underlies dynamic gene expression. *Genes Dev*. 30:660-672.

Noh, K.M., I. Maze, D. Zhao, B. Xiang, W. Wenderski, P.W. Lewis, L. Shen, H. Li, and C.D. Allis. 2015. ATRX tolerates activity-dependent histone H3 methyl/phos switching to maintain repetitive element silencing in neurons. *Proc Natl Acad Sci U S A*. 112:6820-6827.

Nozaki, T., K. Kaizu, C.G. Pack, S. Tamura, T. Tani, S. Hihara, T. Nagai, K. Takahashi, and K. Maeshima. 2013. Flexible and dynamic nucleosome fiber in living mammalian cells. *Nucleus*. 4:349-356.

Ohta, S., J.C. Bukowski-Wills, L. Sanchez-Pulido, L. Alves Fde, L. Wood, Z.A. Chen, M. Platani, L. Fischer, D.F. Hudson, C.P. Ponting, T. Fukagawa, W.C. Earnshaw, and J. Rappsilber. 2010. The protein composition of mitotic chromosomes determined using multiclassifier combinatorial proteomics. *Cell*. 142:810-821.

Ohtsubo, M., H. Okazaki, and T. Nishimoto. 1989. The RCC1 protein, a regulator for the onset of chromosome condensation locates in the nucleus and binds to DNA. *J Cell Biol*. 109:1389-1397.

Okano, M., D.W. Bell, D.A. Haber, and E. Li. 1999. DNA methyltransferases Dnmt3a and Dnmt3b are essential for de novo methylation and mammalian development. *Cell*. 99:247-257.

Okuhara, K., K. Ohta, H. Seo, M. Shioda, T. Yamada, Y. Tanaka, N. Dohmae, Y. Seyama, T. Shibata, and H. Murofushi. 1999. A DNA unwinding factor involved in DNA replication in cell-free extracts of Xenopus eggs. *Curr Biol*. 9:341-350.

Oppikofer, M., T. Bai, Y. Gan, B. Haley, P. Liu, W. Sandoval, C. Ciferri, and A.G. Cochran. 2017. Expansion of the ISWI chromatin remodeler family with new active complexes. *EMBO Rep*. 18:1697-1706.

Osthus, R.C., B. Karim, J.E. Prescott, B.D. Smith, M. McDevitt, D.L. Huso, and C.V. Dang. 2005. The Myc target gene JPO1/CDCA7 is frequently overexpressed in

human tumors and has limited transforming activity in vivo. *Cancer Res*. 65:5620-5627.

Palozola, K.C., G. Donahue, H. Liu, G.R. Grant, J.S. Becker, A. Cote, H. Yu, A. Raj, and K.S. Zaret. 2017. Mitotic transcription and waves of gene reactivation during mitotic exit. *Science*. 358:119-122.

Paulson, J.R., and U.K. Laemmli. 1977. The structure of histone-depleted metaphase chromosomes. *Cell*. 12:817-828.

Peng, A., A.L. Lewellyn, and J.L. Maller. 2008. DNA damage signaling in early Xenopus embryos. *Cell Cycle*. 7:3-6.

Peshkin, L., M. Wuhr, E. Pearl, W. Haas, R.M. Freeman, Jr., J.C. Gerhart, A.M. Klein, M. Horb, S.P. Gygi, and M.W. Kirschner. 2015. On the Relationship of Protein and mRNA Dynamics in Vertebrate Embryonic Development. *Dev Cell*. 35:383-394.

Phelan, M.L., S. Sif, G.J. Narlikar, and R.E. Kingston. 1999. Reconstitution of a core chromatin remodeling complex from SWI/SNF subunits. *Mol Cell*. 3:247-253.

Prescott, J.E., R.C. Osthus, L.A. Lee, B.C. Lewis, H. Shim, J.F. Barrett, Q. Guo, A.L. Hawkins, C.A. Griffin, and C.V. Dang. 2001. A novel c-Myc-responsive gene, JPO1, participates in neoplastic transformation. *J Biol Chem*. 276:48276-48284.

Ramachandran, A., M. Omar, P. Cheslock, and G.R. Schnitzler. 2003. Linker histone H1 modulates nucleosome remodeling by human SWI/SNF. *J Biol Chem*. 278:48590-48601.

Ray-Gallet, D., J.P. Quivy, C. Scamps, E.M. Martini, M. Lipinski, and G. Almouzni. 2002. HIRA is critical for a nucleosome assembly pathway independent of DNA synthesis. *Mol Cell*. 9:1091-1100.

Ray-Gallet, D., J.P. Quivy, H.W. Sillje, E.A. Nigg, and G. Almouzni. 2007. The histone chaperone Asf1 is dispensable for direct de novo histone deposition in Xenopus egg extracts. *Chromosoma*. 116:487-496.

Ren, J., V. Briones, S. Barbour, W. Yu, Y. Han, M. Terashima, and K. Muegge. 2015. The ATP binding site of the chromatin remodeling homolog Lsh is required for nucleosome density and de novo DNA methylation at repeat sequences. *Nucleic Acids Res*. 43:1444-1455.

Ricketts, M.D., B. Frederick, H. Hoff, Y. Tang, D.C. Schultz, T. Singh Rai, M. Grazia Vizioli, P.D. Adams, and R. Marmorstein. 2015. Ubinuclein-1 confers histone H3.3-specific-binding by the HIRA histone chaperone complex. *Nat Commun*. 6:7711.

Rizkallah, R., and M.M. Hurt. 2009. Regulation of the transcription factor YY1 in mitosis through phosphorylation of its DNA-binding domain. *Mol Biol Cell*. 20:4766-4776.

Roberts, C., H.F. Sutherland, H. Farmer, W. Kimber, S. Halford, A. Carey, J.M. Brickman, A. Wynshaw-Boris, and P.J. Scambler. 2002. Targeted mutagenesis of the Hira gene results in gastrulation defects and patterning abnormalities of mesoendodermal derivatives prior to early embryonic lethality. *Mol Cell Biol*. 22:2318-2328.

Robertson, K.D., and A.P. Wolffe. 2000. DNA methylation in health and disease. *Nat Rev Genet*. 1:11-19.

Saitoh, N., I.G. Goldberg, E.R. Wood, and W.C. Earnshaw. 1994. ScII: an abundant chromosome scaffold protein is a member of a family of putative ATPases with an unusual predicted tertiary structure. *J Cell Biol*. 127:303-318.

Sakaguchi, A., and A. Kikuchi. 2004. Functional compatibility between isoform alpha and beta of type II DNA topoisomerase. *J Cell Sci*. 117:1047-1054.

Sakai, A., B.E. Schwartz, S. Goldstein, and K. Ahmad. 2009. Transcriptional and developmental functions of the H3.3 histone variant in Drosophila. *Curr Biol*. 19:1816-1820.

Samejima, K., I. Samejima, P. Vagnarelli, H. Ogawa, G. Vargiu, D.A. Kelly, F. de Lima Alves, A. Kerr, L.C. Green, D.F. Hudson, S. Ohta, C.A. Cooke, C.J. Farr, J. Rappsilber, and W.C. Earnshaw. 2012. Mitotic chromosomes are compacted laterally by KIF4 and condensin and axially by topoisomerase IIalpha. *J Cell Biol*. 199:755-770.

Sampath, S.C., R. Ohi, O. Leismann, A. Salic, A. Pozniakovski, and H. Funabiki. 2004. The chromosomal passenger complex is required for chromatin-induced microtubule stabilization and spindle assembly. *Cell*. 118:187-202.

Sawin, K.E., and T.J. Mitchison. 1991. Mitotic spindle assembly by two different pathways in vitro. *J Cell Biol*. 112:925-940.

Schubert, I., and J.L. Oud. 1997. There is an upper limit of chromosome size for normal development of an organism. *Cell*. 88:515-520.

Schuffenhauer, S., O. Bartsch, M. Stumm, T. Buchholz, T. Petropoulou, S. Kraft, B. Belohradsky, G.K. Hinkel, T. Meitinger, and R.D. Wegner. 1995. DNA, FISH and complementation studies in ICF syndrome: DNA hypomethylation of repetitive and single copy loci and evidence for a trans acting factor. *Hum Genet*. 96:562-571.

Session, A.M., Y. Uno, T. Kwon, J.A. Chapman, A. Toyoda, S. Takahashi, A. Fukui, A. Hikosaka, A. Suzuki, M. Kondo, S.J. van Heeringen, I. Quigley, S. Heinz, H. Ogino, H. Ochi, U. Hellsten, J.B. Lyons, O. Simakov, N. Putnam, J. Stites, Y. Kuroki, T. Tanaka, T. Michiue, M. Watanabe, O. Bogdanovic, R. Lister, G. Georgiou, S.S. Paranjpe, I. van Kruijsbergen, S. Shu, J. Carlson, T. Kinoshita, Y. Ohta, S. Mawaribuchi, J. Jenkins, J. Grimwood, J. Schmutz, T. Mitros, S.V. Mozaffari, Y. Suzuki, Y. Haramoto, T.S. Yamamoto, C. Takagi, R. Heald, K. Miller, C. Haudenschild, J. Kitzman, T. Nakayama, Y. Izutsu, J. Robert, J. Fortriede, K. Burns, V. Lotay, K. Karimi, Y. Yasuoka, D.S. Dichmann, M.F. Flajnik, D.W. Houston, J. Shendure, L. DuPasquier, P.D. Vize, A.M. Zorn, M. Ito, E.M. Marcotte, J.B. Wallingford, Y. Ito, M. Asashima, N. Ueno, Y. Matsuda, G.J. Veenstra, A. Fujiyama, R.M. Harland, M. Taira, and D.S. Rokhsar. 2016. Genome evolution in the allotetraploid frog Xenopus laevis. *Nature*. 538:336-343.

Shechter, D., J.J. Nicklay, R.K. Chitta, J. Shabanowitz, D.F. Hunt, and C.D. Allis. 2009. Analysis of histones in Xenopus laevis. I. A distinct index of enriched variants and modifications exists in each cell type and is remodeled during developmental transitions. *J Biol Chem*. 284:1064-1074.

Shintomi, K., F. Inoue, H. Watanabe, K. Ohsumi, M. Ohsugi, and T. Hirano. 2017. Mitotic chromosome assembly despite nucleosome depletion in Xenopus egg extracts. *Science*. 356:1284-1287.

Shintomi, K., M. Iwabuchi, H. Saeki, K. Ura, T. Kishimoto, and K. Ohsumi. 2005. Nucleosome assembly protein-1 is a linker histone chaperone in Xenopus eggs. *Proc Natl Acad Sci U S A*. 102:8210-8215.

Shintomi, K., T.S. Takahashi, and T. Hirano. 2015. Reconstitution of mitotic chromatids with a minimum set of purified factors. *Nat Cell Biol*. 17:1014-1023.

Sif, S., P.T. Stukenberg, M.W. Kirschner, and R.E. Kingston. 1998. Mitotic inactivation of a human SWI/SNF chromatin remodeling complex. *Genes Dev*. 12:2842-2851.

Singh, H.R., A.P. Nardozza, I.R. Moller, G. Knobloch, H.A.V. Kistemaker, M. Hassler, N. Harrer, C. Blessing, S. Eustermann, C. Kotthoff, S. Huet, F. Mueller-Planitz, D.V. Filippov, G. Timinszky, K.D. Rand, and A.G. Ladurner. 2017. A Poly-ADP-Ribose Trigger Releases the Auto-Inhibition of a Chromatin Remodeling Oncogene. *Mol Cell*. 68:860-871 e867.

Sinha, K.K., J.D. Gross, and G.J. Narlikar. 2017. Distortion of histone octamer core promotes nucleosome mobilization by a chromatin remodeler. *Science*. 355.

Smeets, D.F., U. Moog, C.M. Weemaes, G. Vaes-Peeters, G.F. Merkx, J.P. Niehof, and G. Hamers. 1994. ICF syndrome: a new case and review of the literature. *Hum Genet*. 94:240-246.

Smith, S., and B. Stillman. 1991. Stepwise assembly of chromatin during DNA replication in vitro. *EMBO J*. 10:971-980.

Song, F., P. Chen, D. Sun, M. Wang, L. Dong, D. Liang, R.M. Xu, P. Zhu, and G. Li. 2014. Cryo-EM study of the chromatin fiber reveals a double helix twisted by tetranucleosomal units. *Science*. 344:376-380.

Steegmaier, M., M. Hoffmann, A. Baum, P. Lenart, M. Petronczki, M. Krssak, U. Gurtler, P. Garin-Chesa, S. Lieb, J. Quant, M. Grauert, G.R. Adolf, N. Kraut, J.M. Peters, and W.J. Rettig. 2007. BI 2536, a potent and selective inhibitor of polo-like kinase 1, inhibits tumor growth in vivo. *Curr Biol*. 17:316-322.

Stokes, D.G., and R.P. Perry. 1995. DNA-binding and chromatin localization properties of CHD1. *Mol Cell Biol*. 15:2745-2753.

Sumara, I., E. Vorlaufer, P.T. Stukenberg, O. Kelm, N. Redemann, E.A. Nigg, and J.M. Peters. 2002. The dissociation of cohesin from chromosomes in prophase is regulated by Polo-like kinase. *Mol Cell*. 9:515-525.

Suto, R.K., M.J. Clarkson, D.J. Tremethick, and K. Luger. 2000. Crystal structure of a nucleosome core particle containing the variant histone H2A.Z. *Nat Struct Biol*. 7:1121-1124.

Tada, K., H. Susumu, T. Sakuno, and Y. Watanabe. 2011. Condensin association with histone H2A shapes mitotic chromosomes. *Nature*. 474:477-483.

Tahara, K., M. Takagi, M. Ohsugi, T. Sone, F. Nishiumi, K. Maeshima, Y. Horiuchi, N. Tokai-Nishizumi, F. Imamoto, T. Yamamoto, S. Kose, and N. Imamoto. 2008. Importin-beta and the small guanosine triphosphatase Ran mediate chromosome loading of the human chromokinesin Kid. *J Cell Biol*. 180:493-506.

Talbert, P.B., and S. Henikoff. 2017. Histone variants on the move: substrates for chromatin dynamics. *Nat Rev Mol Cell Biol*. 18:115-126.

Tencer, A.H., K.L. Cox, L. Di, J.B. Bridgers, J. Lyu, X. Wang, J.K. Sims, T.M. Weaver, H.F. Allen, Y. Zhang, J. Gatchalian, M.A. Darcy, M.D. Gibson, J. Ikebe, W. Li, P.A. Wade, J.J. Hayes, B.D. Strahl, H. Kono, M.G. Poirier, C.A. Musselman, and T.G. Kutateladze. 2017. Covalent Modifications of Histone H3K9 Promote Binding of CHD3. *Cell Rep*. 21:455-466.

Terakawa, T., S. Bisht, J.M. Eeftens, C. Dekker, C.H. Haering, and E.C. Greene. 2017. The condensin complex is a mechanochemical motor that translocates along DNA. *Science*. 358:672-676.

Termanis, A., N. Torrea, J. Culley, A. Kerr, B. Ramsahoye, and I. Stancheva. 2016. The SNF2 family ATPase LSH promotes cell-autonomous de novo DNA methylation in somatic cells. *Nucleic Acids Res*. 44:7592-7604.

Teves, S.S., L. An, A.S. Hansen, L. Xie, X. Darzacq, and R. Tjian. 2016. A dynamic mode of mitotic bookmarking by transcription factors. *Elife*. 5.

Teves, S.S., C.M. Weber, and S. Henikoff. 2014. Transcribing through the nucleosome. *Trends Biochem Sci*. 39:577-586.

Thijssen, P.E., Y. Ito, G. Grillo, J. Wang, G. Velasco, H. Nitta, M. Unoki, M. Yoshihara, M. Suyama, Y. Sun, R.J. Lemmers, J.C. de Greef, A. Gennery, P. Picco, B. Kloeckener-Gruissem, T. Gungor, I. Reisli, C. Picard, K. Kebaili, B. Roquelaure, T. Iwai, I. Kondo, T. Kubota, M.M. van Ostaijen-Ten Dam, M.J. van Tol, C. Weemaes, C. Francastel, S.M. van der Maarel, and H. Sasaki. 2015. Mutations in CDCA7 and HELLS cause immunodeficiency-centromeric instability-facial anomalies syndrome. *Nat Commun*. 6:7870.

Toselli-Mollereau, E., X. Robellet, L. Fauque, S. Lemaire, C. Schiklenk, C. Klein, C. Hocquet, P. Legros, L. N'Guyen, L. Mouillard, E. Chautard, D. Auboeuf, C.H. Haering, and P. Bernard. 2016. Nucleosome eviction in mitosis assists condensin loading and chromosome condensation. *EMBO J*. 35:1565-1581.

Tseng, B.S., L. Tan, T.M. Kapoor, and H. Funabiki. 2010. Dual detection of chromosomes and microtubules by the chromosomal passenger complex drives spindle assembly. *Dev Cell*. 18:903-912.

Tuck-Muller, C.M., A. Narayan, F. Tsien, D.F. Smeets, J. Sawyer, E.S. Fiala, O.S. Sohn, and M. Ehrlich. 2000. DNA hypomethylation and unusual chromosome instability in cell lines from ICF syndrome patients. *Cytogenet Cell Genet*. 89:121-128.

Ulyanova, N.P., and G.R. Schnitzler. 2005. Human SWI/SNF generates abundant, structurally altered dinucleosomes on polynucleosomal templates. *Mol Cell Biol*. 25:11156-11170.

Ura, K., K. Nightingale, and A.P. Wolffe. 1996. Differential association of HMG1 and linker histones B4 and H1 with dinucleosomal DNA: structural transitions and transcriptional repression. *EMBO J*. 15:4959-4969.

van den Boogaard, M.L., P.E. Thijssen, C. Aytekin, F. Licciardi, A.A. Kiykim, L. Spossito, V. Dalm, G.J. Driessen, R. Kersseboom, F. de Vries, M.M. van Ostaijen-Ten Dam, A. Ikinciogullari, F. Dogu, M. Oleastro, E. Bailardo, L. Daxinger, E. Nain, S. Baris, M.J.D. van Tol, C. Weemaes, and S.M. van der Maarel. 2017. Expanding the mutation spectrum in ICF syndrome: Evidence for a gender bias in ICF2. *Clin Genet*. 92:380-387.

Van der Laan, M.J., and K.S. Pollard. 2003. A new algorithm for hybrid hierarchical clustering with visualization and the bootstrap. *Journal of Statistical Planning and Inference*. 117:275-303.

Van Holde, K.E. 1989. Chromatin. Springer-Verlag, New York. xii, 497 p. pp.

Viegas-Pequignot, E., and B. Dutrillaux. 1976. Segmentation of human chromosomes induced by 5-ACR (5-azacytidine). *Hum Genet*. 34:247-254.

von Eyss, B., J. Maaskola, S. Memczak, K. Mollmann, A. Schuetz, C. Loddenkemper, M.D. Tanh, A. Otto, K. Muegge, U. Heinemann, N. Rajewsky, and U. Ziebold. 2012. The SNF2-like helicase HELLS mediates E2F3-dependent transcription and cellular transformation. *EMBO J*. 31:972-985.

Walter, J., and J. Newport. 2000. Initiation of eukaryotic DNA replication: origin unwinding and sequential chromatin association of Cdc45, RPA, and DNA polymerase alpha. *Mol Cell*. 5:617-627.

Wan, C., B. Borgeson, S. Phanse, F. Tu, K. Drew, G. Clark, X. Xiong, O. Kagan, J. Kwan, A. Bezginov, K. Chessman, S. Pal, G. Cromar, O. Papoulas, Z. Ni, D.R. Boutz, S. Stoilova, P.C. Havugimana, X. Guo, R.H. Malty, M. Sarov, J. Greenblatt, M. Babu, W.B. Derry, E.R. Tillier, J.B. Wallingford, J. Parkinson, E.M. Marcotte, and A. Emili. 2015. Panorama of ancient metazoan macromolecular complexes. *Nature*. 525:339-344.

Wang, F., J. Dai, J.R. Daum, E. Niedzialkowska, B. Banerjee, P.T. Stukenberg, G.J. Gorbsky, and J.M. Higgins. 2010. Histone H3 Thr-3 phosphorylation by Haspin positions Aurora B at centromeres in mitosis. *Science*. 330:231-235.

Wang, H.B., and Y. Zhang. 2001. Mi2, an auto-antigen for dermatomyositis, is an ATP-dependent nucleosome remodeling factor. *Nucleic Acids Res*. 29:2517-2521.

Wang, W., J. Cote, Y. Xue, S. Zhou, P.A. Khavari, S.R. Biggar, C. Muchardt, G.V. Kalpana, S.P. Goff, M. Yaniv, J.L. Workman, and G.R. Crabtree. 1996. Purification and biochemical heterogeneity of the mammalian SWI-SNF complex. *EMBO J*. 15:5370-5382.

Weemaes, C.M., M.J. van Tol, J. Wang, M.M. van Ostaijen-ten Dam, M.C. van Eggermond, P.E. Thijssen, C. Aytekin, N. Brunetti-Pierri, M. van der Burg, E. Graham Davies, A. Ferster, D. Furthner, G. Gimelli, A. Gennery, B. Kloeckener-Gruissem, S. Meyn, C. Powell, I. Reisli, C. Schuetz, A. Schulz, A. Shugar, P.J. van den Elsen, and S.M. van der Maarel. 2013. Heterogeneous clinical

presentation in ICF syndrome: correlation with underlying gene defects. *Eur J Hum Genet*. 21:1219-1225.

Wiese, C., A. Wilde, M.S. Moore, S.A. Adam, A. Merdes, and Y. Zheng. 2001. Role of importin-beta in coupling Ran to downstream targets in microtubule assembly. *Science*. 291:653-656.

Willhoft, O., R. Bythell-Douglas, E.A. McCormack, and D.B. Wigley. 2016. Synergy and antagonism in regulation of recombinant human INO80 chromatin remodeling complex. *Nucleic Acids Res*. 44:8179-8188.

Winkler, D.D., U.M. Muthurajan, A.R. Hieb, and K. Luger. 2011. Histone chaperone FACT coordinates nucleosome interaction through multiple synergistic binding events. *J Biol Chem*. 286:41883-41892.

Woodcock, C.L. 1994. Chromatin fibers observed in situ in frozen hydrated sections. Native fiber diameter is not correlated with nucleosome repeat length. *J Cell Biol*. 125:11-19.

Wu, H., P.E. Thijssen, E. de Klerk, K.K. Vonk, J. Wang, B. den Hamer, C. Aytekin, S.M. van der Maarel, and L. Daxinger. 2016. Converging disease genes in ICF syndrome: ZBTB24 controls expression of CDCA7 in mammals. *Hum Mol Genet*. 25:4041-4051.

Wuhr, M., R.M. Freeman, Jr., M. Presler, M.E. Horb, L. Peshkin, S.P. Gygi, and M.W. Kirschner. 2014. Deep proteomics of the Xenopus laevis egg using an mRNA-derived reference database. *Curr Biol*. 24:1467-1475.

Wyrick, J.J., F.C. Holstege, E.G. Jennings, H.C. Causton, D. Shore, M. Grunstein, E.S. Lander, and R.A. Young. 1999. Chromosomal landscape of nucleosome-dependent gene expression and silencing in yeast. *Nature*. 402:418-421.

Wysocka, J., T. Swigut, H. Xiao, T.A. Milne, S.Y. Kwon, J. Landry, M. Kauer, A.J. Tackett, B.T. Chait, P. Badenhorst, C. Wu, and C.D. Allis. 2006. A PHD finger of NURF couples histone H3 lysine 4 trimethylation with chromatin remodelling. *Nature*. 442:86-90.

Xi, S., T.M. Geiman, V. Briones, Y. Guang Tao, H. Xu, and K. Muegge. 2009. Lsh participates in DNA methylation and silencing of stem cell genes. *Stem Cells*. 27:2691-2702.

Xu, G.L., T.H. Bestor, D. Bourc'his, C.L. Hsieh, N. Tommerup, M. Bugge, M. Hulten, X. Qu, J.J. Russo, and E. Viegas-Pequignot. 1999. Chromosome instability and immunodeficiency syndrome caused by mutations in a DNA methyltransferase gene. *Nature*. 402:187-191.

Yamagishi, Y., T. Honda, Y. Tanno, and Y. Watanabe. 2010. Two histone marks establish the inner centromere and chromosome bi-orientation. *Science*. 330:239-243.

Yan, Q., E. Cho, S. Lockett, and K. Muegge. 2003. Association of Lsh, a regulator of DNA methylation, with pericentromeric heterochromatin is dependent on intact heterochromatin. *Mol Cell Biol*. 23:8416-8428.

Yang, J.G., T.S. Madrid, E. Sevastopoulos, and G.J. Narlikar. 2006. The chromatin-remodeling enzyme ACF is an ATP-dependent DNA length sensor that regulates nucleosome spacing. *Nat Struct Mol Biol*. 13:1078-1083.

Yokoyama, H., S. Rybina, R. Santarella-Mellwig, I.W. Mattaj, and E. Karsenti. 2009. ISWI is a RanGTP-dependent MAP required for chromosome segregation. *J Cell Biol*. 187:813-829.

Yu, W., C. McIntosh, R. Lister, I. Zhu, Y. Han, J. Ren, D. Landsman, E. Lee, V. Briones, M. Terashima, R. Leighty, J.R. Ecker, and K. Muegge. 2014. Genome-wide DNA methylation patterns in LSH mutant reveals de-repression of repeat elements and redundant epigenetic silencing pathways. *Genome Res*. 24:1613-1623.

Zemach, A., M.Y. Kim, P.H. Hsieh, D. Coleman-Derr, L. Eshed-Williams, K. Thao, S.L. Harmer, and D. Zilberman. 2013. The Arabidopsis nucleosome remodeler DDM1 allows DNA methyltransferases to access H1-containing heterochromatin. *Cell*. 153:193-205.

Zhu, H., T.M. Geiman, S. Xi, Q. Jiang, A. Schmidtmann, T. Chen, E. Li, and K. Muegge. 2006. Lsh is involved in de novo methylation of DNA. *EMBO J*. 25:335-345.

Zierhut, C., C. Jenness, H. Kimura, and H. Funabiki. 2014. Nucleosomal regulation of chromatin composition and nuclear assembly revealed by histone depletion. *Nat Struct Mol Biol*. 21:617-625.